Insights into the biopharmaceutical behavior of oral lipid-based formulations using advanced analytical techniques and mathematical modeling

Inauguraldissertation

zur

Erlangung der Würde eines Doktors der Philosophie

vorgelegt der

Philosophisch-Naturwissenschaftlichen Fakultät

der Universität Basel

von

CORDULA EDITH STILLHART

aus Bütschwil SG

Basel, 2014

Genehmigt von der Philosophisch-Naturwissenschaftlichen Fakultät
auf Antrag von:

Prof. Dr. Georgios Imanidis, Dissertationsleiter
Prof. Dr. Jörg Huwyler, Korreferent
Prof. Dr. Martin Kuentz, Korreferent

Basel, den 15. Oktober 2013

Prof. Dr. Jörg Schibler
Dekan

Namensnennung-Keine kommerzielle Nutzung-Keine Bearbeitung 3.0 Schweiz
(CC BY-NC-ND 3.0 CH)

Sie dürfen: **Teilen** — den Inhalt kopieren, verbreiten und zugänglich machen

Unter den folgenden Bedingungen:

Namensnennung — Sie müssen den Namen des Autors/Rechteinhabers in der von ihm festgelegten Weise nennen.

Keine kommerzielle Nutzung — Sie dürfen diesen Inhalt nicht für kommerzielle Zwecke nutzen.

Keine Bearbeitung erlaubt — Sie dürfen diesen Inhalt nicht bearbeiten, abwandeln oder in anderer Weise verändern.

Wobei gilt:

- **Verzichtserklärung —** Jede der vorgenannten Bedingungen kann **aufgehoben** werden, sofern Sie die ausdrückliche Einwilligung des Rechteinhabers dazu erhalten.
- **Public Domain (gemeinfreie oder nicht-schützbare Inhalte) —** Soweit das Werk, der Inhalt oder irgendein Teil davon zur Public Domain der jeweiligen Rechtsordnung gehört, wird dieser Status von der Lizenz in keiner Weise berührt.
- **Sonstige Rechte —** Die Lizenz hat keinerlei Einfluss auf die folgenden Rechte:
    - Die Rechte, die jedermann wegen der Schranken des Urheberrechts oder aufgrund gesetzlicher Erlaubnisse zustehen (in einigen Ländern als grundsätzliche Doktrin des **fair use** bekannt);
    - Die **Persönlichkeitsrechte** des Urhebers;
    - Rechte anderer Personen, entweder am Lizenzgegenstand selber oder bezüglich seiner Verwendung, zum Beispiel für **Werbung** oder Privatsphärenschutz.
- **Hinweis —** Bei jeder Nutzung oder Verbreitung müssen Sie anderen alle Lizenzbedingungen mitteilen, die für diesen Inhalt gelten. Am einfachsten ist es, an entsprechender Stelle einen Link auf diese Seite einzubinden.

Quelle: http://creativecommons.org/licenses/by-nc-nd/3.0/ch/ Datum: 12.11.2013

Meiner Familie

Science lives not on knowledge alone
but also (and perhaps above all) on dreams.

Gottfried Schatz

Abstract

Lipid-based formulations (LBFs) are effective means for the oral delivery of poorly water-soluble compounds. The drug is already solubilized in the formulation and, thus, the critical dissolution step is circumvented. However, the oral bioavailability is also determined by the fate of the LBF in the gastrointestinal (GI) tract. Formulation dispersion and lipid digestion are particularly critical steps in this regard. The ability to maintain the drug in a solubilized state may be reduced leading to an increased risk of drug precipitation and erratic drug absorption.
The present thesis consists of five studies, which aim at improving the biopharmaceutical understanding of LBF performance in the GI tract. To this end, *in vitro* dispersion and digestion assays are employed along with advanced analytical techniques and mathematical modeling. The findings may improve the predictability of LBF performance upon oral administration.

In the first study, we analyzed surfactant/co-solvent systems during aqueous dilution. A theoretical model was proposed to analyze the role of excipient interaction for drug solubilization during dilution. This model indicated that, in undiluted formulations, co-solvent/surfactant domains were responsible for drug solubilization. In contrast, in diluted formulations the co-solvent partitioned out of the surfactant microstructure. This loss of excipient interaction caused formulation-specific supersaturation, which was indicative for the risk of drug precipitation. The analysis of excipient interactions and drug supersaturation facilitated the identification of critical drug-loadings in LBFs that are prone to drug precipitation.

The second study focused on the *in vitro* lipolysis test. We evaluated Raman spectroscopy as an analytical technique for real-time monitoring of lipolysis-triggered drug precipitation. Despite the complex and varying medium composition, in-line analytics provided robust and highly time-resolved drug precipitation profiles. This allowed further analysis of the precipitation kinetics using a theoretical nucleation and growth model. The combination of real-time Raman spectroscopy and mathematical modeling

provided valuable insights into the time evolution of lipolysis-triggered drug crystallization.

The simulation of formulation digestion in an absorption environment was the purpose of the third study. Current *in vitro* lipolysis tests are performed in a single compartment and, therefore, they include no absorption sink. In this study, we developed a physiologically-based model of formulation digestion in the GI tract based on *in vitro* lipolysis and *in vivo* pharmacokinetic data. The resulting system of differential equations allowed the calculation of drug supersaturation during the intestinal transit of LBFs. This approach provided clear evidence that an absorption sink significantly lowers the risk for lipolysis-triggered drug precipitation. Hence, *in vitro* lipolysis provides the worst case prediction of LBF performance. Moreover, our results suggested that the intestinal digestion of LBFs is less critical than expected with respect to drug precipitation, especially with highly permeable drugs.

The fourth study focused on the solid-state of precipitated weakly basic drugs. Drug-loaded LBFs were dispersed in a simulated intestinal medium with and without digestive enzymes and the resulting precipitate was analyzed by X-ray diffraction and re-dissolution. The study revealed that *in vitro* conditions can influence the solid-state properties of precipitating weak bases. While a crystalline precipitate was observed upon dispersion, the presence of digestive enzymes led to an amorphous precipitate. These findings are of high practical importance for the prediction of LBF performance *in vivo*. In contrast to the crystalline form, an amorphous precipitate may re-dissolve rapidly and, hence, become again available for absorption.

Finally, in the fifth study, Raman spectroscopy and ultrasound resonator technology were evaluated as process analytical tools for drug quantification in LBFs. This study evidenced the excellence of Raman spectroscopy for drug quantification in complex lipidic matrices and was the basis for using Raman spectroscopy with biopharmaceutical tests.

This thesis provided novel insights into the biopharmaceutical behavior of LBFs in the GI tract. The establishment of real-time techniques allowed the examination of highly dynamic formulation changes during dispersion and digestion. Moreover, mathematical modeling provided key insights into biopharmaceutical processes that are hardly accessible using *in vitro* methods. These advancements may improve the ability to predict LBF performance *in vivo*.

Contents

Chapter 1

Introduction

1.1 Background

Oral administration is generally the most convenient way for systemic drug delivery. From a biopharmaceutical perspective, a drug has to overcome two main hurdles in order to become systemically available. First, the drug has to dissolve in the gastrointestinal (GI) fluids and the kinetics and extent of this dissolution are critical for poorly water-soluble compounds. In a second step, the drug must permeate across the intestinal membrane to reach the circulation. Good membrane permeability is fundamental at this stage. The biopharmaceutical classification system (BCS) has been introduced to classify pharmaceutical compounds into four types as a function of their solubility and permeability properties [1]. BCS class II and IV compounds are particularly challenging from a pharmaceutical perspective, but the formulation strategy can help in reducing biopharmaceutical issues, especially with BCS class II drugs. These compounds are poorly water-soluble but well permeable, *i.e.*, the dissolution step is the major cause for limited drug absorption. Drug solubilization is largely influenced by exo- and endogenous factors such as food and bile salts, and as a consequence, the pharmacokinetic profile is often highly variable [2, 3].

Since up to 75% of new low molecular weight compounds are poorly water-soluble [4], the research interest toward robust and effective means for enhancing oral bioavailability increased tremendously over the past decades. Several formulation principles have been identified, which principally improve either the solubility or the dissolution rate of the drug [5, 6]. This can be achieved, for example, by altering the solid-state (*e.g.*, by selecting superior polymorphs) or by developing more soluble salts or hydrates. Other mechanisms include the reduction of particle size of the solid drug (*i.e.*, variation of the specific surface area) and the generation of solid dispersions. The dissolution step can

even be entirely circumvented by administering the active compound in a solubilized state. This strategy is applied with lipid-based formulations (LBFs) and is the main focus of the present thesis.

LBFs are not a recent pharmaceutical innovation [7]. However, the raising number of poorly water-soluble drug candidates notably increased the research interest toward oral LBFs in the past decade. The successful launch of some lipid-based products, such as Sandimmun Neoral®, Invirase®, and Norvir®, has additionally promoted this formulation strategy [8].

Oral LBFs are simple oil solutions or more complex mixtures of lipidic excipients, in which the drug is incorporated in the solubilized form [9, 10]. The circumvention of the dissolution step and the higher apparent drug solubility in GI fluids are certainly major advantages of LBFs [11]. However, there are additional mechanisms, which can improve the oral bioavailability. Certain lipidic excipients may interact with membrane transporters and, thus, increase drug uptake in enterocytes [12, 13]. LBFs can also have a protective effect against presystemic degradation. Since formulation absorption generally occurs via the lymphatic system, first-pass metabolism is significantly reduced [14–17].

After oral administration, LBFs experience several processing steps in the GI tract. The aqueous environment in the stomach leads to the formation of small oil droplets, emulsions, and/or micellar structures. This dispersion process is generally spontaneous and occurs rapidly on contact with the aqueous fluids. In the intestinal lumen, formulation lipids are then digested by lipolytic enzymes. During digestion, oil droplets are reduced to smaller colloidal structures from which drug absorption is facilitated.

Although these structural changes are necessary for promoting formulation dispersion, in some instances they can also compromise drug absorption [11]. During dispersion, hydrophilic excipients often migrate into the aqueous bulk, which may significantly reduce the drug solubilization capacity of the formulation. Similarly, excipient digestion generates comparatively hydrophilic lipolysis products, such as monoglycerides and fatty acids. The formulation becomes more polar, and as a consequence, the drug can precipitate. A poorly water-soluble compound is generally not expected to re-dissolve during GI transit. Hence, such intralumenal precipitation is highly undesired and may seriously compromise drug absorption.

The prediction of LBF behavior is very important for effective formulation development. Several *in vitro* methods have been developed to simulate formulation dispersion and digestion in biorelevant media [18]. However, the prediction of *in vivo* performance is still poor and only a rank-order level of correlation has been evidenced so far [19–25].

It is a main focus of current LBF research to improve biopharmaceutical *in vitro* assays

[26–30]. One major limitation is the lack of appropriate analytical techniques for characterizing formulation changes. Formulation dispersion and digestion are highly dynamic processes and traditional analytical instrumentations often fail in capturing these events accurately [31, 32]. Moreover, there is increasing evidence that drug precipitation does not necessarily impair oral bioavailability [23, 33–35]. In contrast to the crystalline form, an amorphous precipitate may re-dissolve rapidly upon precipitation and become again available for absorption. Hence, the solid-state of a precipitate is a major determinant of oral bioavailability. A further critical limitation is the absence of an absorptive sink in *in vitro* assays [36–38]. This is particularly relevant for poorly water-soluble drugs, which easily attain the saturation level, especially in a closed compartment.
As a result, there is still an incomplete mechanistic understanding of LBF performance in the digestive tract. More research is required in this field of drug delivery.

1.2 Objectives

The general aim of this thesis is to improve the biopharmaceutical understanding of LBF performance in the GI tract using *in vitro* tests. To this end, advanced analytical techniques are introduced, which provide insights into the highly dynamic processes of formulation dispersion/digestion and drug precipitation. Moreover, mathematical models are implemented to describe the processes of drug solubilization on a mechanistic basis. The thesis is subdivided into six chapters, which address analytical and mechanistic aspects of LBF performance during *in vitro* dispersion and digestion.

The theoretical section (Chapter 2) aims at reviewing *in vitro* assays and analytical techniques currently adopted for biopharmaceutical characterization of oral LBFs. Particular attention is also directed to the technical limitations of *in vitro* assays.

Chapter 3 focuses on the process of LBF dispersion of surfactant/co-solvent systems. The aim is to elucidate the mechanism of drug solubilization upon aqueous dilution in order to identify LBFs with a low risk for drug precipitation.

The first purpose in Chapter 4 is to implement a real-time analytical technique for monitoring drug precipitation during *in vitro* lipolysis. *In situ* analytics is required to reduce the temporal delay involved with off-line techniques and to obtain highly time-resolved data. Based on this advanced analytics, the second aim is to study the kinetics of drug crystallization using a theoretical nucleation and growth model.

The aim in Chapter 5 is to examine the effect of an absorptive sink on the extent of drug supersaturation during formulation lipolysis. Due to the absence of multi-compartmental

in vitro assays, we aim at developing a physiologically-based mathematical model that simulates formulation digestion in the intestine.

The solid-state of weakly basic drugs precipitated during LBF dispersion and digestion is the focus in Chapter 6. The purpose is to assess the influence of *in vitro* conditions (dispersive *versus* digestive) on the solid-state properties and re-dissolution behavior of precipitated weak bases.

Finally, Chapter 7 focuses on the application of Raman spectroscopy and ultrasound resonator technology as process analytical tools for drug quantification in LBFs. The aim is to identify analytical techniques which are particularly appropriate for quantitative analyses in complex lipidic matrices.

Chapter 2

Theoretical section

2.1 Oral lipid-based formulations

Oral LBFs have gained increasing attention as a drug delivery strategy for poorly water-soluble compounds. These formulations are mixtures of up to five excipients, including oils, lipophilic or hydrophilic surfactants, and co-solvents [8], in which the drug is administered in a solubilized state. In 2000, Pouton introduced the Lipid Formulation Classification System (LFCS) that categorizes LBFs into five classes according to their composition (Table 2.1) [9, 10]. Type I formulations are the most lipophilic formulations and are composed from digestible oils only (*e.g.*, Miglyol N 812, olive oil). These formulations form coarse oil droplets in contact with aqueous media and have to be digested to promote dispersion and drug absorption. Type II formulations contain additionally a hydrophobic surfactant (*e.g.*, Tween® 85), which facilitates self-emulsification. They generate coarse emulsions of 200 nm to 1 μm in diameter and digestion is often necessary to reduce particle size and facilitate drug absorption. Type III formulations are composed of lipids, hydrophilic surfactants (*e.g.*, Cremophor® EL, Tween® 80), and eventually co-solvents (*e.g.*, ethanol, Transcutol®). This class is subdivided into two types to discern between formulations with larger amounts of oil (type IIIA) and formulations with less than 20% w/w oil (type IIIB). The hydrophilic surfactants generally accelerate self-emulsification and produce fine emulsions of less than 200 nm in diameter. Finally, type IV formulations are lipid-free and are composed of surfactants and co-solvents only. These systems disperse very easily forming micellar structures in aqueous milieu and, since surfactants are generally poorly lipolised, formulation digestion is less relevant. Strickley [8, 39] and Hauss [18] provided thorough reviews of excipients used in commercially available LBFs.

TABLE 2.1: Composition of LBFs (% w/w) according to the LFCS [9, 10].

Excipient	Type I	Type II	Type IIIA	Type IIIB	Type IV
Oils	100	40-80	40-80	<20	-
Lipophilic surfactants (HLB<12)	-	20-60	-	-	0-20
Hydrophilic surfactants (HLB>12)	-	-	20-40	20-50	30-80
Co-solvents	-	-	0-40	20-50	0-50

LBFs are developed in an empirical way to date and several procedural methods can be found in the literature [6, 40, 41]. The development of a LBF usually starts with the identification of excipients (oils, surfactants, and co-solvents) that provide adequate drug solubilization [42]. This screening is performed via experimental solubility measurement to date, but much effort is currently directed to the development of automated high-throughput solubility assays [43] and *in silico* methods for solubility prediction [44–47]. Such advanced approaches are desirable since conventional solubility measurement in lipidic and/or semi-solid matrices is labor-intensive and time-consuming.
Once adequate excipients have been identified, different mixtures of ingredients are evaluated in terms of miscibility via ternary phase diagrams [10, 48]. This screening allows the identification of stable formulations that provide homogeneous drug solubilization. Further criteria of formulation selection include toxicity and impurity issues as well as capsule compatibility [49].
Successful formulation candidates are finally tested with respect to their biopharmaceutical performance. The primary aim is to assess the capacity of the formulation to maintain the drug in the solubilized state after oral administration. Two processes are particularly critical in this regard: formulation dispersion in the aqueous environment and formulation digestion by intestinal lipases. These processing steps can lead to a restructuring and a change in polarity of lipidic excipients, which may affect the microenvironment of the drug. The solubilization capacity of the formulation often decreases, and as a result, the drug can precipitate. Because a poorly water-soluble compound may barely re-dissolve during GI transit, such intralumenal precipitation is highly undesired and can result in reduced and erratic drug absorption. Appropriate *in vitro* tools are therefore necessary to identify viable formulation candidates.

Several *in vitro* methods for biopharmaceutical testing of LBFs are described in the literature but, unfortunately, there is still a lack of standardized, compendial assays [6, 30]. The most used *in vitro* assays are dilution, dispersion, and lipolysis tests. *In vitro* dilution testing assesses the performance of LBFs in contact with aqueous media qualitatively. It is a simple test, and thus, appropriate for high-throughput formulation screening. However, the simulated environment is rather far from physiological conditions. For more biorelevant characterization, other tests may be applied, as for example

TABLE 2.2: Comparison of the three main *in vitro* assays for simulating LBF performance in the GI tract (modified from [29]).

	Dilution test	Dispersion test	Lipolysis test
Experimental simplicity	++	+	−
Proximity to *in vivo* conditions	−/+	+	++
Miniaturization for high-throughput screening	++	+	−
Testing of the final dosage form (*e.g.*, capsule)	−	++	−[a]
Quantification of the extent of precipitation	−/+	++	++
Determination of supersaturation and kinetics of precipitation	−/+	++	++
Solid-state analysis of precipitate	−/+	++	++

[a] Limited physiological relevance.

an *in vitro* dispersion test. This test is usually performed in a compendial USP 2 dissolution apparatus and it provides the drug solubilization *versus* time profile of a LBF. Due to the similarity to dissolution testing with solid dosage forms, *dispersion*, *dissolution*, and *drug-release* testing are often used as synonyms. However, the term *dissolution* should not be used when the drug is not in a solid form in the formulation. The test offers more standardized conditions (*e.g.*, hydrodynamics) compared to simple *in vitro* dilution. Finally, *in vitro* lipolysis testing is applied to characterize LBF performance in digestive environment. This test involves a simulated intestinal medium with lipolytic enzymes and provides the closest conditions to the *in vivo* physiology. However, *in vitro* lipolysis is comparatively time-consuming, and thus, less adequate for high-throughput analyses. Key aspects of *in vitro* dilution, dispersion, and lipolysis tests are listed in Table 2.2.

The development of standardized *in vitro* assays is a major focus in current LBF research [26–29]. Several limitations have been identified and much efforts were directed to the optimization of testing protocols [26, 29, 31, 37, 50–52]. Moreover, particular attention has been directed to selection of appropriate analytical instrumentation for LBF characterization [31–33, 53]. The accurate monitoring and interpretation of formulation properties is, indeed, the basis for any biopharmaceutical investigation.
The present theoretical section summarizes recent advancements in *in vitro* testing of LBFs. First, two important parameters affecting drug absorption are discussed, *i.e.*, drug supersaturation and the solid-state of a precipitate. The second part provides an overview of current methods for *in vitro* dilution, drug-release, and lipolysis testing. A particular focus is directed to the analytical techniques for biopharmaceutical characterization of LBFs. Finally, current challenges of *in vitro* LBF testing are discussed.

2.2 Important parameters affecting drug absorption from LBFs

A major aim in biopharmaceutical testing of LBFs is to assess whether the drug remains in solution during formulation dispersion and digestion. Drug absorption can be significantly reduced in case of intralumenal precipitation, and thus, such biorelevant characterization is of primary importance. In addition to the intrinsic solubilization capacity of the LBF, oral bioavailability can also be influenced by other formulation- and drug-related factors. Formulation-related factors include, for example, biological effects of lipidic excipients on intestinal based efflux and lymphatic transport [14, 54]. Drug-related factors include more biophysical aspects of drug precipitation. There is a growing realization that the occurrence of drug precipitation *in vitro* does not directly imply a reduced drug absorption *in vivo* [36, 38, 55–62]. Important determinants are the extent of drug supersaturation and the solid-state of precipitating material, which will be discussed in the present section.

2.2.1 Drug supersaturation

The process of precipitation basically occurs in three stages [63]. In the initial stage, the drug is completely solubilized, but its concentration exceeds the solubility at equilibrium. This so-called supersaturated state is thermodynamically unstable and provides the driving force for drug precipitation. Once a critical degree is attained, drug molecules begin to form small aggregates. During this nucleation phase, an initial energy barrier must be exceeded until these aggregates grow to a critical size [64]. As soon as stable nuclei are formed, they act as centers for crystallization and grow to larger crystals. Crystal growth is the third stage of precipitation.

From a biopharmaceutical perspective, the initial induction period is particularly important. Supersaturated drug is thermodynamically unstable, and hence, prone to precipitation. However, the time point when nucleation begins is variable. For low degrees of supersaturation and in the absence of external triggers, the nucleation period can be in the order of years. In contrast, when a critical degree of supersaturation is exceeded, the induction time reduces dramatically and nucleation may begin within seconds to minutes [63]. This duration is particularly relevant when drug supersaturation occurs in an absorptive environment [36]. Supersaturated drug is, indeed, still available for absorption, and the longer the induction period, the more drug can be absorbed prior to precipitation. In the best case, supersaturation falls below a critical level and precipitation is ultimately prevented.

Four different mechanisms can basically induce drug supersaturation after oral administration of a LBF [59]. Formulation dispersion [48] and excipient digestion [56] are certainly of major importance, but recent studies have evidenced other triggers of supersaturation. It was shown that the inclusion of bile salt micelles into lipid-rich mixed-micelles containing lipolysis products decreases the solubilization capacity of basic drugs [55, 65]. This influence is, however, assumed to be drug specific and may be less critical for neutral drugs [65]. Furthermore, supersaturation can also be generated by the absorption of lipolysis products, and hence, the removal of solubilizing agents. Particularly important is here the microenvironment at the unstirred water layer. The lower pH favors protonation of fatty acids, the dissociation from colloidal structures, and finally, fatty acid absorption [66].

Much attention is directed to the prevention of high degrees of supersaturation *in vivo*, but supersaturation *per se* can also be a desirable outcome in drug delivery. Indeed, the thermodynamic activity of a supersaturated drug is comparatively high, and thus, the drug flux across the intestinal membrane is favored [36, 58, 67, 68]. This property has clearly beneficial effects on drug absorption. The extent of supersaturation and the place where supersaturation occurs within the GI lumen are particularly important in this respect. Moderate supersaturation near to the absorptive membrane is expected to favor drug absorption, and as a consequence, the risk of drug precipitation is rather low. In contrast, extensive supersaturation in a poorly absorptive environment (*e.g.*, in the stomach) is more critical.

The potential of maintaining drug in a supersaturated state has also influenced formulation strategies with poorly water-soluble compounds [69–72]. In particular, supersaturable LBFs and supersaturated self-nanoemulsifying drug delivery systems (super-SNEDDS) have attracted increasing attention. Supersaturable LBFs aim at generating high levels of supersaturation upon aqueous dispersion of the formulation and at decelerating the rate of drug precipitation to enable drug absorption. To this end, low amounts of surfactant and a polymeric precipitation inhibitor (*e.g.*, hydroxypropyl methylcellulose) are added to the formulation [73–75]. A similar approach is followed with super-SNEDDS. In these formulations, the drug is incorporated at a concentration that exceeds its solubility in the pure formulation. Hence, super-SNEDDS are thermodynamically unstable already in the undispersed state, but allow a higher drug-load compared to supersaturable LBFs [23, 34].

The degree of supersaturation is generally expressed as (super-)saturation ratio, SR, which is the ratio of the actual concentration of solubilized drug, C_{sol}, and the equilibrium solubility of the drug, C^*:

$$SR = \frac{C_{sol}}{C^*} \tag{2.1}$$

For $SR \leq 1$, the system is thermodynamically stable, whereas for $SR > 1$, supersaturation is reached and the drug may precipitate to restore saturation.
The extent of supersaturation can be indicative for the likelihood of drug precipitation during LBF dispersion and digestion. This measure has therefore attracted increasing attention in recent LBF research [28, 36, 38, 55–58, 61, 65, 70, 76, 77]. For example, drug precipitation was shown to be unlikely on a physiologically relevant time-scale at $SR < 2$, whereas rapid drug precipitation was observed at $SR > 4$ during *in vitro* dispersion of LBFs [48, 77]. Particularly challenging is the determination of a critical SR with lipolysis-triggered drug precipitation. Drug solubility is here continuously changing due to the hydrolysis of formulation lipids, and hence, the SR is not constant. Accordingly, a formulation can be below saturation upon dispersion (without lipolysis), but then exhibit a dramatic loss in solubilization capacity upon digestion [31]. Williams *et al.* proposed a modified SR for assessing the theoretical thermodynamic instability of the drug in digested formulation. This potential maximum supersaturation ratio, SR^M, is the ratio of the maximum theoretical concentration of solubilized drug and the minimum drug solubility in the digest [28]:

$$SR^M = \frac{\text{Max.}C_{sol}\text{in digest}}{\text{Min.}C^*\text{during digestion}} \tag{2.2}$$

Based on a range of compounds and LBFs, it appeared that the risk of drug precipitation was particularly high for $SR^M > 3$ [28, 56]. The correlation was remarkable, thus, indicating that it is a practical approach for identifying drug-loads with an increased risk of precipitation. However, it must be noted that the SR^M value is obtained from formulation digestion *in vitro* and it gives no information about the time evolution of drug supersaturation. This can be a limitation, for example, for evaluating the risk of drug precipitation in an absorptive environment.

2.2.2 Solid-state of precipitated drug

It was generally assumed that drug precipitation directly reduces the absorbable drug dose because of the poor re-dissolution capacity of a poorly water-soluble substance [10]. However, recent studies suggested that this assumption is not valid for every type of precipitate. A significant determinant of drug absorption is the solid-state of the precipitate, which can be either oily, amorphous, or crystalline [78].
Crystalline material is characterized by a highly periodical three-dimensional pattern and long distance order of the molecules in the crystal lattice. This is the most stable solid structure from a thermodynamic perspective. In an amorphous precipitate, the molecules have no long-range order, whereas in the oil state, molecules are randomly arranged. The oil state is considered as an additional liquid phase and is generated at

very high degrees of supersaturation [78].

The dissolution behavior of a drug is highly dependent from its solid-state [79]. The free energy needed to mobilize drug molecules from oil and amorphous precipitates is much lower than for crystalline solids. Such precipitates are therefore expected to re-dissolve notably faster and to reach higher apparent solubilities compared to crystalline drug (Figure 2.1). Moreover, the higher apparent solubility enhances drug flux across the intestinal membrane, which provides a further advantage for drug absorption [62].

Sassene *et al.* recently observed that cinnarizine precipitated in an amorphous form during *in vitro* lipolysis of a self-emulsifying formulation. Subsequent re-dissolution experiments confirmed that this precipitate dissolved much faster than the crystalline counterpart [33]. Interestingly, a solubility advantage was also observed *in vivo*, where extensive drug absorption occurred after oral administration of the LBFs [80]. However, to confirm the causal relationship between amorphous precipitate and drug absorption, further studies are necessary, which possibly analyze the solid-state of a precipitate directly in intestinal aspirates. Such analyses were recently performed by Psachoulias *et al.*, for simple drug solutions without LBFs [61].

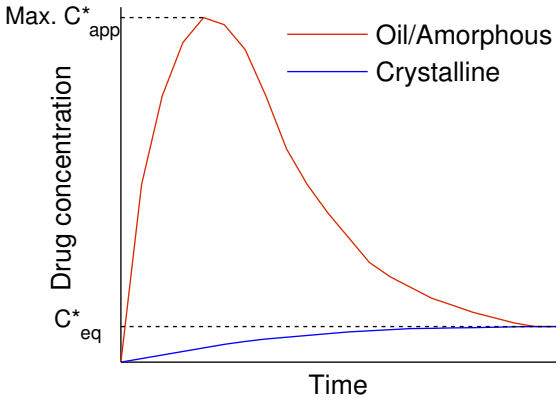

FIGURE 2.1: Re-dissolution behavior of precipitated drug in the oil/amorphous state (red) and in the crystalline state (blue). Although the final equilibrium solubility, C^*_{eq}, is equal for each solid-state, the highest apparent solubility, C^*_{app}, of high energy materials such as oil or amorphous precipitates can be a multiple of the solubility at equilibrium (adapted from [38]).

2.3 *In vitro* assessment of LBF dilution/dispersion

Formulation dispersion is the first process that occurs after LBF administration and capsule disintegration in the GI fluids. Due to the partial immiscibility of lipidic excipients in polar fluids, the dispersion step often leads to a considerable restructuring of formulation components [10, 48]. For example, the addition of small amounts of water

to an LFCS type III formulation leads to the swelling of inverse micelles. More water causes the formation of a water-in-oil emulsion, and in the presence of equal amounts of water and formulation, the system becomes bicontinuous. Finally, the vehicle passes over to an oil-in-water emulsion [10]. This restructuring can significantly impair the drug solubilization capacity of the formulation, especially with hydrophilic systems such as LFCS type III and IV formulations [48, 77]. The loss of drug solubilization capacity can result in a supersaturated state and in undesired drug precipitation.

2.3.1 *In vitro* dilution test

In vitro dilution is a simple test that is usually applied in early formulation development. The primary aim is to assess the spontaneity of self-emulsification and the characteristics of the resulting dispersion. This information reveals the capacity of the LBF to form physically stable and homogeneous emulsions upon oral administration. A second aim is to gain first, qualitative information about the drug solubilization capacity of the formulation in an aqueous environment.
For dilution testing, a formulation is mixed with water (or an aqueous buffer) at one to three different dilution ratios. Experiments are perfomed at either room temperature or 37°C and under mild agitation conditions [81–86]. It is recommendable to select more than one dilution ratio to learn about the LBF performance at different stages of formulation restructuring. Low dilution ratios (*e.g.*, 1:2 w/w) simulate the formulation behavior near to the bicontinuous phase, whereas high dilution ratios (*e.g.*, 1:200 w/w) hold for the final dilution in GI fluids [77, 87].

2.3.1.1 Analytical tools for studying aqueous dilution of LBFs

In the early development of LBFs, the dilution behavior is generally evaluated with standard analytical methods. Visual inspection is particularly important in this context and provides first information about the spontaneity of self-emulsification and the presence of a precipitate. Instrumental methods include primarily dynamic light scattering (DLS), turbidimetry, and conductivity measurement, which are particularly convenient in terms of availability and costs [48, 71, 88]. DLS measures the size of dispersed particles (*e.g.*, oil droplets) in a colloidal range [89, 90]. The sample is illuminated by a laser beam and the backscattered light is detected at a certain angle by a photon detector. The diffusion coefficient of particles is then used to calculate their hydrodynamic radius via the Stokes-Einstein equation. The particle size is, however, not the only relevant information resulting from DLS measurements. Another important parameter is the particle size distribution, often expressed as polydispersity index (PDI), which indicates

the uniformity of the dispersed formulation. This technique is well-established in LBF research and has found broad application in both industrial and academic laboratories [88, 91]. Turbidimetry is particularly appropriate to determine the spontaneity of self-emulsification and the phase stability of an emulsion. A nephelometer is used, which determines the forward light scattering of a sample, and hence, the degree of obscuration based on the scattered signal. The possibility of *in situ* measurement is a great advantage of turbidimetric analysis. Moreover, the technique can be miniaturized, and therefore, it has found application as a high-throughput method for formulation screening [43, 92]. Turbidimetry was also proposed for flow-through analysis of the dispersion properties of self-emulsifying formulations [83].
Conductivity measurement allows for the analysis of the phase behavior of formulations during aqueous dilution [48, 93–95]. The phase change at the oil to water continuous/bicontinuous region is particularly well detectable, as the conductivity notably increases when water becomes the continuous phase in a diluted system.
Visual inspection and turbidimetry can also be used to detect drug precipitation during formulation dilution, by direct comparison of drug-free and drug-loaded formulation [43, 71, 72, 77]. Higher turbidity in the drug-loaded system may indicate the presence of a precipitate. However, the clear detection of such a precipitate is sometimes challenging. Solid drug can be hardly visible due to the intrinsic turbidity of the emulsified formulation, especially with LFCS type II and IIIA systems [29]. Other limitations are typically the low overall amount of drug, especially at high dilution levels, and the effect of drug inclusion on the droplet size of emulsified formulations [96]. An increase in droplet size, and thus, and increase in turbidity, may then be erroneously interpreted as drug precipitation. In these cases, additional methods, such as optical microscopy, may be necessary to confirm the presence of a precipitate [29].

The mechanistic elucidation of formulation behavior is more complex and sophisticated methods are required for this purpose.
Microscopy techniques such as transmission electron microscopy (TEM) has been often applied for studying formulation morphology in the dispersed state [94, 97–102]. Traditional electron microscopes work under high-vacuum to avoid electron scattering by gas molecules. Hence, to analyze hydrated structures such as colloids, a cryo preparation is generally required to prevent the damage of the native morphology [103]. Polarized light microscopy (PLM) is instead particularly appropriate for detecting liquid crystalline mesophases, which appear as birefringent structures in the microscopy images [83, 104].
Dynamic viscosity and ultrasound resonator technology (URT) were used for the analysis of LBF performance at varying dilution ratios. Dynamic viscosity was measured

with a rotational viscosimeter and provided information about the size and attractive interactions between microemulsion droplets [94, 95, 105, 106]. Instead, URT was applied to determine the difference in ultrasound velocity between diluted formulation and a reference medium, *i.e.*, water. In a homogeneous ideal liquid, the velocity of a sound wave is known to depend on the density, ρ, and the apparent compressibility, κ, of the fluid, as described by the Newton-Laplace equation, $U = 1/\sqrt{\rho\kappa}$ [107]. Thus, a change in ultrasound speed was attributable to a change in apparent density or compressibility, and hence to a structural transition of the formulation. Such analysis was recently performed with surfactant/co-solvent systems. It was demonstrated that these formulation pass a main structural transformation at a dilution ratio of 1:1 to 1:5 w/w in water, whereas almost no further change occurred at higher dilution [77].

Advanced light scattering techniques have also found broad application in elucidating structural changes during LBF dispersion. The scattering behavior of photons is determined by the relative wavelength of radiation compared to the dimension of the scattering material. To analyze structures with colloidal dimensions, radiation sources providing X-rays and neutrons are particularly appropriate (wavelength ∼1 Å). In this context, small-angle neutron scattering (SANS) and small-angle X-ray scattering (SAXS) provided essential structural information about the atomic order and the interatomic distance and angle in colloids [108–113]. Phan *et al.* recently applied SAXS to investigate the interplay between lipid-based liquid crystalline structures and drug release from LBFs [114]. These studies showed that drug release was faster from bicontinuous cubic structures than from other phases, which indicated that the properties of water compartments have a pronounced influence on the kinetics of drug release. Thorough reviews about the application of light scattering techniques with LBFs were provided by Moulik and Paul [90] and Yaghmur and Rappolt [115].

Nuclear magnetic resonance (NMR) spectroscopy provides information on the molecular interactions, the structural rearrangement, and the microenvironment of the drug during formulation dispersion [80, 104, 116]. Larsen *et al.* applied pulsed field gradient stimulated echo NMR to measure the apparent diffusion coefficient of a model drug in a self-nanoemulsifying system [80]. These experiments revealed details about the drug partitioning in LBFs that were dispersed in different pH environments. Similarly, electron paramagnetic resonance (EPR) spectroscopy was applied for studying the microenvironment of a drug [87, 117–119]. This technique makes use of paramagnetic molecules (*e.g.*, nitroxides), which are incorporated into the tested system. The interaction between electrons and an externally applied magnetic field indicates the polarity and viscosity of the microenvironment surrounding the probe molecules.

2.3.2 *In vitro* dispersion test

The purpose of dispersion testing is to determine how fast and to which extent a drug is available for absorption after oral administration of a LBF (without considering formulation digestion). The terminology is not consistent in the literature and *(dynamic) dispersion*, *drug-release*, and *dissolution* are often used as synonyms. The term *dissolution* testing is misleading, because the drug is already dissolved in the formulation and is not subjected to a real dissolution process during *in vitro* testing. *Dispersion* and *drug-release* are more appropriate. Indeed, it is assumed that the drug must be dissolved in either the dispersed formulation or in the bulk aqueous medium to be available for absorption [14, 120]. As a matter of clarity, only the term *dispersion* is used in this chapter.

The underlying principle of dispersion testing is analogous to dissolution testing with conventional oral dosage forms. Briefly, a dosing unit is immersed in a compendial dissolution vessel, containing an aqueous medium, and the concentration of solubilized drug is measured at intervals. Bulk formulation and precipitated drug are then separated, *e.g.*, via filtration, to finally measure the concentration of solubilized drug in dispersed formulation and in the aqueous bulk. In general, the focus of dispersion testing is not the velocity of formulation dispersion, but the capacity of the formulation to maintain the drug in the solubilized form. This is a major difference to conventional dissolution testing.

The composition of dissolution media used for dispersion testing is highly variable in the literature [69, 81, 84, 85, 121–129]. The medium can notably affect formulation dispersion and drug solubilization [128–132], and as a result, cross-comparison of experimental data is often challenging. For simple experimental setups, such as in routine quality control, purified water [81, 84] and acidic or basic aqueous solutions [69, 85, 121–124] are generally adequate. The low drug solubilization capacity can be a limiting factor and a surfactant such as sodium dodecylsulfate (SDS) or polysorbate 80 may be added to generate sink conditions [124–126]. This strategy has also been included in the chapter on dissolution testing of the United States Pharmacopeia (USP) [133]. However, it is less appropriate for the biopharmaceutical characterization of LBFs, since it would reduce the discriminatory power of the test. A more physiological alternative is the use of biorelevant media, which contain bile salts and phospholipids as solubilizing agents. The media developed by Dressman *et al.* are frequently employed in this context, most importantly the fasted state simulated gastric and intestinal media (FaSSGF and FaSSIF, respectively) and the fed state simulated intestinal medium (FeSSIF) [127–129]. These media contain bile salts and phospholipids at physiological concentrations. The presence of surface active compounds is important when testing poorly water-soluble compounds, as they significantly influence the wettability and drug solubility in GI fluids [134–136].

TABLE 2.3: Experimental issues related to sample filtration and centrifugation.

Filtration	Centrifugation
Nuclei and small crystals may not be retained by conventional 0.22μm and 0.45μm filters	Emulsified formulation may separate into an oil and an aqueous phase
Larger emulsion droplets may be retained by the filter	Time delay between sampling and analysis (>15–30 minutes) allows further LBF dispersion and/or drug precipitation
Possible drug adsorption on filter material	

2.3.2.1 Analytical tools for studying LBF dispersion

The concentration of drug in dispersed LBFs is usually determined using off-line analytical techniques. Accordingly, an aliquot of acceptor medium is removed at intervals and the concentration of solubilized drug is measured, *e.g.*, via high-performance liquid chromatography (HPLC).

In this regard, it is important to select an appropriate technique with the goal to separate solubilized drug from undispersed formulation and unsolubilized drug. Sample filtration [29, 37, 128] and sample centrifugation [28, 48, 81] were typically employed, but both techniques present assets and drawbacks when working with LBFs. Sample centrifugation is effective in separating molecularly dissolved drug from undissolved particles, but it also implies a critical time lag between sample removal and analysis. This delay could lead to further formulation dispersion, to drug precipitation, or to a solid-state transformation of precipitated drug. Hence, the resulting drug concentrations may not reflect the real formulation dispersion and drug solubilization profile.

Sample filtration is less critical in this respect, since the separation of the solid and the liquid phase occurs almost immediately. A critical factor is, however, the pore size of filter material, as it determines the cut-off for retention of solid drug and undispersed formulation. Sample filtration during *in vitro* dispersion testing is usually done with a 0.45 μm filter membrane [29, 37, 128]. This pore size is expected to be larger than precipitated drug particles, and hence, small nuclei and crystals may not be retained; in the opposite case, when filter pores are too small, emulsion droplets containing solubilized drug may be erroneously retained by the filter. It was recently shown that filters with a pore size of less than 100 nm are able to separate molecularly dissolved drug from colloidal and undissolved particles [137]. Such filters are therefore particularly appropriate for detecting drug precipitation, but care is certainly needed when studying LBFs with droplet size of more than 100 nm in diameter (*e.g.*, LFCS type I and II formulations). Table 2.3 lists experimental issues related to filtration and centrifugation as separation techniques.

In the light of these experimental limitations, on-line techniques appear to be most interesting for detecting drug precipitation. Gao *et al.* pioneered the use of focused beam reflectance measurement (FBRM) for studying drug precipitation during LBF dispersion [75]. FBRM consists of an in-process probe which directs a rotating laser beam into the process stream (Figure 2.2). Laser light is reflected each time the beam encounters a particle and, based on this back-scattered light, the chord length distribution of particles is calculated [138, 139]. Several applications in the field of LBF testing showed that drug precipitation was clearly detectable despite the high turbidity of dispersed formulation droplets [29, 75, 77]. The detection limit of FBRM is around 1 μm (chord length).
For quantitative monitoring of drug precipitation, FBRM is often combined with other *in situ* techniques, such as Raman or infrared (IR) spectroscopy [140–142]. These methods have several advantages. They are not only highly specific for chemical compounds, but can also differentiate between physical states and are suitable for analyses in aqueous media. Arnold *et al.* presented the use of FBRM and Raman spectroscopy for monitoring drug precipitation in simulated intestinal fluid [142]. Interestingly, despite the complex medium composition and the presence of excipients, the instruments were able to clearly differentiate between nucleation and particle growth.

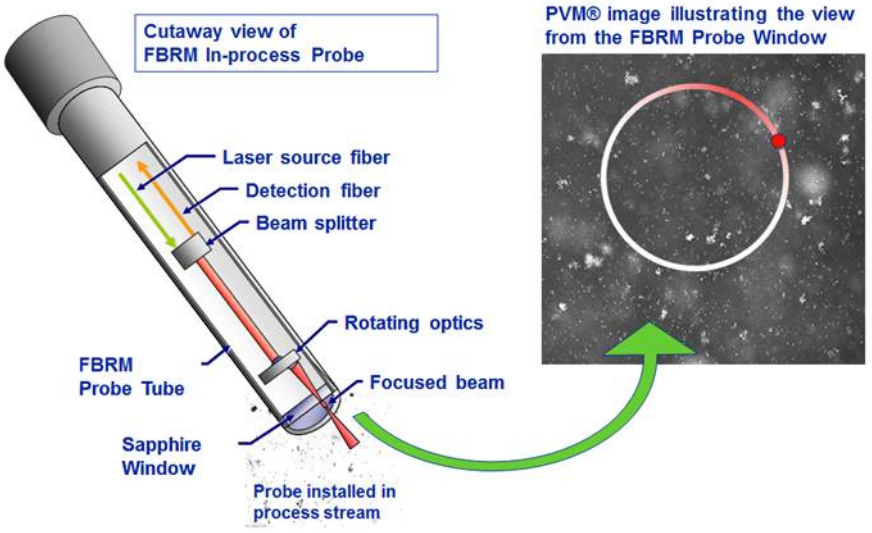

FIGURE 2.2: FBRM in-process probe (Source: Mettler-Toledo, Switzerland).

2.4 *In vitro* assessment of LBF digestion

Formulation digestion is the second critical processing step during GI transit of LBFs. Lipid digestion occurs primarily in the intestine and is catalyzed by the pancreatic lipase

and co-lipase, the pancreatic lipase related proteins, and the carboxyl ester hydrolase [143]. Di- and triglycerides are hydrolyzed at the *sn*-1 and *sn*-3 ester bonds generating *sn*-2 monoglycerides and fatty acids as final lipolysis products. Monoglycerides and fatty acids form vesicular structures and, in the presence of bile salts, they can be incorporated into more complex colloidal species [14]. These structures provide a solubilizing compartment for lipophilic molecules and facilitate drug absorption. For oil-rich formulations, the digestion process is therefore essential for promoting formulation processing and drug absorption. However, digestion products are more hydrophilic than the undigested lipids and this change in polarity may reduce the solubilization capacity of the formulation. It is therefore possible that formulation digestion results in undesired intralumenal drug precipitation.

2.4.1 *In vitro* lipolysis test

The main objective of *in vitro* lipolysis testing is to assess the drug solubilization capacity of a LBF in the digestive environment. Very first assays were developed by Reymond and Sucker [144] and Patton and Carey [145], which provided the basis for todays commonly used *in vitro* lipolysis methods. These include the protocols developed by Sek *et al.* [146] and by Zangenberg *et al.* [147, 148], which are also known as *Monash* and *Copenhagen* methods, respectively. Moreover, several additional methods were described in the literature, which present rather minor differences to those of Sek *et al.* and Zangenberg *et al.* [25, 33, 118, 127, 128, 149–152].
The underlying principle for lipolysis testing is generally the same [30]. In brief, an aliquot of formulation is dispersed in an aqueous buffer containing bile salts and phospholipids ("lipolysis medium"). After a short equilibration, the pancreatic enzymes are added to initiate digestion. The hydrolysis reaction generates fatty acids, which lower the medium pH and, to restore the original value, NaOH is added via an automated titration unit (Figure 2.3). This titration profile reveals the amount of liberated fatty acids, and hence, the extent of LBF digestion.

One major difference between the lipolysis method of Sek *et al.* [146] and of Zangenberg *et al.* [147, 148] is the strategy of calcium addition. Calcium ions remove fatty acids from the surface of oil droplets via precipitation of calcium soaps. This removal mimics the absorption of fatty acids *in vivo*, which would otherwise progressively inhibit the lipolytic enzymes [153, 154]. Sek *et al.* proposed the direct calcium addition [146], *i.e.*, calcium is already present in the lipolysis medium on digestion initiation. In contrast, with the method of Zangenberg *et al.*, calcium is continuously added during formulation lipolysis [147, 148]. The advantage of the first method is the proximity to physiological conditions, where lipolysis products are removed quite rapidly from the surface of oil

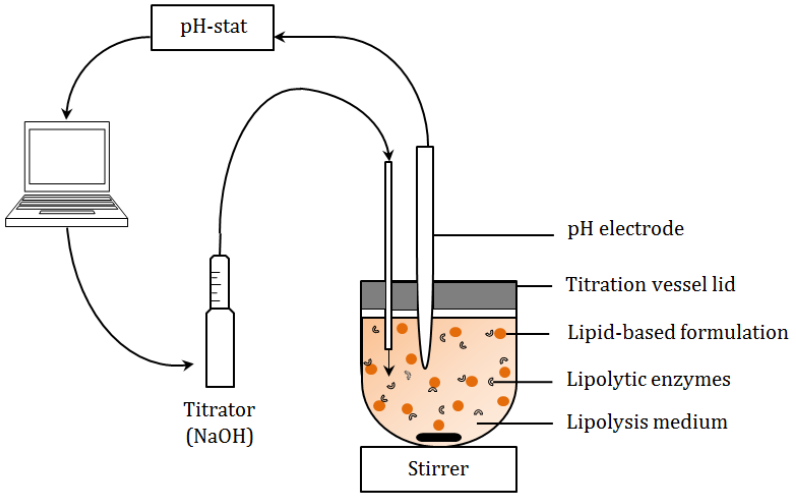

FIGURE 2.3: *In vitro* lipolysis model by Sek *et al.* [146].

droplets *in vivo*. The purpose of the continuous calcium addition is to directly control the lipolysis rate by taking advantage of the inhibitory effect of fatty acids on lipoyltic enzymes. This method allows the analysis of LBF digestion at a higher temporal resolution, but it may be rather critical for determining lipolysis-triggered drug precipitation. For such analysis, the physiological lipolysis rate is highly relevant, and thus, direct calcium addition might be more appropriate.

Other differences in experimental methods concern the composition of the digestion medium (pH, bile salts, phospholipids), the preparation of lipolytic enzymes, and the amount of digested formulation (Table 2.4). It is well-known that minor changes in experimental conditions can notably influence the kinetics of formulation digestion [26]. As a consequence, the cross-comparison of experimental results is often difficult. Much research effort has been directed to the standardization of testing protocols and this is also a major aim of the LFCS consortium [155], a collaborative project between industry and academia. Several studies were release by this consortium and a standardized method for *in vitro* lipolysis was recently proposed, as detailed in Table 2.4 [26–28].

2.4.2 Analytical tools for measuring lipolysis-triggered drug precipitation

One objective of *in vitro* lipolysis testing is to assess the drug solubilization capacity of a LBF during digestion. The drug concentration *versus* time profile is usually determined and this analysis is performed on a sampling regime. According to the state of the art methods of lipolysis testing, an aliquot of digest is removed at intervals and, after ultracentrifugation, the amount of solubilized and/or precipitated drug is measured by HPLC [26, 146, 147]. Ultracentrifugation is necessary for separating undigested oil from

TABLE 2.4: Currently most used *in vitro* lipolysis models [146, 147] and standard *in vitro* lipolysis model proposed by the LFCS consortium [26–28].

		Sek *et al.* [146]	Zangenberg *et al.* [147]	LFCS consortium [26–28]
Composition of digestion medium	Tris-maleate	50 mM	2 mM	2 mM
	NaCl	150 mM	150 mM	150 mM
	Ca^{2+}	5 mM	0.5 M (0.045-0.181 mmol/min)	1.4 mM
	Bile salts	5-20 mM (NaTDC)	5-30 mM Porcine bile extract	3 mM (NaTDC)
	Phospholipids	1.25 mM (Lecithin from egg yolk)	1.25 mM (Phosphatidylcholine from soja)	0.75 mM (Phosphatidylcholine from egg yolk)
	pH	7.5	6.5	6.5
Lipolytic enzymes	Source	Porcine pancreatin (8xUSP)	Porcine pancreatin (>3xUSP)	Porcine pancreatin (8xUSP)
	Preparation	1g pancreatin per 5ml digestion buffer, stirring, centrifugation (1600xg, 5°C, 15 min)	Pancreatin suspended in water (37°C), stirring, centrifugation (4000 rpm, 37°C, 7 min)	1g pancreatin per 5ml digestion buffer (5°C), stirring, centrifugation (2800xg, 5°C, 15 min)
Lipolysis test	Amount of LBF	1g per 40ml lipolysis medium	1.3–3g in 300ml lipolysis medium[a]	1g per 40ml lipolysis medium
	Final lipase activity	1000 TBU/ml[b]	800 USP/ml	1000 TBU/ml[b]
	Duration	30 min	60 min	30 to 60 min
	Sample processing	Ultracentrifugation (334,000xg, 37°C, 30 min)	Ultracentrifugation (540,000xg, 37°C, 30 min)	Ultracentrifugation (400,000xg, 37°C, 30 min) or bench-top centrifugation (21,000xg, 37°C, 30 min)[c]

[a] [33, 96, 156]
[b] Corresponding to 620 USP units/ml
[c] Ultracentrifugation is recommended for poorly digested, lipophilic formulations; bench-top centrifugation is recommended for extensively digested, hydrophilic formulations [26]

the aqueous bulk.
Such a sampling procedure implies the same experimental drawbacks as discussed for dispersion testing (Section 2.3.2.1). There is a considerable delay between sample removal and analysis, which can lead to further drug precipitation or to a solid-state conversion of the precipitate. This behavior was observed in recent studies, where ultracentrifugation was used as a separation technique to determine lipolysis-triggered drug precipitation. The concentration profiles of solubilized drug were rather biased due to ongoing drug precipitation, so that they reflected concentrations close to the equilibrium. The true kinetic concentrations were therefore barely measurable [31]. Nanofiltration was recently proposed as an alternative method to ultracentrifugation [31]. However, as previously discussed, care is needed when testing emulsions with comparatively large formulation droplets.
The LFCS consortium proposed bench-top centrifugation as an alternative separation technique. The higher sample throughput is a major advantage because it allows faster sample processing. Moreover, smaller sample volumes are required and the technique is more convenient in terms of availability and cost. Unfortunately, the separation of undigested oil was more difficult using bench-top centrifugation, so that the technique appeared more appropriate for hydrophilic formulations (*e.g.*, type IIIB and IV), which contain low amount of oil [26].
The use of *in situ* techniques is highly recommendable for detecting lipolysis-triggered drug precipitation, since both formulation lipolysis and drug precipitation are dynamic processes. The first in-line method for detecting drug precipitation during *in vitro* lipolysis was recently presented by Stillhart *et al.* [31]. Technical challenges were due to the complex and varying medium composition, the high turbidity, and the low concentration of analyte. Therefore, selection of appropriate instrumentation appeared to be essential. Raman spectroscopy was selected as analytical technique, as it provides high chemical specificity and the capacity to discern between different physical states. A large spot-size Raman probe was employed to reduce the effects of varying particle size and turbidity, while chemometrical procedures were applied to remove spectral information that was uncorrelated with the signal of the analyte. Hence, it was shown that *in situ* analysis of lipolysis-triggered drug precipitation is basically possible, but it requires advanced analytical techniques and chemometrical procedures to increase the accuracy of the method.

In vitro lipolysis testing has recently been combined with the solid-state characterization of precipitated drug using X-ray powder diffraction (XRPD) [23, 28, 31, 33, 34]. The pellet phase obtained from lipolysis of drug-loaded formulation was directly analyzed after ultracentrifugation. As a reference, the same analysis was performed with the pellet phase obtained from lipolysis of drug-free formulation that was spiked with an equal

amount of pure drug (as used for formulation preparation).
For an amorphous precipitate, the influence of drug precipitation on drug absorption is expected to be minimal, as it may rapidly re-dissolve in the aqueous fluids. This solubility advantage can be proved via a so-called *re-dissolution* experiment [33, 34]. To this end, the pellet phase obtained from drug-loaded formulation is isolated and immersed in a USP 2 paddle dissolution apparatus containing simulated intestinal medium. The concentration of solubilized drug is then measured at intervals, analogous to compendial dissolution testing. As a reference, the experiment is repeated with the pellet phase obtained from drug-free formulation spiked with crystalline drug.

2.4.3 Analytical tools for monitoring the extent of hydrolysis and structural changes during formulation digestion

In vitro lipolysis is not only of interest for assessing lipolysis-triggered drug precipitation. An important aspect is to learn about the susceptibility of LBFs toward digestion and structural changes occurring on formulation digestion. This knowledge is essential for a rational development of formulations. This section focuses on the analytical techniques for quantification of lipolysis products as well as on biophysical tools for the analysis of colloidal structures evolving during formulation digestion.
During *in vitro* lipolysis, the extent of formulation digestion is usually assessed via the direct titration of fatty acids and the so-called *back-titration* procedure to correct for the amount of unionized fatty acids [157, 158]. For standard formulation characterization, this procedure is generally adequate. However, for a differentiated analysis of lipolysis products, more specific analytical techniques are required. High-performance thin-layer chromatography (HPTLC) has been frequently used for this purpose [118, 146, 151, 159, 160]. Due to the lack of chromophoric groups, lipids and lipolytic products are indeed hardly detectable via traditional analytical methods. A more simple and accessible method was recently proposed by Lee *et al.*, who used HPLC with refractive index detection to quantify lipids and lipid digestion products in gastrointestinal aspirates [161]. Other quantification techniques for lipolysis products include flame ionization detection [162] and gas chromatography [163].
The structure of colloidal phases formed with intermediate digestion products has been intensively explored using microscopy techniques [101, 145, 164–168]. Standard light microscopy provided very first images of fat digestion and revealed a lamellar liquid crystalline and a viscous isotropic phase at the surface of oil droplets [145]. Later, the availability of advanced microscopical techniques significantly improved the quality of images in terms of contrast and resolution. Rigler *et al.* used freeze fracture electron microscopy to identify multilamellar and vesicular lipolytic products in the range of 20

nm as intermediate phases of fat digestion [164]. More recent studies were performed using cryogenic transmission electron microscopy (Cryo-TEM) [101, 165–168]. The advantage of Cryo-TEM is that samples are not fixed on a sample grid, and hence, artifacts induced by staining are generally avoided. These studies provided key insights into the transient structures occurring on formulation digestion such as micelles, sperical and elongated unilamellar vesicles. Atomic force microscopy (AFM) provides information about the surface topology of lipidic structures. It requires no sample processing and was most recently applied to characterize colloidal structures in human intestinal fluids *ex vivo* [166]. In this study, the combination of Cryo-TEM and AFM demonstrated the presence of unilamellar vesicles, oil droplets, and facetted vesicles in the aqueous micellar phase.

Although key structural information was obtained, these microscopical techniques failed in reproducing the highly dynamic process of formulation digestion with appropriate temporal resolution. Day *et al.* pioneered in using multiplex coherent anti-Stokes Raman scattering (CARS) microscopy to investigate lipid digestion in real-time [169]. CARS is a non-invasive technique that allows *in situ* imaging with submicrometer resolution and millimolar sensitivity. It provided information about the local chemical composition and the phase behavior inside the oil droplets, without the need to label molecules. The spatial resolution of CARS is around 0.3 to 1 μm. This resolution was too low for imaging drug molecules within colloidal structures, but it was shown to be adequate for monitoring drug partitioning from the excipient into the lipolytic products [169].

Light scattering techniques have also become increasingly important for studying transient liquid crystalline structures formed during LBF digestion. Fatouros *et al.* pioneered the use of small-angle X-ray scattering (SAXS) in the field of pharmaceutical lipid-based drug carriers [156]. This off-line method was able to detect the nano-scale architecture of colloids formed during LBF digestion with excellent spatial resolution. However, real-time structural data were not accessible, and for this reason, Warren *et al.* presented the application of synchrotron SAXS [32]. In this study, the time evolution of liquid crystalline nanostructures during LBF digestion was monitored. This technique is certainly less convenient in terms of cost and availability, but it provides clear advantages over benchtop SAXS source. It allowed the analysis of weakly scattering materials due to the high-intensity light source ($\sim$1000 times more intense than benchtop SAXS [170]) and was shown to be well suited for studying real-time processes in a high-throughput manner [32, 168].

Recently, another new analytical method has been introduced to study LBFs, *i.e.*, diffusing wave spectroscopy (DWS) [171, 172]. DWS is an optical technique that is derived from DLS. It provides key information about the viscoelastic properties of supramolecular structures in a continuous phase. These properties are derived from the dynamics of scattered light, but, while DLS is restricted to systems in which light is scattered

once, DWS is applied to systems that exhibit multiple light scattering. The technique is therefore particularly appropriate for the examination of highly turbid systems and has found application in the field of LBF digestion. Marze *et al.* recently resolved the structural transition from a droplet to vesicles and then to micelles during lipid digestion [172].
Finally, NMR and EPR spectroscopy have also been implemented in the analysis of LBF digestion. NMR is particularly appropriate for following phase transfer of molecules [172, 173] and, similarly, EPR spectroscopy provided a deeper understanding of the interaction between drug and lipids during formulation lipolysis [117, 118].

2.5 Current challenges in *in vitro* LBF testing

The possibility to perform predictive *in vitro* tests is a prerequisite for rational development of drug delivery systems. For this purpose, several studies analyzed the *in vitro–in vivo* correlation of LBF performance. In some cases, it was possible to predict the rank order of formulations based on *in vitro* dispersion and digestion testing [19–23, 29, 52, 174–176]. In other studies, however, no correlation was evident at all [24, 25]. These findings suggested that *in vitro* conditions should be optimized to better simulate formulation performance *in vivo*. Critical parameters of current *in vitro* dispersion and lipolysis assays are discussed in the present section.

Conventional dispersion and lipolysis assays are usually one-compartmental tests. This experimental setup is, however, often problematic when testing formulations with poorly water-soluble compounds. Drug solubility in the testing medium is generally low and, in the absence of an absorptive sink, the degrees of supersaturation can be notably higher than *in vivo*.
Some advanced strategies for generating an absorptive sink have been described in the literature. Shi *et al.* developed a biphasic system for dispersion testing, which consisted of an aqueous buffer and octanol as organic acceptor phase [50]. The LBF was loaded into a flow cell (USP 4) and the aqueous medium was circulated between the USP 2 vessel and the flow cell as seen in Figure 2.4. dispersion was measured in the acceptor compartment, and interestingly, a good correlation was obtained with *in vivo* pharmacokinetic data. Such an approach should certainly be further considered and validated with more LBFs. It would be advantageous to use biorelevant media instead of a simple aqueous buffer, to include the influence of bile salts on emulsification and drug solubilization. However, the presence of surface-active compounds may increase the solubility of the organic phase in the aqueous bulk, which could also be a major drawback for bi-phasic assays with *in vitro* lipolysis.

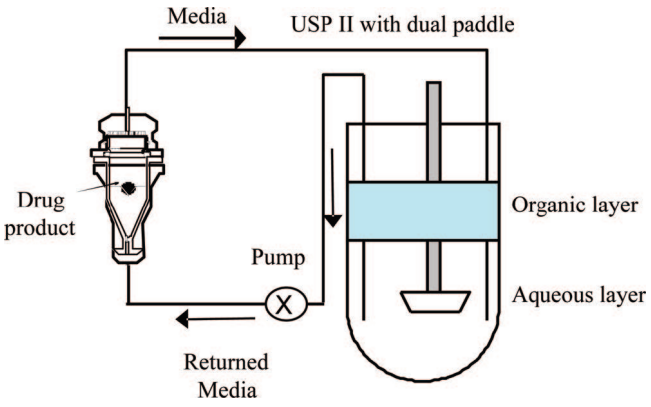

FIGURE 2.4: Schematic representation of the biphasic dissolution test developed by Shi *et al.* [50]. The aqueous layer was a simple aqueous buffer and the organic layer consisted of octanol.

Kataoka *et al.* provided an absorptive sink via an alternative approach. A two-compartment system was established consisting of an apical and a basal chamber separated by a Caco-2 cell membrane [51]. The LBF was dispersed in the apical chamber (without lipolytic enzymes) and drug absorption was then measured in the basal compartment. The use of a biological membrane is highly valuable from a biopharmaceutical perspective because it provides the most physiological simulation of drug absorption. This is particularly relevant when studying lipidic excipients, which are known to affect drug permeability, for example via the inhibition of P-gp transporters [12, 13, 177–180]. Unfortunately, this assay revealed only a limited correlation with *in vivo* drug absorption data [51]. The low surface-to-volume ratio could be critical in this regard, as the area for absorption *in vitro* is much smaller than *in vivo*. Hence, this method is less suitable to generate a realistically high absorptive sink.

The establishment of two-compartmental tests with *in vitro* lipolysis is expected to be even more challenging, due to cell toxicity caused by lipidic excipients and pancreatic enzymes [86, 181]. Dahan and Hoffmann proposed *in vitro* lipolysis with consecutive drug permeability studies using an intestinal epithelium (*ex vivo* from rats) [19]. This is an interesting approach for studying the impact of formulation lipolysis on the intestinal drug permeability. However, the processes of lipolysis and drug absorption do not occur simultaneously in this assay, which limits its biopharmaceutical relevance.

A very new approach for biopharmaceutical characterization of LBFs was most recently presented by Fei *et al.* [37]. In this study, self-microemulsifying drug delivery systems were tested using the *in vitro* dispersion test (without digestive enzymes) and, based on these data, an *in vitro–in silico–in vivo* approach was followed to study formulation performance upon oral administration. The process of drug absorption was, hence, included via a computational simulation. This approach provided a remarkably accurate prediction of drug concentration profiles in human plasma. The combination of *in vitro*

data with simulations *in silico* appears to be a very promising approach for studying biopharmaceutical processes that can be hardly simulated with *in vitro* tools only.

Beyond the lack of an absorptive sink, there are other factors, which may limit the predictability of formulation performance *in vivo*.
Current *in vitro* lipolysis assays simulate only intestinal formulation digestion. However, it was estimated that the human gastric lipase performs ∼25% of GI lipolysis [143, 182]. Although this contribution is comparatively low, it could be relevant for certain formulations, *e.g.*, for LBFs with acidic drugs. An *in vitro* lipolysis assay simulating both, gastric and intestinal lipolysis has been proposed by Fernandez *et al.* [183], but its biopharmaceutical relevance still needs to be confirmed.
Another difference to *in vivo* performance is the fate of lipolysis products during *in vitro* digestion. During GI transit, fatty acids and monoglycerides are solubilized in the aqueous bulk and form mixed micellar or vesicular structures before being absorbed [14]. In contrast, during *in vitro* lipolysis, fatty acids are rapidly removed from solution via the precipitation of calcium soaps, whereas the concentration of monoglycerides is progressively increasing due to the absence of an absorptive sink. The kinetic concentrations and resulting phase behavior of lipolysis products is therefore considerably different, which may directly affect the drug solubilization capacity. The formation of insoluble calcium soaps reduces the ability of fatty acids to solubilize drug in mixed micellar structures and vesicles [184], while the accumulation of monoglycerides may increase the drug solubility. Hence, biopharmaceutical assays including an absorptive sink would also provide the advantage of simulating the removal of lipolysis products.
An accurate prediction of *in vivo* bioavailability should also include post-absorptive processes. For example, it has been shown that lymphatic drug transport is lower with medium-chain lipids than with long-chain lipids. Hence, a drug that is extensively metabolized in the liver may rather profit from long-chain LBFs, than from medium-chain lipids [25, 185]. Similarly, saturation or inhibition of intestinal metabolic enzymes or transporters by drug or excipients could affect the extent of drug absorption [12, 13, 23, 177–180].
Finally, particular attention must be directed to the selection of the animal model for studying *in vitro–in vivo* correlations. The physiology of the GI tract can be substantially different among animal species [186, 187]. Particularly relevant are differences in lipolytic activity of digestive enzymes [188] and in the composition of GI fluids. For example, rats have a continuous bile secretion into the intestine, irrespective of the nutritional state [189]. This difference can notably influence the self-emulsification behavior of LBFs and the drug solubilization in GI fluids [52].

Chapter 3

Study of drug supersaturation for rational early formulation screening of surfactant/co-solvent drug delivery systems

Summary

The objective of this study was to advance *in vitro* screening of surfactant/co-solvent formulations in early development by considering drug supersaturation and the mechanism of solubilization upon aqueous dilution. Two surfactant/co-solvent model systems were studied at practically relevant aqueous dilution ratios. Precipitation of the model drug fenofibrate was characterized by focused beam reflectance measurement, X-ray diffraction, and Raman spectroscopy. We calculated drug supersaturation in diluted systems and introduced a theoretical model to study the role of excipient interaction in the process of drug solubilization. Finally, vehicle phase changes upon dilution were examined using dynamic light scattering and ultrasound analysis.

Phase changes occurred at low dilution levels, while more extensive dilution barely led to further structural changes. In undiluted formulations, ethanol-surfactant domains were responsible for fenofibrate solubilization. In dispersed formulations, however, the co-solvent partitioned out of the surfactant microstructure, leading to drug solubilization by independent micellization and co-solvency. This loss of excipient interaction caused formulation-specific supersaturation, which was indicative for the risk of drug

Stillhart C. *et al.* Study of drug supersaturation for rational early formulation screening of surfactant/co-solvent drug delivery systems. *Journal of Pharmacy and Pharmacology*, **2012**, 65, 181–192.

precipitation. Experimental protocols of *in vitro* formulation screening should include both low and high dilution levels of physiological relevance. The study of excipient interaction and estimation of supersaturation allows the identification of formulations that are prone to drug precipitation.

3.1 Introduction

Drug solubilization in the gastrointestinal tract is of pivotal importance for adequate oral bioavailability. This is a particular challenge for poorly water-soluble drugs that often exhibit incomplete or variable drug absorption. Lipid-based formulations, such as oil solutions or self-(micro)-emulsifying drug delivery systems (S(M)EDDS), can overcome this limiting step by keeping the drug in solubilized form *in vivo* [9, 190]. Moreover, these formulations often protect the drug against chemical and enzymatic degradation in an aqueous environment and may circumvent hepatic first-pass metabolism by enhancing lymphatic drug transport [191, 192].

SEDDS are complex mixtures, comprising up to five excipients (triglyceride oils, mixed glycerides, lipophilic surfactants, hydrophilic surfactants, and water-soluble co-solvents). The addition of small amounts of water to SEDDS leads to the swelling of inverse micelles. Larger amounts of water cause the formation of water-in-oil emulsions and, if water and formulation are present in similar amounts, the systems may become bicontinuous. Finally, at high dilution levels, oil-in-water dispersions are generated [10]. During these phase changes, a compound that is solubilized in the SEDDS will migrate into oil-rich or water-rich domains, depending on its physicochemical properties (*e.g.*, log$P$). This migration, in turn, presents an enhanced risk of drug precipitation [10]. Drug precipitation in the crystalline form is particularly critical, since re-dissolution of drug crystals is often rather slow, resulting in incomplete drug absorption *in vivo*.

It is therefore important to study formulation behavior upon aqueous dilution to anticipate the fate of a lipid-based system in the gastrointestinal lumen. Dilution tests, comprising one to three dilution ratios in an aqueous medium, are a typical industrial screening tool for early formulation development. This simple testing procedure gives a first indication of whether the formulation is able to keep the drug solubilized in aqueous dispersions. However, profound knowledge of the formulation changes occurring upon aqueous dilution may minimize this experimental work and rationalize the development of new lipid-based formulations.

Several approaches have been adopted in recent years to gain a better insight into the dispersion process of lipid-based formulations. Phase changes in these systems are often hardly detectable by the naked eye, so that sophisticated physical methods are needed for

improved structural analysis. Several techniques have been used, such as small-angle X-ray scattering (SAXS), small-angle neutron scattering (SANS), dynamic laser light scattering (DLS), nuclear magnetic resonance (NMR), time-resolved fluorescence quenching (TRFQ), conductance, viscosimetry, and ultrasonic velocimetry [90, 94, 95, 193]. Recently, electron paramagnetic resonance (EPR) spectroscopy was successfully adopted to study microstructural changes of dispersed SMEDDS [87, 117]. Other groups employed analytical ultrasound techniques to characterize phase changes in SEDDS [194, 195]. Mohsin *et al.* investigated precipitation of fenofibrate following the dispersion of lipid-based formulations (Pouton type I–IV systems) in water [48]. The authors reported that the drug precipitated mostly from formulations with a high content of hydrophilic excipients. Such systems are particularly interesting for studying structural changes upon aqueous dilution and the effect on drug solubilization.

This study focuses on Pouton type IV systems, which are typically mixtures of a hydrophilic surfactant and co-solvent and do not contain any oil [10]. Such formulations can lead to high supersaturation upon dilution, which is accompanied by a risk of drug precipitation [38, 71]. However, there is still a lack of reliable techniques to predict the risk of drug precipitation for a given lipid-based formulation. An improved understanding is needed of how phase changes during dispersion affect drug solubilization and supersaturation.

The aim of this work was to study how drug supersaturation and precipitation can result from aqueous dilution of Pouton type IV systems. Specifically, we aimed to gain a better understanding of the dispersion process to provide a rationale for the selection of dilution levels in early formulation screening. We studied the features of aqueous dispersions obtained from two hydrophilic surfactant systems with ethanol as co-solvent and fenofibrate as the model drug. To describe excipient effects on drug solubilization in the undiluted and the diluted state, we employed a theoretical concept termed *non-interacting model*, which assumed a drug to be independently solubilized by the surfactant and the co-solvent. Moreover, theoretical supersaturation as a function of the dilution level was estimated for both systems.

3.2 Materials and methods

3.2.1 Materials

Polysorbate 80 was purchased from Hänseler AG (Herisau, Switzerland), Cremophor® RH 40 from BASF AG (Ludwigshafen, Germany), and ethanol from Baker (Deventer,

Netherlands). Fenofibrate (2-[4-(4- chlorobenzoyl)phenoxy]-2-methylpropanoic acid isopropyl ester; ⩾99%) was obtained from Sigma-Aldrich Chemie GmbH (Buchs, Switzerland).

3.2.2 Preparation of formulations

Two different Pouton type IV formulations were used for this study: one was composed of Cremophor RH 40 and ethanol (1:1 w/w, cremophor system), and the other consisted of polysorbate 80 and ethanol (1:1 w/w, polysorbate system). Cremophor RH 40 was melted on a heating plate (40°C) and, while cooling down to room temperature, ethanol was added. The polysorbate system was prepared by directly adding ethanol to the surfactant. Excipients were mixed on a magnetic stirrer until a homogeneous, clear solution was obtained.

The poorly water-soluble fenofibrate ($\log P$ 5.24 [196]) was selected as model drug. Drug formulations were prepared by loading the cremophor system and polysorbate system with fenofibrate at a concentration corresponding to 80% of drug solubility. The formulations were stirred until a clear solution was obtained.

To determine fenofibrate solubility in the formulations, we mixed the systems with an excess of fenofibrate on a magnetic stirrer (500 rpm) for 24 h in hermetically sealed glass vials at 37°C. The suspensions were then filtered through a 0.45-μm polytetrafluoroethylene (PTFE) membrane to remove the excessive solid drug, and the concentrations were determined by UV spectrometry. We used a SpectraMax M2 microplate photometer (Molecular Devices, Sunnyvale, CA, USA) to measure the absorbance at 286 nm. Solubility measurements were performed in four replicates.

3.2.3 Dilution behavior of fenofibrate formulations and drug-free formulations

Cremophor formulation and polysorbate formulation with and without fenofibrate were dispersed in demineralized water at six dilution ratios (1:1, 1:2, 1:5, 1:10, 1:20, 1:50, and 1:100 w/w) at 37°C. These ratios were expressed as dilution factors and labelled as 1, 2, 5, 10, 20, 50, and 100, respectively. The low dilutions (*i.e.*, dilution factors 1–20) were included because the main structural changes were expected to occur in this concentration range. Higher levels of dilution (*i.e.*, dilution factors 50 and 100) were included in this study because of their physiological relevance.

We first compared the dispersion behavior of systems containing fenofibrate and drug-free systems visually and then by means of focused beam reflectance measurement

(FBRM). When precipitation occurred, we analyzed the solid phase using X-ray powder diffraction (XRPD) and Raman spectroscopy.

3.2.3.1 Focused beam reflectance measurement

A Lasentec FBRM D600L probe (Lasentec, Redmond, WA, USA) was used to detect precipitation of drug particles after formulation dispersion (dilution factors 1, 2, 5, 10, 20, 50, and 100). The probe was positioned at an angle of 30° in a thermostated glass vessel (37°C) and the dispersion was stirred at 500 rpm. Measurements were recorded every 2 s for 5 min using the iC FBRM software version 4.0 (Mettler-Toledo AutoChem, Columbia, MD, USA). The formulations were dispersed and measured in triplicate.

3.2.3.2 X-ray diffraction

Dispersions that contained solid structures were filtered after 30 min of dispersion, and an X-ray diffraction pattern was immediately recorded using a theta-theta X-ray powder diffractometer (R-XRD Phaser D2; Bruker AXS GmbH, Karlsruhe, Germany) equipped with a Co and Cu KFL tube (30 kV, 10 mA) as radiation source and a Lynxeye® detector. The single sample was scanned in the angular range of 5° (2θ) to 40 (2θ) with a step size of 0.1° (2θ) and a count time of 5 s per step. The result was compared with the reference diffraction pattern of pure fenofibrate.

3.2.3.3 Raman spectroscopy

We prepared the samples for Raman spectroscopy analogously to those for the X-ray analysis. Thus, following a 30-min dispersion period, the samples containing precipitated drug were filtered and a Raman spectrum of the solid material was recorded. As a reference, we acquired the spectrum of pure, crystalline fenofibrate as used for the formulation preparation.

We used a Raman RXN1 analyzer (Kaiser Optical Systems, Inc., Ann Arbor, MI, USA) in the backscattering mode, equipped with a charge-coupled device (CCD) camera and a diode laser operating at a wavelength of 785 nm. The spectra were recorded with a laser power of 400 mW and background Rayleigh scattering was removed by a holographic filter during spectra acquisition. We used a multi-fibre P^{h}AT probe having a non-contact sampling device with a laser spot diameter of 6 mm. Scattered radiation was collected by an array of 50 optical fibers and was transmitted to the CCD detector. The sample was positioned in a sample holder consisting of a black metal block to shield the samples from external light. Spectra were collected at a resolution of 4 cm^{-1} and an acquisition

time of 500 ms using the iC Raman Instrument software (Version 3.0; Mettler-Toledo AutoChem Inc., Columbia, MD, USA).

3.2.4 Determination of theoretical supersaturation

The difference in chemical potential $\Delta\mu$ of a supersaturated solution (μ) and a thermodynamically stable, saturated solution (μ_{eq}) is the driving force for drug precipitation. Assuming that the activity coefficients of a solute in the saturated and supersaturated state are the same, the relationship between the difference in chemical potential and supersaturation can be described by the equation $\Delta\mu = \mu - \mu_{eq} = kT\ln(S)$, where k is the Boltzmann constant, T the temperature, and S the supersaturation ratio [197]. We calculated S as a measure of the difference in chemical potential, $\Delta\mu$, present in the aqueous dispersions. We determined a theoretical value, S_{theor}, in the formulations dispersed at a given ratio according to $S_{theor} = C_{theor}/C_{eq,meas}$, where C_{theor} is the calculated concentration of fenofibrate resulting after dispersion of the formulation (containing fenofibrate at 80% of its solubility, *i.e.*, S_{theor} of 0.8 for the undiluted formulation) and $C_{eq,meas}$ is the equilibrium solubility of the drug in a given aqueous dispersion. To measure $C_{eq,meas}$, the placebo cremophor system and polysorbate system were dispersed in demineralized water at dilution factors of 1, 2, 5, 10, 20, 50, and 100, and an excess amount of fenofibrate was added to the mixtures. Samples were left to stir on a magnetic stirrer at 500 rpm for 24 h in a water bath at 37°C using hermetically sealed glass vials. The suspensions were then filtered through a 0.45-μm PTFE membrane to separate the excess of solid drug, and the concentration was determined in the samples by UV spectrometry at 286 nm (n=4, freshly prepared analysis samples per dilution level). To calculate S_{theor}, we used the mean value of $C_{eq,meas}$ (n=4 at each dilution factor).

3.2.5 Determination of drug solubility in dispersed excipients and data modeling

We measured fenofibrate solubility in the pure, as well as diluted, excipients (polysorbate 80, Cremophor RH 40, and ethanol) corresponding to a dilution factor of 1, 2, 5, 10, 20, 50, and 100. Fenofibrate solubility in the diluted surfactant or co-solvent was labelled as $C_{eq,surf}$ or $C_{eq,co}$, respectively. Thus, the individual excipients were dispersed in demineralized water, and an excess amount of fenofibrate was added to the mixtures. Samples were left to stir on a magnetic stirrer at 500 rpm for 24 h in a water bath at 37°C using hermetically sealed glass vials. We measured drug solubility at the highest and lowest excipient concentration after 24, 48, and 72 h of equilibration (analytical

bracketing). Since after 24 h the equilibrium was reached in these solubility experiments, this time was selected for all other solubility tests. The same procedure was pursued for solubility measurement in undiluted excipients. The suspensions were then filtered through a 0.45-μm PTFE membrane to separate the excess of solid drug, and the concentrations ($C_{eq,surf}$ and $C_{eq,co}$) were determined by UV spectrometry (286 nm). All solubility values were determined in four replicates.

Fenofibrate solubility was then modeled as a function of the excipient concentration. The calculations were based on a linear regression for the surfactants (cremophor and polysorbate), while a log-linear regression was employed for the co-solvent (ethanol). We used the software Statgraphics Centurion XV Professional (StatPoint Technologies Inc., Warrenton, VA, USA) and determined the R^2 and p-values for each model fit. The model p-value demonstrated whether the relationship between the two variables was significant at a 95.0% confidence level. Based on drug solubility in the pure excipients, $C_{eq,surf}$ and $C_{eq,co}$, we calculated the theoretically expected fenofibrate solubility, $C_{eq,model}$, in the undiluted and diluted formulations, assuming that the excipients were not interacting. Finally, the calculated values were compared with the experimental solubility values, $C_{eq,meas}$, measured in the dispersed formulations, as depicted in Figure 3.1.

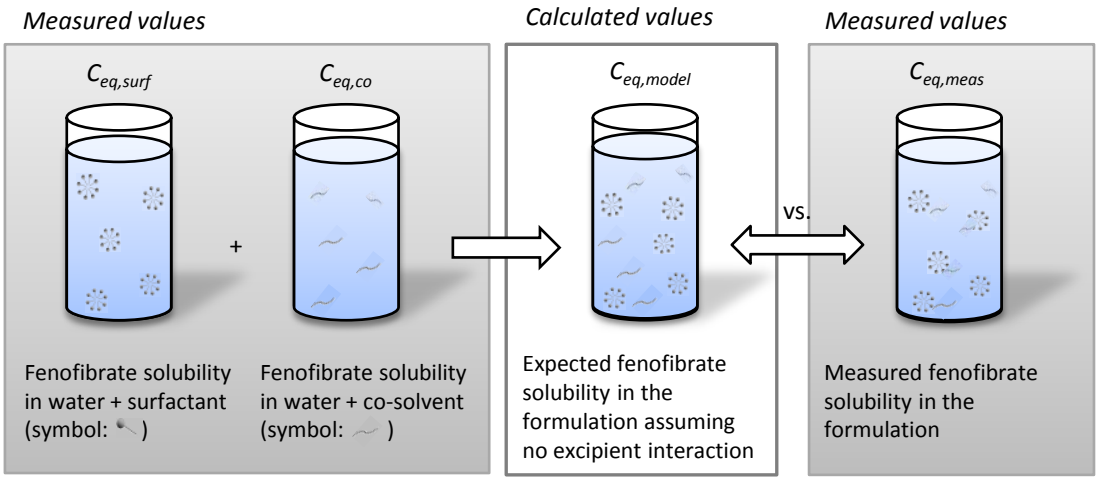

FIGURE 3.1: Illustration of the *non-interacting model* of drug solubilization.

3.2.6 Physical characterization of placebo dispersions

3.2.6.1 Dynamic laser light scattering

Particle size of dispersed placebo cremophor systems and polysorbate systems was measured by means of DLS at 37°C. We dispersed the formulations in demineralized water

(dilution factors of 1, 2, 5, 10, 20, 50, and 100) and measured particle size using a Zetasizer Nano ZS (Malvern Instruments Ltd, Malvern, UK) equipped with a 4 mW He-Ne laser operating at a wavelength of 633 nm. The scattering signal was detected at an angle of 173°, and each sample was measured for 10 min. The Dispersion Technology Software DTS 5.0 (Malvern Instruments Ltd, Malvern, UK) was used to calculate the mean hydrodynamic particle diameter, expressed as z-average (nm), and the polydispersity index (PDI). The formulations were dispersed and measured in triplicate.

3.2.6.2 Ultrasonic resonator technology

Ultrasound velocity, U (m/s), was measured using a ResoScan® system (TF Instruments Inc., Monmouth Junction, NJ, USA). The instrument was equipped with two identical parallel resonator cells (sample volume 200 μl) having a path length of 7.0 mm (ground wave $\lambda = 14$ mm) with a fundamental frequency of approximately 10 MHz. Since the ultrasound velocity is strongly temperature dependent, a thermostat controlled with a Peltier element ensured a highly stable temperature in the resonator cavities (resolution 1 mK, stability ±5 mK). Ultrasound velocity was measured in the range 1100–1900 m/s.

The relative value of ultrasound speed, U (*i.e.*, $U_{cell\ 2} - U_{cell\ 1}$), was considered for analysis. Thus, we measured the difference of ultrasound velocity, ΔU, between water (filled in cell 1) and the samples at the defined dilution factors of 1, 2, 5, 10, 20, 50, and 100 (filled in cell 2) at 37°C. ΔU was measured every 10 s for 5 min, and the mean value was determined subsequently. The dispersions were freshly prepared in triplicate for the analysis.

Finally, we used an Olympus BX 61 polarized light microscope (Olympus Corp., Tokyo, Japan) to confirm the presence of birefringent structures in the samples at dilution factor 1.

3.2.6.3 Density measurement

The density of the diluted systems was determined using a DA-110 M density meter from Mettler-Toledo GmbH (Greifensee, Switzerland), which was equipped with a Peltier thermostat for temperature control. We measured the density of samples (1 ml) at the defined dilution factors of 1, 2, 5, 10, 20, 50, and 100 at 37°C. Three replicates were measured and the mean value and standard deviation were calculated for each dilution factor.

3.2.7 Statistical methods

The effects of dilution on the onset time of precipitation (induction time, t_{ind}) were evaluated using the Friedman's test. The induction time was arbitrarily defined as the time when the counts of particles with a chord length below 10 μm exceeded 50, because this FBRM signal was above the range of instrumental noise. The Kruskal–Wallis test was performed to analyze the effects of dilution on the PDI and ΔU values, respectively. A significance level of 95.0% ($p<0.05$) was selected in all cases. We used the software Statgraphics Centurion XV Professional for all statistical data treatments. Error bars in graphical plots represented standard deviations in all cases.

3.3 Results

3.3.1 Macroscopic dilution behavior

We studied the dilution of two Pouton type IV model formulations. One consisted of equal amounts (w/w) of Cremophor RH 40 and ethanol (cremophor system), while the other contained polysorbate 80 and ethanol at the same mixing ratio (polysorbate system). At 37°C, fenofibrate solubility was 14.56 ± 1.87 mg/ml and 105.96 ± 0.82 mg/ml in the cremophor and polysorbate systems, respectively.
The drug-free (placebo) formulations appeared both as homogeneous and transparent mixtures that remained clear even following dispersion in water (Figure 3.2a and 3.2c). The undiluted fenofibrate formulations were also clear mixtures, but differences were observed upon aqueous dispersion. Dilution of the polysorbate system containing fenofibrate resulted in considerable turbidity within a few seconds, but this did not occur with the cremophor system (Figure 3.2b and 3.2d).

3.3.2 Characterization of precipitation

Appearance of particles after aqueous dispersion of the fenofibrate and placebo formulations was monitored by FBRM. This technique consisted of an in-process probe, which detected the chord length distribution of particles. This laser scanning technique has been used before to characterize drug precipitation [75] and the general measurement principle was described by Ruf *et al.* [138].
No FBRM signal was detected upon dispersion of the cremophor system (fenofibrate and placebo) and placebo polysorbate system. In contrast, the polysorbate system containing fenofibrate led to increasing particle counts at different levels of dilution. To

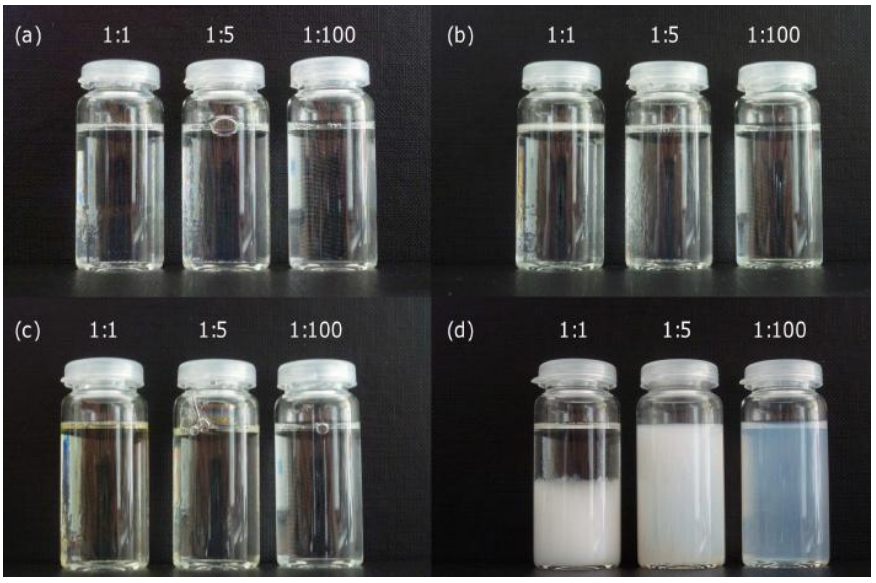

FIGURE 3.2: Macroscopic dilution behavior of the placebo cremophor system (a), verum cremophor system (b), placebo polysorbate system (c), and verum polysorbate system (d) in water. Verum systems contained fenofibrate at 80% of its solubility in the formulation. All diluted systems were clear except the verum polysorbate formulation (d), which exhibited pronounced drug precipitation.

follow the number of evolving particles over time, we selected only counts with a chord length of less than 10 μm, which minimized the noise from those counts resulting from aggregated particles (Figure 3.3). However, it should be noted that the detection is

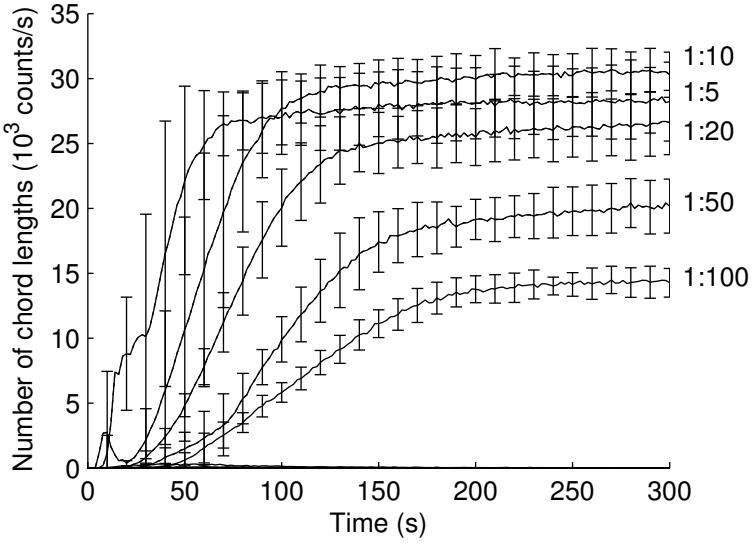

FIGURE 3.3: Particles counts (chord length $< 10\mu$m) upon dilution of the verum polysorbate system by using FBRM. The level of dilution is referred on the right side ($n = 3$ for each level of dilution).

limited to particles with a chord length of more than 1 μm. The lowest dilution ratios

(1:1 and 1:2 w/w) could not be measured since the large amount of particles hampered the homogeneous mixing of the sample. The dilutions of 1:5 and 1:10 displayed a sharp initial increase of counts, while a less pronounced increase was noted for more diluted samples. From Figure 3.3 we can infer that the initial count rate seemed to be indirectly proportional to the onset of particle counts. The Friedman's test proved that the induction time was significantly different for the more diluted systems ($p = 0.027$), spanning a rather narrow range from a few seconds to nearly a minute.

We further studied the solid-state properties of the formed particles. Figure 3.4 displays the X-ray diffractograms and Raman spectra of the precipitated material and of crystalline fenofibrate as used in the formulation. From the obtained patterns it could be clearly observed that the solid-state form of the precipitate corresponded to that of crystalline fenofibrate.

It was remarkable that only the polysorbate-containing formulation exhibited drug precipitation when water was added, even though both model systems had the same initial drug saturation ratio of 0.8 before aqueous dilution.

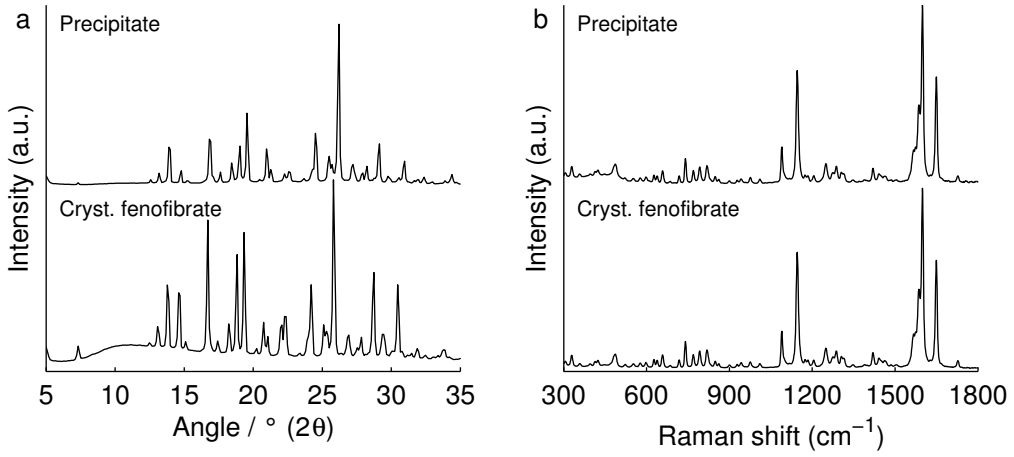

FIGURE 3.4: X-ray diffraction pattern (a) and Raman spectra (b) of the precipitate and the crystalline fenofibrate as used for formulation preparation.

3.3.3 Calculation of the theoretical supersaturation, S_{theor}

FBRM indicated that the polysorbate system went through an initial supersaturated state, which lasted for only a short time. To determine the initial supersaturation in dispersed systems, we used the value C_{theor} calculated based on the amount of fenofibrate added to the water for each dilution ratio. Figure 3.5 depicts the values of S_{theor} of the two systems as a function of the dilution ratio. The dispersed cremophor system reached a supersaturation of about 2. In contrast, supersaturation in the polysorbate system was

about 10-fold higher than in the cremophor system, reaching a ratio of more than 20. Interestingly, the polysorbate system displayed a lower supersaturation level at dilution factor 1 and reached a peak at dilution factor 2. Supersaturation in the cremophor system, however, was almost constant over all dilution levels.

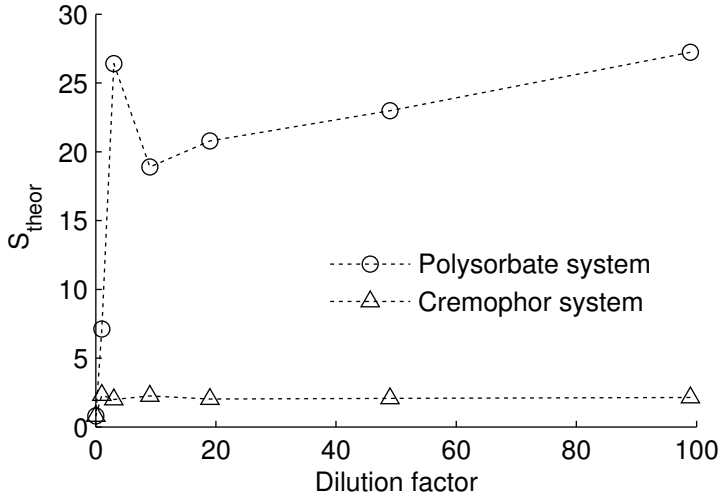

FIGURE 3.5: Theoretical fenofibrate supersaturation (S_{theor}) in the cremophor system and polysorbate system at different dilution ratios.

3.3.4 Fenofibrate solubilization in excipients and formulations

We analyzed the solubility of fenofibrate in the pure excipients (ethanol, Cremophor RH 40, and polysorbate 80) to compare these values with fenofibrate solubility in the cremophor system and polysorbate system.

Figure 3.6 depicts the solubility of fenofibrate in undiluted and diluted co-solvent (ethanol) as a function of ethanol concentration. In line with theoretical expectations [198], we found a log-linear relationship between fenofibrate solubility in the co-solvent, $C_{eq,co}$, and the co-solvent concentration, C_{co} ($R^2 = 0.978$; $p<0.0001$) according to:

$$\log C_{eq,co} = \log C_{eq,w} + \sigma' \cdot C_{co} \tag{3.1}$$

where σ' is the co-solvent solubilization power. We labeled this parameter differently from Yalkowsky *et al.* [198], since the constant σ' was obtained from co-solvent concentrations in units of % w/w. The intercept provided a calculated aqueous solubility ($C_{eq,w}$) of 0.011 mM, which agreed well with the experimental value (0.010 ± 0.003 mM). Subsequently, we determined the surfactant-mediated solubility, $C_{eq,surf}$, at different dilution levels. The relationship between the surfactant concentration, C_{surf}, and the drug solubility, $C_{eq,surf}$, was in good agreement with the expected linearity. In theory,

micelle-mediated solubility is a linear function of the surfactant concentration minus the critical micelle concentration (CMC) [199]. However, the latter value is often neglected

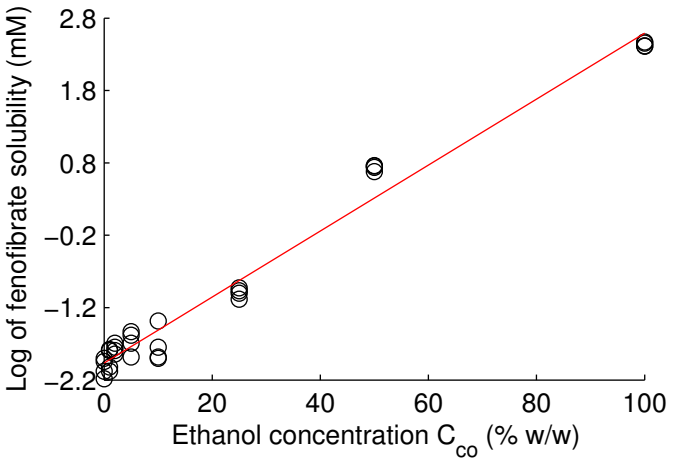

FIGURE 3.6: Fenofibrate solubility in the aqueous dilution of co-solvent, $C_{eq,co}$. The red line represents the regression line and it has to be noted that the solubility is expressed in the log-scale.

at much higher surfactant concentrations than the CMC [200], leading to the following equation:

$$C_{eq,surf} \cong C_{eq,w} + \kappa' \cdot C_{surf} \tag{3.2}$$

An adequate linear regression was obtained in the case of Cremophor RH 40 (R^2 = 0.997; p<0.0001) with a κ' of 0.30 ± 0.007. Similarly, polysorbate 80 provided a slope of

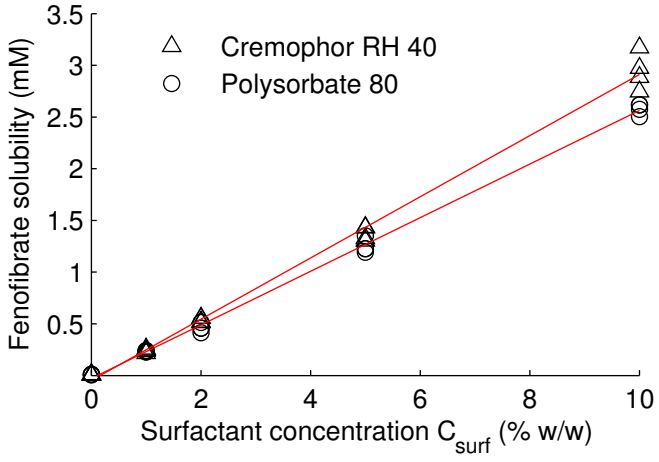

FIGURE 3.7: Fenofibrate solubility in the aqueous dilution of the surfactants, $C_{eq,surf}$ (Cremophor RH 40 and polysorbate 80, respectively). The red lines represent the linear regression lines.

0.26 ± 0.003 ($R^2 = 0.999$; $p<0.0001$). Both cases of pure surfactant-dependent fenofibrate solubility can be inferred from Figure 3.7 . Only the range of non-gelling dilution samples was considered.

Based on these results, we combined Eq. 3.1 and Eq. (3.2) to construct the *non-interacting model* of drug solubility:

$$C_{eq,model} \cong C_{eq,w} \cdot (1 + 10^{\sigma' \cdot C_{co}}) + \kappa' \cdot C_{surf} \tag{3.3}$$

The theoretical values ($C_{eq,model}$) were then compared with the experimental fenofibrate solubility values ($C_{eq,meas}$). Figure 3.8 shows a good agreement between $C_{eq,model}$ and $C_{eq,meas}$, primarily in the diluted state. However, the measured solubility in the undiluted cremophor formulation was more than double the theoretical estimate ($C_{eq,meas}$

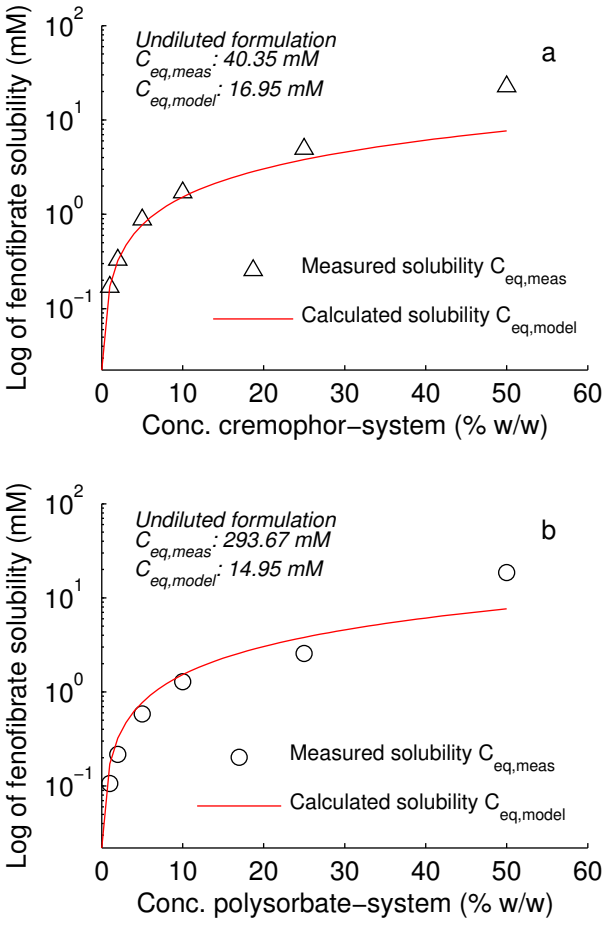

FIGURE 3.8: Fenofibrate solubility (mM) in the diluted cremophor system (a) and polysorbate system (b). Red lines hold for calculated values according to the *non-interacting model*, while measured values of fenofibrate solubility are represented by triangles (cremophor system) and circles (polysorbate system).

40.35 mM *versus* $C_{eq,model}$ 16.95 mM). This gap was even more pronounced in the undiluted polysorbate system, for which the measured solubility was nearly 20 times the calculated solubility (293.67 mM *versus* 14.95 mM, respectively) according to the non-interacting model (Eq. (3.3)).

3.3.5 Structural changes of the vehicle upon aqueous dilution

After characterizing the two formulations in terms of fenofibrate solubilization in the dispersed state, we further studied the physical changes of the formulation during aqueous dilution. Thus, both surfactant/co-solvent systems (drug-free) were analyzed at the different dilution levels using DLS as well as ultrasound analysis.

3.3.5.1 Dilution analysis by dynamic light scattering

Along with measuring the particle size, we applied DLS primarily to trace the polydispersity of micellar particles arising from the dilution of the two drug-free model formulations. There was a pronounced variation of PDI depending on the dilution level (Figure 3.9), which was significant for both systems (p=0.008 and 0.007 for the polysorbate and the cremophor system, respectively).
At low dilution, samples were highly polydisperse and an effective mean particle size was not detectable. On the other hand, rather monodisperse systems (PDI<0.2) were obtained for more diluted samples so that it was possible to determine the mean diameter of colloidal particles. The abrupt decrease of polydispersity was remarkable. The cremophor system exhibited a constant particle diameter of 13–14 nm beyond a dilution factor of 20, while the polysorbate system exhibited a particle diameter of <10 nm beyond a dilution factor of 5.

3.3.5.2 Dilution analysis by ultrasonic resonator technology

Finally, we studied the structural changes of dispersed Pouton type IV systems by using ultrasound propagation. The speed of ultrasound waves is known to depend on a sample's density and compressibility [107, 201, 202]. Phase changes of a lipid-based system in water are therefore expected to influence this acoustic response. We measured the difference in ultrasound velocity, ΔU, between water and the formulations at different dilution ratios (Figure 3.10).
The qualitative change of the acoustic response was similar for the two systems. ΔU reached a peak at dilution factor 2 and decreased again at higher dilution ratios. When

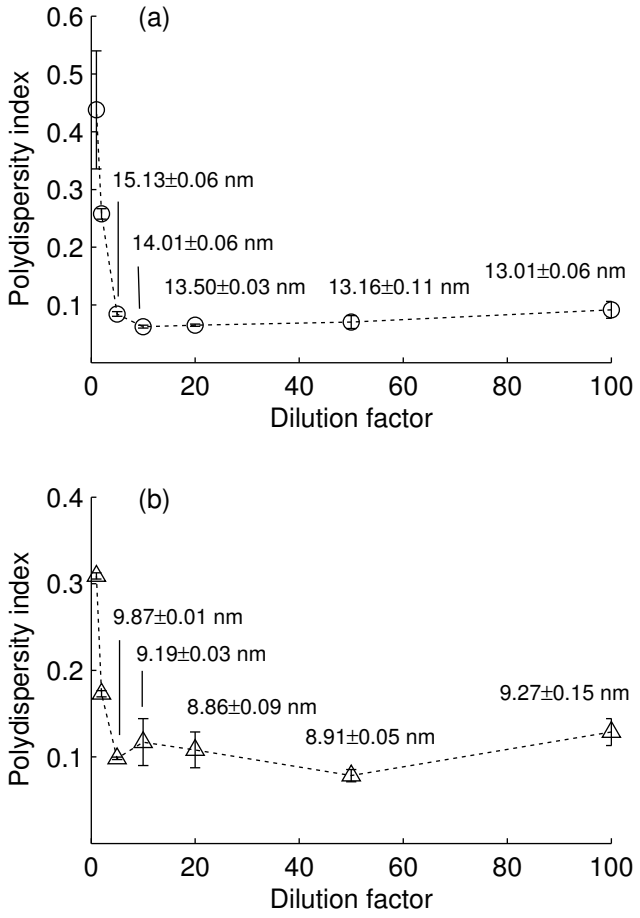

FIGURE 3.9: Polydispersity index and particle size of diluted (a) cremophor system and (b) polysorbate system. The particle size is specified only for systems with a PDI smaller than 0.2.

plotting the acoustic response as a function of the formulation concentration, an approximately linear dependency was revealed between ΔU and the formulation concentration for most samples. However, the highest concentration (corresponding to dilution factor 1) was clearly outside this linear range. At this level of dilution we observed optical birefringence by polarized light microscopy. The Kruskal–Wallis test proved a statistically significant change in ΔU as a function of the dilution factor (p=0.004 and 0.003 for the polysorbate and the cremophor system, respectively).

The density of the diluted systems followed a nearly linear decay for the different dilution levels. However, in contrast to ultrasound values, this trend included even the samples of dilution factor 1.

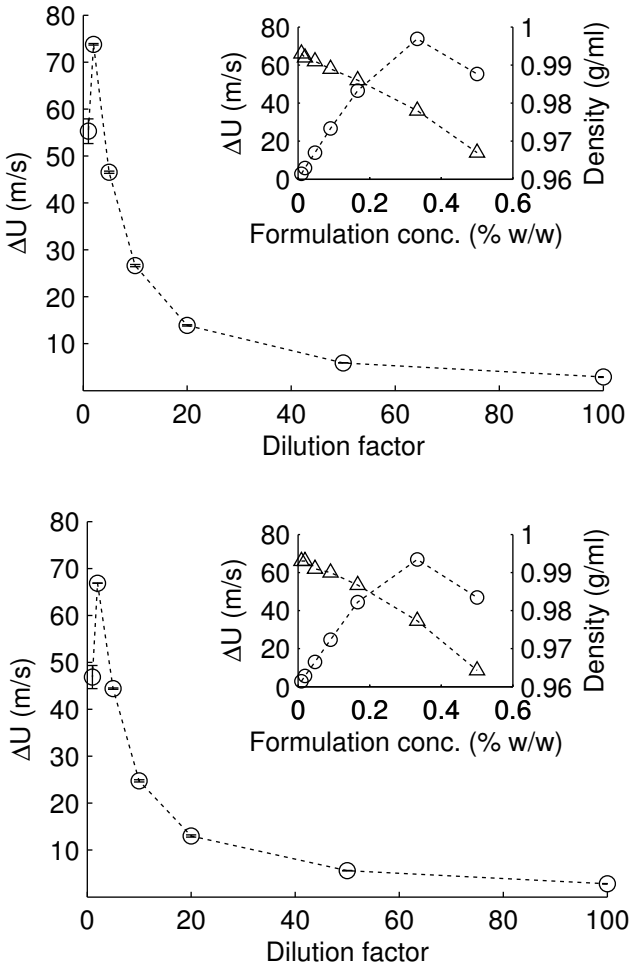

FIGURE 3.10: Difference of ultrasound velocity, ΔU (◯), measured between water and the diluted cremophor system (a) and polysorbate system (b) as a function of the dilution factor (large charts) and the formulation concentration (small charts). The variation of density as a function of dilution is displayed in the insets (△, $n = 3$).

3.4 Discussion

The analyzed Pouton type IV formulations had a similar composition (*i.e.*, a hydrophilic surfactant mixed with ethanol 1:1 w/w). Moreover, the two fenofibrate systems had the same relative drug concentration, corresponding to 80% of drug solubility. However, once dispersed in water, there was a clear difference regarding their ability to keep the drug in solution. Considerable drug precipitation resulted with the polysorbate system but not with the cremophor system.

FBRM measurements showed that precipitation started within several seconds after formulation dispersion. The XRPD pattern confirmed that the precipitate corresponded to crystalline fenofibrate. Therefore, re-dissolution of this poorly soluble drug is expected to be critically slow and, as a consequence, such a formulation could lead to erratic drug

absorption *in vivo*.

Due to the observed differences in the dilution behavior (presence or absence of drug precipitation), the cremophor system and polysorbate system were particularly suited as model formulations, while keeping in mind that capsule compatibility and long-term stability were not determined in this study. We selected several dilution levels that were of relevance for industrial dispersion tests. Despite the practical orientation of the work, the driving force of drug precipitation was of interest to understand differences in dispersion behavior. The value of estimated supersaturation, S_{theor}, proved to be helpful in assessing the risk of drug precipitation. In fact, this parameter was about 10-fold higher in the diluted polysorbate system than in the cremophor system. Due to rather low supersaturation, the latter formulation was able to keep the drug in solution, suggesting that the presence of surfactant inhibited drug precipitation. However, there is a non-linear relationship between drug supersaturation and the risk of precipitation. At a high level of supersaturation there is a pronounced driving force towards drug precipitation, which limits the ability of a surfactant to prevent drug precipitation. Thus, excipient-mediated stabilization of this metastable state is not an absolute effect but depends on the extent of supersaturation [38].

Similarly, the authors of a recent study observed that the dispersion of a self-emulsifying formulation containing polysorbate 80 led to high supersaturation and precipitation of crystalline AMG 517, a poorly water-soluble drug candidate [75]. Interestingly, the presence of small amounts of hydroxypropylmethylcellulose retarded drug precipitation, due to drug stabilization in the supersaturated state. Other stabilizing polymers were investigated and recently reviewed by Warren *et al.* [71]. In the present case with the polysorbate formulation, we observed a supersaturation that was obviously too high to allow stabilization by the surfactant alone. However, the addition of a polymeric precipitation inhibitor might have sustained this metastable state and prolonged the induction time. Further studies are needed to clarify the combined effects of surfactants and polymers on drug precipitation.

From a mechanistic point of view, the newly introduced *non-interacting model* of drug solubilization was particularly interesting. This model was able to demonstrate how solubility was mediated at different levels of aqueous dilution. It was evident from the formulation composition that drug solubilization in both formulations was facilitated by either co-solvency, pure surfactant micelles or interaction between co-solvent and micelles. The last situation may exist in different forms, depending on the level of dilution. In the undiluted formulation, microdomains of surfactant and co-solvent can be present. In the diluted state, interaction between co-solvent and surfactant may be due again to two different structures: depending on the dilution level, it is either a bicontinuous phase including a coherent network of surfactant and co-solvent, or, alternatively swollen micelles.

The *non-interacting model* is a theoretical concept that describes drug solubility in a system where solubility arises from independent micelle inclusion and co-solvency. Therefore, good agreement between modeled and measured data indicated that solubility was independently mediated by ethanol and the surfactant. The ability of the model to describe the experimental solubility at high dilution was remarkable, keeping in mind that this equation was a theoretical simulation. Thus, we can deduce that in diluted samples drug solubilization resulted from co-solvency and micellization independently. However, at the lowest level of dilution (1:1 w/w), the *non-interacting model* did not accurately describe drug solubility. This difference was even more pronounced in the undiluted formulations, indicating that interaction of the excipients accounted for enhanced solubility. In the pure formulations, the ratio of observed to modeled solubility was around 2 for the cremophor system and almost 20 for the polysorbate system. This suggests that the solubilization ability of ethanol–polysorbate microdomains was much higher than ethanol–cremophor structures. Once water was added to the formulations, ethanol migrated out of the interacting structures and, at dilution factors higher than 5, excipient interaction was completely lost. Loss of microdomains was particularly critical for the polysorbate system, leading to a high level of supersaturation upon aqueous dispersion.

The DLS results showed that the two Pouton type IV systems reached a threshold value of polydispersity around dilution factor 5. This observation confirmed the extensive restructuring of the systems at low levels of dilution, which was interpreted as the transition from a bicontinuous structure to dispersion of discrete micelles. In fact, this is in good agreement with the transition from a bicontinuous system to discrete micelles recently observed with SMEDDS [87]. The mean particle sizes at high dilution levels were comparable to the mean micelle size of diluted, pure polysorbate 80 and Cremophor RH 40 [91]. This confirmed the assumption that micelles did not swell in the presence of co-solvent, since ethanol diffused out of micelles.

Ultrasound analysis showed as well a transition of the formulation structure as a function of dilution level. In a homogeneous ideal liquid, the velocity of a sound wave is known to depend on the density, ρ, and the compressibility, κ, of the fluid, as described by the Newton–Laplace equation, $U = 1/\sqrt{\rho\kappa}$. Thus, a change in ultrasound speed is attributed to a difference in apparent density or compressibility of the medium. In our systems we observed a concentration-dependent linear variation of ΔU and of the density between dilution factors 2 and 100. This result was expected for solutions with solubilized or dispersed particles, where equal microstructures but different particle concentrations are present [76]. However, the trend of ΔU was interrupted at the highest level of dilution, while a similar change was not observed with the density. Based on the Newton–Laplace equation, we deduced that the medium compressibility and, thus, the microstructure was changing at dilution factor 1. High ΔU values, such as those present

at low dilution levels, are typical for elevated stiffness (corresponding to low medium compressibility), arising from the existence of coherent liquid-crystalline structures [194]. Polarized light microscopy indeed confirmed the presence of optical birefringence in samples at dilution factor 1. Further dilution led to a pronounced decrease in ΔU indicating a loss of mechanical stiffness, which was expected for isolated micelles in water. This was also described by Fanun *et al.* [94], who analyzed the viscosity of diluted SMEDDS. These authors observed maximum viscosity around a dilution factor of 1. Interestingly, the ΔU values obtained from the two formulations were similar. Thus, the structural properties affecting ultrasound speed were comparable for the two formulations. This indicates that ultrasound wave propagation was barely influenced by the type of surfactant (Cremophor RH 40 and polysorbate 80).

This study focused on how the drug solubilization capacity of two surfactant/co-solvent systems changed upon aqueous dispersion. Understanding such changes in drug solubilization and supersaturation is important to predict the fate of a lipid-based system upon dispersion. However, with respect to the formulation behavior *in vivo*, further aspects have to be considered. First, simple *in vitro* methods, such as the dilution test, do not have a sink compartment that simulates drug absorption across the intestinal membrane. If a drug is rapidly absorbed, the resulting supersaturation could be lower and, as a consequence, the risk of precipitation is reduced [76]. Secondly, the gastrointestinal fluid is a complex matrix consisting of various exogenous and endogenous components, such as bile salts and phospholipids. The individual composition of the intestinal fluid *in vivo* influences the resulting drug solubility. Intestinal fluids also contain digestive enzymes, which can degrade lipid-based excipients and, thus, change their physicochemical properties and solubilization capacity [203]. Finally, both the reduction of supersaturation by drug absorption and the presence of exogenous and endogeneous colloids may affect the nature of the precipitating material. Amorphous or co-crystallized drug potentially shows a largely different biopharmaceutical behavior compared with the crystalline form [61]. Such a precipitate is expected to re-dissolve faster than the crystalline material [33] and, as a consequence, oral bioavailability might be impaired to a lesser extent than predicted from *in vitro* tests.

Despite the known complexity *in vivo*, simple *in vitro* models are still needed from a pharmaceutical development perspective. Especially in the early stages of lipid-based formulation screening, dilution and dispersion tests have their merits [41]. Using the *non-interacting model* provided a better understanding of the *in vitro* results, which is needed to rationally select experimental protocols. Moreover, modeling the effects of excipients on drug solubilization and supersaturation will certainly be important for the future *in silico* prediction of drug absorption.

3.5 Conclusions

Our study of the dilution of two Pouton type IV formulations demonstrated that the testing of formulation candidates only at a single, high dilution level (*e.g.*, 1:100 w/w) representing physiological conditions may be insufficient. Structural changes that are relevant for drug solubilization occur at comparatively low dilution levels. Moreover, a low dilution results in a high absolute drug concentration, which facilitates the detection of precipitated material.

Screening of experimental formulations should therefore include at least one rather low dilution level (*i.e.*, 1:5 w/w or lower). This seems also reasonable with respect to the *in vivo* situation. Formulation dispersion *in vivo* does not immediately reach the final state but rather passes through a low dilution state, especially when viscous bicoherent structures are present. Such dynamic effects, lasting seconds to minutes, can reach the duration of nucleation induction time, and therefore become relevant for drug precipitation.

We introduced a theoretical *non-interacting model* to investigate the mechanism of drug solubilization of two model systems at relevant dilution ratios. Our results suggested that drug solubilization in the undiluted systems was mainly dominated by microdomains caused by surfactant/co-solvent interaction. In contrast, drug solubilization in the dispersed systems was due to independent mechanisms of co-solvency and micellization. Additional surfactants and co-solvents should be tested to predict how broadly the concept of non-interacting excipients can be applied. Finally, pharmacokinetic studies would be of interest to compare the obtained results with *in vivo* drug precipitation and absorption.

Chapter 4

Insights into drug precipitation kinetics during *in vitro* digestion of a lipid-based drug delivery system using in-line Raman spectroscopy and mathematical modeling

Summary

The aim was to determine drug precipitation during *in vitro* lipolysis of a lipid-based drug delivery system (LBDDS) using Raman spectroscopy as a real-time monitoring technique. A second aim was to describe the kinetics of lipolysis-triggered drug precipitation using a theoretical nucleation and growth model. A model LBDDS containing different concentration of fenofibrate was digested *in vitro* and drug precipitation was determined after ultracentrifugation and nanofiltration (off-line methods), as well as by Raman spectroscopy (in-line method). Subsequently, a theoretical nucleation and growth model was fitted to the obtained drug crystallization profiles by considering the lipolysis-triggered change in drug solubility.

Compared with standard off-line measurements, Raman spectroscopy enabled a more

Stillhart C. *et al.* Insights into drug precipitation kinetics during *in vitro* digestion of a lipid-based drug delivery system using in-line Raman spectroscopy and mathematical modeling. *Pharmaceutical Research*, **2013**, 30(2), 3114–3130.

robust and highly time-resolved analysis of lipolysis-triggered drug precipitation. Although the formulation was rapidly digested, fenofibrate remained in a supersaturated state for several minutes before beginning to crystallize. The *in vitro* digestion results were in excellent agreement with the theoretical model. The combination of real-time Raman spectroscopy and mathematical modeling provided insights into the kinetics of lipolysis-triggered drug crystallization. This knowledge allows a better biopharmaceutical understanding and will, ultimately, lead to the improved development of LBDDS.

4.1 Introduction

Contemporary drug discovery screening has generated an increasing number of highly active but poorly water-soluble drug candidates. Lipid-based drug delivery systems (LBDDS) are an innovative strategy that significantly enhances the oral bioavailability of such compounds. Because the formulated drug is already in a dissolved state, the critical dissolution step is circumvented. This is, however, only one mechanism by which LBDDS can enhance oral drug absorption. Drug solubilization in the intestinal medium is generally improved in the presence of lipidic excipients. Furthermore, these excipients can stabilize a supersaturated drug, may reduce pre-systemic clearance, and can promote lymphatic absorption [14, 54, 56, 75].

The improvement of oral bioavailability is largely governed by the fate of the LBDDS in the gut. In addition to formulation dispersion, digestion represents a particularly critical step, because hydrolyzed glycerides and some surfactants exhibit a change in polarity [146, 203, 204]. Thus, the capacity of a formulation to solubilize a drug may be progressively reduced, developing an increased risk of drug precipitation. To predict the fate of a drug in the gastrointestinal lumen therefore requires adequate *in vitro* tests. Although no standard compendial methods have been established so far, first attempts have been made in this direction [134, 146–148]. Most recently, the Lipid Formulation Classification System Consortium released a collaborative work, which was aimed at standardizing *in vitro* methods to assess the performance of LBDDS, with a particular focus on lipolysis testing [26, 27].

A lipolysis test should primarily reveal whether a formulation keeps the drug solubilized. According to the current procedure, samples are removed at given time intervals during a digestion experiment [26, 30]. After enzyme inhibition, the digests are separated by ultracentrifugation into a pellet phase (containing precipitated drug), an oil phase, and an aqueous phase. The drug distribution in these phases is crucial, because the solubilized drug is expected to approximate the dose fraction that is available for absorption [120].

The influence of lipid digestion on drug solubilization is the result of a complex interplay

between several factors. Relevant for solubilization are the properties of the drug and of the lipolysis products in the presence of bile salts and phospholipids. It is assumed that colloidal structures, which are generated during formulation lipolysis, largely define drug solubilization. Although these structures have been characterized in several studies [48, 101, 102, 145, 156, 205, 206], it is difficult to predict the resulting drug solubilization. The difficulty arises not only from dynamic changes in the medium but also from the possibility of drug supersaturation. Indeed, if the period of supersaturation is long enough to enable drug absorption, then intestinal drug precipitation might be prevented. Thus, considerable research efforts have focused on drug supersaturation in biorelevant media, with and without the aid of lipid-based excipients [56, 57, 70]. As well as drug supersaturation, the solid-state properties of precipitated drug are of biopharmaceutical relevance. Sassene *et al.* recently observed the precipitation of amorphous cinnarizine during digestion of a self-emulsifying system [33]. Drug re-dissolution was measured *in vitro* and proved to be faster than from its crystalline form. Such knowledge appears to be critical to the development of a formulation and indicates that more research is needed in this pharmaceutical field.

Formulation digestion and drug solubilization are highly dynamic processes, but the lack of real-time information limits the feasibility of exploring *in vitro* digestion. Warren *et al.* recently demonstrated the importance of using an *in situ* method (synchrotron small-angle X-ray scattering) to gain insight into a rapidly proceeding digestion process [32]. Significant transformations of the formulation typically occur within a short time frame and the sampling regime of traditional methods almost precludes the detection of transient solubility effects.

The use of Raman spectroscopy is an efficient approach to the real-time monitoring of crystallization processes during chemical production [207–212]. The method allows rapid spectra collection in a contact-free manner and with high chemical specificity. Recently, Raman spectroscopy has been applied successfully to study drug precipitation in a biorelevant medium [213] and for process monitoring in complex multiphasic systems [214]. These are promising features with respect to real-time monitoring of drug crystallization during *in vitro* digestion. However, the complexity of the medium and the varying composition during lipolysis are particularly challenging for any spectroscopic application.

The first aim of the study was to evaluate the potential of Raman spectroscopy for real-time monitoring of drug precipitation during *in vitro* lipolysis. Based on this *in situ* information, the second aim was to describe the kinetics of drug precipitation using a theoretical model of nucleation and particle growth, including the lipolysis-triggered change in drug solubility. Finally, using the combination of real-time spectroscopy and mathematical modeling, we aimed to gain a better quantitative understanding of lipolysis-triggered drug precipitation.

4.2 Materials and methods

4.2.1 Materials

We obtained fenofibrate (≥99%), Trizma® maleate, calcium chloride dihydrate (≥99%), pancreatin (from porcine pancreas, 8xUSP specifications), 4-bromophenylboronic acid (4-BPBA, ≥95.0%), chloroform, and acetonitrile from Sigma-Aldrich Chemie GmbH (Buchs, Switzerland), and sodium chloride (≥99%) from Carl Roth GmbH (Karlsruhe, Germany). Lipoid E PC S (phosphatidylcholine from egg yolk) was supplied by Lipoid GmbH (Ludwigshafen, Germany), sodium taurodeoxycholate by Prodotti Chimici e Alimentari S.p.A. (Basaluzzo, Italy), and sodium hydroxide 1 M by Scharlab S.L. (Sentmenat, Spain). Imwitor® 988 was purchased from Sasol Germany GmbH (Witten, Germany), Miglyol 812 N from Hänseler AG (Herisau, Switzerland), and Cremophor® RH 40 from BASF AG (Ludwigshafen, Germany). Imwitor 988 was a blend of medium-chain mono-, di-, and triglycerides (54.6% monoglyceride [MG], 38.0% diglyceride [DG], and 7.1% triglyceride [TG]) consisting of 98.7% w/w caprylic acid (C8), 1.1% w/w capric acid (C10), and 0.1% w/w caproic acid (C6), with average molecular weights of 197, 340, and 483 g/mol for MG, DG, and TG, respectively (according to the certificate of analysis, lot no. 003041, Cremer Oleo GmbH). Miglyol 812 N was a medium-chain TG consisting of 57.9% w/w caprylic acid (C8), 41.2% w/w capric acid (C10), 0.5% w/w lauric acid (C12), and 0.1% w/w caproic acid (C6) with an average molecular weight of 517 g/mol (according to the certificate of analysis, lot no. 2008111435, Hänseler AG). Purified water was prepared with an Arium® 61215 water-purification system from Sartorius Stedim Biotech GmbH (Göttingen, Germany). We used Anotop® 25 Plus filters (aluminum oxide, 0.1 μm) purchased from Whatman GmbH (Dassel, Germany) for nanofiltration.

4.2.2 Preparation of the formulation

A self-microemulsifying drug delivery system (SMEDDS) was selected as the model formulation. The SMEDDS was composed of 40% w/w Miglyol 812, 20% w/w Imwitor 988, and 40% w/w Cremophor RH 40. The components were mixed on a magnetic stirrer at 40°C until a clear solution was obtained and then slowly cooled to room temperature. Fenofibrate (log$P$ 4.6) was used as a poorly water-soluble model drug. The compound was incorporated into the formulation at levels of 20, 30, 40, 50, 60, 70, and 80 mg/g (C_{form}). All formulations were visually assessed for absence of undissolved drug particles.

4.2.3 *In vitro* lipolysis test

The *in vitro* lipolysis test was performed as described in the literature [146]. We prepared a micellar solution containing 1.25 mM phosphatidylcholine (PC) and 5 mM sodium taurodeoxycholate (NaTDC) to simulate fasted state intestinal conditions. PC was dissolved in chloroform and the solvent was evaporated under vacuum (Rotavapor RE 120, Büchi, Switzerland). NaTDC and digestion buffer (50 mM Trizma maleate, 150 mM NaCl, and 5 mM $CaCl_2 \cdot 2H_2O$; pH 7.5) were then added and the mixture was stirred for 12 h (450 rpm, 5°C). To prepare the pancreatin extract, we mixed 1 g of porcine pancreatin powder per 5 ml of digestion buffer (5°C), stirred for 15 min, and then centrifuged the suspension (15 min, 1,600xg, 5°C). Finally, the supernatant was collected and the pH adjusted to 7.5, which corresponded to the pH of the lipolysis medium. The pancreatin extract was freshly prepared each day and stored on ice until use.

The micellar solution (108 ml) was transferred to a thermostated glass vessel (37.0 ± 0.5°C) and the formulation (2.6 g) was added. The mixture was stirred for 10 min for complete dispersion, thermal equilibration, and pH adjustment to 7.500 ± 0.001. For mixing, we used a magnetic stirrer (3 cm in diameter) at a speed of 450 rpm. Digestion was initiated by the addition of 12 ml pancreatin extract (final nominal lipase activity: 1000 tributyrin units per ml). The free fatty acids (FA) produced during lipolysis were titrated using 1 M NaOH to maintain pH 7.500 using a pH-stat apparatus (842 Titrando and 800 Dosino, Metrohm AG, Switzerland), which was operated using the Tiamo® 1.2 software package (Metrohm AG, Switzerland). Lipolysis was allowed to proceed for 30 min.

To determine the NaOH consumption caused by digestion of the blank digestion medium, we performed the lipolysis test with pure digestion medium without formulation (n=3). Fenofibrate formulations with varying drug loads (20, 30, 40, 50, 60, 70, and 80 mg/g) were digested in triplicate and the amount of precipitated and/or solubilized drug was assayed using three different procedures, *i.e.*, ultracentrifugation, nanofiltration, and Raman spectroscopy.

4.2.3.1 "Back-titration" and calculation of free fatty acids liberated during digestion

It was previously shown that the titrated NaOH volume represents only an approximation of the free fatty acids (FA) liberated during lipolysis. Some FA exist in their unionized state, according to the pK_a value, leading to an underestimation of the total FA liberation. This must be corrected by a procedure that was previously termed "back-titration" [157, 158]. We performed the back-titration experiment as described

in the literature, with minor changes. At the end of the 30 min digestion period, the pH was rapidly increased to 9 by addition of 1M NaOH for complete FA ionization (deprotonation). The experiment was also done with blank digestion buffer including pancreatin extract (without formulation, PC, and NaTDC) to determine the NaOH volume needed to increase the pH in the absence of lipolysis products. The latter volume was subtracted from the total back-titration volume obtained in the presence of lipolysis products to obtain the value of FA_{titr}(back-titration). The correction factor was calculated according to the formula:

$$\text{Correction factor} = \frac{FA_{titr}(\text{direct titration}) + FA_{titr}(\text{back-titration})}{FA_{titr}(\text{direct titration})} \tag{4.1}$$

where FA_{titr}(direct titration) is the amount of FA titrated after the 30 min digestion period.

A correction factor was calculated for both the lipolysis of formulations and the lipolysis of pure digestion medium (without formulation). Finally, the amount of FA liberated from the pure digestion medium was subtracted from the total amount of FA titrated in presence of the formulation.

4.2.4 Determination of drug precipitation

4.2.4.1 Ultracentrifugation method

During formulation lipolysis, aliquots (2.7 ml) were taken from the digestion media after a 1, 2.5, 5, 7.5, 10, 12.5, 15, 20, 25, and 30 min digestion period. We immediately added 20 μl of a 4-BPBA solution (1 M in methanol) to inhibit further lipolysis [215] and ultracentrifuged the samples (80,000xg, 37°C, 90 min) in a Centrikon T-1180 ultracentrifuge equipped with a TFT-80.4 fixed-angle rotor (Kontron Instruments, Milan, Italy). The aqueous phase was then diluted with acetonitrile and centrifuged (16,000xg, 15 min). The pellet was suspended in purified water, diluted in acetonitrile, and centrifuged (16,000xg, 15 min). Finally, all samples were analyzed using high-performance liquid chromatography (HPLC).

4.2.4.2 Nanofiltration method

A 2 ml sample was withdrawn from the lipolysis medium after 1, 2.5, 5, 7.5, 10, 12.5, 15, 20, 25, and 30 min. The samples were directly passed through an Anotop 25 Plus syringe filter (pore size 0.1 μm, aluminum oxide filter membrane) [137] and the filtrate was immediately diluted in acetonitrile to stop further lipolysis. The samples were then

centrifuged (16,000xg, 30 min) and analyzed by HPLC. We verified experimentally that no loss of dissolved substance occurred through adsorption onto the filter material.
The Mann–Whitney test was performed to compare the concentration of solubilized drug after 0 and 1 min of lipolysis. For statistical treatments we used the software Statgraphics® Centurion XV Professional (Statpoint Technologies Inc. Warrenton, USA) and selected a significance level of 95.0% (p<0.05).

4.2.4.3 In-line determination of drug precipitation using Raman spectroscopy

A multi-fiber Raman P^{h}AT probe was used to determine the course of fenofibrate precipitation *in situ*. The titration vessel was covered with a custom-built vessel lid (Metrohm AG, Zofingen, Switzerland) with an extra cavity for the P^{h}AT probe, which was positioned 1 cm above the initial level of the lipolysis medium (Fig. 4.1). A comparatively large titration vessel, and thus a relatively high volume of digestion medium, were required because of the P^{h}AT probe size (outer diameter: 32 mm). The entire lipolysis vessel was wrapped in aluminum foil and the laboratory was darkened to avoid the influence of external light on the Raman signal.
We used a Raman RXN1 analyzer (Kaiser Optical Systems, Inc., Ann Arbor, MI, USA) equipped with a charge-coupled device (CCD) camera and a diode laser operating at a wavelength of 785 nm. The spectra were acquired with a laser power of 400 mW

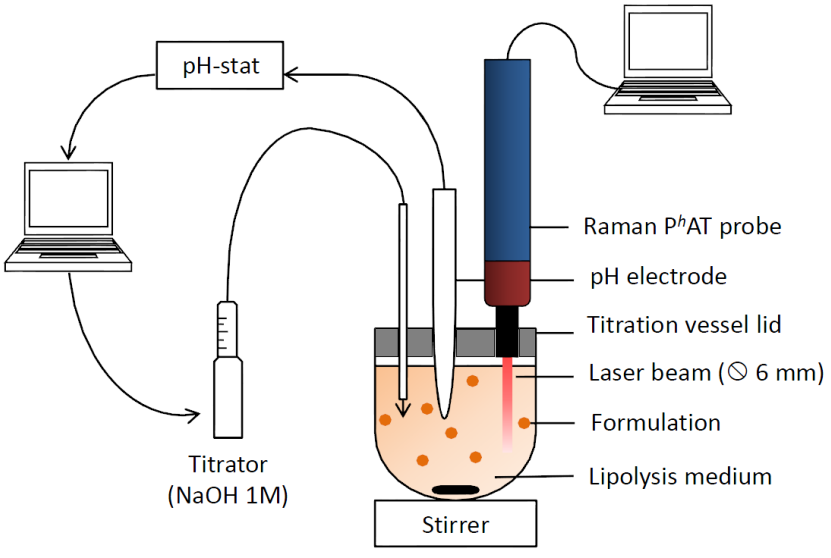

FIGURE 4.1: Experimental setup of the *in vitro* lipolysis test combined with Raman spectroscopy. The P^{h}AT probe consisted of a non-contact optic device and provided a large laser spot area (6 mm in diameter).

and background Rayleigh scattering was removed by a holographic filter during spectra acquisition. A single spectrum was acquired every 20 s (acquisition time 18.5 s) with a resolution of 4 cm^{-1} using the iC Raman® Instrument software (Version 3.0, Mettler-Toledo AutoChem Inc., Columbia, MD, USA). The Raman P^hAT probe was a multi-fiber probe with a non-contact sampling optic device having a laser spot diameter of 6 mm. The scattered radiation was collected by an array of 50 optical fibers and delivered to the CCD camera.

To remove sources of non-linearity and spectral information that was uncorrelated with the concentration of the analyte, the spectra were subjected to several preprocessing algorithms, *i.e.*, the multiplicative scatter correction (MSC) [216], the standard normal variate (SNV) transformation [217], and the Savitzky–Golay (SG) polynomial derivative filter [218]. All data were mean-centered and, finally, a calibration model was built by partial least-squares (PLS) regression [219]. The optimal number of PLS factors was defined where the root-mean-square error of cross-validation (RMSECV) reached a minimum (<1% of spectral variation). Cross-validation was performed with the leave-one-out method. We evaluated different spectral ranges to include in the PLS regression model, *i.e.*, the entire spectrum (500–1800 cm^{-1}), the fingerprint range of fenofibrate (1000–1800 cm^{-1}), and specific fenofibrate peaks (1132–1164 cm^{-1}, 1550–1615 cm^{-1}, and 1635–1663 cm^{-1}). Spectral preprocessing and PLS regression analysis were calculated using Matlab® (MathWorks, Naticks, MA, USA). The calibration models were evaluated in terms of the correlation coefficient R^2, the cross-validation coefficient Q^2, the root-mean-square error of calibration (RMSEC), and the RMSECV.

4.2.5 Drug solubilization upon dispersion without lipolysis

Drug solubilization under non-digesting conditions was determined to assess whether fenofibrate precipitated spontaneously upon aqueous dispersion of the formulation (without lipolysis). Thus, 2.6 g of formulation with 80 mg/g fenofibrate were dispersed in 108 ml of digestion buffer (containing NaTDC and PC) in a glass vessel at 37°C and stirred at 450 rpm. After equilibrating the system for 10 min, 12 ml of pure digestion buffer (without pancreatin extract) were added and the medium was stirred for 30 min. Subsequently, three 2 ml aliquots were centrifuged for 30 min (16,000xg, 37°C) and the concentration of solubilized and precipitated fenofibrate was measured by HPLC. The experiment was carried out in triplicate.

4.2.6 Determination of drug solubility

Drug solubility was determined in the undiluted formulation (C^*_{form}). Excess solid drug was added to a 2 ml aliquot of blank formulation and stored in hermetically sealed glass vials during equilibration (37°C, 450 rpm). After 24 h, 48 h, and 72 h the samples were centrifuged (37°C, 16,000xg, 30 min) and the supernatant was analyzed by HPLC. Equilibrium was assumed when two consecutive solubility samples varied by <5% (w/w). Furthermore, we determined the drug solubility ($C^*_{m,t}$) in the lipolysis medium containing drug-free formulation after a 1, 2.5, 5, 7.5, 10, 12.5, 15, 20, 25, and 30 min digestion period. The enzyme inhibitor (4-BPBA, 1M in methanol, 9 μl per ml of digest) was added to the medium at the aforementioned time points to stop further digestion. Excess solid drug was transferred to a 10 ml aliquot of the lipolysis medium and was hermetically sealed in glass vials. After equilibration (450 rpm, 37°C), the samples were ultracentrifuged (80,000xg, 37°C, 90 min). The liquid phase was then diluted in acetonitrile, centrifuged (16,000xg, 15 min), and finally analyzed by HPLC. Because the solubilities were found to decrease at equilibration times longer than 24 h, we considered the value obtained at 24 h of equilibration as the relevant solubility. The observed decrease in solubility was attributed to kinetic instability of the colloidal structures in digested medium [27, 56]. Whenever a lipid phase was obtained upon ultracentrifugation, the lipid and the aqueous phase were re-emulsified, to measure the overall concentration of solubilized drug. The drug solubility experiments were carried out in triplicate.

4.2.7 High-performance liquid chromatography (HPLC)

For HPLC analysis (Agilent Technologies 1200 Series) we used an autosampler (G1329A), an isocratic pump (G1310A), and a variable wavelength detector (G1310A). All measurements were done on a LiChrospher® 60, RP select B 125-4 (5 μm) column (Merck, Darmstadt, Germany), using a flow rate of 1 ml/min, a UV detection wavelength of 287 nm, and an injection volume of 20 μl. The mobile phase consisted of acetonitrile and ammonium acetate buffer (pH 3.5; 25 mM) at a ratio of 65:35 v/v [220]. All sample measurements were in the linear range of calibration.

4.2.8 Dynamic light scattering (DLS)

We measured the particle size of the dispersed formulation before lipolysis initiation by DLS using a Zeta Sizer Nano ZS (Malvern Instruments, Malvern, UK), equipped with a 4 mW He-Ne Laser operating at a wavelength of 633 nm. The scattering signal was detected at an angle of 173° and each sample was measured in triplicate for 10 min. The

result was expressed as intensity averaged particle diameter (nm) and as polydispersity index (PDI).

4.2.9 X-ray powder diffraction (XRPD)

The pellet phase that was obtained upon digestion and ultracentrifugation of the drug-containing formulation was analyzed by XRPD. The formulation with 80 mg/g fenofibrate was digested for 30 min in the *in vitro* lipolysis test and, after enzyme inhibition, an aliquot was ultracentrifuged (80,000xg, 37°C, 90 min). The pellet phase was immediately isolated and an X-ray diffractogram was recorded. The same procedure was followed with the pellet phase obtained from a 30 min lipolysis experiment with drug-free formulation, which was spiked with an equal amount of pure fenofibrate (as used for formulation preparation). Moreover, we recorded the X-ray diffractogram of crystalline fenofibrate as a reference.
We used a theta-theta X-ray powder diffractometer (R-XRD Phaser D2, Bruker AXS GmbH, Karlsruhe, Germany) equipped with a Co and Cu KFL tube (30 kV, 10 mA) as radiation source and a Lynxeye® detector. The samples were scanned in the angular range of 5° (2θ) to 40° (2θ) with a step size of 0.1° (2θ) and a count time of 5s per step.

4.2.10 Modeling the kinetics of lipolysis-triggered drug precipitation

The increased chemical potential of a supersaturated solution, in which the actual concentration of solubilized drug exceeds its solubility, is the driving force for drug precipitation. Precipitation can be described by two consecutive processes, *i.e.*, nucleation and particle growth. The relationship between precipitation and supersaturation is reflected in the expressions describing the kinetics of these processes. According to the classical nucleation theory, the nucleation rate, J ($m^{-3}s^{-1}$), is given by [64]:

$$J = \frac{dC'_{pr}}{dt} = A'Se^{-\frac{B}{\ln^2 S}} \tag{4.2}$$

where C'_{pr} is the number of nuclei formed per unit volume and S is the degree of supersaturation given by $S = C/C^*$, with C being the actual drug concentration and C^* its solubility in the medium. Parameter A' ($m^{-3}s^{-1}$) holds for the kinetic component of nucleation and is proportional to the number of nucleation-active centers. Its value differs between volume-diffusion-controlled and interface-controlled nucleation and is many orders of magnitude smaller for heterogeneous nucleation than for homogeneous nucleation [197]. B stands for the thermodynamic component of the process and is given by:

$$B = 16\pi\nu_0^2\gamma^3/3(kT)^3 \tag{4.3}$$

where ν_0 is the molecular volume of the crystalline phase, γ is the interfacial energy per unit area of the crystal, k is the Boltzmann constant, and T is the temperature. In the case of heterogeneous nucleation, the work of nucleation is reduced because of the lower interfacial energy, leading to smaller values of B.
The particle growth rate G ($\mathrm{m{\cdot}s^{-1}}$) is often expressed heuristically as a power-law [63]:

$$G = k_g^{'}(C - C^*)^g \tag{4.4}$$

where $k_g^{'}$ is the particle growth coefficient, and g is the order of particle growth.
To apply Eqs. 4.2 and 4.4 for modeling the kinetics of lipolysis-triggered drug precipitation, the changes in C^* and S as a function of time had to be considered. Fenofibrate solubility depends on the concentration of lipids in the medium and is therefore affected by the lipolysis, which changes the lipid composition over time. Hence, solubility was expressed as a function of time by a heuristic equation, which considered the contribution of different lipid species to solubility.
Considering the lipolysis kinetics on the one hand, and the specificity/activity of digestive enzymes (*i.e.*, pancreatic lipase, co-lipase, and carboxyl ester hydrolase [146, 157–159]) on the other, we subdivided the lipolysis of the formulation (containing TG, DG, and MG) into two kinetic stages. TG and DG were assumed to be digested rapidly by the pancreatic lipase and co-lipase (first stage), while MG were digested slowly by the carboxyl ester hydrolase (second stage). The time point of transition between the first and second stages, t_x, was obtained graphically from the experimental FA titration curve. Based on the titration data and the stoichiometry of glyceride lipolysis, we calculated the moles of TG and DG ($M_1(t)$) digested into MG during the first stage and the moles of MG ($M_2(t)$) digested during the second stage. The course of drug solubility in both stages was modeled using Eqs. 4.5 and 4.6:

$$C^*_{m,t}(\text{stage 1}) = C^*_{m,0} \cdot \left(1 - \frac{M_1(t)}{M_0}\right) + C^*_{m,tx} \cdot \left(\frac{M_1(t)}{M_0}\right) \tag{4.5}$$

$$C^*_{m,t}(\text{stage 2}) = (C^*_{m,tx} - C^*_{m,30}) \cdot \left(1 - \frac{M_2(t)}{M_{tx}}\right) + C^*_{m,30} \tag{4.6}$$

where $C^*_{m,0}$, $C^*_{m,tx}$, and $C^*_{m,30}$ are the experimental drug solubility values in the lipolysis medium at times 0, t_x, and 30 min, respectively. M_0 is the molar quantity of TG and DG at 0 min, and M_{tx} is the molar quantity of MG in the medium at t_x. $M_1(t)$ and $M_2(t)$ were proportional to the logarithm of time.
The kinetics of lipolysis-triggered drug precipitation was modeled by adapting Eqs. 4.2 and 4.4, and combining them with Eqs. 4.5 and 4.6. Three time intervals were defined

that were delimited by t_0 (beginning of the experiment), t_n (beginning of nucleation), t_g (beginning of particle growth), and t_{30} (end of the experiment). Thus, the model comprised the following system of ordinary differential equations:

$$t_0 < t < t_n: \quad \frac{\mathrm{d}C_{pr}}{\mathrm{d}t} = 0 \tag{4.7}$$

$$t_n < t < t_g \text{ and } t < t_x: \quad \frac{\mathrm{d}C_{pr}}{\mathrm{d}t} = ASe^{-\frac{B}{\ln^2 S}} \quad \text{with } S = \frac{C}{C^*_{m,t}(\text{stage 1})} \tag{4.8}$$

$$t_n < t < t_g \text{ and } t > t_x: \quad \frac{\mathrm{d}C_{pr}}{\mathrm{d}t} = ASe^{-\frac{B}{\ln^2 S}} \quad \text{with } S = \frac{C}{C^*_{m,t}(\text{stage 2})} \tag{4.9}$$

$$t_g < t < t_{30} \text{ and } t < t_x: \quad \frac{\mathrm{d}C_{pr}}{\mathrm{d}t} = k_g \cdot (C - C^*)^g \quad \text{with } S = C^*_{m,t}(\text{stage 1}) \tag{4.10}$$

$$t_g < t < t_{30} \text{ and } t > t_x: \quad \frac{\mathrm{d}C_{pr}}{\mathrm{d}t} = k_g \cdot (C - C^*)^g \quad \text{with } S = C^*_{m,t}(\text{stage 2}) \tag{4.11}$$

C_{pr} refers to the mass concentration of precipitated drug. During the induction time (between t_0 and t_n), no precipitation takes place (Eq. 4.7). During nucleation, the degree of supersaturation S may be given by Eqs. 4.8 and 4.9 depending on the position of t_x relative to t_n and t_g. Analogously, during particle growth, the expression of solubility C^* may depend on the position of t_x with respect to t_n and t_g (Eqs. 4.10 and 4.11).
The values of parameters A, B, k_g, g, t_n, and t_g, were estimated by regressing this system of differential equations to the concentration data obtained by Raman spectroscopy. Mean C_{pr} values of each drug load between 40 and 80 mg/g (n=3) were used.
Calculations were carried out using Matlab. For parameter estimation we used the Matlab optimization algorithm *fminsearch*, which is based on the simplex procedure. The ordinary differential equations were numerically solved using the Matlab *ode45* solver and the model quality was assessed based on the R^2 value and the root-mean-square error (RMSE).

4.3 Results

4.3.1 Formulation characteristics

The lipid-based system emulsified spontaneously within 10 s, resulting in a fine emulsion with a droplet diameter of 39.5 ± 0.3 nm and a PDI of 0.047 ± 0.018 (mean ± standard deviation (SD), n=3). No drug precipitation was measured 30 min after dispersion under non-digesting conditions. Fenofibrate solubility in the undigested lipolysis medium

was 2.60 ± 0.44 mg/ml. However, upon addition of pancreatin extract, the solubility dropped rapidly to a value of 0.403 ± 0.006 mg/ml within the first minute of digestion. By the end of the lipolysis experiment (t=30 min), solubility further decreased to 0.129 ± 0.005 mg/ml. On the other hand, fenofibrate solubility in the undispersed formulation,C^*_{form}, was 139.6 ± 0.7 mg/g.

Before lipolysis initiation, fenofibrate was below saturation, even at the highest drug load. As a consequence of the rapid decrease in drug solubility with formulation lipolysis, fenofibrate became supersaturated within the first minute of digestion. At the highest drug load (80 mg/g) the supersaturation ratio reached a value of 4.19 ± 0.03 (1 min of digestion), whereas at a drug load of 20 mg/g, the corresponding supersaturation ratio was 1.04 ± 0.02.

Figure 4.2 shows the NaOH titration profile obtained from formulation lipolysis. Immediately after initiation of digestion, the hydrolysis was fast, while after approximately 1 min the rate had clearly decreased. No clear differences were observed between the lipolysis profiles of formulations with different drug loads.

Because not all FA were expected to be ionized at the pH of the assay, we employed the "back-titration" procedure. We obtained a back-titration factor of 1.09 for the formulation lipolysis, implying that 9% of the free FA were protonated at pH 7.5 and, thus, not determined by direct titration. The lipolysis and back-titration of pure digestion medium (without SMEDDS) resulted in a correction factor of 1.77.

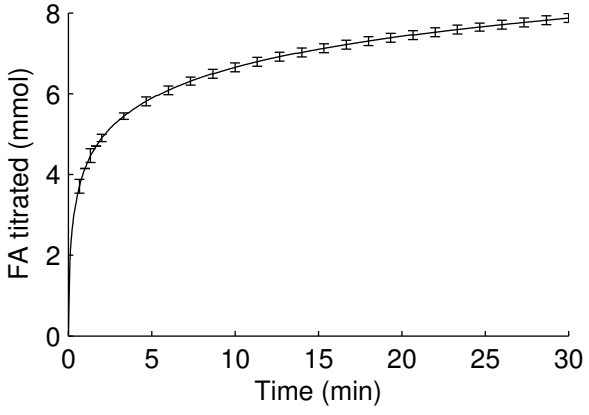

FIGURE 4.2: Free FA originating from formulation digestion as a function of time. Values (means ± SD, n = 3) were corrected for background lipolysis (pure lipolysis medium) and include additional FA detected by back-titration.

4.3.2 Detection of drug precipitation during lipolysis

4.3.2.1 Ultracentrifugation method

To determine the amount of precipitated drug, we first applied ultracentrifugation for sample preparation, which appeared to be the most widespread method in this field of *in vitro* testing. Following ultracentrifugation, only two phases were obtained, *i.e.*, an aqueous and a pellet phase. No oil phase was visually detectable with the given samples. This was, as expected, different from the samples that were not digested (t=0), in which an oil phase was additionally observed.

Figure 4.4a displays the fenofibrate precipitation profiles of formulations with varying drug loads, as obtained using ultracentrifugation. Drug precipitation started rapidly upon initiation of digestion and leveled off after approximately 2.5 min for formulations with drug loads of 40 to 80 mg/g. Formulations with a lower drug load displayed some drug precipitation as well but the rates and extents were moderate.

Drug concentration in the aqueous phases decreased over time, in parallel to the increase in precipitation. After a 2.5 min digestion period, the concentrations of solubilized drug approached the equilibrium values, $C^*_{m,t}$, for all formulations with a drug load of 40–80 mg/g.

We recorded the XRPD pattern of pure fenofibrate, of the pellet containing precipitated fenofibrate, and of a reference pellet. This reference was the pellet obtained after lipolysis of drug-free formulation, which was spiked with crystalline fenofibrate. As seen in

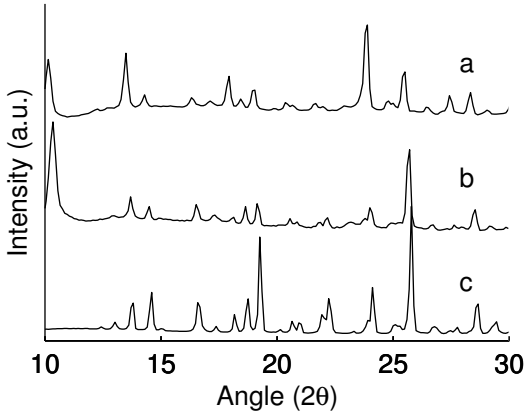

FIGURE 4.3: XRPD pattern of the pellet phase obtained upon ultracentrifugation and resulting from (a) the formulation with 80 mg/g fenofibrate, (b) the pellet phase of drug-free formulation spiked with crystalline fenofibrate, and (c) pure crystalline fenofibrate.

Fig. 4.3, the angular range of peaks of the pellet containing precipitated drug corresponded to that of the reference pellet. Therefore, apparently, fenofibrate precipitated in the crystalline form during lipolysis.

4.3.2.2 Nanofiltration method

The nanofiltration method allowed the determination of solubilized fenofibrate in the filtrate. Therefore, the concentration of precipitate was calculated as the difference between the total drug concentration and the amount of solubilized drug (Fig. 4.4b). Similar to the ultracentrifugation method, we observed significant drug precipitation within 30 min of lipolysis with all formulations having a drug load of 40 mg/g and more. However, the time course was different, as there was an initial lag phase without precipitation before the drug finally started to precipitate out. Thus, for the SMEDDS with the highest drug load, precipitation started after approximately 2.5 min, while for the formulation with a drug load of 30 mg/g, drug precipitated after about 15 min. The concentration of solubilized drug did not significantly change within the first minute of digestion for each drug load (p>0.05). Finally, only minimal precipitation was observed in the formulation with a 20 mg/g drug load.

4.3.2.3 Raman spectroscopy

The Raman spectra of fenofibrate in the crystalline and solubilized forms displayed a characteristic pattern, as seen in Fig. 4.5a. Unprocessed spectra are depicted, which were recorded during the lipolysis experiment at different time points (drug load: 70 mg/g). Moreover, the Raman spectra of crystalline fenofibrate and of the drug-free lipolysis medium are shown. The spectra recorded after 40 s, 5 min, and 30 min of lipolysis displayed noticeable variations in the range of 1132–1164 cm^{-1} and 1550–1663 cm^{-1}. A PLS model was built for the concentration of crystallized fenofibrate based on a set of 42 spectra, as detailed in Table 4.1.

Table 4.1: Calibration set as used for quantitative application of Raman spectroscopy.

C_{pr} (mg/g)	Time span of acquisition (s)	C_{pr} (mg/ml)	Total number of calibration spectra
20, 30, 40, 50, 60, 70	20–40	0	18
50, 60, 70, 80	1480–1500	C_{pr} [a]	12
50, 60, 70, 80	1780–1800	C_{pr} [a]	12

[a] Results obtained using the ultracentrifugation method.

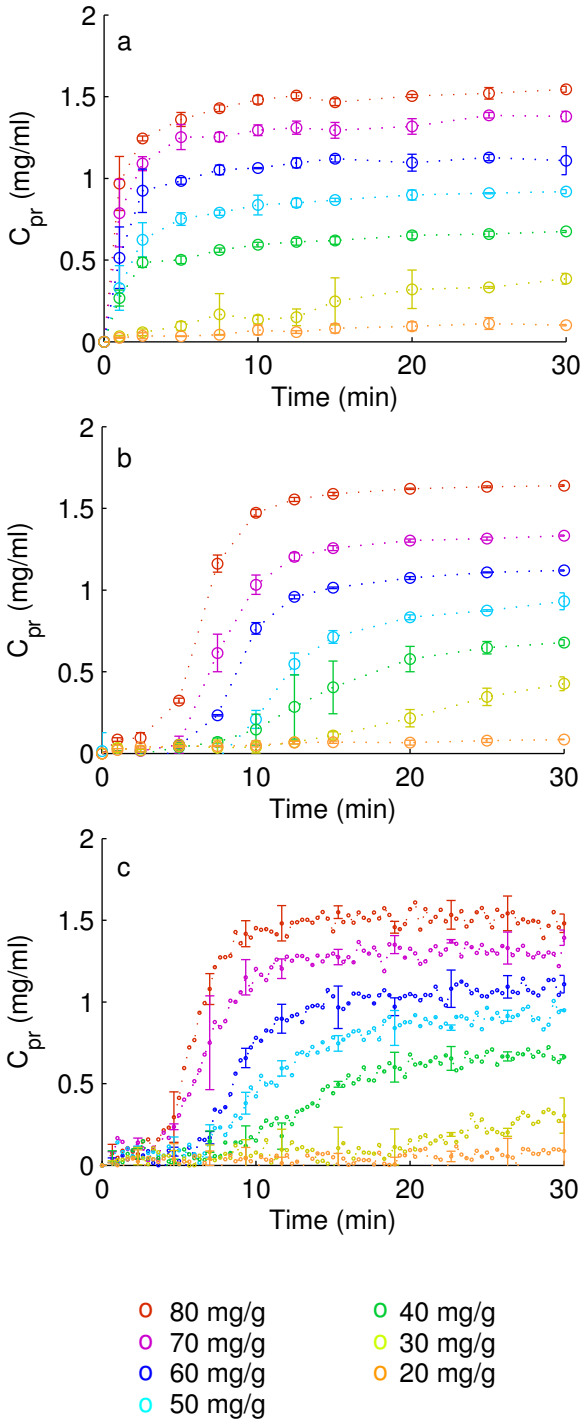

FIGURE 4.4: Time course of fenofibrate precipitation during formulation lipolysis as detected (a) upon ultracentrifugation, (b) upon nanofiltration and (c) with Raman spectroscopy. Each color represents a single drug loading, C_{form}. Values are expressed as means ± SD (n=3).

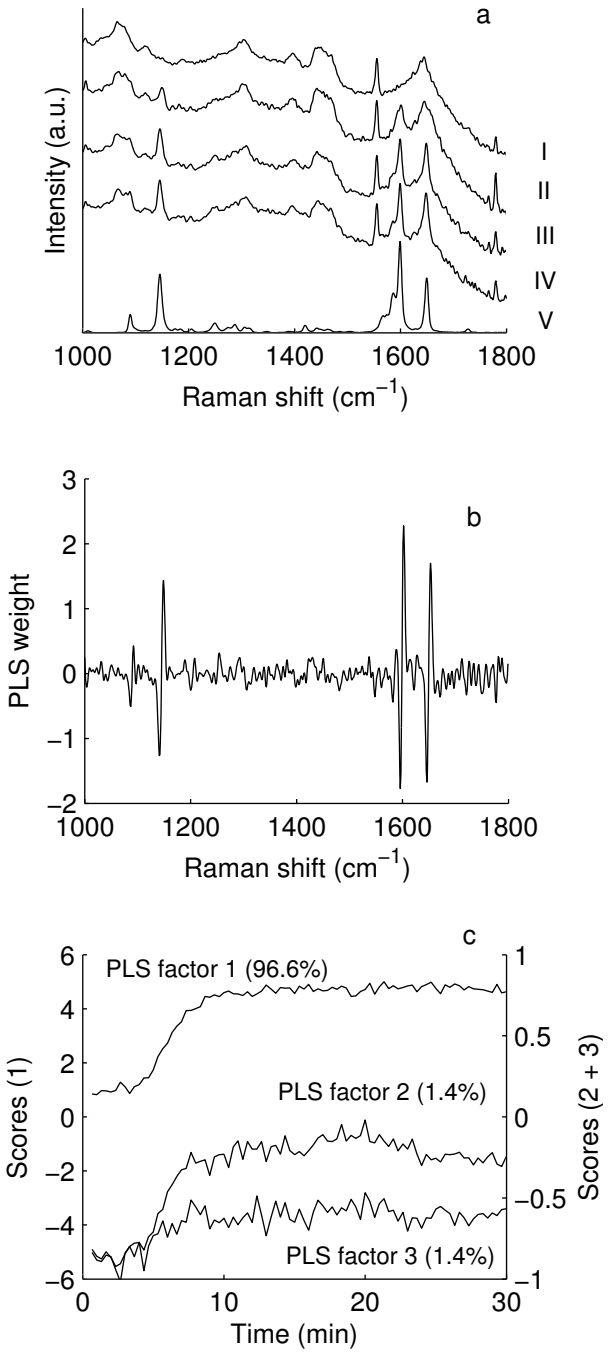

FIGURE 4.5: Part (a) depicts the unprocessed Raman spectra of drug-free lipolysis medium (I), lipolysis medium with fenofibrate after 40 s (II), 5 min (III), and 30 min (IV) digestion periods, and pure fenofibrate (V). Plots of the weights of the first PLS factor (b) and scores over time of all three PLS factors used in the PLS model (c). The numbers in (c) represent the variance captured in the corresponding PLS factor. All plots are offset for clarity.

The reference values were mostly selected from concentrations and time points that demonstrated consistent results in both off-line methods (*i.e.*, ultracentrifugation and nanofiltration). The concentrations in samples with a drug load of 50–80 mg/g, assayed at 25 and 30 min of digestion, were consistent between the two methods and were therefore used for model calibration of the corresponding spectra. To further include spectra of digests without precipitate, we relied on the data from the nanofiltration method. According to these results, the concentration of solubilized drug after 1 min of lipolysis was not significantly different from the concentration before initiation of lipolysis ($p>0.05$ in all cases). This observation indicates that no precipitation occurred during the first minute of digestion. Therefore, for model calibration we selected the earliest spectrum (*i.e.*, the spectrum that was acquired 40 s after lipolysis initiation) of each formulation with a drug load of 20–70 mg/g and set C_{pr} equal to zero. The 80 mg/g drug load was excluded from this part of the calibration.

We evaluated different methods for data preprocessing. Two scatter-correction methods (MSC, SNV) and a derivative method (SG) were compared [216–218]. Moreover, three different spectral ranges were considered for model calibration. Table 4.2 compares the performance of calibration models that were obtained using the different pre-processing methods and spectral ranges. The best calibration model was attained with the SG algorithm (1^{st} derivative) and a spectral range between 1000 and 1800 cm^{-1}. Three PLS factors described 99.4% of the spectral variation, with an R^2 value of 0.994, while the first, second, and third factors accounted for 96.6%, 1.4%, and 1.3% of the variation, respectively. Only the first PLS factor is shown in Fig. 4.5b, as it accounted for most of the variation. Herein, three ranges with a high PLS weight were identified, which corresponded to the peaks of the crystalline fenofibrate. The second and the third factors contributed to the model variation to a lower extent. However, they may account for residual non-linearity in the data set as seen in Fig. 4.5c. The cross-validation procedure yielded a Q^2 value of 0.972 and an RMSECV of 0.111 mg/ml, indicating a robust calibration model.

Finally, we applied this calibration model to all other Raman spectra to determine the precipitation profiles over a 30 min digestion period. Figure 4.4c shows that fenofibrate precipitated after an initial lag time in all formulations with drug loads of more than 30 mg/g. Minimal drug precipitation was observed for the formulation with a drug load of 20 mg/g.

In summary, the comparison of fenofibrate precipitation profiles (Fig. 4.4a, 4.4b, and 4.4c) demonstrated an excellent agreement between the nanofiltration and the spectroscopic methods. Both methods suggested that drug precipitated only after an initial lag phase. This was in contrast to the ultracentrifugation method, which indicated precipitation almost immediately after digestion started.

Table 4.2: PLS analysis result of Raman spectroscopy

Pre-processing method	Spectral range[b]	PLS factors	R^2	Q^2	RMSEC (mg/ml)	RMSECV (mg/ml)
None	A	5	0.985	0.969	0.0142	0.113
	B	4	0.985	0.959	0.0104	0.129
	C	3	0.979	0.960	0.0501	0.112
SNV	A	3	0.984	0.907	0.0298	0.194
	B	3	0.988	0.962	0.0199	0.152
	C	4	0.953	0.962	0.0108	0.124
MSC	A	4	0.985	0.958	0.0129	0.132
	B	3	0.978	0.958	0.0133	0.132
	C	3	0.982	0.966	0.0158	0.117
SG[a]	A	3	0.993	0.971	0.0083	0.117
	B	3	0.994	0.972	0.0079	0.111
	C	3	0.990	0.969	0.0099	0.111

[a] Parameters used in the SG algorithm: window size 10 points, 1^{st} derivative, 2^{nd} polynomial.
[b] Spectral ranges: A=500–1800 cm^{-1}; B=1000–1800 cm^{-1}; C=1132–1164, 1550–1615, 1635–1663 cm^{-1}.

4.3.3 Modeling the kinetics of lipolysis-triggered drug precipitation

The high temporal resolution of in-line Raman spectroscopy encouraged a more detailed analysis of drug precipitation kinetics. The theories of nucleation and growth (Eqs. 4.2 and 4.4) were applied to model the course of lipolysis-triggered drug precipitation. Before lipolysis initiation, drug concentration in the lipolysis medium was below saturation. Enzymatic digestion of lipids resulted in a diminished drug solubilization, which in turn induced supersaturation and led to drug precipitation. Because the drug solubility changed continuously through ongoing lipolysis, an expression for time-dependent solubility was introduced.

The progress of lipolysis is reflected by the amount of FA titrated as a function of time (Fig. 4.2). These data show that lipolysis occurred rapidly at first and then slowed down considerably. By drawing two straight lines through the data points between 0 and 40 s, and between 16.6 and 30 min, we found the intersection point, t_x, at 82.1 s. This time point was used to define the transition of the initial rapid lipolysis stage to the second, slow lipolysis stage. Based on the titration data and the stoichiometry of hydrolysis, we calculated the amount of glycerides that were apparently hydrolyzed in these two stages (Fig. 4.6a), and compared it with the amount of formulation lipids. The good agreement between experimental data (Fig. 4.6a), and the formulation composition (Table 4.3) supports the view that the first stage corresponded primarily to the hydrolysis of TG and DG, whereas the second stage was attributable to the hydrolysis of MG. The latter value included MG, those present in the formulation (Imwitor 988) and

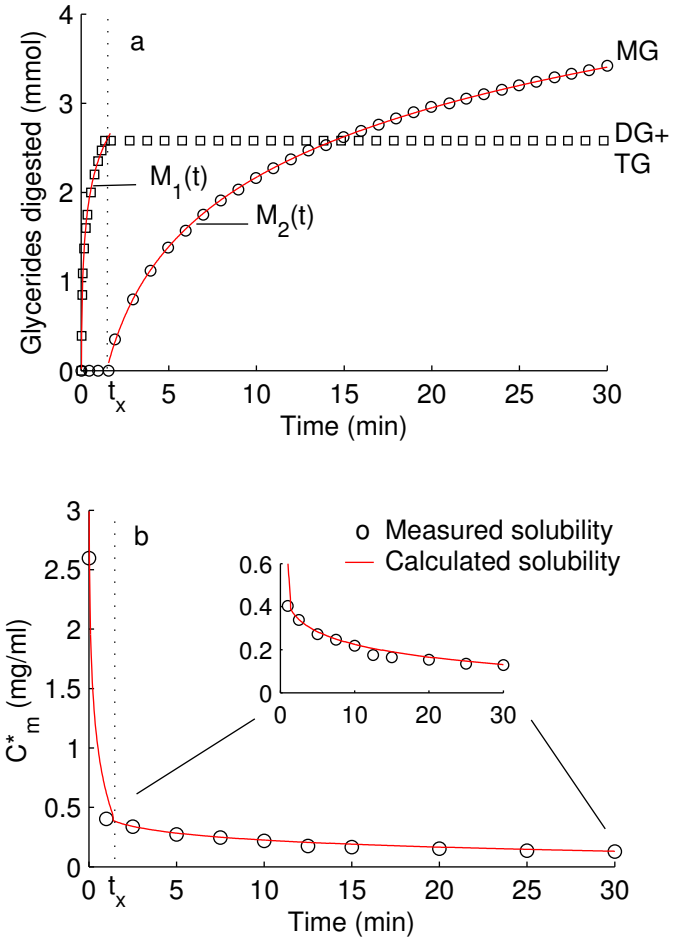

FIGURE 4.6: TG and DG digestion (*white square*) and *sn*-1 MG digestion (*white circle*) over time, as calculated based on titrated FA and the stoichiometry of glyceride hydrolysis according to the literature (a). The red lines represent logarithmic functions of the time fitted to these time courses ($M_1(t) = 0.57\ln(t)+2.37$ and $M_2(t) = 1.12\ln(t)-0.419$, respectively). (b) Fenofibrate solubility in the lipolysis medium as determined experimentally at different lipolysis times (*circles*) and as calculated from Eqs. 4.5 and 4.6 (*red line*).

those generated from the lipolysis of *sn*-1,3 DG. In contrast, *sn*-2 MG resulting from the digestion of TG were assumed not to be further hydrolyzed [159]. With respect to the different enzyme activities, we expected rapid digestion of DG and TG by the pancreatic lipase and co-lipase, whereas the activity of the carboxyl ester hydrolase is known to be comparatively low [157, 158]. This difference in lipolysis rates was in good agreement with our observations, as DG and TG were digested considerably faster than MG. The amount of digested TG and DG ($M_1(t)$) and of digested MG ($M_2(t)$) was found to be well described by a logarithmic function of time ($R^2 > 0.99$), as shown by the fitted lines in Fig. 4.6a.

TABLE 4.3: Estimation of the amount of FA liberated from 2.6 g SMEDDS according to assumptions inferred from the literature [157–159] and maximal amount of hydrolysable ester bonds in 2.6 g SMEDDS.

Excipient	Composition in SMEDDS (% w/w)	Excipient composition (% w/w)	Excipient in 2.6 g formulation[b] (mmol)	FA liberation according to the literature[a] (mmol)	Max. available FA (mmol)
Miglyol 812	40	100 (TG)	2.01	4.03†	6.04
Imwitor 988	20	54.6 (TG)	1.45‡	1.45	1.45
		38.0 (TG)	0.58	0.58† and 0.58‡	1.16
		7.1 (TG)	0.077	0.15†	0.23
Cremophor RH 40	40	100 (TG)	0.39‡	0.09	1.16

[a] TG in Miglyol 812 and Imtiwor 988 are digested to *sn*-2 MG and 2 FA; *sn*-1,3 DG in Imwitor 988 are digested to *sn*-1 MG and 1 FA, and then to glycerol and 1 FA; *sn*-1 MG in Imwitor 988 are digested to glycerol and FA; Cremophor RH 40 was assumed to be hydrolyzed by 7.5% (w/w) according to Cuine *et al.* [203]. Digestion of TG to *sn*-1,2 DG and *sn*-2 MG and of *sn*-1,3 DG to *sn*-1 MG was assumed to occur rapidly (†, first stage), while the digestion of Cremophor RH 40 and of *sn*-1 MG to glycerol and FA was supposed to occur slowly (‡, second stage).
[b] Average molecular weights (g/mol) used for calculation: 516.8 (Miglyol 812), 196.2 (MG in Imwitor 988), 339.4 (DG in Imwitor 988), 482.6 (TG in Imwitor 988), 2699 (Cremophor RH 40 [203]).

These findings of lipolysis kinetics were used to propose a mathematical expression for solubility as a function of time. It was assumed that two phases contributed to overall solubility. An oil phase consisted of TG and DG, whereas a colloidal phase consisted primarily of MG. Both contributions to the total solubility were considered additively. Therefore, drug solubility in the first and second stages of lipolysis was given by Eqs. 4.5 and 4.6, respectively. Figure 4.6b demonstrates that the curve, which was calculated (not fitted) using these equations, accurately reflected the experimental solubility values. The drug solubility at 82.1 s was found by interpolation and corresponded to a value of 0.39 mg/ml. It must be mentioned that no single mathematical expression was able to describe adequately the change in drug solubility over the entire time course of lipolysis. Eqs. 4.2 and 4.4 were combined with Eqs. 4.5 and 4.6 to give the system of differential equations (Eqs. 4.7–4.11), which was fitted to the concentration data obtained by Raman spectroscopy. The model was found to excellently describe the experimental concentrations of precipitated drug ($R^2 > 0.975$) at all drug loads (Fig. 4.7). Table 4.4 details the values of A, B, k_g, g, t_n, and t_g that were estimated from this optimization. The nucleation parameters A and B had comparable values for all studied drug loads, while the nucleation induction time, t_n, increased with decreasing drug load. The growth parameters exhibited values within a similar range for each drug load. No fitting was carried out for the smallest drug loads of 20 and 30 mg/g because of the large scatter in Raman data.

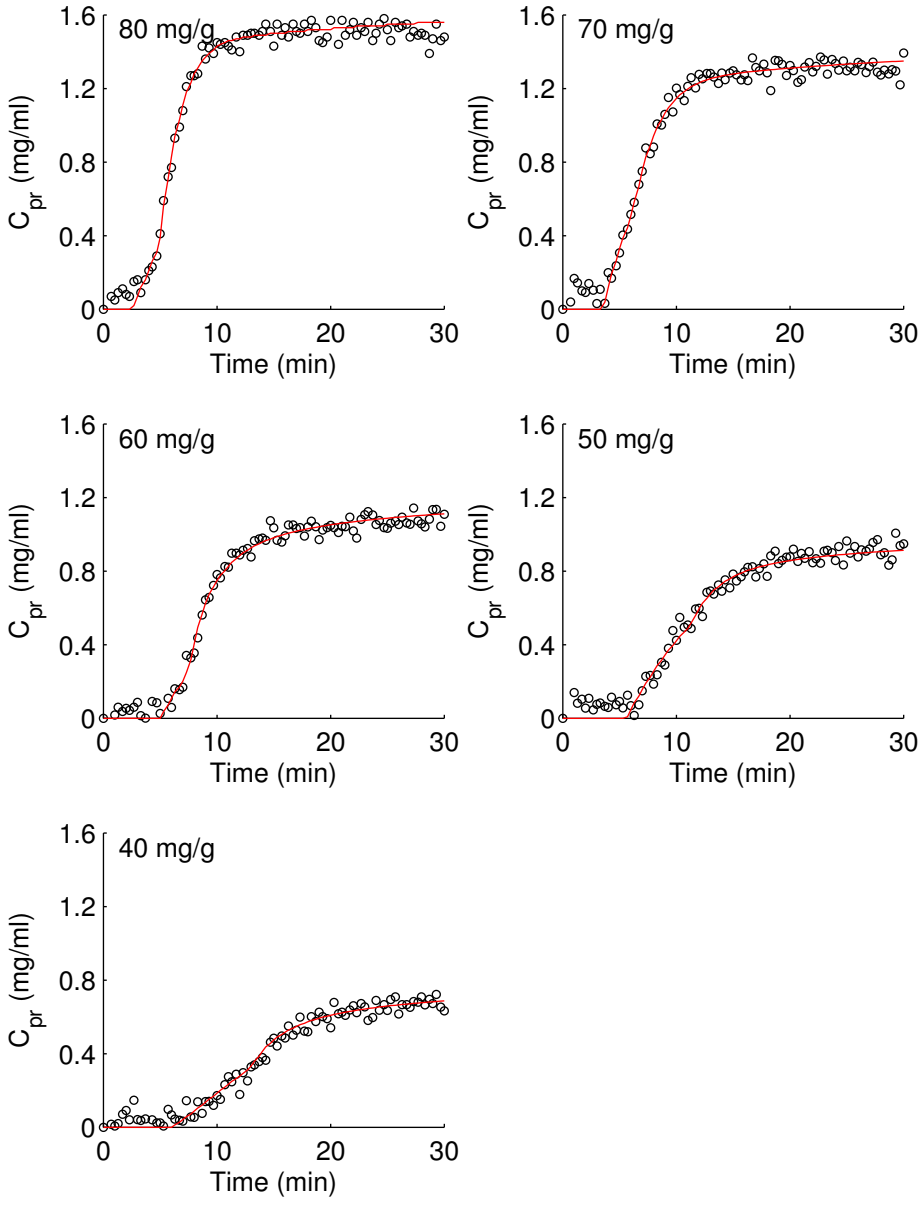

FIGURE 4.7: Concentration profile of precipitated fenofibrate as measured with Raman spectrocopy (*circles*) and as obtained from mathematical modeling (*red lines*). Each plot represents the result of a single drug loading and the circles are mean values of three experiments.

TABLE 4.4: Results of parameter estimation of drug precipitation kinetics.

C_{form} (mg/g)	A (μg·ml/s)	B	t_n (s)	t_g (s)	k_g (10^{-3}/s)	g	R^2	RMSE (mg/ml)
80	2.0	6.1	149.0	291.0	9.0	0.8	0.990	0.052
70	2.9	4.8	210.5	395.2	7.3	0.9	0.987	0.052
60	2.0	6.6	300.2	478.7	9.0	1.4	0.992	0.041
50	2.8	6.3	335.9	671.7	8.4	1.2	0.978	0.051
40	1.6	6.2	362.0	824.8	8.2	1.3	0.976	0.040

4.4 Discussion

4.4.1 Detection of drug precipitation during *in vitro* lipolysis

The fate of a LBDDS in the gastrointestinal tract is decisive for drug absorption and, therefore, for the performance of the formulation. Poorly water-soluble drugs often precipitate from lipid-based systems already upon dispersion in aqueous fluids. Such potentially inferior systems can be identified early in formulation screening using simple *in vitro* dilution and dispersion tests [41]. Other formulations exhibit drug precipitation in the course of formulation digestion. The analysis of such lipolysis-triggered drug precipitation was the main focus of the present work.

Traditionally, drug solubilization during *in vitro* lipolysis is analyzed using methods that rely on a sampling regime. Accordingly, aliquots of the digest are drawn from the lipolysis medium at defined time points and the concentration of solubilized and/or precipitated drug is usually measured following ultracentrifugation. This approach has so far provided fundamental knowledge on the lipolysis of lipid-based systems as well as the *in vitro* fate of poorly water-soluble drugs. However, real-time monitoring seems to be essential to further analyze the dynamic changes of the formulation and to study effects of drug supersaturation.

The first aim of this study was to evaluate Raman spectroscopy for real-time monitoring of drug precipitation during *in vitro* lipolysis. A model SMEDDS containing fenofibrate was digested using a common lipolysis test [146]. The application of Raman spectroscopy to *in vitro* lipolysis represented a particularly challenging case for monitoring of crystallization. While classical crystallization monitoring in chemical processes usually involves high drug concentrations and a constant medium, the present application of Raman spectroscopy had to cope with low analyte concentrations in a changing

digestion medium. The hydrolysis products interfered with the drug-related Raman signal and had to be considered in the interpretation of spectra. Moreover, the two off-line methods (ultracentrifugation and nanofiltration) revealed some conflicting results, which led to an even more challenging development of a robust calibration model. Hence, an accurate selection of instrumental parameters, chemometric procedures, and reference measurements was required.

The time courses of drug precipitation obtained from the two off-line sample preparation methods were dissimilar, particularly in the initial stage of precipitation. This difference was likely due to additional drug precipitation occurring during sample ultracentrifugation. Even though ultracentrifugation was proven to separate the solid, aqueous, and oil phases efficiently [26], the influence of sample preparation on drug precipitation can barely be avoided. First, there was an unavoidable time delay of up to 30 min between sample removal and ultracentrifugation. Second, we allowed ultracentrifugation to proceed for 90 min. This step usually takes a shorter time (30 min [26]), but we deliberately selected an extreme condition (90 min [25]) to simulate a worst-case sample preparation. These steps introduced time delays during which the drug could further precipitate. Therefore, the results of the ultracentrifugation method might not provide the actual kinetic concentration but rather an advanced stage of drug precipitation. This assumption was supported by the observation that drug concentrations in the aqueous phase, as measured upon ultracentrifugation, were almost equal to the corresponding solubilities. In contrast, the nanofiltration method allowed a more rapid separation of the liquid phase. This method has proven to effectively separate undissolved drug from colloidal drug solutions in biorelevant release tests [137].

The selection of calibration spectra and reference measurements relied on these previous findings. According to the nanofiltration results, the concentration of solubilized drug did not significantly change within the first minute of lipolysis. This observation proved that fenofibrate did not precipitate instantaneously when lipolysis was started, but only after an initial lag phase. It was therefore justified to include the earliest spectra and the corresponding nanofiltration result within the calibration set. Between 25 and 30 min of digestion, the nanofiltration and ultracentrifugation methods yielded consistent results and thus the corresponding spectra and reference values were included in the calibration set. Finally, between 40 s and 25 min there was a lack of reliable reference measurements, hence those spectra were excluded from the set of calibration spectra.

The generation of lipolysis products led to a notable increase in medium turbidity. This light scattering originated mostly from FA precipitation in the presence of calcium and from precipitated drug. To reduce particle-size effects, we selected adequate sampling optics consisting of a large spot-size Raman probe [221]. Furthermore, we evaluated different pre-processing algorithms for the entire set of Raman spectra prior to PLS regression analysis. This was necessary to correct for light scattering and residual particle-size

effects [219]. We found that an SG smoothing and differentiation filter (1^{st} derivative) was best for reducing this systematic variation. Residual sources of non-linearity were finally corrected by a three-component PLS regression model, while cross-validation demonstrated good robustness.

After spectra pre-processing and calibration, we applied the resultant quantification model to the entire data set. The real-time data demonstrated that drug started to precipitate after a lag phase of three to six min, while this period decreased with increasing drug load. Interestingly, there was excellent agreement between the course of drug precipitation obtained from Raman spectroscopy and from the nanofiltration method, even though only spectra from the initial and final time points were included in the calibration set.

Raman spectroscopy demonstrated clear advantages compared with the traditional ultracentrifugation method. The main issue in the latter method was the time delay caused by sample preparation. The application of benchtop centrifugation instead of ultracentrifugation, as proposed in a recent publication [26], could reduce this time delay. However, temporal resolution is still better using an *in situ* method such as Raman spectroscopy.

In contrast to ultracentrifugation, conventional Raman spectroscopy may be barely able to determine drug solubilization in the aqueous and the oil phases separately. However, the authors of a recent study suggested that the concentration of solubilized drug in the entire medium (and not only in the aqueous phase) may be the relevant measure for predicting intestinal permeation of a drug [120]. In this respect, Raman spectroscopy can provide the relevant data for estimating the absorbable dose fraction. Even though Raman spectroscopy was applied to the quantification of crystalline drug in the present case, the technique would also be able to quantify amorphous drug precipitation. This is certainly an advantage over, for example, *in situ* XRPD. However, the combination of XRPD and Raman spectroscopy is certainly of interest for studying transient polymorphic changes [222].

4.4.2 Kinetics of lipolysis-triggered drug precipitation

The second aim of the study was to determine the kinetics of drug precipitation during formulation lipolysis. Modeling precipitation kinetics may offer advantages in the biopharmaceutical characterization of lipid-based systems. Indeed, the amount of drug available for absorption does not only depend on whether or not the drug precipitates in the gastrointestinal lumen. Besides improving drug solubility, lipid-based formulations can increase bioavailability by the temporary stabilization of a drug in the supersaturated state. Although it is in a metastable condition, this induction time is particularly

relevant for compounds with good permeability. Indeed, supersaturation generates an increased flux across the intestinal membrane and precipitation *in vivo* may be reduced or even be absent. This awareness is crucial for formulation development. Drug supersaturation and the solid-state properties of a precipitate are often neglected during industrial screening tests of lipid-based formulations. Such candidate systems generally drop out of screening programs and, consequently, there is a risk of excluding candidate formulations that may still exhibit sufficient oral availability *in vivo*. Physiologically based pharmacokinetic (PBPK) models are valuable tools for predicting the formulation behavior *in vivo* on the basis of characteristics that are measured *in vitro* [41]. These models consider drug release and absorption as a dynamic interplay to predict the bioavailability of a drug. However, to obtain a precise estimation, PBPK modeling requires accurate prediction of supersaturation and potential drug precipitation during formulation dispersion and/or lipolysis.

4.4.2.1 Nucleation and growth model

We presented a nucleation and growth model that considered the dynamic changes in drug solubility during formulation digestion. The new model successfully described the data of lipolysis-triggered fenofibrate precipitation and yielded reasonable parameter values. The kinetic and thermodynamic pre-factors of the nucleation rate, A and B, respectively, were consistent for different drug loads and are in good agreement with the literature [197]. For such comparison, it has to be noted that the pre-factor A is here expressed as a mass concentration per unit time. The growth constant k_g and the exponent g were also in accordance with previously reported values [63].
When comparing the kinetics of drug precipitation with the kinetics of formulation lipolysis, we observed a non-linear correlation between the two variables (Fig. 4.8). This was interesting in relation to the findings of Sassene *et al.*, who observed linearity between precipitated cinnarizine and titrated FA using a self-microemulsifying formulation [33]. In this previous study, continuous calcium addition and the different sample preparation method (ultracentrifugation) may have influenced the observed kinetics. To clarify such effects, more studies that compare the different lipolysis tests using the same drug formulation are certainly needed.

Our study indicates that the nucleation time t_n decreased with increasing drug load, *i.e.*, with higher levels of supersaturation, in good agreement with expectation, as the degree of supersaturation generally decreases the induction period [63]. This dependence is highly relevant for selecting the adequate dose strength. Accordingly, the administration of a single lipid-based capsule with high dose strength might result in a different pharmacokinetic profile compared with the administration of multiple units at lower

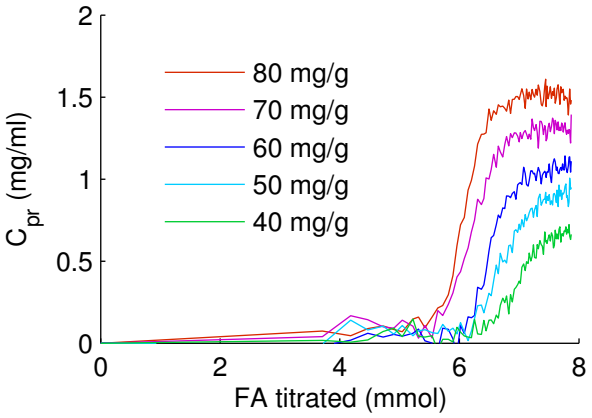

FIGURE 4.8: Fenofibrate precipitation as a function of titrated FA. Each color represents a single drug loading and is the mean value of three experiments.

dose strength. These considerations are in good agreement with a recent attempt to study the effects of drug loading on the lipolysis of lipid-based formulations [34].
Several studies used the *in vitro* digestion model to predict formulation performance *in vivo*. However, limited correlation between *in vitro* solubilization and *in vivo* exposure was often apparent. For instance, in an attempt to prove supersaturation stabilization in SEDDS with polymers, Anby *et al.* showed a clearly beneficial effect of polymer addition upon *in vitro* digestion, but no correlation was found with *in vivo* data [56]. Other studies showed an agreement between *in vitro* and *in vivo* data, but primarily as a rank-order correlation [19–21, 25, 223]. An improved characterization of drug supersaturation, precipitation, and re-dissolution might be the key to better understand the pharmacokinetic processes *in vivo*. To this end, real-time Raman spectroscopy, together with mathematical modeling of lipolysis-triggered drug precipitation, could play an important role. These techniques may become part of future drug absorption modeling and improve the predictivity of *in vitro–in vivo* correlations.

4.4.2.2 Drug solubility as a function of time

An important part of the presented nucleation and growth model was to consider the change in drug solubility as a function of time. The proposed heuristic function was in line with previous studies that proved a direct correlation between drug solubility and the concentration of formulation components and digestion products [102, 224, 225]. However, some discussion is needed to explain why the present heuristic approach was proposed. The pancreatin extract consisted of a mixture of digestive enzymes and co-enzymes, most importantly pancreatic lipase and co-lipase, as well as carboxyl ester hydrolase [226, 227]. These enzymes exhibit different lipolytic activities and substrate

specificities, as described previously [143, 157–159]. These properties of lipolytic enzymes and the composition of the model formulation suggested that lipolysis occurred in two stages. Pancreatic lipase and co-lipase are known to rapidly hydrolyze TG and DG at the *sn*-1,3 position, yielding *sn*-2 MG and FA as digestion products. It is assumed that this substrate specificity is due to the high affinity of the pancreatic lipase and co-lipase to insoluble lipids [157, 158]. In contrast, the second stage was likely characterized by the digestion of MG, which is catalyzed mostly by carboxyl ester hydrolase. This enzyme has high affinity to lamellar structures and micelles containing MG and its lipolytic activity is lower than that of pancreatic lipase [157, 158]. Although the regioselectivity of carboxyl ester hydrolase is still a debated topic, it is assumed to cleave MG preferentially at the *sn*-1 position [143, 228]. Sek *et al.* quantified the digestion products of medium-chain and long-chain glycerides upon *in vitro* digestion, using the same experimental conditions as in the present study [159]. Interestingly, *sn*-2 MG were weakly digested by porcine digestive enzymes, whereas *sn*-1 MG were hydrolyzed to a large extent. For this reason, we assumed that primarily *sn*-1 MG were digested in the second stage of lipolysis.

The amounts of DG and TG hydrolyzed during the first stage of lipolysis (as obtained from the titration data) were in good agreement with the nominal amount of lipids that was present in the formulation. For the second stage of lipolysis, we expected *sn*-1 MG and a small fraction of Cremophor RH 40 to be hydrolyzed (Table 4.3, FA liberation according to the literature). Interestingly, considering these assumptions, the amount of titrated FA exceeded the expected FA liberation. This observation could originate from higher Cremophor RH 40 hydrolysis than the reported fraction of 7.5% [203]. This value was obtained from the *in vitro* lipolysis of pure excipient and it might not be the same for Cremophor RH 40 digestion in a lipid mixture. Care is needed when assuming that a single excipient is digested equally to when it is present in combination with an oil phase in a formulation. The situation is particularly complex for surfactants, as they are known to act as substrates and as inhibitors of lipolytic enzymes [203]. A further explanation for the observed lipolysis degree is that some *sn*-2 MG were further digested. Mattson and Volpenhein observed that a small fraction of *sn*-2 MG exhibited a non-enzymatic isomerization to *sn*-1 MG [229]. In line with their observation, it seems possible that a small amount of *sn*-2 MG exhibited isomerization and was further digested.

As a result, the proposed equation for fenofibrate solubility as a function of time was in very good agreement with the experimental solubility values. DG and TG were the most lipophilic glycerides present in the formulation. Therefore, the removal of these compounds was correlated with a pronounced decrease in fenofibrate solubilization. In contrast, we measured a less pronounced decrease during the second stage of lipolysis because of the smaller contribution of MG to solubilization.

4.5 Conclusions

Real-time analytics is fundamental to gain an improved understanding of the highly dynamic processes of formulation digestion. In this study we evaluated the quantitative application of Raman spectroscopy for real-time monitoring of drug precipitation during *in vitro* lipolysis. The method was compared with two off-line procedures, which were based on a sampling regime. Raman spectroscopy measured fenofibrate precipitation with a high temporal resolution and minimal experimental bias. In contrast, care is needed when determining the kinetics of drug precipitation by methods that require sample preparation. Indeed, the lag time between sample removal and analysis could lead to further drug precipitation.

The precipitation profiles obtained by Raman spectroscopy were used to model the kinetics of lipolysis-triggered drug precipitation. We introduced a mathematical model, which was based on theoretical equations of nucleation and growth by considering solubility changes over time. This model provided an excellent prediction of fenofibrate crystallization during lipolysis. The drug began to precipitate after an initial lag phase of supersaturation. The temporary supersaturation is not only of theoretical interest. This metastable state is particularly important for poorly water-soluble compounds with high permeability, *i.e.*, when the process of drug precipitation occurs in a similar time span as drug absorption.

The proposed model for lipolysis-triggered drug precipitation may be part of more complex pharmacokinetic models. Physiologically based drug absorption models are particularly interesting in this aspect. More refined mechanistic modeling of this type will ultimately help to better predict the fate of a LBDDS *in vivo*.

Chapter 5

Biopharmaceutical modeling of drug supersaturation during lipid-based formulation digestion considering an absorption sink

Summary

In vitro lipolysis is widely utilized for predicting *in vivo* performance of oral lipid-based formulations (LBFs). However, evaluation of LBFs in the absence of an absorption sink may have limited *in vivo* relevance. This study aimed at employing biopharmaceutical modeling to simulate LBF digestion and drug supersaturation in a continuous absorptive environment. Three fenofibrate-loaded LBFs were characterized *in vitro* (dispersion and lipolysis) and drug precipitation was monitored using in-line Raman spectroscopy. *In vitro* data were combined with pharmacokinetic data derived from an *in vivo* study in pigs to simulate intestinal LBF transit. This biopharmaceutical model allowed calculation of lipolysis-triggered drug supersaturation while drug and lipolysis products are absorbed from the intestine. The biopharmaceutical model predicted that, in a continuous absorption environment, fenofibrate supersaturation was considerably lower compared to *in vitro* lipolysis (non-sink). Hence, the extensive drug precipitation observed *in vitro* was predicted to be unlikely *in vivo*. The absorption of lipolysis products increased drug supersaturation, but drug precipitation was unlikely for highly permeable

Stillhart C. *et al.* Biopharmaceutical modeling of drug supersaturation during lipid-based formulation digestion considering an absorption sink, *Pharmaceutical Research*, **2014**, in press.

drugs. Biopharmaceutical modeling is a valuable approach for predicting LBFs performance *in vivo*.

5.1 Introduction

Low aqueous solubility and poor dissolution in the gastrointestinal (GI) fluids are major reasons for limited oral absorption of poorly water-soluble compounds. Such drug candidates may therefore exhibit low and variable oral bioavailability, which hinders effective drug development. Lipid-based formulations (LBFs) are gaining increasing interest as a drug delivery strategy for poorly water-soluble compounds. The improvement in oral bioavailability is obtained via several mechanisms. The critical dissolution step is circumvented and the apparent drug solubility in GI fluids is generally increased in presence of lipidic excipients. Additionally, lipid excipients may increase drug permeability across the intestinal membrane and promote drug uptake via the intestinal lymphatics [190].

The improvement of oral absorption from LBFs is also significantly influenced by the fate of the LBF in the GI tract. Digestion of lipidic excipients by endogenous lipases is particularly critical due to the formation of more polar lipolysis products (*i.e.*, monoglycerides (MGs) and fatty acids (FAs)) and the potential of drug precipitation. Such drug precipitation *in vivo* is undesirable, as subsequent re-dissolution is likely to delay and/or reduce the overall extent of drug absorption. The solid-state properties of the precipitate that forms *in vivo* therefore become critical. While it has been shown for some drugs that the formation of an amorphous precipitate may be favorable in terms of higher apparent solubility and facilitated re-dissolution, this is not the case in all drug types [33, 34]. There is growing evidence that the kinetics of precipitation is also a significant determinant of LBF performance *in vivo* [38, 56]. From a biopharmaceutical perspective, the initial induction period of drug nucleation is highly relevant, as during this stage the actual drug concentration exceeds equilibrium solubility, *i.e.*, the drug is supersaturated. Although being thermodynamically unstable, this supersaturated state promotes absorptive flux across the intestinal membrane, and hence, the longer the induction period, the more drug can be absorbed [38]. To maximize the biopharmaceutical benefit, supersaturation should be high enough to enhance drug uptake, but without inducing nucleation of drug particles in a physiologically relevant time span.

An *in vitro* lipolysis assay is commonly employed to study the impact of digestion on the drug solubilization capacity of LBFs [146, 147]. Formulation digestion is performed using simulated intestinal medium and pancreatic enzymes, and the digestion is monitored by direct titration of the liberated FAs. Several reports categorized LBFs in terms of their propensity for lipolysis-triggered precipitation *in vitro*, but the *in vivo* performance was

successfully predicted only in few studies and mainly rank-order correlations have been observed [230]. Strategies are therefore necessary to improve accuracy of *in vitro–in vivo* correlation (IVIVC) for LBFs. It is hypothesized that a major limitation of the current *in vitro* lipolysis test is the absence of an absorptive sink compartment. Given that the current test is a closed system (*i.e.*, no absorption sink), the drug concentrations may differ from those observed *in vivo*, especially for highly permeable compounds, which are continuously removed via absorption.

In an attempt to improve the relevance to the *in vivo* situation, Shi *et al.* developed a biphasic system, comprising an aqueous buffer and an organic solvent as acceptor phase [50]. Although a good IVIVC was obtained, this approach was only suitable for simulating LBF dispersion in the absence of biorelevant media. Alternative approaches using artificial or biological membranes [51] have also been applied, but in addition to the increased model complexity, critical parameters, such as the appropriate filter membrane selection (regarding molecular cut-off) as well as the small surface area for absorption require careful consideration.
Computational methods are a promising alternative for simulating complex biopharmaceutical processes. Most recently, Fei *et al.* presented such an *in silico* approach for modeling the GI performance of self-emulsifying formulations [37]. Thus, *in vitro* dissolution data (without digestive enzymes) were incorporated in a biopharmaceutical model to simulate simultaneous formulation dispersion and drug absorption. The resulting *in silico* model suitably predicted oral bioavailability in humans. The LBFs comprised mostly surfactants (SFs) with comparatively low amounts of digestible lipids, and hence, LBF dispersion was considered the most critical step with respect to drug precipitation. However, in presence of larger amounts of digestible lipids, formulation digestion may become increasingly critical. For such formulations, the possibility to model formulation lipolysis and lipolysis-triggered drug precipitation is highly desirable. Recently we introduced a mathematical nucleation and growth model that described drug precipitation during formulation lipolysis [31]. This model was based on *in vitro* lipolysis data that were acquired under standard conditions, *i.e.*, without an absorption sink.

The purpose of the present study was to develop a computational approach to predict the impact of formulation digestion in an absorption environment. To this end, using both *in vitro* and *in vivo* data, we developed an *in silico* biopharmaceutical model of LBF digestion and simultaneous drug absorption. Intestinal drug concentration profiles were derived from an *in vivo* study (in pigs) following oral administration of three fenofibrate-loaded LBFs [29]. A mathematical model simulating the time evolution of drug solubility in the intestine was developed based on *in vitro* solubility and *in vitro* lipolysis data. The biopharmaceutical model was then used to calculate intralumenal

drug supersaturation to predict the likelihood of lipolysis-triggered drug precipitation *in vivo*.

5.2 Materials and methods

5.2.1 Materials

Fenofibrate (2-[4-(4-chlorobenzoyl)phenoxy]-2-methylpropionic acid 1-methylethyl ester, ≥99%), olive oil Ph. Eur., Tween® 85, Trizma® maleate, calcium chloride dihydrate (≥99%), pancreatin (from porcine pancreas, 8xUSP specifications), chloroform, and acetonitrile were obtained from Sigma-Aldrich Chemie GmbH (Buchs, Switzerland), and sodium chloride (≥99%) from Carl Roth GmbH (Karlsruhe, Germany). Lipoid® E PC S (phosphatidylcholine from egg yolk) was supplied by Lipoid GmbH (Ludwigshafen, Germany), sodium taurodeoxycholate by Prodotti Chimici e Alimentari S.p.A. (Basaluzzo, Italy), sodium hydroxide 1 M by Scharlab S.L. (Sentmenat, Spain), and 4-bromophenylboronic acid (4-BPBA, ≥95.0%) by AK Scientific (Union City, CA, USA). Miglyol® 812 N was purchased from Hänseler AG (Herisau, Switzerland), and Cremophor® RH 40 from BASF AG (Ludwigshafen, Germany). Purified water was prepared using an Arium® 61215 water-purification system from Sartorius Stedim Biotech GmbH (Göttingen, Germany). We used Anotop® 25 Plus filters (aluminum oxide, 0.1 μm) purchased from Whatman GmbH (Dassel, Germany) for nanofiltration.
Miglyol 812 N was a medium-chain triglyceride (TG) consisting of 57.9% w/w caprylic acid (C8), 41.2% w/w capric acid (C10), 0.5% w/w lauric acid (C12), and 0.1% w/w caproic acid (C6) with an average molecular weight of 517 g/mol (according to the certificate of analysis, Hänseler AG, Switzerland). Olive oil Ph. Eur. is a natural TG principally composed of oleic acid (C18, 80%) and linoleic acid (C18, ∼20%). Tween 85 is a polyoxyethylene sorbitan trioleate surfactant (HLB 11) and Cremophor RH 40 is polyoxyl 40 hydrogenated castor oil (HLB 15).

5.2.2 Preparation of formulations

The compositions of the three LBFs used in this study are summarized in Table 5.1. The model LBFs comprised two SFs (Cremophor RH 40 and Tween 85) at a fixed ratio of 1:2 w/w. Formulation IIIB/IV was a surfactant-only system, whereas IIIA LC and IIIA MC additionally comprised an oil component of 40% w/w olive oil (long-chain TG) and 40% w/w Miglyol 812 (medium-chain TG), respectively.

The excipients were weighted and mixed until a clear solution was obtained. Fenofibrate was then incorporated into the formulations at 80 mg/g, which corresponded to a saturation level of 56%, 83%, and 77% in formulation IIIA LC, IIIA MC, and IIIB/IV, respectively [29]. The blends were stirred at 50°C for 30 min and stored overnight at 37°C to ensure complete dissolution of the drug. All formulations were visually assessed for absence of undissolved drug particles prior to use.

TABLE 5.1: Composition of the formulations IIIA LC, IIIA MC, and IIIB/IV.

Component	IIIA LC	IIIA MC	IIIB/IV
Olive oil	40 % w/w	-	-
Miglyol 812	-	40 % w/w	-
Cremophor RH 40	20 % w/w	20 % w/w	33 % w/w
Tween 85	40 % w/w	40 % w/w	67 % w/w
Fenofibrate	80 mg/g	80 mg/g	80 mg/g

5.2.3 *In vitro* lipolysis

The *in vitro* lipolysis test was performed as described in the literature [146]. Briefly, 108 ml of a micellar solution (50 mM Trizma maleate, 150 mM NaCl, and 5 mM $CaCl_2{\cdot}2H_2O$; pH 7.5) were heated in a thermostated glass vessel (37.0 ± 0.5°C) and the formulation (3 g) was added. The mixture was stirred (450 rpm, 10 min) for complete dispersion, thermal equilibration, and pH adjustment to 7.5. Digestion was initiated with the addition of 12 ml pancreatin extract (final nominal lipase activity: 1000 tributyrin units per ml) obtained from porcine pancreatin powder [146].
The free FAs produced during lipolysis were titrated using 1 M NaOH to maintain pH 7.5 using a pH-stat apparatus (842 Titrando and 800 Dosino, Metrohm AG, Switzerland), with the Tiamo 1.2 software package (Metrohm AG, Switzerland). Lipolysis was allowed to proceed for 60 min. To determine the NaOH consumption caused by digestion of the blank digestion medium, lipolysis experiments were run with pure digestion medium without formulation. *In vitro* lipolysis was assayed in triplicate with each formulation.
To determine the total amount of FAs released during formulation digestion a so-called "back-titration" was conducted as previously described [31]. This was necessary because some FAs exist in their unionized state, according to the pK_a value, leading to an underestimation of the amount of total FAs liberated.
The extent of formulation digestion was calculated according to:

$$\text{Extent of digestion} = \frac{\text{FA}_{titr}^{tot}}{\text{Theor. amount of digestible FAs in LBF}} \tag{5.1}$$

where FA_{titr}^{tot} was the total amount of ionized and unionized FAs liberated by 60 min of digestion. The theoretical amount of digestible FAs in LBFs was calculated assuming that each TG and SF molecule liberated two FAs.

5.2.4 Quantification of drug precipitation using Raman spectroscopy

Raman spectroscopy was used to quantify fenofibrate precipitation during *in vitro* lipolysis as previously described [31]. A multi-fiber Raman P^hAT probe and a Raman RXN1 analyzer (Kaiser Optical Systems, Inc., Ann Arbor, MI, USA) equipped with a diode laser (wavelength of 785 nm, laser power of 400 mW) were used. A single spectrum was collected every 20 s (acquisition time 18.5 s) with a resolution of 4 cm^{-1} using the iC Raman Instrument software (Version 3.0, Mettler-Toledo AutoChem Inc., Columbia, MD, USA).

To remove sources of non-linearity and spectral information that was uncorrelated with the concentration of the analyte, the spectra were subjected to the Savitzky–Golay polynomial derivative filter [31]. The spectral range corresponding to the fingerprint range of fenofibrate (1000–1800 cm^{-1}) was used for drug quantification. All data were mean-centered and, finally, a calibration model was built by partial least-squares (PLS) regression [219]. The optimal number of PLS factors was defined for which the root-mean-square error of cross-validation reached a minimum (<1% of spectral variation). Cross-validation was determined with the leave-one-out method; spectral preprocessing and PLS regression were calculated using Matlab® (MathWorks, Naticks, MA, USA). The calibration models were evaluated in terms of the correlation coefficient, R^2, the cross-validation coefficient, Q^2, the root-mean-square error of calibration (RMSEC), and of cross-validation (RMSECV).

The concentration of solubilized drug in the digests was determined using an off-line method as reference for the calibration of Raman spectra [31]. A 2 ml sample was removed from the lipolysis medium prior to and after 5, 10, 15, 20, 25, 30, 40, 50, 60 min of lipolysis. The samples were directly passed through an Anotop 25 Plus syringe filter (pore size 0.1 μm, aluminum oxide filter membrane) and the filtrate was immediately diluted in acetonitrile to halt further lipolysis. Control experiments were also performed that verified that no loss of dissolved drug occurred via potential filter adsorption. The samples were then centrifuged (16,000xg, 30 min) and analyzed by HPLC [31].

5.2.5 X-ray powder diffraction

X-ray powder diffraction (XRPD) was used to determine the solid-state properties of fenofibrate precipitating during *in vitro* lipolysis. LBFs containing fenofibrate were digested for 60 min and, after enzyme inhibition, an aliquot was ultracentrifuged (80,000xg, 37°C, 90 min) in a Centrikon T-1180 ultracentrifuge equipped with a TFT-80.4 fixed-angle rotor (Kontron Instruments, Milan, Italy). The pellet phase was immediately isolated and an X-ray diffractogram was recorded. The same procedure was followed with the pellet phase obtained from a 60 min lipolysis experiment with drug-free formulation, which was spiked with an equal amount of pure fenofibrate (as used for LBF preparation). Moreover, the X-ray diffractogram of crystalline fenofibrate was recorded as reference. We used a theta-theta X-ray powder diffractometer (R-XRD Phaser D2, Bruker AXS GmbH, Karlsruhe, Germany) equipped with a Co and Cu KFL tube (30 kV, 10 mA) as radiation source and a Lynxeye® detector. The samples were scanned in the angular range of 5° (2θ) to 40° (2θ) with a step size of 0.1° (2θ) and a count time of 5 s per step.

5.2.6 Measurement of fenofibrate solubility in lipolysis medium at different lipolysis times

The solubility of fenofibrate in lipolysis medium containing LBF was determined at different lipolysis times ($C^*_{m,t}$). *In vitro* lipolysis with drug-free formulation was performed as described and enzyme inhibitor (4-bromophenylboronic acid, 1M in methanol, 9 μl per ml of digest) was added to the medium at defined time points to stop further digestion. An aliquot was transferred to hermetically sealed glass vials and excess solid fenofibrate was added. The samples were equilibrated (450 rpm, 37°C), and an aliquot was centrifuged after 4 h, 8 h, and 24 h (16,000xg, 37°C, 30 min). The solubilities were found to decrease after 24 h of equilibration, which was attributed to kinetic instability of the colloidal structures in digested medium [27, 31, 56]. The liquid phase was diluted in acetonitrile, centrifuged (16,000xg, 15 min), and finally analyzed by HPLC. Whenever a distinct lipid phase was obtained upon centrifugation, the lipid and the aqueous phase were re-emulsified to measure the overall concentration of solubilized drug. Drug solubility experiments were carried out in triplicate with each formulation.

5.2.7 Determination of the *in vivo* bioavailability of fenofibrate-loaded LBFs

The pharmacokinetic (PK) profiles of fenofibric acid after peroral (p.o.) administration of formulation IIIA LC, IIIA MC, and IIIB/IV and after intravenous (i.v.) administration of a fenofibrate solution were obtained from the literature [29]. Briefly, six male landrace pigs (15–20 kg, mean 17.5 kg) were fasted for 16 h prior to experiments. On day 1, an indwelling i.v. catheter was inserted into the jugular vein under general anaesthesia. On day 3, following an overnight fast, the oral formulations were administered in gelatine capsules with the aid of a dosing gun, after which the pigs received ∼50 ml of tap water via a syringe. The animals had continuous access to water during the study and were fed 8 h after LBF administration. Blood samples (4 ml) were collected pre-dosing and 0.5, 1, 2, 3, 4, 6, 8, 12, 24, and 48 h post-dosing. The study was conducted as a three way cross-over, with a 7 day washout period. For the i.v. dosing, a separate group of four pigs were administered 25 mg fenofibrate dissolved in ethanol-based solution. The solution was administered by slow infusion (over 2 min) of 3 ml of a solution containing 8.33 mg/ml fenofibrate in 80% w/w ethanol (96% w/v) and 20% saline into an ear vein. Blood sampling was performed as outlined above, with an additional three blood samples taken at 0.0833, 0.25, 0.75 h post-dose. The concentration of the active metabolite fenofibric acid was then determined in blood samples, since fenofibrate is rapidly and completely transformed to fenofibric acid by tissue and plasma esterases [231].

5.3 Theoretical section

A mathematical model that simulates the time course of drug supersaturation in the intestine after oral administration of LBFs was developed. This profile was then used to estimate the likelihood of lipolysis-triggered drug precipitation in an absorption environment. In order to model intestinal drug supersaturation, the concentration of solubilized drug and drug solubility in intestinal fluids was required. The intralumenal concentrations of solubilized drug were derived from *in vivo* plasma concentration *versus* time data. The time evolution of drug solubility in the intestinal fluids was calculated by combining *in vitro* solubility and lipolysis data with the pharmacokinetic parameters derived from the *in vivo* studies.

5.3.1 Modeling the drug concentration profile in the intestine

To model the profile of solubilized fenofibrate in the intestinal lumen, $C_{id}(t)$, we fitted a physiologically based pharmacokinetic model to the *in vivo* PK data obtained from pig studies. The plasma profile of fenofibric acid obtained after i.v. administration was used to estimate the rate constants of drug disposition (k_{pt}, k_{tp}) and elimination (k_{el}), as well as the volume of distribution in the plasma compartment (V_d) by fitting a two-compartment model to the experimental data according to the equations:

$$\frac{\mathrm{d}D_p(t)}{\mathrm{d}t} = -k_{el} \cdot D_p(t) - k_{pt} \cdot D_p(t) + k_{tp} \cdot D_t(t) \tag{5.2}$$

$$\frac{\mathrm{d}D_t(t)}{\mathrm{d}t} = k_{pt} \cdot D_p(t) - k_{tp} \cdot D_t(t) \tag{5.3}$$

$$C_p(t) = \frac{D_p(t)}{V_d} \tag{5.4}$$

where D_p and C_p are the drug mass and concentration in the plasma, respectively; D_t is the drug mass in the peripheral tissue; k_{pt} and k_{tp} are the rate constants for drug disposition from plasma to peripheral tissue and from peripheral tissue to plasma, respectively.

The PK profiles obtained after oral administration of LBFs were then described using Eqs. 5.5–5.11 (Figure 5.1):

$$\frac{\mathrm{d}D_{gu}(t)}{\mathrm{d}t} = -k_{gd} \cdot D_{gu}(t) - k_{ge} \cdot D_{gu}(t) \tag{5.5}$$

$$\frac{\mathrm{d}D_{gd}(t)}{\mathrm{d}t} = k_{gd} \cdot D_{gu}(t) - k_{ge} \cdot D_{gd}(t) \tag{5.6}$$

$$\frac{\mathrm{d}D_{iu}(t)}{\mathrm{d}t} = k_{ge} \cdot D_{gu}(t) - k_{id} \cdot D_{iu}(t) \tag{5.7}$$

$$\frac{\mathrm{d}D_{id}(t)}{\mathrm{d}t} = k_{ge} \cdot D_{gd}(t) + k_{id} \cdot D_{iu}(t) - P_{eff,FF} \cdot \frac{2}{r} \cdot f \cdot D_{id}(t) \cdot 3600 \tag{5.8}$$

$$\frac{\mathrm{d}D_p(t)}{\mathrm{d}t} = P_{eff,FF} \cdot \frac{2}{r} \cdot f \cdot D_{id}(t) \cdot 3600 - k_{el} \cdot D_p(t) - k_{pt} \cdot D_p(t) + k_{tp} \cdot D_t(t) \tag{5.9}$$

$$C_p(t) = \frac{D_p(t)}{V_d} \cdot F_a \tag{5.10}$$

$$C_{id}(t) = \frac{D_{id}(t)}{V_i} \tag{5.11}$$

D_{gu} and D_{gd} are the drug mass in undispersed and dispersed LBF in the stomach, respectively; D_{iu} and D_{id} are the drug mass in undispersed and dispersed LBF in the intestine, respectively. We assumed an effective permeability coefficient for fenofibrate, $P_{eff,FF}$, of $2.66{\cdot}10^{-5}$ cm/s [37], an intestinal radius, r, of 1.5 cm [186], and an effective surface expansion factor, f, of 30 [232]. A volume of intestinal fluids, V_i, of 50 ml was assumed, which corresponded to the volume of co-administered water. The gastric emptying constant, k_{ge}, and the fraction absorbed, F_a, were estimated by regressing Eqs. 5.5–5.11 to the plasma concentration profiles obtained after p.o. administration of formulations IIIA LC, IIIA MC, and IIIB/IV.

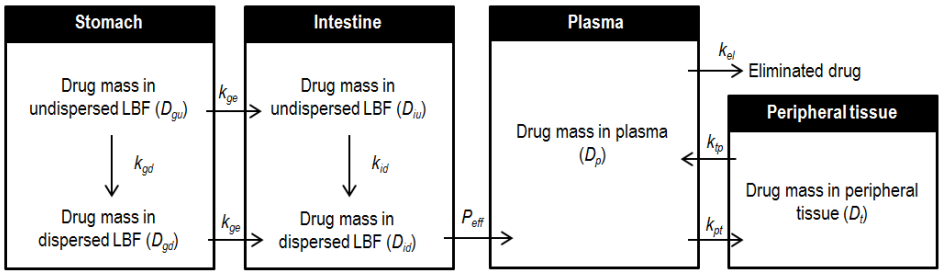

FIGURE 5.1: Scheme of model parameters describing drug transit after oral administration of LBFs.

The dispersion rate constants in gastric fluid, k_{gd}, and in intestinal fluid, k_{id}, were obtained from the results of *in vitro* dissolution/dispersion testing reported by Griffin *et al.* [29]. This test was performed using a mini-vessel dissolution apparatus containing fasted-state simulated gastric fluid (FaSSGF) and fasted-state simulated intestinal fluid (FaSSIF-v2). The constants k_{gd} and k_{id} were obtained by fitting a first-order kinetic equation to the dispersion profiles measured in FaSSGF and FaSSIF-v2, respectively (Table 5.2).

TABLE 5.2: Dispersion rate constants (value ± 95% CI) in FaSSGF and FaSSIF-v2, as obtained from the fitting of data described in the literature [29]. The distinction between dispersed an undispersed formulation was given by the experimental mini-vessel test. The dispersion rates were described excellently by a first order kinetic equation ($R^2 > 0.93$).

Formulation	k_{gd} (h^{-1})	k_{id} (h^{-1})
IIIA LC	10.9 ± 1.3	15.2 ± 1.5
IIIA MC	7.4 ± 3.1	7.2 ± 1.9
IIIB/IV	9.0 ± 1.8	6.4 ± 0.6

It should be noted that this biopharmaceutical model assumed no drug precipitation in the GI lumen. Moreover, the model assumptions included that drug absorption occurred only in the intestine and only from dispersed formulation (*i.e.*, no absorption occurred in the stomach and from undispersed formulation). Modeling was performed using Matlab. The differential equations were numerically solved using the *ode45* solver, and optimization procedures were carried out with the *fminsearch* algorithm.
To evaluate the goodness of fit (modeled *versus* experimental plasma data), the similarity factor, f_2, was calculated as follows:

$$f_2 = 50 \cdot \log\left(\sqrt{1 + \frac{1}{n} \cdot \sum_{i=1}^{n} (M_i - T_i)^2} \cdot 100\right) \tag{5.12}$$

where n is the number of sampling time points, M_i is the ratio between the plasma concentration at time point i and the maximum plasma concentration in the modeled profile, and T_i is the ratio between the plasma concentration at time point i and the maximum value in the experimental plasma concentration profile [233].

5.3.2 Modeling the time evolution of drug solubility during LBF digestion

A mathematical approach to model drug solubility during formulation lipolysis in the intestinal environment was developed. Initially, a general model of drug solubility during *in vitro* formulation lipolysis was developed. Subsequently, this model was applied to simulate drug solubility in the intestinal environment (*i.e.*, under continuous absorptive conditions). This solubility profile is finally used to calculate the time course of drug supersaturation and, hence, to estimate the likelihood of precipitation from LBFs under physiological conditions.

5.3.2.1 Theoretical concept

Previously, we have reported a heuristic approach to model the time evolution of drug solubility during *in vitro* lipolysis [31]. This approach assumed that different lipidic species contributed additively to the overall drug solubility. Therefore, drug solubility was proportional to the concentration of lipids and of lipolysis products (LPs). A similar assumption was applied to the current study to model the time evolution of drug solubility during LBF digestion. However, the model was intended to simulate drug solubility not only during *in vitro* lipolysis (closed system), but also during the intestinal transit of LBFs (open system). Some adaptations of the previous mathematical model

were therefore necessary.

The theoretical concept of solubility modeling is represented graphically in Figure 5.2. The amount of TGs and SFs decreases during formulation digestion. As it can be assumed that there is linearity between the concentration of lipids and drug solubility [199, 234], the drug solubilization caused by these excipients reduces accordingly ($C^*_{TG,t}$ and $C^*_{SF,t}$, respectively). At the same time, the hydrolysis of TGs and SFs liberates LPs, which can contribute to drug solubilization. This increasing solubility is represented by $C^*_{LP1,t}$ and $C^*_{LP2,t}$, where LP1 are lipolysis products liberated from TGs and LP2 are lipolysis products liberated from SFs. Fenofibrate solubility in pure lipolysis medium (without LBF) was comparatively small and was hence considered negligible for solubility modeling.

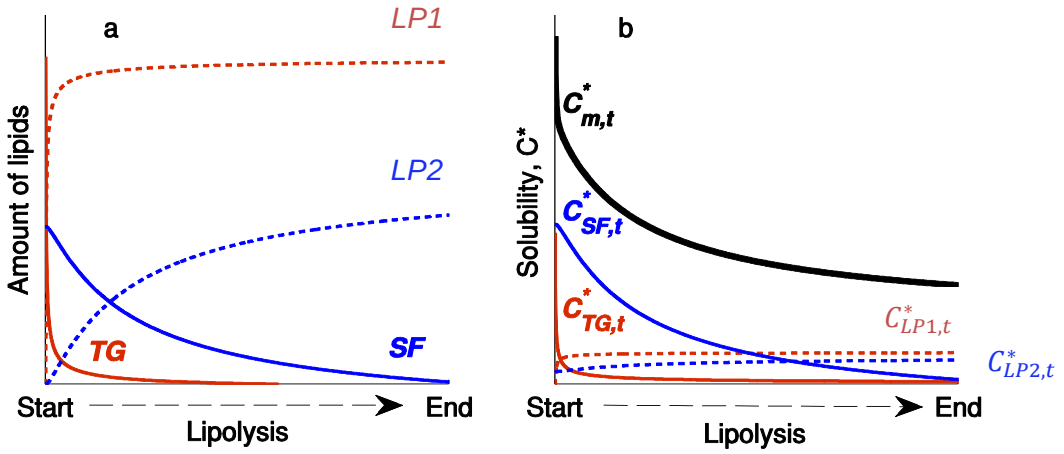

FIGURE 5.2: Time evolution of (a) lipidic species and (b) drug solubilities in the lipolysis medium during LBF digestion (assuming no LPs absorption). Colored lines represent the amounts and solubility contributions of the single lipidic species and the black line represents the resulting overall drug solubility.

In summary, the overall drug solubility in the lipolysis medium, $C^*_{m,t}$, was calculated by considering the contribution of each lipidic species additively:

$$C^*_{m,t} = C^*_{TG,t} + C^*_{SF,t} + C^*_{LP1,t} + C^*_{LP2,t} \tag{5.13}$$

To determine these contributions, a relative drug solubility value was introduced, which was the amount of drug that is solubilized by 1 mmol of excipient per ml of lipolysis medium at equilibrium ($\mathrm{mg \cdot ml^{-1} \cdot mmol^{-1}}$). Thus, the product of the relative fenofibrate solubility and the corresponding amount of excipient as a function of time (mmol) determined the time course of each partial contribution to drug solubility:

$$C^*_{m,t}(t) = \hat{C}^*_{TG} \cdot TG(t) + \hat{C}^*_{SF} \cdot SF(t) + \hat{C}^*_{LP1} \cdot LP1(t) + \hat{C}^*_{LP2} \cdot LP2(t) \tag{5.14}$$

where $\hat{C}^*_{TG}$, $\hat{C}^*_{SF}$, $\hat{C}^*_{LP1}$, and $\hat{C}^*_{LP2}$ are the relative fenofibrate solubilities in TGs, SFs, LP1, and LP2, respectively, and *TG(t)*, *SF(t)*, *LP1(t)*, and *LP2(t)* are the molar amounts of excipient at time *t*.
Formulation IIIB/IV contained only SF and, thus, the overall drug solubility was calculated according to:

$$C^*_m(t) = \hat{C}^*_{SF} \cdot SF(t) + \hat{C}^*_{LP2} \cdot LP2(t) \tag{5.15}$$

The values of $\hat{C}^*_{TG}$, $\hat{C}^*_{SF}$, $\hat{C}^*_{LP1}$, and $\hat{C}^*_{LP2}$ were derived from experimental solubility data as described in the next section. Modeling and simulation of solubility profiles was performed using Matlab.

5.3.2.2 Calculation of relative drug solubilities

The relative drug solubilities $\hat{C}^*_{TG}$, $\hat{C}^*_{SF}$, $\hat{C}^*_{LP1}$, and $\hat{C}^*_{LP2}$ were obtained from experimental solubility values with undigested (for $\hat{C}^*_{TG}$ and $\hat{C}^*_{SF}$) and digested (for $\hat{C}^*_{LP1}$ and $\hat{C}^*_{LP2}$) formulations.
Formulation IIIB/IV was composed of SFs only and, hence, the drug solubilities measured in undigested and digested formulation IIIB/IV were used to calculate $\hat{C}^*_{SF}$ and $\hat{C}^*_{LP2}$, respectively. $\hat{C}^*_{SF}$ corresponded to the solubility $C^*_{m,0}$ (*i.e.*, drug solubility in 100% undigested SF) divided by the molar amount of SF in dispersion at t=0, SF_{tot} (Eq. 5.16). $\hat{C}^*_{LP2}$ was the relative drug solubility in completely digested formulation IIIB/IV (*i.e.*, only LP2). An experimental value was not available, because formulation IIIB/IV was only partially digested by 60 min of *in vitro* lipolysis. However, it is known from literature that there is a linear relationship between the concentration of a SF and drug solubility [199]. Thus, we determined $\hat{C}^*_{LP2}$ via linear extrapolation based on the measured drug solubility $C^*_{m,60}$ and the extent of digestion by 60 min of lipolysis; the resulting value was then divided by the molar amount of LP2 at the end of digestion, $\mathrm{LP2}_{tot}$ (Eq. 5.17). It has to be noted that formulation IIIA LC and IIIA MC also contained Cremophor RH 40 and Tween 85 at a ratio of 1:2. Thus, the calculated values of $\hat{C}^*_{SF}$ and $\hat{C}^*_{LP2}$ were the same for each formulation.
The relative solubility $\hat{C}^*_{TG}$ was calculated for the oil-containing formulations IIIA LC and IIIA MC only. Prior to lipolysis, fenofibrate was solubilized by undigested SF and TG. Thus, the contribution of TGs to drug solubility was the difference between the overall drug solubility, $C^*_{m,0}$, and the contribution of SFs, C^*_{SF}. C^*_{SF} was the product of the relative solubility $\hat{C}^*_{SF}$ and the molar amount of undigested SF prior to lipolysis, (SF_0). This difference was then divided by the molar amount of TGs in dispersion at $t = 0$, TG_{tot} (Eq. 5.18).
Finally, $\hat{C}^*_{LP1}$ was obtained by regressing Eq. 5.14 to the experimental solubility values,

$C^*_{m,t}$ for formulations IIIA LC and IIIA MC.

$$\hat{C}^*_{SF} = C^*_{m,0}/\mathrm{SF}_{tot} \tag{5.16}$$

$$\hat{C}^*_{LP2} = \left(C^*_{m,0} - \frac{C^*_{m,0} - C^*_{m,60}}{\text{Extent of digestion}} \right) / \mathrm{LP2}_{tot} \tag{5.17}$$

$$\hat{C}^*_{TG} = \left(C^*_{m,0} - \hat{C}^*_{SF} \cdot \mathrm{SF}_0 \right) / \mathrm{TG}_{tot} \tag{5.18}$$

5.3.2.3 Determination of the kinetics of TG and SF digestion

The kinetics of formulation digestion was determined using *in vitro* lipolysis data. First, the course of TG and SF digestion was determined from the FA titration profiles by considering the stoichiometry of hydrolysis. It was assumed that TGs were digested rapidly on lipolysis initiation, whereas SFs were digested more slowly in a second stage of lipolysis. This two-step lipolysis kinetics arises from the different hydrolysis rates of lipolytic enzymes present in the pancreatic extract. The pancreatic lipase and co-lipase preferentially bind insoluble lipids and, therefore, they hydrolyze primarily TGs and DGs. In contrast, the carboxyl ester hydrolase shows higher affinity to lamellar and micellar structures containing SFs [157, 158]. Moreover, the lipolytic activity of the pancreatic lipase and co-lipase is higher compared to that of the cholesterol ester hydrolase [157, 158]. For formulation IIIA LC and IIIA MC, two time profiles were anticipated: one for the digested TGs (first stage) and one for the digested SFs (second stage). Instead, only one stage of lipolysis was assumed for the surfactant-only formulation IIIB/IV. Based on the resulting profiles of undigested glycerides (mmol) *versus* time, we defined a general power-law describing the digestion rate as a function of the amount of available substrate:

$$\frac{\mathrm{dTG}(t)}{\mathrm{d}t} = -k_{dig,TG} \cdot (\mathrm{TG})^{n_{TG}} \tag{5.19}$$

$$\frac{\mathrm{dSF}(t)}{\mathrm{d}t} = -k_{dig,SF} \cdot (\mathrm{SF})^{n_{SF}} \tag{5.20}$$

where $k_{dig,TG}$ and $k_{dig,SF}$ are the digestion rate constants, and n_{TG} and n_{SF} are the order of kinetics for TG and SF digestion, respectively. These constants were estimated by regressing Eqs. 5.19 and 5.20 to the experimental values.

5.3.2.4 General model of formulation digestion used for solubility modeling

To describe the kinetics of LBF digestion with a time-independent transition from the first to the second stage of hydrolysis, formulation digestion was modeled using Eqs. 5.21 and 5.22–5.24. According to the two-step kinetics, SFs were expected to be digested after forming micelles. The kinetics of micelles formation was assumed to correspond to the kinetics of TG digestion. Hence, Eq. 5.22 and 5.23 describe the time evolution of SFs in oil droplets and in micelles, respectively. The total amount of undigested SFs, which is ultimately used for solubility modeling, is described by Eq. 5.24. The generation of LP1 (Eq. 5.25) and LP2 (Eq. 5.26) corresponded to the kinetics of TG and SF digestion, respectively, according to the stoichiometry of lipolysis.

$$\frac{\mathrm{dTG}(t)}{\mathrm{d}t} = -k_{dig,TG} \cdot (\mathrm{TG}(t))^{n_{TG}} \tag{5.21}$$

$$\frac{\mathrm{dSF}_{oil}(t)}{\mathrm{d}t} = -k_{dig,TG} \cdot (\mathrm{TG}(t))^{n_{TG}} \cdot \frac{N_{SF}}{N_{TG}} \tag{5.22}$$

$$\frac{\mathrm{dSF}_{mic}(t)}{\mathrm{d}t} = k_{dig,TG} \cdot (\mathrm{TG}(t))^{n_{TG}} \cdot \frac{N_{SF}}{N_{TG}} - k_{dig,SF} \cdot (\mathrm{SF}_{mic}(t))^{n_{SF}} \tag{5.23}$$

$$\frac{\mathrm{dSF}(t)}{\mathrm{d}t} = -k_{dig,SF} \cdot (\mathrm{SF}_{mic}(t))^{n_{SF}} \tag{5.24}$$

$$\frac{\mathrm{dLP1}(t)}{\mathrm{d}t} = k_{dig,TG} \cdot (\mathrm{TG}(t))^{n_{TG}} \tag{5.25}$$

$$\frac{\mathrm{dLP2}(t)}{\mathrm{d}t} = k_{dig,SF} \cdot (\mathrm{SF}_{mic}(t))^{n_{SF}} \tag{5.26}$$

N_{SF}/N_{TG} is the ratio of molar amounts of SFs and TGs in undigested formulation.
To model the lipolysis-triggered change in drug solubility during *in vitro* lipolysis (closed system), we inserted the numerical solutions of Eqs. 5.21, 5.24, 5.25, and 5.26 into Eqs. 5.14 and 5.15.

5.3.2.5 Modeling intestinal formulation digestion and drug solubility

Intestinal formulation lipolysis and drug solubility were simulated using the general model of formulation digestion (Eqs. 5.21 and 5.22–5.24) and the physiological parameters describing the GI transit of LBFs. As a first approximation, we assumed that (i) there is no lipolysis in the stomach; (ii) TGs and DGs are not absorbed from the GI tract; (iii) LPs are absorbed only in the intestine.
The kinetics of undigested lipid-based excipients in the GI tract can be described as

follows:

$$\frac{\mathrm{d}X_{gu}(t)}{\mathrm{d}t} = -k_{gd} \cdot X_{gu}(t) - k_{ge} \cdot X_{gu}(t) \tag{5.27}$$

$$\frac{\mathrm{d}X_{gd}(t)}{\mathrm{d}t} = k_{gd} \cdot X_{gu}(t) - k_{ge} \cdot X_{gd}(t) \tag{5.28}$$

$$\frac{\mathrm{d}X_{iu}(t)}{\mathrm{d}t} = k_{ge} \cdot X_{gu}(t) - k_{id} \cdot X_{iu}(t) \tag{5.29}$$

where X holds for amount of TGs or SFs; X_{gu} and X_{gd} are the amounts of excipient in the stomach in undispersed and dispersed formulation, respectively, and X_{iu} is the amount of undispersed excipients in the intestine. The time evolution of dispersed TGs and SFs in the intestine depends on the lipolysis rate of the specific glyceride and was described by the following equations:

$$\frac{\mathrm{dTG}_{id}(t)}{\mathrm{d}t} = k_{ge} \cdot \mathrm{TG}_{gd}(t) + k_{id} \cdot \mathrm{TG}_{iu}(t) - k_{dig,TG} \cdot (\mathrm{TG}_{id}(t))^{n_{TG}} \tag{5.30}$$

$$\frac{\mathrm{dSF}_{id,oil}(t)}{\mathrm{d}t} = k_{ge} \cdot \mathrm{SF}_{gd}(t) + k_{id} \cdot \mathrm{SF}_{iu}(t) - k_{dig,TG} \cdot (\mathrm{TG}(t))^{n_{TG}} \cdot \frac{N_{SF}}{N_{TG}} \tag{5.31}$$

$$\frac{\mathrm{dSF}_{id,mic}(t)}{\mathrm{d}t} = k_{dig,TG} \cdot (\mathrm{TG}(t))^{n_{TG}} \cdot \frac{N_{SF}}{N_{TG}} - k_{dig,SF} \cdot (\mathrm{SF}_{id,mic}(t))^{n_{SF}} \tag{5.32}$$

$$\frac{\mathrm{dSF}_{id}(t)}{\mathrm{d}t} = k_{ge} \cdot \mathrm{SF}_{gd}(t) + k_{id} \cdot \mathrm{SF}_{iu}(t) - k_{dig,SF} \cdot (\mathrm{SF}_{id,mic}(t))^{n_{SF}} \tag{5.33}$$

$$\frac{\mathrm{dLP1}(t)}{\mathrm{d}t} = k_{dig,TG} \cdot (\mathrm{TG}_{id}(t))^{n_{TG}} - P_{eff,LP} \cdot \frac{2}{r} \cdot f \cdot \mathrm{LP1}(t) \cdot 3600 \tag{5.34}$$

$$\frac{\mathrm{dLP2}(t)}{\mathrm{d}t} = k_{dig,SF} \cdot (\mathrm{SF}_{id,mic}(t))^{n_{SF}} - P_{eff,LP} \cdot \frac{2}{r} \cdot f \cdot \mathrm{LP2}(t) \cdot 3600 \tag{5.35}$$

Eq. 5.30 denotes the time course of undigested TGs and Eqs. 5.31 and 5.32 describe the time evolution of undigested SFs in oil droplets and in micelles, respectively. The time evolution of LP1 is determined by the lipolysis kinetics of TGs and the absorption rate of LP (Eq. 5.34), and that of LP2 is given by the lipolysis kinetics of SFs and the absorption rate of LP (Eq. 5.35). $P_{eff,LP}$ is the effective permeability of LPs and the same value was assumed for LP1 and LP2.

Drug solubility in the intestine was finally modeled by inserting the numerical solutions of Eqs. 5.30, 5.33, 5.34, and 5.35 into Eqs. 5.14 and 5.15. We simulated only intestinal drug solubility, because this compartment is the primary site of formulation lipolysis. The GI transit of excipients after p.o. administration of the LBFs is visualized in Figure 5.3.

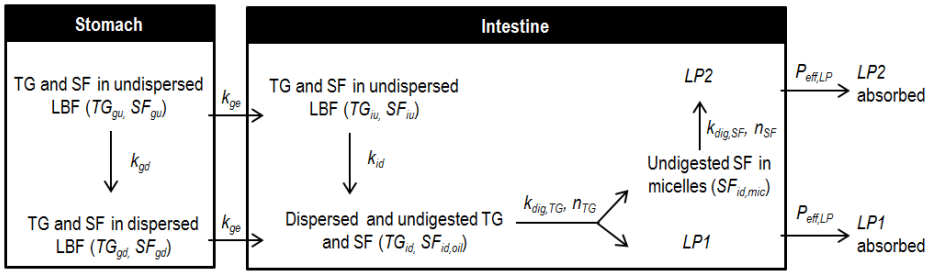

FIGURE 5.3: Scheme of model parameters describing the GI transit of excipients after oral administration. The distinction between dispersed and undispersed formulation was given by the experimental mini-vessel test in [29].

5.3.3 Calculation of the saturation ratio during LBF digestion

The drug saturation ratio, *SR*, during formulation lipolysis was calculated according to:

$$SR(t) = \frac{C_{sol}(t)}{C^*(t)} \tag{5.36}$$

where $C_{sol}(t)$ is the actual concentration of solubilized drug and $C^*(t)$ the drug solubility. SR(t) during *in vitro* lipolysis was calculated using the $C_{sol}(t)$ obtained from Raman spectroscopy, whereas SR(t) in the *in vivo* situation was calculated using the $C_{sol}(t)$ values obtained from Eq. 5.11.

For *in vitro* lipolysis, the recently proposed maximum supersaturation ratio, SR^M, was calculated according to [26]:

$$SR^M = \frac{C_{sol,max}}{C^*_{m,60}} \tag{5.37}$$

where $C_{sol,max}$ is the maximum attainable concentration of fenofibrate in solution assuming no precipitation and $C^*_{m,60}$ is the lowest fenofibrate solubility in the lipolysis medium during digestion (t=60 min).

5.3.4 Parameter sensitivity analysis

The impact of the LP absorption rate on intralumenal drug solubility and supersaturation was studied. Thus, a $P_{eff,LP}$ of 0, 10^{-7}, 10^{-5}, and 10^{-3} cm/s was inserted in Eqs. 5.34 and 5.35 to simulate no absorption as well as slow, moderate, and fast LP absorption, respectively. The resulting drug solubility and supersaturation profiles were

analyzed.

Moreover, the intestinal drug supersaturation profiles were simulated for different drug permeability values, P_{eff}, and lipolysis rates. P_{eff} was varied in the range of 0.1 to 10 times the nominal value of $2.66 \cdot 10^{-5}$ cm/s and the lipolysis rate was varied in the range of 0.01 to 100 times the lipolysis rates obtained from *in vitro* experiments. The result was depicted as a 3D surface plot showing the peak saturation ratio as a function of P_{eff} and lipolysis rate.

5.4 Results

5.4.1 Rate and extent of LBF digestion

The digestion of three LBFs was studied employing a commonly used *in vitro* lipolysis method [31]. The amount of unionized FAs was measured via back-titration and the resulting correction factors were 1.61, 1.10, and 1.30 for formulation IIIA LC, IIIA MC, and IIIB/IV, respectively. Hence, the largest fraction of unionized FAs was measured with long-chain FAs (61% in formulation IIIA LC and 30% in formulation IIIB/IV). This result was a consequence of the higher pK_a of long-chain FAs compared to medium-chain FAs and was in agreement with previously reported values [26].

Different rates and extents of digestion were observed among the three formulations (Figure 5.4). A two-stage profile resulted from the digestion of IIIA LC and IIIA MC, consisting of an initial stage of rapid lipolysis followed by a second stage of slower lipolysis. These two formulations were completely hydrolized within 60 minutes resulting in

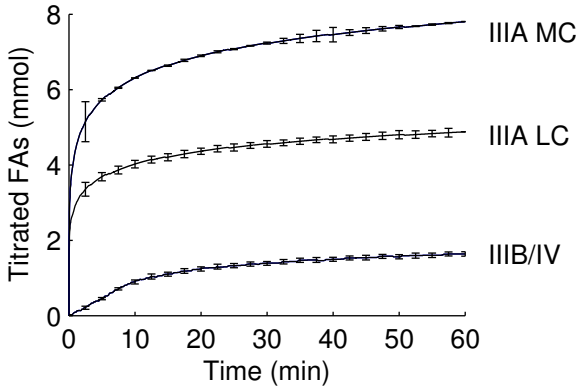

FIGURE 5.4: Digestion profiles of the three model LBFs containing 80 mg/g fenofibrate (*in vitro* lipolysis according to Sek *et al.* [146]). The NaOH volume obtained from direct titration was adjusted for the amount of protonated FAs at pH 7.5 (via back-titration) and the NaOH consumption caused by the digestion phospholipids was subtracted from the total volume (mean ± 1 SD, n=3).

an extent of digestion of 109.4 ± 5.9% and 103.3 ± 0.03% (mean ± 1 SD, n=3), respectively. Lipolysis of formulation IIIB/IV was comparatively slow and only 56.0 ± 2.0% of excipients were digested. The two-stage lipolysis profile of formulations IIIA LC and IIIA MC agreed with our assumption of fast TG and slow SF digestion. Analogously, only one stage of lipolysis was observed with formulation IIIB/IV, due to the presence of only SFs and the absence of an oil phase.

The amount of digested glycerides was calculated based on the titration profiles in Figure 5.4 and the stoichiometry of lipolysis. The rate of TG and SF lipolysis was then determined according to Eqs. 5.19 and 5.20, and the resulting kinetic constants $k_{dig,TG}$, $k_{dig,SF}$, n_{TG}, and n_{SF} are detailed in Table 5.3. The power-laws described the profiles of glyceride digestion accurately, resulting in $R^2 > 0.92$.

Table 5.3: Kinetic constants (value ± 95% CI) for glyceride digestion.

LBF	TG digestion			SF digestion		
	$k_{dig,TG}$	n_{TG}	R^2	$k_{dig,SF}$	n_{SF}	R^2
IIIA LC	587.7 ± 95.9	1.35 ± 0.18	0.9628	25.93 ± 0.55	2.17 ± 0.04	0.9937
IIIA MC	276.5 ± 13.6	2.30 ± 0.15	0.9768	18.08 ± 0.36	1.29 ± 0.03	0.9851
IIIB/IV	n/a	n/a	n/a	1.18 ± 0.03	5.32 ± 0.06	0.9216

5.4.2 Determination of lipolysis-triggered drug precipitation (*in vitro*)

The three formulations containing 80 mg/g fenofibrate were digested *in vitro* and the course of drug precipitation was monitored using in-line Raman spectroscopy. A specific calibration model was built for each formulation based on a set of 30 reference spectra spanning the entire concentration range of precipitated drug. Accurate calibration models were obtained with R^2 values of 0.9862 to 0.9974 and a RMSEC between 0.0124 and 0.0046 mg/ml. The cross-validation procedure yielded Q^2 values of 0.9244 to 0.9561 and RMSECV smaller than 0.16 mg/ml, indicating robust calibrations.

These PLS models were then applied to all Raman spectra of the corresponding LBF to determine the drug solubilization profiles over the 60 min digestion period. As a result, each LBF demonstrated extensive drug precipitation as seen in Figure 5.5, showing the kinetics of solubilized drug. With formulations IIIA LC and IIIB/IV, fenofibrate started to precipitate after an initial lag phase of 10 to 15 min. In contrast, with formulation IIIA MC, drug precipitation started rapidly after lipolysis initiation and reached equilibrium after ∼10 min.

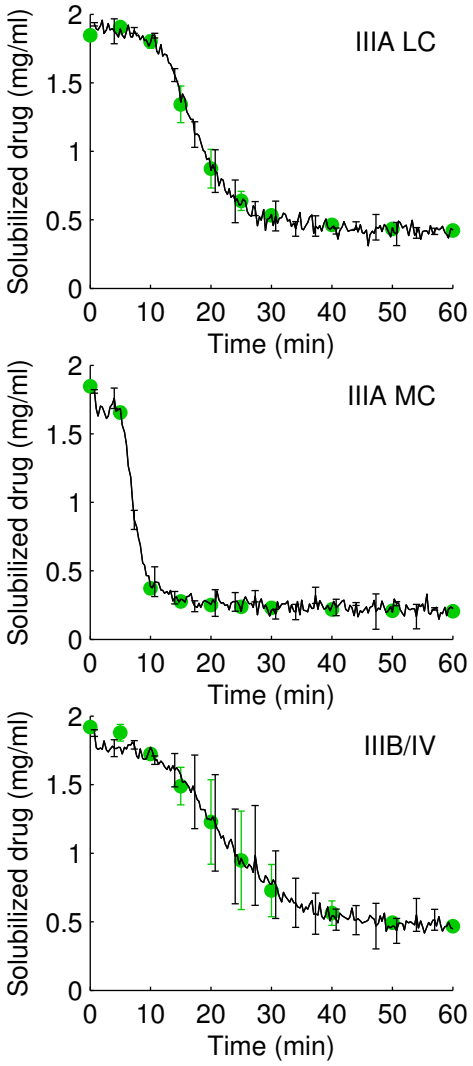

FIGURE 5.5: Drug solubilization profiles measured with in-line Raman spectroscopy during *in vitro* lipolysis of LBF IIIA LC, IIIA MC, and IIIB/IV. Decreasing concentrations of solubilized drug indicated precipitation. The black line represent the concentration profiles determined via Raman spectroscopy and green circles are reference values measured upon nanofiltration (mean ± 1 SD, n=3).

Interestingly, Griffin *et al.* [29] reported notably different precipitation profiles. Only formulation IIIB/IV resulted in comparable extent drug precipitation (∼70%), whereas less than 10% of the drug precipitated with IIIA LC and IIIA MC. These differences in the extent of precipitation between the two studies were most likely due to the different drug contents in the lipolysis assay (80 mg *versus* 240 mg), different amounts of formulation lipid (1 g *versus* 3 g), and a minor difference in digestion media (*i.e.*, type of bile salts).

To study the solid-state of precipitated drug, a pellet was isolated after ultracentrifugation at the end of the *in vitro* lipolysis experiment and then analyzed by XRPD.

Figure 5.6 depicts the resulting XRPD spectra of the pellet phases obtained by ultracentrifugation, of pure crystalline fenofibrate, and of a reference pellet. This reference was the pellet obtained after lipolysis of drug-free formulation, which was spiked with crystalline fenofibrate. The angular range of peaks of the pellets containing precipitated drug corresponded to that of the reference pellet. Therefore, XRD analyses suggested the precipitation of fenofibrate in a crystalline state during lipolysis with each formulation. This observation was in good agreement with Raman spectroscopy data, which showed a clear shift of fenofibrate peaks toward the position of crystalline reference material.

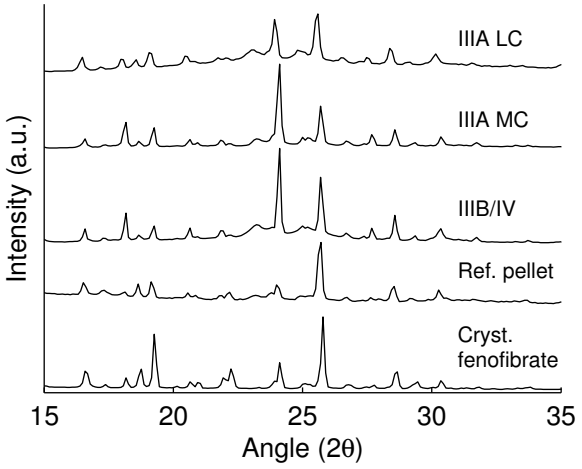

FIGURE 5.6: XRPD pattern of the pellet phase obtained upon lipolysis of LBF IIIA LC, IIIA MC, and IIIB/IV. The reference was the pellet phase obtained from lipolysis of drug-free formulation, which was spiked with crystalline fenofibrate. The XRPD pattern of reference pellets were almost equal for formulation IIIA LC, IIIA MC, and IIIB/IV, and hence, only the pattern obtained from formulation IIIA MC is depicted.

5.4.3 Drug solubility during *in vitro* lipolysis

Fenofibrate solubility in lipolysis medium, $C^*_{m,t}$, was determined at different digestion times. The highest initial solubility, $C^*_{m,0}$, was obtained with formulation IIIA MC (2.19 ± 0.01 mg/ml), followed by IIIA LC (1.41 ± 0.03 mg/ml) and IIIB/IV (0.93 ± 0.01 mg/ml). On lipolysis initiation, the solubilities decreased in each case due to the generation of comparatively hydrophilic lipolysis products. This decrease in drug solubility was most extensive with IIIA MC, where 80% lower solubility was measured at 5 min of digestion ($C^*_{m,5}$: 0.44 ± 0.01 mg/ml), and less pronounced with IIIA LC and IIIB/IV, which resulted in a $C^*_{m,5}$ of 0.81 ± 0.03 and 0.67 ± 0.07 mg/ml, respectively. By 60 min of digestion, the total loss of solubilization capacity was 72.3%, 87.6%, and

50.0% for formulation IIIA LC, IIIA MC, and IIIB/IV, respectively.
The relative fenofibrate solubilities $\hat{C}^*_{TG}$, $\hat{C}^*_{SF}$, $\hat{C}^*_{LP1}$, and $\hat{C}^*_{LP2}$ were calculated based on measured drug solubility values and the molar amounts of excipients in the LBFs. As seen in Table 5.4, the relative fenofibrate solubility in long-chain TGs was lower than in medium-chain TGs (0.631 *versus* 0.701 mg·ml^{-1}·mmol^{-1}). In contrast, drug solubility in long-chain LPs was higher than in medium-chain LPs (0.369 *versus* 0.093 mg·ml^{-1}·mmol^{-1}). To calculate $\hat{C}^*_{SF}$ and $\hat{C}^*_{LP2}$ no differentiation was done between Cremophor RH 40 and Tween 85.

TABLE 5.4: Relative fenofibrate solubility in dispersed TG, SF, LP1, and LP2 (mg·ml^{-1}·mmol^{-1}). $\hat{C}^*_{LP1}$ was estimated via parameter fitting (value ± 95% CI).

LBF	$\hat{C}^*_{TG}$	$\hat{C}^*_{SF}$	$\hat{C}^*_{LP1}$	$\hat{C}^*_{LP2}$
IIIA LC	0.631	0.640	0.369 ± 0.001	0.069
IIIA MC	0.701	0.640	0.093 ± 0.011	0.069
IIIB/IV	n/a	0.640	n/a	0.069

5.4.3.1 Modeling drug solubility and supersaturation during *in vitro* lipolysis

The drug solubility as a function of time during *in vitro* lipolysis (without absorption sink) was modeled initially, given that these experimentally determined solubility values were available for model validation. Figure 5.7 displays the experimental (circles) and modeled (continuous lines) drug solubility profiles. There were excellent correlations between experimental and modeled profiles (R^2 >0.89).
The SRs during *in vitro* lipolysis were calculated according to Eq. 5.36 based on the concentrations of solubilized drug obtained from Raman spectroscopy and the modeled drug solubility profiles. Prior to lipolysis, dispersed formulations IIIA LC and IIIB/IV were slightly supersaturated (SR of 1.36 and 1.94, respectively). In contrast, IIIA MC was initially below saturation (SR of 0.83) but rapidly became supersaturated on lipolysis initiation. The SRs of all three formulations increased following initiation of lipolysis reaching a peak SR value of 2.62, 3.34, and 2.31 with formulations IIIA LC, IIIA MC, and IIIB/IV, respectively.
For comparison, the SR^M values were also calculated, which is the ratio of the highest drug concentration in solution to the lowest drug solubility (*i.e.*, $C^*_{m,60}$). This theoretical value has been previously defined to indicate the maximum SR obtainable during *in vitro* lipolysis [28]. The values were generally higher than the SR and the rank order was slightly different, *i.e.*, IIIA MC (6.81)>III B (3.70)>IIIA LC (3.17).

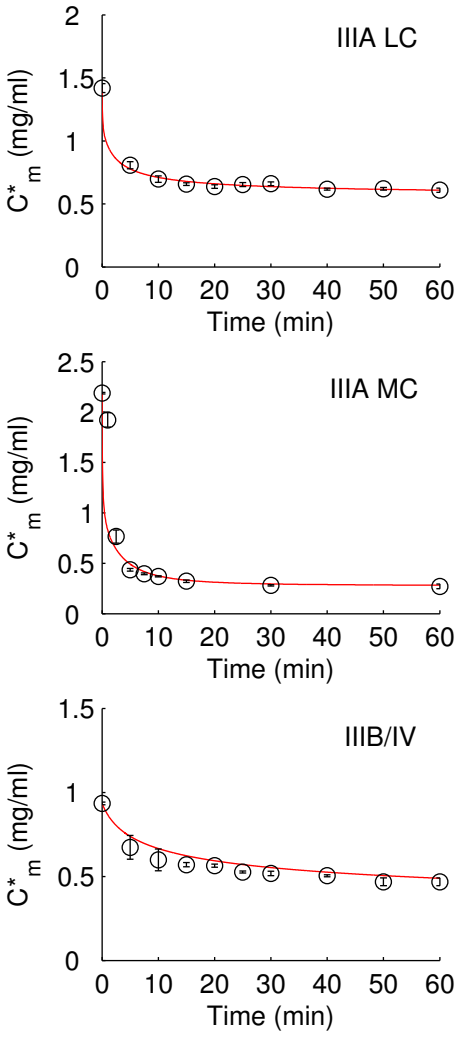

FIGURE 5.7: Fenofibrate solubility during *in vitro* lipolysis of formulation IIIA LC, IIIA MC, and IIIB/IV. There was a very good agreement between experimental solubility data (circles) and the mathematical model of drug solubility (red lines), resulting in a R^2 of 0.9952, 0.9941, and 0.8930 for IIIA LC, IIIA MC, and IIIB/IV, respectively.

5.4.4 Modeling lipolysis-triggered drug supersaturation in the intestinal lumen

5.4.4.1 *In vivo* LBF performance and estimation of PK parameters

Griffin *et al.* [29] previously reported absolute oral bioavailabilities of 65.6%, 70.7%, and 71.7% for formulation IIIA LC, IIIA MC, IIIB/IV, respectively. These relatively high and similar oral bioavailabilities suggested that intralumenal fenofibrate precipitation was either absent or only minimal and similar for the three formulations. The *in vivo* data were used to estimate the PK parameters as well as the intralumenal drug concentration profiles of fenofibrate.

The plasma concentrations obtained after i.v. administration of fenofibrate allowed an estimation of V_d, k_{el}, k_{pt}, and k_{tp} and the resulting parameter values were 6.4 ± 0.2 L, 0.187 ± 0.008 h^{-1}, 0.093 ± 0.046 h^{-1}, and 0.179 ± 0.025 h^{-1} (estimated value ± 95% CI), respectively (R^2=0.9963, Figure 5.8). The similarity factor f_2 of 61.1 indicated that the difference between modeled and experimental plasma concentration profiles was less than 10%.

The plasma concentrations obtained after p.o. administration of fenofibrate were then modeled using Eqs. 5.5–5.11. This model assumed that the entire oral dose was available for absorption, *i.e.*, that no precipitation occurred in the GI lumen. As seen in Figure 5.8, the plasma profiles of fenofibric acid were described accurately by the mathematical model.

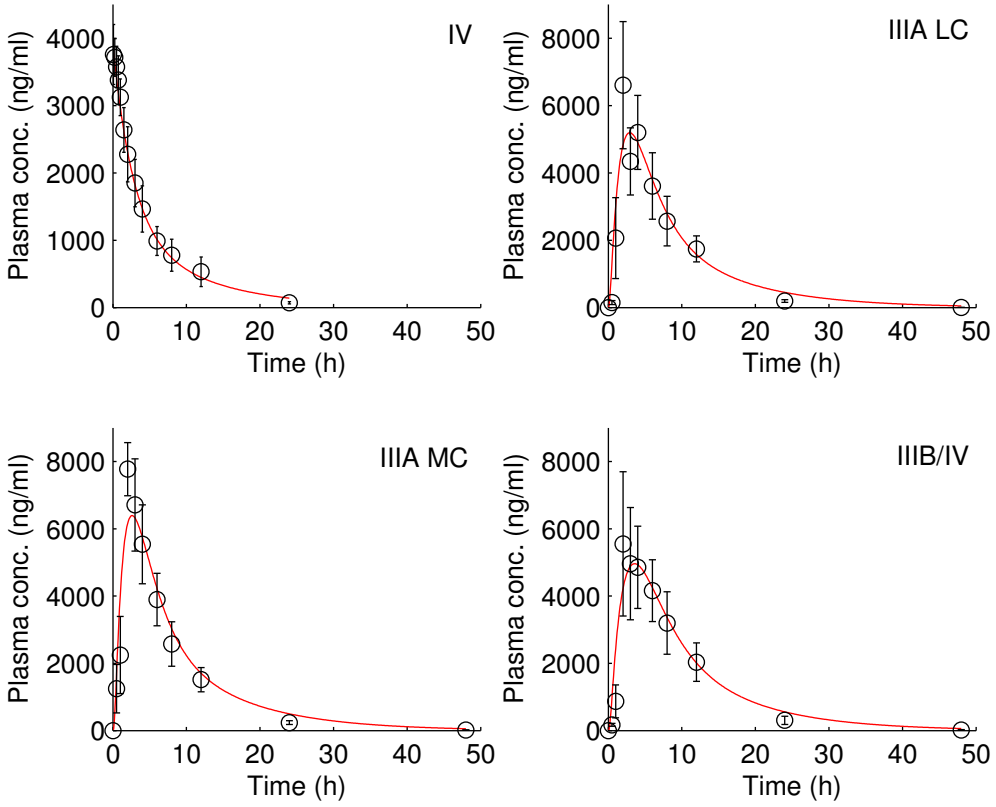

FIGURE 5.8: Experimental (circles) and modeled (red lines) plasma concentration profiles obtained after administration of fenofibrate.

The similarity factor f_2 was higher than 36 with each formulation, indicating that the average difference between experimental and modeled plasma concentration profiles was less than 20%. The largest deviation was observed at peak plasma concentrations, where the physiologically-based model slightly underestimated the real plasma concentrations.

The values of k_{ge} and F_a obtained by regressing Eqs. 5.5–5.11 to the plasma concentration profiles are detailed in Table 5.5.

TABLE 5.5: Pharmacokinetic parameters (value ± 95% CI) estimated from plasma data after p.o. administration of the three LBFs (96 mg fenofibrate).

LBF	k_{ge} (h^{-1})	F_a (%)	f_2	R^2
IIIA LC	0.555 ± 0.327	68.3 ± 16.7	37.9	0.8777
IIIA MC	0.681 ± 0.347	78.1 ± 15.3	41.8	0.9119
IIIB/IV	0.377 ± 0.178	75.7 ± 17.1	42.9	0.8995

5.4.4.2 Simulating formulation digestion and drug solubility in the intestinal lumen

Using this model, the fenofibrate concentration profile in the intestinal lumen after p.o. administration of the three formulations. Figure 5.9a shows that maximum drug concentrations were reached ∼1 h after administration and that the drug was almost completely absorbed within 6 h. To simulate the amount of excipients in the intestinal lumen, the PK parameters obtained from *in vivo* data and the digestion rate of formulation lipids (calculated from *in vitro* lipolysis experiments) were utilized. The resulting time evolution of formulation lipids is depicted in Figure 5.9 c–f.

Low amounts of undigested TGs were available in the intestine, indicating that TGs were rapidly digested (Figure 5.9c). In contrast, the amount of intralumenal SFs was notably higher, especially with formulation IIIB/IV (Figure 5.9d). Figures 5.9 e and f show the time course of LP1 and LP2 assuming no LPs absorption (continuous lines) and rapid LPs absorption ($P_{eff,LP}$ of 10^{-4} cm/s, dotted lines). Because LPs absorption was much faster than formulation digestion, the LPs concentrations in the absorption environment were very low.

The time evolution of drug solubility in the intestinal lumen was then calculated based on the profiles of TGs, SFs, LP1, and LP2, and the relative fenofibrate solubilities listed in Table 5.4. Figure 5.9b shows the solubility profiles of the three LBFs assuming no LPs absorption (continuous lines) and rapid LPs absorption (dotted lines). During the first hour of intestinal transit, the drug solubility was similar for the three formulations (assuming no LP absorption). At later time points, the solubility with formulation IIIB/IV was higher, followed by IIIA LC and IIIA MC. The impact of LPs absorption on drug solubility was particularly pronounced with formulation IIIA LC and IIIA MC, with substantially lower concentrations in the intestinal lumen under rapid LP absorptive conditions. In contrast for the Type IIIB/IV formulations the impact of LPs absorption was negligible.

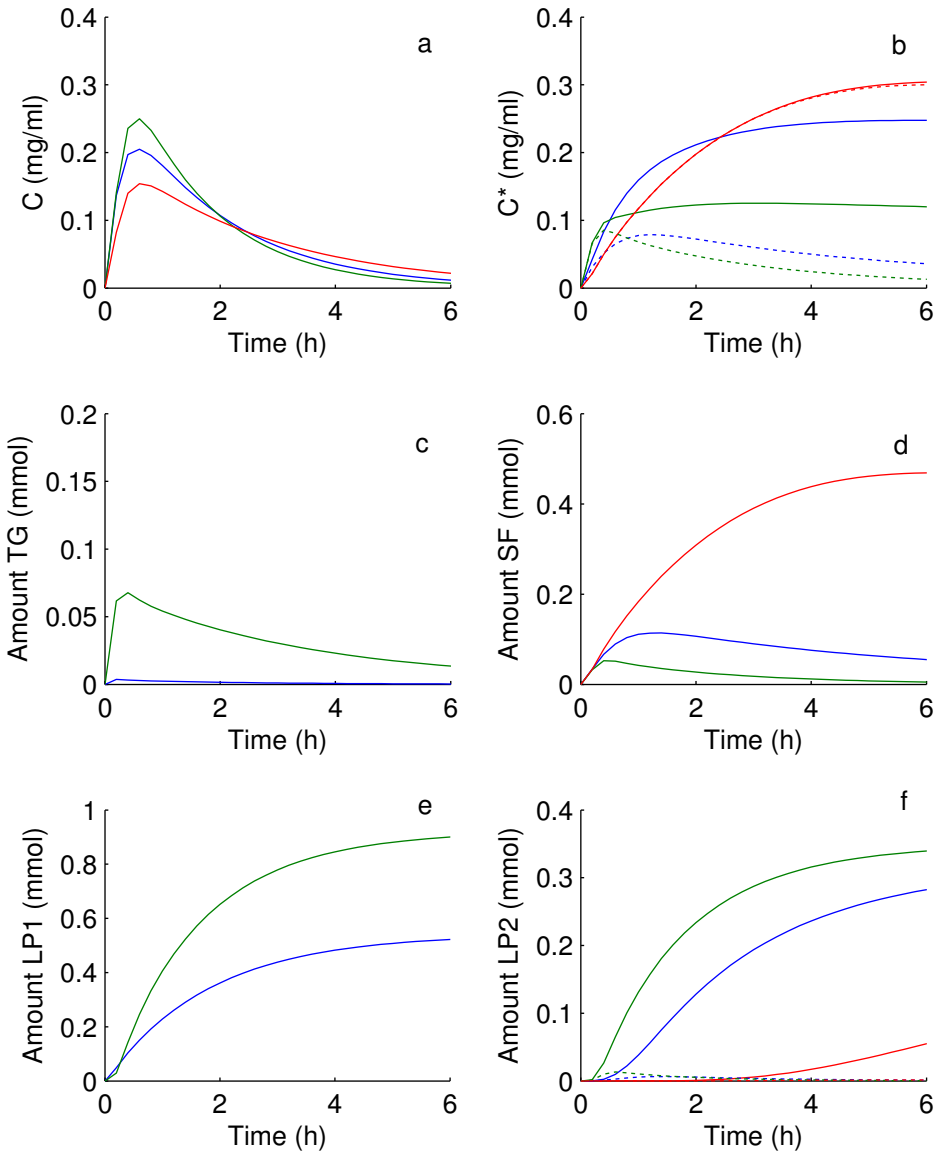

FIGURE 5.9: Time evolution of (a) fenofibrate concentration and (b) fenofibrate solubility, and of the amounts of (c) TG, (d) SF, (e) LP1, and (f) LP2 in the intestinal lumen upon p.o. administration of formulation IIIA LC (blue), IIIA MC (green), and IIIB/IV (red). Simulations were performed assuming no LPs absorption (continuous lines) and rapid LPs absorption (dotted lines). Only the first 6 h of GI transit are depicted in the plots, which corresponds to the estimated gastric and small intestinal emptying time [235, 236].

5.4.4.3 Drug supersaturation in intestinal fluids

The intralumenal drug concentration and solubility profiles were then used to calculate the SR in the intestinal fluids according to Eq. 5.36. This SR profiles provided the basis for evaluating the risk of lipolysis-triggered drug precipitation in an absorptive environment.

Figure 5.10a shows the profile of drug supersaturation assuming the nominal fenofibrate permeability ($P_{eff,FF}$ of $2.66{\cdot}10^{-5}$ cm/s) and rapid LPs absorption ($P_{eff,LP}$ of 10^{-4} cm/s). We focused on the initial 6 h of intestinal transit as this was the estimated residence

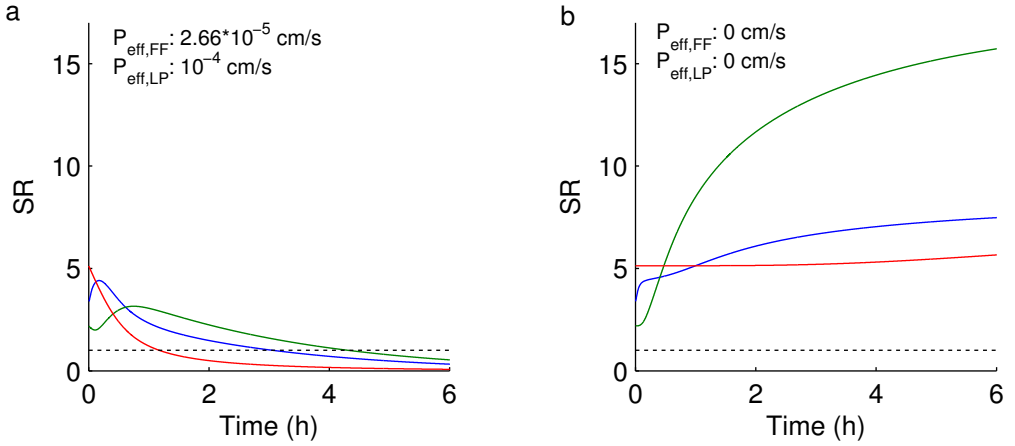

FIGURE 5.10: Time evolution of the SR in intestinal fluids assuming (a) sink conditions ($P_{eff,FF}$ $2.66{\cdot}10^{-5}$ cm/s and$P_{eff,LP}$ 10^{-4} cm/s) and (b) non-sink conditions for formulation IIIA LC (blue), IIIA MC (green), and IIIB/IV (red). Only the first 6 h of GI transit are depicted in the plots, which corresponds to the estimated gastric and small intestinal emptying time in the fasted state [235, 236].

time of drug formulation in the gut [235, 236]. With the Type IIIB/IV and IIIA LC formulations, the highest SRs reached a value of ∼4, but then rapidly decreased and fell below saturation after 1.5 and 3 h, respectively. With formulation IIIA MC, the peak SR value was slightly lower (∼3), but the drug remained supersaturated for the longest period of time (>4 h).

In vitro lipolysis simulates conditions without an absorptive environment, and for comparison, it was interesting to calculate the time evolution of supersaturation in the intestinal lumen assuming no fenofibrate and LPs absorption. As seen in Figure 5.10b, each formulation became highly supersaturated. The rank-order of formulations obtained was similar to that observed with the *in vitro* lipolysis test, with highest SRs for formulation IIIA MC, followed by IIIA LC, and IIIB/IV. The SRs were particularly high with formulation IIIA MC where, after 6 h of digestion, values of ∼16 were obtained.

5.4.4.4 Impact of LPs absorption on drug solubility and supersaturation

In the previous simulation, we assumed rapid LPs absorption to simulate the worst case in terms of drug solubility. To better understand the influence of LPs absorption, we examined the intralumenal SR assuming a range of different $P_{eff,LP}$ values. The result of this simulation is depicted in Figure 5.11 for the absence of LPs absorption ($P_{eff,LP} = 0$ cm/s), as well as for slow ($P_{eff,LP} = 10^{-7}$ cm/s), moderate ($P_{eff,LP} = 10^{-5}$ cm/s), and fast ($P_{eff,LP} = 10^{-3}$ cm/s) LPs absorption.
With formulations IIIA LC and IIIA MC, the intralumenal drug solubility was substantially lower when assuming high $P_{eff,LP}$ values ($> 10^{-5}$ cm/s). This effect was particularly pronounced with formulation IIIA LC (Fig. 5.11a), which was not only extensively digested, but also resulted in LPs with relatively high drug solubilization ($\hat{C}^*_{LP1}$: 0.369 mg/ml). In contrast, the solubilization capacity of medium-chain LPs was rather low ($\hat{C}^*_{LP1}$: 0.093 mg/ml) and, thus, the influence of LPs absorption on drug solubility was less pronounced (Fig. 5.11c). With formulation IIIB/IV, drug absorption was much faster than formulation digestion and, as a consequence, LPs absorption had a negligible influence on drug solubility and supersaturation (Fig. 5.11e).
The SR in intestinal lumen as a function of time are shown in Figure 5.11b, d, and f. A notable increase in SR was observed when $P_{eff,LP}$ exceeded $P_{eff,FF}$, as seen with formulation IIIA LC and IIIA MC (red profiles in Fig. 5.11b and d). In contrast, when drug absorption was much faster than formulation lipolysis and/or LPs absorption, the SR was minimally affected by LPs absorption (Fig. 5.11f).

5.4.4.5 Impact of drug permeability and lipolysis rate on drug supersaturation

The influence of drug permeability and lipolysis rate on the extent of intralumenal supersaturation was subsequently evaluated. The supersaturation profile was determined assuming drug permeabilities, P_{eff}, in the range of 0.1 to 10 times the nominal value for fenofibrate ($2.66 \cdot 10^{-5}$ cm/s) and assuming digestion rates in the range of 0.01 to 100 times the experimental lipolysis rate. The peak SRs occurring during intestinal transit were then mapped as a function of P_{eff} and the relative lipolysis rate (Figure 5.12).
The resulting surface plots for the formulations IIIA LC and IIIA MC were significantly different from that of formulation IIIB/IV. With formulation IIIA LC and IIIA MC, the peak SRs were highly dependent on the drug absorption and formulation lipolysis rates. The SRs became critically high (*i.e.*, exceeding a value of ~3 [6]) under low permeability conditions (*i.e.*, $P_{eff} < 10^{-5}$ cm/s) and/or for relative lipolysis rates higher than 1. In contrast, for high permeability and/or slow formulation lipolysis, the intestinal SRs remained at a constant low level of less than 4. With formulation IIIB/IV, the impact of

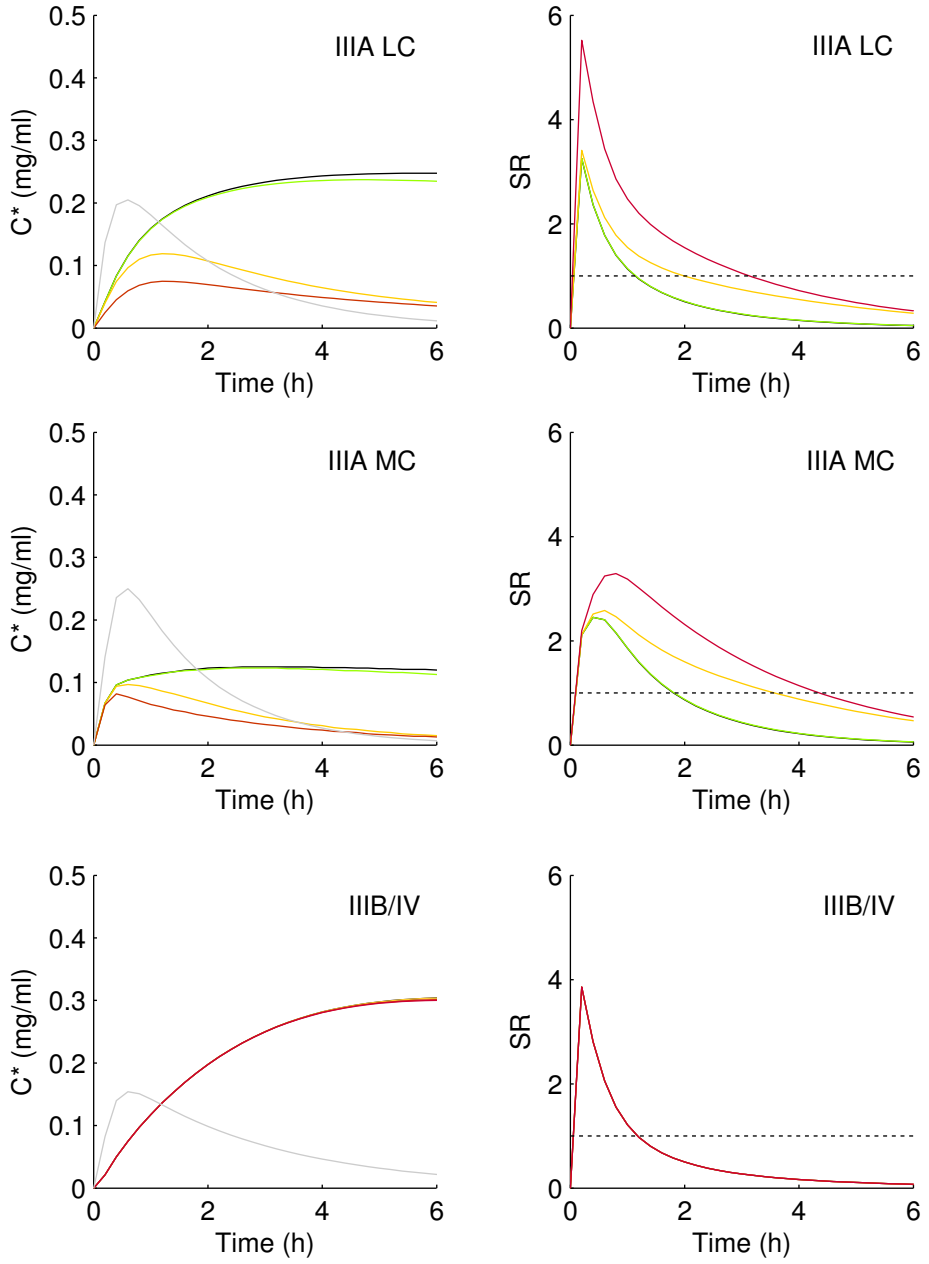

FIGURE 5.11: Influence of LPs absorption on intralumenal drug solubility (C^*) and SR for formulations IIIA LC, IIIA MC, and IIIB/IV. Different $P_{eff,LP}$ values were assumed, which resulted in different LP absorption rates, *i.e.*, 0 (black), 10^{-7} (green), 10^{-5} (orange), and 10^{-3} (red) cm/s. The gray line shows the time evolution of intralumenal fenofibrate concentration assuming a $P_{eff,FF}$ of $2.66{\cdot}10^{-5}$ cm/s. Only the first 6 h of GI transit are depicted in the plots and the horizontal dotted lines correspond to a SR of 1.

drug absorption and lipolysis rate on the intralumenal SR was negligible and the highest SR was much less pronounced.

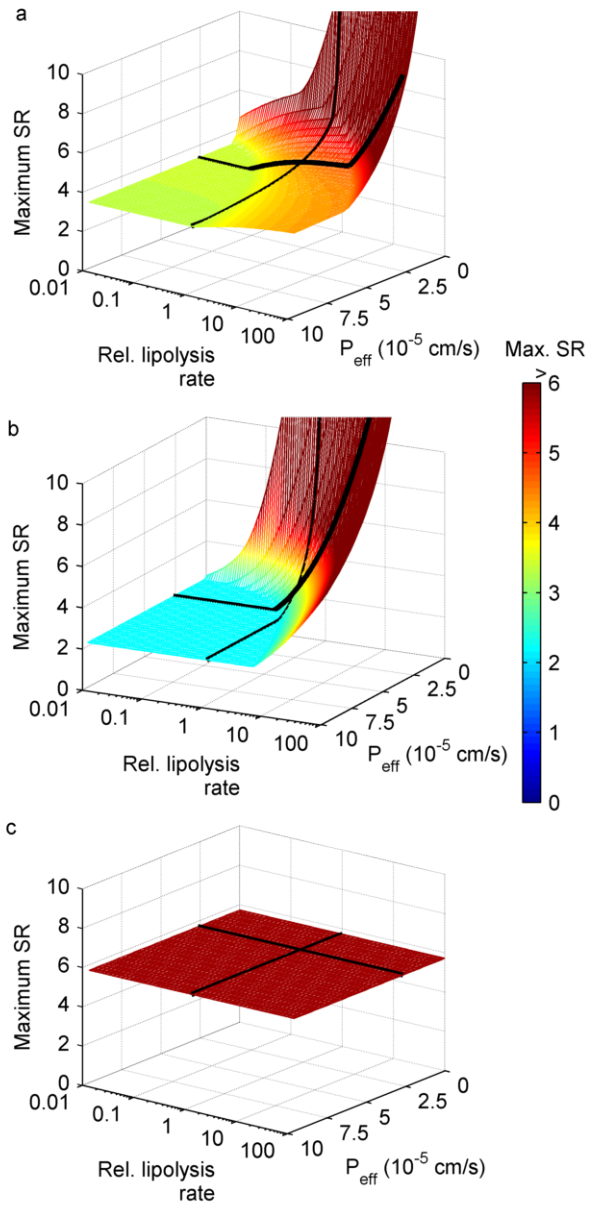

FIGURE 5.12: 3D surface plot showing the impact of drug permeability and lipolysis rate on the intralumenal SR for formulation (a) IIIA LC, (b) IIIA MC, and (c) IIIB/IV. The SR values corresponding to a P_{eff} of $2.66{\cdot}10^{-5}$ cm/s and and to the experimental lipolysis rate are shown by the black lines. The 3D surface plots were truncated for SR values higher than 10.

5.5 Discussion

In the present study, we analyzed three fenofibrate-loaded LBFs that showed a poor correlation between formulation performance *in vitro* and *in vivo*. Using *in vitro* lipolysis testing without an absorption sink, all formulations resulted in extensive drug precipitation of crystalline material. This result suggested a notable loss in absorbable drug dose in the intestinal lumen. However, the PK profile obtained after p.o. administration of the LBFs to pigs showed that ∼70% of the administered drug dose was absorbed and no substantial difference in oral bioavailability was observed among the three formulations [29].Thus, it would appear that the extensive precipitation observed *in vitro* did not adversely impact drug absorption *in vivo*. Such poor correlations have been previously reported [230] and there is a clear need for more predictive *in vitro* assays for LBFs.
The aim of this study was to examine LBF lipolysis in an absorptive environment by introducing a predictive biopharmaceutical model of formulation digestion and drug absorption. This model revealed the drug supersaturation profile in the intestinal lumen, which provided a basis for estimating the risk of drug precipitation *in vivo*. It should be noted that this simulation was based on conservative assumptions, which resulted in worst-case prediction of *in vivo* LBF performance.

5.5.1 Biopharmaceutical model of drug supersaturation during LBF digestion

The novel biopharmaceutical model enabled analysis of drug supersaturation, and hence, of the risk of drug precipitation in the intestinal environment. A key aspect of supersaturation modeling was the simulation of drug solubility during intestinal transit of LBFs. To this end, we used a mathematical approach that was previously developed for modeling drug solubility in closed systems [31]. However, drug solubilization in the GI tract is more dynamic and some adaptations were therefore necessary. The basic assumption was that each lipidic species (*i.e.*, TGs, SFs, and LPs) contributed additively to drug solubilization at equilibrium and that there was a linear relationship between drug solubility and the concentration of excipients [31, 199, 234]. The resulting solubility model was validated using experimental data obtained during *in vitro* lipolysis and resulted in an excellent correlation.
This strong correlation was a key requirement to simulate, in a second step, the time evolution of drug supersaturation *in vivo*. As a first evaluation, we simulated intestinal lipolysis with simultaneous drug and LPs absorption assuming the nominal fenofibrate permeability ($P_{eff,FF}$: $2.66{\cdot}10^{-5}$ cm/s) and rapid LP absorption ($P_{eff,LP}$: 10^{-4} cm/s).

This $P_{eff,LP}$ value was deliberately sselected to simulate worst-case in terms of drug solubilization capacity in the intestinal lumen. For comparison, we calculated the intralumenal supersaturation profile assuming no absorptive environment, which corresponded with the conditions used during routine *in vitro* lipolysis.
This comparison showed that the extent of fenofibrate supersaturation was dramatically lower assuming sink conditions than for non-sink conditions (Figure 5.10a and b). For example, with formulation IIIA MC the peak SR in a non-sink environment was around 15, which indicated a highly unstable system and a substantial risk of drug precipitation. In contrast, assuming an absorption sink, the SRs were below 3. Similarly, the other formulations resulted in peak SRs in the range of 2.5 to 6.
These smaller degrees of supersaturation certainly involved a much reduced risk of drug precipitation compared to non-sink conditions. However, since the concentration of solubilized drug still exceeded the saturation level, the drug remained at risk for precipitation. It is important to consider that the model assumptions were simulating a worst-case situation. Some physiological parameters were associated with a relatively high degree of uncertainty and for these parameters conservative assumptions were employed (*e.g.*, the surface expansion actor, *f*, and the volume of intestinal fluids, V_i). The volume of intestinal fluid in which the drug dose was diluted prior to absorption is particularly relevant in this regard. To our knowledge, no reference volume of intestinal fluids is available for pigs, and hence, we assumed a volume of 50 ml. This was the amount of water administered to the animals on formulation dosing and did not include intestinal secretions and the continuous access to water. A sensitivity analysis is straightforward in this case and demonstrates that the SR is highly dependent from V_i. If for example the V_i is doubled (*i.e.*, 100 ml), which may reflect a more physiologically relevant scenario, the extent of supersaturation is divided in half resulting in SRs in the range of 1.25 to 3. Such values certainly suggest a substantially lower risk of drug precipitation.

A second aspect to consider is the definition of critical supersaturation. From a thermodynamic perspective, any saturation ratio >1 will lead to drug precipitation if sufficient time is given. The induction period for precipitation can be in the range of months to years for very low degrees of supersaturation, but becomes very short (seconds to minutes) when a critical range of supersaturation is exceeded [63]. The critical supersaturation ratio is therefore very important from a biopharmaceutical perspective.
Williams *et al.* recently addressed the importance of this parameter for drug precipitation during *in vitro* lipolysis [28]. They proposed the SR^M value as a measure for evaluating the risk of drug precipitation and found a critical threshold in the range of 2.5 to 3. Accordingly, drug precipitation was very likely to occur if the SR^M exceeded this critical range during LBF lipolysis. Consistent results were found for several drugs

(danazol, fenofibrate, and tolfenamic acid) and different types of LBFs (LFCS type II–IV) [28, 56].
Care is certainly needed when applying a critical supersaturation ratio obtained from *in vitro* experiments to formulation lipolysis *in vivo*. The critical supersaturation ratio is, indeed, not the only determinant for drug precipitation in an absorptive environment. Important additional factors are the drug absorption rate and the duration of the induction period prior to precipitation. When the SR exceeds a critical level, drug precipitation becomes highly probable, but the induction period still provides the opportunity for the drug to be absorbed. In case of a long induction period and/or fast drug absorption, the SR can rapidly fall below the critical value and drug precipitation may ultimately be prevented. It is therefore likely that the driving force (*i.e.*, the supersaturation ratio) must be higher for inducing drug precipitation *in vivo* than during *in vitro* lipolysis.

The biopharmaceutical model assumed that the drug was directly available for intestinal absorption once the formulation was dispersed. In this regard, we did not differentiate between drug that was solubilized in oil droplets, mixed micelles, and free drug in the aqueous bulk. Such a partitioning step is likely to have limited relevance on the overall drug absorption rate, as was recently suggested by Vertzoni *et al.* [120]. However, there were other cases where only the free drug was directly available for absorption [68]. This influence might be drug and formulation specific, and more studies are required to elucidate the mechanism of drug absorption.An additional drug partitioning step is expected to decelerate drug absorption. Neglecting this drug partitioning would therefore lead to an overestimation of the absorption rate. Such an overestimation was, however, not confirmed by the modeled data. On the contrary, the model described *in vivo* data very accurately with the exception of maximum plasma concentrations, which were slightly underestimated. However, due to this uncertainty, we also performed a parameter sensitivity analysis assuming a range of drug permeabilities, as will be discussed later in this section.

5.5.2 Influence of LPs absorption, drug permeability, and lipolysis rate on intralumenal drug supersaturation

The biopharmaceutical model of drug supersaturation provided the unique possibility to estimate the impact of LPs absorption on the solubilization capacity of LBFs during digestion, and hence, to assess the risk of lipolysis-induced precipitation under continuous absorptive conditions.
We analyzed the impact of LPs absorption as a parameter sensitivity analysis while assuming a range of different $P_{eff,LP}$ values. Precise estimates of the effective permeability

of LPs are difficult to obtain. One major reason is the fact that LPs are converted back into TGs in the enterocytes. Hence, conventional methods for permeability measurement cannot be applied in this particular case. Moreover, the flux of LPs across biological membranes might be influenced by the composition of the formulation (*e.g.*, via the interaction with membrane transporters or the temporary residence of LPs at the oil-to-water interface).

We observed that the influence of LPs absorption on fenofibrate solubility varied substantially among the formulations. The most pronounced decrease in solubility was observed with formulation IIIA LC and IIIA MC. Formulation IIIA LC was rapidly digested and the long-chain LPs liberated from olive oil exhibited relatively high solubilization capacity. Hence, the removal of long-chain LPs had a pronounced influence on intestinal solubility. In contrast, the solubilization capacity of LPs liberated from Miglyol and from SFs was comparatively low and, although formulation IIIA MC was rapidly digested, there resulted a moderate influence of LPs removal on the overall drug solubility. The effect of LPs absorption on the SR was largely determined by the relative rates of drug and LPs absorption. Indeed, the SR was only affected when the absorption of LPs was faster than the absorption of fenofibrate. This observation indicated that, although the impact of LPs on the intestinal SR was minimal for fenofibrate, it might be critical in case of poorly permeable drug compounds, especially when LPs provide substantial drug solubilization.

A comparatively different behavior was observed with formulation IIIB/IV. This formulation was digested slowly and the resulting LPs had low drug solubilization capacity. As a result, LPs absorption had almost no influence on intralumenal supersaturation.

It should also be noted that the relative solubilities $\hat{C}^*_{LP1}$ and $\hat{C}^*_{LP2}$ were obtained from drug solubility studies using digests from *in vitro* lipolysis. These values theoretically included the contribution of monoglycerides, monosorbitanesters, and FAs to drug solubilization. However, in the *in vitro* lipolysis model, the FAs are largely removed from solution via precipitation of calcium soaps and micellization with bile salts. The solubilization capacity of these precipitated FAs is expected to be lower than that of the solubilized products [184]. Hence, these experimental solubilities may slightly underestimate the real solubilization capacity of digested formulations *in vivo*.

Finally, we examined the intralumenal SR for different lipolysis and drug absorption rates (Figure 5.12). This analysis was motivated by potential differences between the formulation lipolysis rates *in vitro* and *in vivo*. Similarly, the drug absorption rate could be influenced by the presence of lipid-based colloids, and thus, deviate from the nominal value of $2.66 \cdot 10^{-5}$, as previously discussed. To examine how drug supersaturation is affected by these parameters, we mapped the peak saturation ratio occurring during intestinal transit as a function of both lipolysis rate and effective permeability.

The results were significantly different among the three formulations. With formulation IIIB/IV the peak saturation ratio was not affected by the lipolysis and/or drug absorption rate (Figure 5.12c). This result was due to the fact that formulation IIIB/IV became supersaturated upon simple dispersion (peak SR=5.7 assuming a V_i of 50 ml) and, since formulation lipolysis was always slower than drug absorption, this SR was never exceeded. Such a behavior might be typical for surfactant-only systems, for which formulation dispersion is generally more critical than formulation digestion [48].
IIn contrast, with the extensively digested formulations IIIA LC and IIIA MC, the resulting SRs were largely influenced by the rates of lipolysis and drug absorption (Figures 5.12a and 5.12b, respectively). Assuming fast drug absorption (*i.e.*, P_{eff} >10^{-5} cm/s), the peak SRs remained below ∼4 even for very fast digestion rates. In contrast, for slower absorption rates, the intralumenal supersaturation rapidly increased, particularly for relative lipolysis rates higher than one.
These results suggested that, for highly permeable drugs, intestinal lipolysis is less critical regarding drug precipitation, even if the formulation is extensively digested. This situation is clearly different for drugs with low permeability characteristics. These compounds are at higher risk for lipolysis-triggered supersaturation and may result in relevant drug precipitation prior to absorption. With surfactant-only formulations, lipolysis generally plays a minor role, but drug precipitation can be induced by simple formulation dispersion, especially at higher drug loads. For this type of LBF, the *in vitro–in silico–in vivo* approach presented by Fei *et al.* might be appropriate to simulate formulation behavior *in vivo*, although it did not include formulation digestion [37].

5.6 Conclusions

This study introduced the first biopharmaceutical model of lipolysis-triggered drug supersaturation during intestinal LBF digestion. We analyzed three fenofibrate-loaded LBFs that resulted in extensive drug precipitation during *in vitro* lipolysis, but led to good oral bioavailability *in vivo*. The biopharmaceutical model showed that, for these formulations, the extent of supersaturation was considerably lower when lipolysis occurred in a continuous absorptive environment. This novel approach provided strong evidence of the importance of an absorption sink to estimate drug supersaturation, and hence, the risk of precipitation. Current *in vitro* assays simulate the worst-case with respect to drug precipitation, due to the absence of an absorption sink. Drug supersaturation is considerably higher than in the intestinal lumen and, as a consequence, drug precipitation is more likely to be observed *in vitro*.

Biopharmaceutical modeling was useful for gaining a deeper understanding of LBF performance in the GI tract. For highly permeable compounds, drug absorption is rather fast compared to formulation digestion and critical degrees of supersaturation may therefore be avoided. Thus, the digestion of LBFs containing highly permeable drug compounds is less critical than previously assumed. This realization is highly encouraging with respect to the use of LBFs for oral administration of poorly water-soluble, but highly permeable drugs.

In the absence of *in vitro* tools simulating an absorption sink, such biopharmaceutical modeling should be further considered in LBF research and development. This strategy offers several opportunities for improving the prediction of LBF performance *in vivo*. A drug precipitation step could be included in the simulation and, to this end, the complex interplay between formulation digestion, drug supersaturation, and precipitation must be further investigated. Future biopharmaceutical modeling may also include biological effects of drug and excipients on oral absorption, such as the influence on efflux transporters or on the lymphatic drug transport.

Chapter 6

Toward an improved understanding of the precipitation behavior of weakly basic drugs from oral lipid-based formulations

Summary

The aim of this study was to analyze the impact of lipid-based formulation (LBF) dispersion and digestion on the precipitation behavior of weakly basic drugs. Loratadine and carvedilol were formulated in a range of LBFs and drug solubilization was analyzed under simulated dispersive and digestive conditions (fasted state). The extent of supersaturation and drug precipitation as well as the solid-state properties and re-dissolution behavior of precipitated drugs were assessed.

Carvedilol precipitated in a crystalline form upon dispersion, but interestingly, this drug gave an amorphous precipitate during lipolysis. In contrast, loratadine precipitated as crystalline material during both formulation dispersion and digestion. No influence of the formulation composition on the type of precipitation was observed. These results suggested that *in vitro* conditions (dispersive *vs.* digestive) largely determined the solid-state properties of precipitating weak bases. Solid-state characterization of precipitated drugs under different experimental conditions should be routinely performed in formulation screening to better understand the biopharmaceutical behavior of LBFs. Hence, these findings are of high practical importance for the pharmaceutical development and *in vitro* assessment of LBFs using weakly basic drugs.

Stillhart C. *et al.* Toward an improved understanding of the precipitation behavior of weakly basic drugs from oral lipid-based formulations *Journal of Pharmaceutical Sciences*, **2014**, 103(4):1194-203.

6.1 Introduction

Poorly water-soluble drug candidates often show reduced and variable systemic bioavailability upon oral administration. The solubility issue is particularly complex in the case of ionizable drugs such as poorly water-soluble weak bases. These compounds are influenced by the pH gradient experienced during transition from the gastric in the intestinal environment. The gastric pH favors ionization of a basic drug, depending on pK_a, which generally results in adequate solubilization in the stomach. However, following transfer into the intestinal fluid, deprotonation to the free base can occur, leading to comparatively lower aqueous solubility. Depending on the administered dose, this decrease in drug solubility may cause drug supersaturation, with a risk of precipitation.

Drug precipitation is generally undesirable, because re-dissolution is typically incomplete for poorly soluble compounds within the time span of intestinal transit. For this reason, the fraction of precipitated drug is frequently assumed not to be available for absorption. However, there is increasing evidence that the impact of drug precipitation on oral bioavailability does not only depend on the extent of precipitation. A significant determinant is the physical state of precipitated drug. Indeed, high-energy solids such as amorphous materials have higher apparent solubilities and might therefore re-dissolve faster compared with their crystalline counterparts [60, 79]. The drug may have sufficient time to re-dissolve during intestinal transit and to become available for absorption. It is also important to consider the stability and extent of drug supersaturation, which is the driving force for drug precipitation. Although it is a metastable state, drug supersaturation defines the time span during which the drug is solubilized and becomes available for absorption [38, 56].
It has recently been shown that the stability toward intestinal precipitation of a weakly basic drug can be increased by a LBF [237]. This is, however, only one mechanism by which LBFs possibly enhance oral drug bioavailability. The drug is already in a dissolved state when it is administered and thus the critical dissolution step is circumvented. Lipidic excipients also often increase the apparent solubility of the drug in intestinal fluids, may reduce pre-systemic clearance, and can enhance drug permeation across the intestinal membrane [6, 14]. Although LBFs offer a great potential for the oral administration of poorly water-soluble compounds, the improvement in oral bioavailability is ultimately governed by the fate of the formulation in the gut. Formulation dispersion and excipient digestion represent particularly critical steps because they change the micro-environment of a drug. Therefore, the capacity of a formulation to keep the drug in solution may be progressively reduced, developing an increased risk of drug precipitation.

There is considerable research interest in the factors that determine the precipitation of weakly basic compounds upon oral administration. Few studies have analyzed the

features of intestinal drug precipitation *in vivo* by aspirating intestinal content [61, 238]. However, as the *in vivo* evaluation of intraluminal content is inherently difficult, drug precipitation has generally been studied using *in vitro* assays. One- or two-compartment experimental setups were developed and simulated gastrointestinal media were usually employed to simulate the transfer from the stomach into the small intestine [213, 239–242]. These assays simulate dispersive conditions without digestive enzymes and can provide valuable information about the intrinsic pH-induced precipitation behavior of weakly basic compounds (in the presence of bile salts and phospholipids).
Other studies used digestive conditions to analyze the precipitation behavior of lipophilic weak bases in LBFs [23, 33, 34] and particular attention has been paid to the solid-state of precipitated drugs. The results of Sassene *et al.* [33], reporting the formation of an amorphous precipitate in the course of formulation digestion of the drug cinnarizine, are particularly interesting. Also important were the findings of the Lipid Formulation Classification System (LFCS) consortium, which studied fenofibrate and tolfenamic acid in different LBFs [28]. While the precipitates of fenofibrate appeared to be of the same crystalline form as the reference drug, tolfenamic acid crystallized, at least partially, in a different polymorphic form. The latter work underlined the necessity to study the formulation behavior upon lipolysis, with a special emphasis on the solid-state characterization of potential precipitate.

Despite the importance of this research field, little information is currently available regarding the impact of specific formulation processing, *i.e.*, dispersion *versus* digestion, on the precipitation behavior of weak bases. Moreover, there is a lack of understanding about the influence of formulation composition on the solid-state properties of a precipitate. Such understanding is fundamental for more rational development of pharmaceutical LBFs and for selecting appropriate *in vitro* assays for formulation screening. The present study focused on the precipitation behavior of lipophilic, weakly basic drugs from LBFs. A major aim was to investigate the influence of dispersion and digestion on the precipitation behavior of model bases. Therefore, the effect of pure dispersion was analyzed separately from the dispersion in a digestive environment. Particular attention was directed to the extent of drug supersaturation and precipitation, as well as to the solid-state properties and re-dissolution behavior of evolving precipitates. A further aim was to evaluate the influence of the LBF composition on dispersion- and lipolysis-triggered drug precipitation. The present study offers an improved understanding of the fate of LBFs with poorly soluble weak bases in the intestinal lumen.

6.2 Methods

6.2.1 Materials

We obtained loratadine, carvedilol, and 4-bromophenylboronic acid (4-BPBA, ≥95.0%) from AK Scientific (Union City, CA, USA). Trizma® maleate, calcium chloride dihydrate (≥99%), pancreatin (from porcine pancreas, 8xUSP specifications), sodium chloride (≥99%), ammonium acetate (≥99%), chloroform, and acetonitrile were from Sigma-Aldrich Chemie GmbH (Buchs, Switzerland). Lipoid E PC S (phosphatidylcholine from egg yolk) was supplied by Lipoid GmbH (Ludwigshafen, Germany), sodium taurodeoxycholate by Prodotti Chimici e Alimentari S.p.A. (Basaluzzo, Italy), and sodium hydroxide 1 M by Scharlab S.L. (Sentmenat, Spain). Imwitor® 988 was purchased from Sasol Germany GmbH (Witten, Germany), Miglyol® 812 N from Hänseler AG (Herisau, Switzerland), and Cremophor® EL from BASF AG (Ludwigshafen, Germany). Ethanol was obtained from Baker (Deventer, Netherlands). Transcutol® HP and Capryol® 90 were kindly donated by Gattefosse (Saint-Priest, France). Purified water was prepared with an Arium® 61215 water-purification system from Sartorius Stedim Biotech GmbH (Göttingen, Germany).

Imwitor 988 was a blend of medium-chain glycerides (54.6% monoglycerides, 38.0% diglycerides, and 7.1% triglycerides) with average molecular weights of 197, 340, and 483 g/mol, respectively (according to the certificate of analysis, Cremer Oleo GmbH). Miglyol 812 N was a medium-chain triglyceride consisting of 57.9% w/w caprylic acid (C8), 41.2% w/w capric acid (C10), 0.5% w/w lauric acid (C12), and 0.1% w/w caproic acid (C6) with an average molecular weight of 517 g/mol (according to the certificate of analysis, Hänseler AG). Capryol 90 was composed from propylene glycol monocaprylate (99.9% caprylic acid (C8), certificate of analysis, Gattefosse AG) and the surfactant Cremophor EL consisted of polyoxyl 35 castor oil.

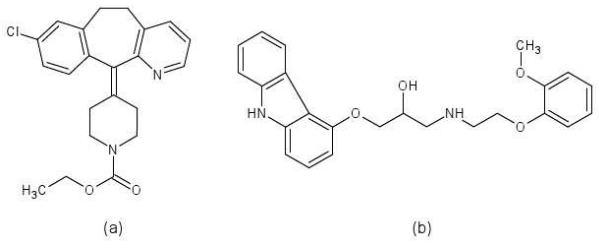

FIGURE 6.1: Chemical structures of the model drugs (a) loratadine (pK_a 5.3 [243], log$P$ 3.9) and (b) carvedilol (pK_a 7.8 [243], log$P$ 4.1).

6.2.2 Preparation of formulations

Three LBF were selected as model formulations and the compositions are detailed in Table 6.1. The lipidic components were mixed on a magnetic stirrer at 40°C until a clear solution was obtained. The mixtures were then slowly cooled to room temperature and finally the co-solvent (ethanol or Transcutol HP) was added.
We selected loratadine and carvedilol as lipophilic, weakly basic model compounds (Fig. 6.1). The formulations were loaded with the free bases at 80% of their saturation solubility in the corresponding formulation. All formulations were visually assessed for absence of undissolved drug particles prior to use.

Table 6.1: Composition of drug-free lipid-based formulations.

Excipient	Formulation F1 (% w/w)	Formulation F2 (% w/w)	Formulation F3 (% w/w)
Migliol 812	30.0	12.5	-
Imwitor 988	30.0	12.5	-
Cremophor EL	30.0	65.0	44.6
Ethanol	10.0	10.0	-
Capryol 90	-	-	33.0
Transcutol HP	-	-	22.4

6.2.3 Preparation of simulated intestinal medium and pancreatic extract

The simulated intestinal medium was composed of an aqueous buffer, 1.25 mM phosphatidylcholine (PC), and 5 mM sodium taurodeoxycholate (NaTDC) at concentrations simulating fasted state intestinal conditions. PC was dissolved in chloroform, and the solvent was evaporated under vacuum (Rotavapor RE 120, Büchi, Switzerland). NaTDC and digestion buffer (50 mM Trizma maleate, 150 mM NaCl, and 5 mM $CaCl_2 \cdot 2H_2O$; pH 7.5) were then added and the mixture was stirred for 12 h (450 rpm, 5°C).
To prepare the pancreatin extract, we mixed 1 g of porcine pancreatin powder per 5 ml of digestion buffer (5°C), stirred for 15 min, and then centrifuged the suspension (15 min, 1600xg, 5°C). Finally, the supernatant was collected and the pH adjusted to 7.5, which corresponded to the pH of the lipolysis medium. The pancreatin extract was freshly prepared each day and stored on ice until use.

6.2.4 Drug solubilization upon dispersion without lipolysis

We assessed the amount of precipitated loratadine and carvedilol during simple dispersion in the simulated intestinal medium (without digestive enzymes). Drug-containing formulation (3.0 g) was dispersed in 108 ml of digestion buffer (containing NaTDC and PC) in a glass vessel at 37°C and stirred at 450 rpm. After equilibrating the system for 10 min, 12 ml of pure digestion buffer (without pancreatic extract) were added and the medium was stirred for 1 h. A 2 ml aliquot was removed prior to and after 10, 30, and 60 min of dispersion. The samples were immediately filtered through a 0.1 μm polytetrafluoroethylene (PTFE) syringe filter [31] and diluted with acetonitrile (loratadine) and methanol (carvedilol). After centrifugation (16,000xg, 25°C, 30 min), the concentration of solubilized drug was measured by HPLC. The experiments were carried out in triplicate. We verified experimentally that no loss of dissolved substance occurred through adsorption onto the filter material.

6.2.5 *In vitro* lipolysis test

The *in vitro* lipolysis test was performed as described in the literature [146]. Simulated intestinal medium (108 ml) was transferred to a thermostated glass vessel (37.0 ± 0.5°C), and the formulation (3.0 g) was added. The mixture was stirred during 10 min for complete dispersion, thermal equilibration, and pH adjustment to 7.500 ± 0.001. For mixing, we used a magnetic stirrer (3 cm in diameter) at a speed of 450 rpm. Digestion was initiated by the addition of 12 ml pancreatin extract (final nominal lipase activity: 1000 tributyrin units per ml). The free fatty acids (FA) produced during lipolysis were titrated using 1 M NaOH to maintain pH 7.500 using a pH-stat apparatus (842 Titrando and 800 Dosino, Metrohm AG, Switzerland), which was operated using the Tiamo® 1.2 software package (Metrohm AG). Lipolysis was allowed to proceed for 30 min, and each experiment was carried out in triplicate.

6.2.5.1 "Back-titration" and determination of the extent of formulation digestion

It was previously shown that the titrated NaOH volume represents only an approximation of the free FA liberated during lipolysis. Some FA persist in the unionized state, according to the pK_a value, leading to an underestimation of the total FA liberation. To account for these unionized molecules, the so-called back-titration procedure was applied according to a previously described method [31]. Briefly, at the end of the 30 min

digestion period, the pH was rapidly increased to 9 by addition of 1 M NaOH for complete deprotonation. The pH increase was also performed with blank digestion buffer including pancreatic extract (without formulation, PC, and NaTDC) to determine the back-titration volume in the absence of lipolysis products. The latter volume was subtracted from the total back-titration volume to obtain the value of FA_{titr}(back-titration). The correction factor was calculated according to the formula:

$$\text{Correction factor} = \frac{FA_{titr}(\text{direct titration}) + FA_{titr}(\text{back-titration})}{FA_{titr}(\text{direct titration})} \tag{6.1}$$

where FA_{titr}(direct titration) is the cumulative amount of FA titrated by 30 min of digestion. The NaOH consumption caused by digestion of formulation lipids was finally obtained by subtracting the consumption due to lipolysis of the blank digestion medium (n=3). The extent of formulation digestion was calculated according to:

$$\text{Extent of digestion} = \frac{FA_{titr}^{tot}}{\text{Theor. max. amount of FA in LBF}} \tag{6.2}$$

where FA_{titr}^{tot} is the cumulative amount of ionized and unionized FA liberated by 30 min of digestion. The theoretical maximal amount of FA in the LBF was calculated assuming that each triglyceride molecule would liberate two FA and that diglyceride and monoglyceride molecules initially present in the formulation liberate one FA. Cremophor EL was assumed to be digested to an extent of 30% [203].

6.2.5.2 Quantification of lipolysis-triggered drug precipitation

The three formulations containing loratadine and carvedilol, respectively, were digested and the amount of precipitated and solubilized drug was assayed in the digests. Thus, after the 30 min digestion period, we immediately added a 4-BPBA solution (1 M in methanol, 9 μL per ml of digest) to inhibit further lipolysis [215], re-adjusted the pH, and ultracentrifuged the samples (80,000xg, 37°C, 90 min) in a Centrikon T-1180 ultracentrifuge equipped with a TFT-80.4 fixed-angle rotor (Kontron Instruments, Milan, Italy). The aqueous phase was then diluted with acetonitrile and centrifuged (16,000xg, 15 min). The pellet was suspended in purified water, diluted in acetonitrile, and centrifuged (16,000xg, 15 min). Finally, all samples were analyzed using high-performance liquid chromatography (HPLC).

6.2.6 Determination of drug solubility in the formulations and in digestive media

Drug solubility was determined in the undiluted formulation at 37°C. Excess solid drug was added to a 2 ml aliquot of blank formulation and stored in hermetically sealed glass vials during equilibration (37°C, 450 rpm). After 24, 48, and 72 h the samples were centrifuged (37°C, 16,000xg, 30 min) and, after dilution in solvent, the supernatant was analyzed by HPLC. Equilibrium was assumed when two consecutive solubility samples varied by ≤5% w/w.

Furthermore, we determined drug solubility in the lipolysis medium containing drug-free formulations prior to and after a 30 min digestion period. For the latter measurement, enzyme inhibitor (4-BPBA, 1M in methanol, 9 μl per ml of digest) was added to the medium after 30 min digestion and the pH was re-adjusted. Excess solid drug was transferred to an aliquot of the lipolysis medium and was hermetically sealed in glass vials. After an equilibration period of 4, 8, and 24 h (450 rpm, 37°C), the samples were centrifuged (16,000xg, 37°C, 15 min). The supernatant was then diluted in solvent, centrifuged (16,000xg, 15 min), and finally analyzed by HPLC. Whenever a lipid phase was obtained upon centrifugation, the lipid and the aqueous phase were re-emulsified, to measure the overall concentration of solubilized drug. Drug solubility experiments were carried out in triplicate. Equilibrium was assumed when two consecutive solubility samples varied by ≤5% w/w.

The maximal supersaturation ratios, SR^M, of the drug-containing formulations in the simulated intestinal media prior to and after digestion were calculated according to the equation $SR^M = C/C^*$, where C is the maximum concentration of solubilized drug and C^* was the solubility prior to and after 30 min lipolysis, respectively [26].

6.2.7 Physical characterization of precipitated drug

The precipitated drug following dispersion and the pellet phase that was obtained upon digestion and ultracentrifugation of the drug-containing formulation, were analyzed by X-ray powder diffraction (XRPD). The precipitate obtained after 1 h of dispersion was collected by filtration using a 0.1 μm polycarbonate filter membrane and immediately analyzed. To analyze the precipitate evolving during formulation lipolysis, the formulations were digested *in vitro* for 30 min, and after enzyme inhibition and pH re-adjustment, an aliquot was ultracentrifuged (80,000xg, 37°C, 90 min). The pellet phase was immediately isolated and an X-ray diffractogram was recorded. The same procedure was followed with the pellet phase obtained from a 30 min lipolysis experiment with drug-free formulation, which was spiked with an equal amount of pure drug (as used for the

formulation preparation). Moreover, we recorded the X-ray diffractograms of crystalline loratadine and carvedilol as a reference.
For X-ray analysis, we used a theta-theta X-ray powder diffractometer (R-XRD Phaser D2, Bruker AXS GmbH, Karlsruhe, Germany) equipped with a Co and Cu KFL tube (30 kV, 10 mA) as radiation source and a Lynxeye® detector. The samples were scanned in the angular range of 5° (2θ) to 40° (2θ) with a step size of 0.1° (2θ) and a count time of 5 s per step.

6.2.8 Re-dissolution of precipitated drug

Re-dissolution of loratadine and carvedilol that precipitated during formulation lipolysis was analyzed in an Erweka DT600 USP 2 paddle dissolution apparatus. Drug-free digestion buffer (containing NaTDC and PC) was preheated in dissolution vessels (37°C, 75 rpm) and the pH was adjusted to 7.5. The volume of the dissolution medium was large enough to ensure sink conditions. After formulation lipolysis (30 min) and enzyme inhibition, the digest was ultracentrifuged (80,000xg, 37°C, 90 min) and the resulting pellet phase was collected. The pellet was re-suspended in 5 ml digestion buffer and added to the re-dissolution medium. Samples (2 ml) were removed after 1, 2, 5, 10, 20, 30, 40, 60, 120, and 180 min of re-dissolution, filtered through a polyvinyl difluoride (PVDF) syringe filter (0.45 μm) and subsequently analyzed by HPLC.
Re-dissolution was studied with pellets obtained after lipolysis of the formulations containing loratadine and carvedilol as well as with a reference pellet. This reference was a pellet obtained from 30 min lipolysis of drug-free formulation, which was spiked with an equal amount of pure crystalline drug. All experiments were conducted in triplicate.

6.2.9 Dynamic light scattering

We measured the particle size of the dispersed formulations before lipolysis initiation by dynamic light scattering using a Zeta Sizer Nano ZS (Malvern Instruments, Malvern, UK), equipped with a 4 mW He-Ne laser operating at a wavelength of 633 nm. Since the formulations were highly diluted in an aqueous medium, the viscosity of water was assumed. The scattering signal was detected at an angle of 173° and measurements were performed at 37°C. Each sample was measured in triplicate and the result was expressed as intensity averaged particle diameter (nm).

6.2.10 High-performance liquid chromatography (HPLC)

For HPLC analysis (Agilent Technologies 1200 Series) we used an autosampler (G1329A), an isocratic pump (G1310A), and a variable wavelength detector (G1310A). A Zorbax® Eclipse Plus C18 (5 μm) column (Agilent Technologies, Santa Clara, CA, USA) was used for all experiments. Loratadine and carvedilol were detected at wavelengths of 248 and 254 nm, respectively. Loratadine was eluted with 40% acetonitrile and 60% phosphate buffer (20 mM, pH 2.5) and carvedilol with 35% acetonitrile and 65% acetate buffer (20 mM, pH 2.5). All sample measurements were within the linear range of calibration.

6.3 Results

6.3.1 Characterization of the LBFs

Three different LBFs (F1, F2, and F3, see Table 6.1) in combination with two lipophilic, weakly basic compounds (loratadine and carvedilol) were selected as model systems. All formulations were self-emulsifying and dispersed rapidly in simulated intestinal medium. The evolving systems ranged from a sub-micron emulsion to colloidal dispersions exhibiting mean droplet diameters of 171.6 ± 11.5, 26.74 ± 0.04, and 34.34 ± 0.13 nm, for formulations F1, F2, and F3, respectively (n=3).
The digestion profiles of the three model formulations are depicted in Figure 6.2. All formulations were hydrolyzed in the presence of digestive enzymes. After 30 min of digestion, formulations F1 and F2 were almost completely digested and formulation F3 was digested to the extent of ∼85.7%. Thus, all dispersions changed substantially over the course of formulation digestion.

6.3.2 Determination of drug solubility and supersaturation ratio

The solubilities of loratadine and carvedilol were determined in the three undiluted formulations, in pure lipolysis medium (without LBF and lipolytic enzymes), as well as in the dispersed systems prior to and after lipolysis. The solubilities of loratadine and carvedilol in pure lipolysis medium were 0.039 ± 0.001 and 0.049 ± 0.007 mg/ml, respectively. The undiluted formulations demonstrated high solubilization capacities with drug solubilities of 130.5 to 165.2 mg/g for loratadine and 78.4 to 145.4 mg/g for carvedilol 6.2. Comparatively lower drug solubilities were found with the dispersed formulations, as expected. In dispersed, undigested formulations, loratadine solubilities were in the range of 1.23 to 2.59 mg/ml, while carvedilol solubilities were between 0.602 and 1.506

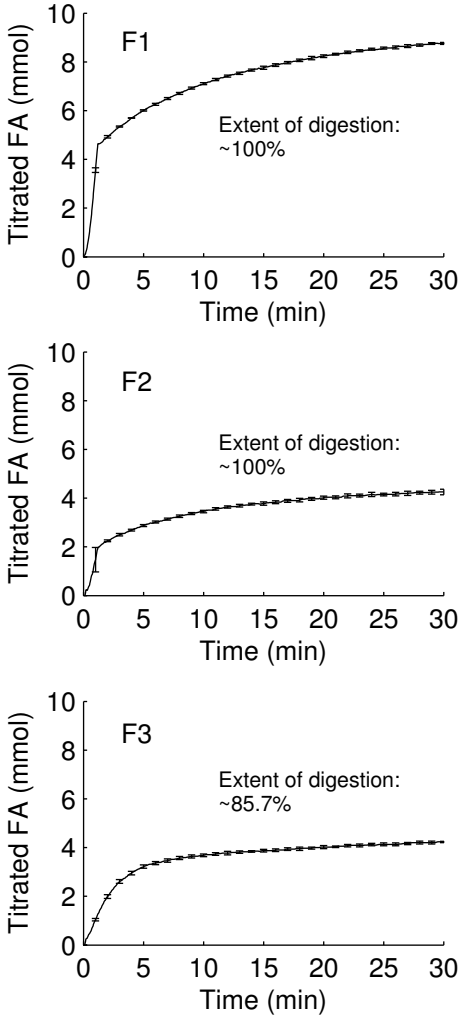

FIGURE 6.2: Titration profile of FA obtained during the 30 min lipolysis of formulations F1, F2, and F3 (mean ± SD, n=3). The titration profiles were corrected with the back-titration factor, and the NaOH consumption caused by the digestion of blank digestion medium was subtracted. The extent of formulation digestion was ∼100% for formulations F1 and F2, and ∼85.7% for formulation F3.

mg/ml. In digested formulations, loratadine solubilities were in the range of 0.63 to 0.79 mg/ml, while carvedilol solubilities were between 0.49 and 1.02 mg/ml.

While all pre-concentrates were below saturation (saturation ratio of 0.8), the dispersed and digested formulations became supersaturated. We calculated the supersaturation ratio SR^M for each dispersed formulation, prior to and after 30 min lipolysis. SR^M is the ratio of the maximum drug concentration (that is attained *in vitro*) and drug solubility [26, 77]. It is a measure of the driving force for drug precipitation; *i.e.*, the higher SR^M, the higher the likelihood for drug precipitation. The dispersed, undigested systems were slightly supersaturated with SR^M values of 1.17 to 2.55. This was different for the digested formulations, where the SR^M increased in each formulation (Table 6.2).

Drug supersaturation was most pronounced with formulation F3, resulting in a more than three times higher SR^M value at the end of lipolysis compared with that at the beginning. With formulation F1, which liberated the largest amount of FA, the supersaturation ratio almost doubled over the course of lipolysis. Finally, with formulation F2, the increase in supersaturation were comparatively moderate (1.6 and 1.1 times the SR^M values prior to lipolysis, respectively).

TABLE 6.2: Drug solubility in the undiluted formulations and saturation ratios (mean ± SD) at the beginning and after a 30 min digestion period. The SR^M is calculated for the formulations containing drug at a concentration corresponding to 80% of solubility (*i.e.*, saturation of 0.8 in each pre-concentrate). The table also details the solid-state of precipitating material during formulation dispersion and digestion.

Compound	LBF	Solubility,	Supersaturation ratio, SR^M		Solid-state of precipitate	
		C^* (mg/g)	Dispersion	Lipolysis	Dispersion	Lipolysis
Loratadine	F1	165.2 ± 3.3	2.23 ± 0.02	5.15 ± 0.08	No precip.	Crystalline
	F2	130.5 ± 5.0	2.02 ± 0.02	3.21 ± 0.10	Crystalline	Crystalline
	F3	156.2 ± 2.9	1.17 ± 0.02	4.16 ± 0.04	No precip.	Crystalline
Carvedilol	F1	78.4 ± 5.6	2.55 ± 0.01	4.34 ± 0.44	No precip.	Amorphous
	F2	145.4 ± 3.7	2.29 ± 0.01	2.59 ± 0.16	Crystalline	Amorphous
	F3	139.6 ± 4.1	1.78 ± 0.04	5.63 ± 0.22	No precip.	Amorphous

6.3.3 Drug solubilization upon dispersion without lipolysis

The drug solubilization capacity was first studied for each drug-loaded formulation upon dispersion only. The dispersion medium was identical to the medium used for lipolysis but without digestive enzymes. As seen in Figure 6.3a and b, formulations F1 and F3 were able to maintain the compounds in solution during the 1 h dispersion period. In contrast, formulation F2 resulted in drug precipitation, and after 1 h, only 71.2 ± 6.9% of loratadine and 61.6 ± 13.9% of carvedilol remained in solution.

Drug material that precipitated from formulation F2 was collected and analyzed using XRPD. As seen in Figure 6.4, the angular range of peaks of precipitated loratadine and carvedilol mostly corresponded to those of the reference patterns (pure, crystalline drugs). Therefore, apparently, loratadine and carvedilol precipitated in a crystalline form during dispersion.

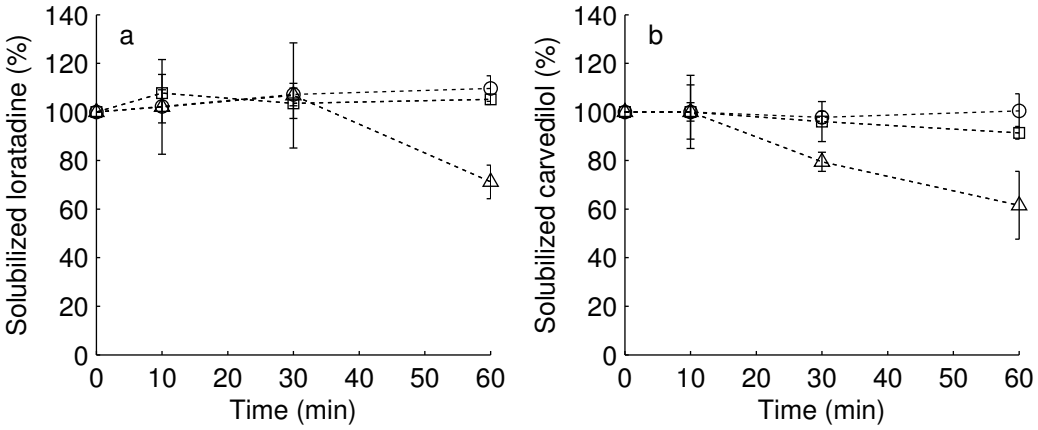

FIGURE 6.3: Percentage of solubilized loratadine (a) and carvedilol (b) after dispersion of formulations F1 (◯), F2 (△), and F3 (□) under non-digesting conditions (mean ± SD, n=3). Only formulation F2 resulted in relevant precipitation of loratadine and carvedilol after 60 min of dispersion.

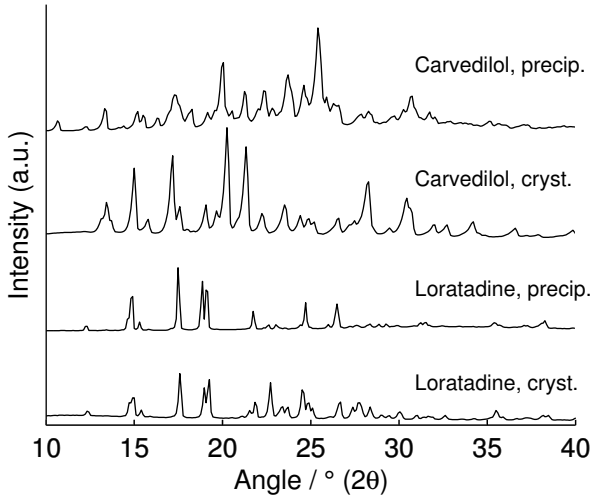

FIGURE 6.4: XRPD patterns of precipitated loratadine and carvedilol collected after 1 h of dispersion of formulation F2. The angular range of peaks of precipitated loratadine and carvedilol corresponded to that of the reference pattern (pure, crystalline drug). This result suggests that loratadine and carvedilol precipitated in the crystalline form during dispersion of formulation F2.

6.3.4 Drug precipitation under digesting conditions

The three formulations containing loratadine and carvedilol were digested for 30 min and the amounts of precipitated drug determined after sample ultracentrifugation. Each formulation resulted in extensive drug precipitation. For formulations with loratadine, approximately 70% of the drug was precipitated after 30 min of digestion. Formulations with carvedilol showed a slightly larger extent of precipitation, ranging from 78.2 to 91.8% (Fig. 6.5). No oil phase was visually detectable in ultracentrifuged samples, which supports the observation that the formulations were almost completely digested by the end of the experiment. With formulations F1 and F3, precipitation of loratadine and carvedilol was only triggered by formulation digestion. Instead, with formulation F2, the main trigger of drug precipitation was formulation dispersion, whereas the contribution of formulation digestion was moderate (2.6% and 16.6% of total drug precipitation for loratadine and carvedilol, respectively).

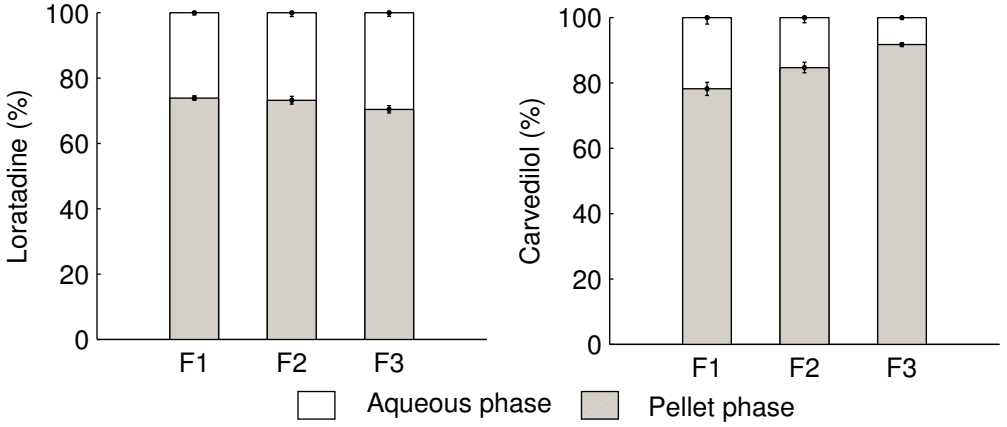

FIGURE 6.5: Amount of loratadine (left plot) and carvedilol (right plot) in the aqueous and pellet phase obtained upon digestion of the three formulations F1, F2, and F3 (mean ± SD, n=3). Approximately 70% of loratadine was precipitated after 30 min of digestion, whereas the extent of carvedilol precipitation was slightly higher (78.2 to 91.8%). The total extent of precipitation was very similar amongst the formulations of a given drug and no oil phase was visually detectable in ultracentrifuged samples.

The pellet phases containing precipitated drug were further analyzed by XRPD. Figure 6.6 depicts the XRPD patterns of pure loratadine and carvedilol, of the pellets containing precipitated drug, and of a reference pellet. This reference was the pellet obtained after lipolysis of drug-free formulation spiked with crystalline drug. The XRPD patterns of these reference pellets displayed the typical diffraction patterns of crystalline loratadine and carvedilol, respectively. For the pellets with precipitated loratadine, the

angular range of peaks corresponded to that of the reference pellet.

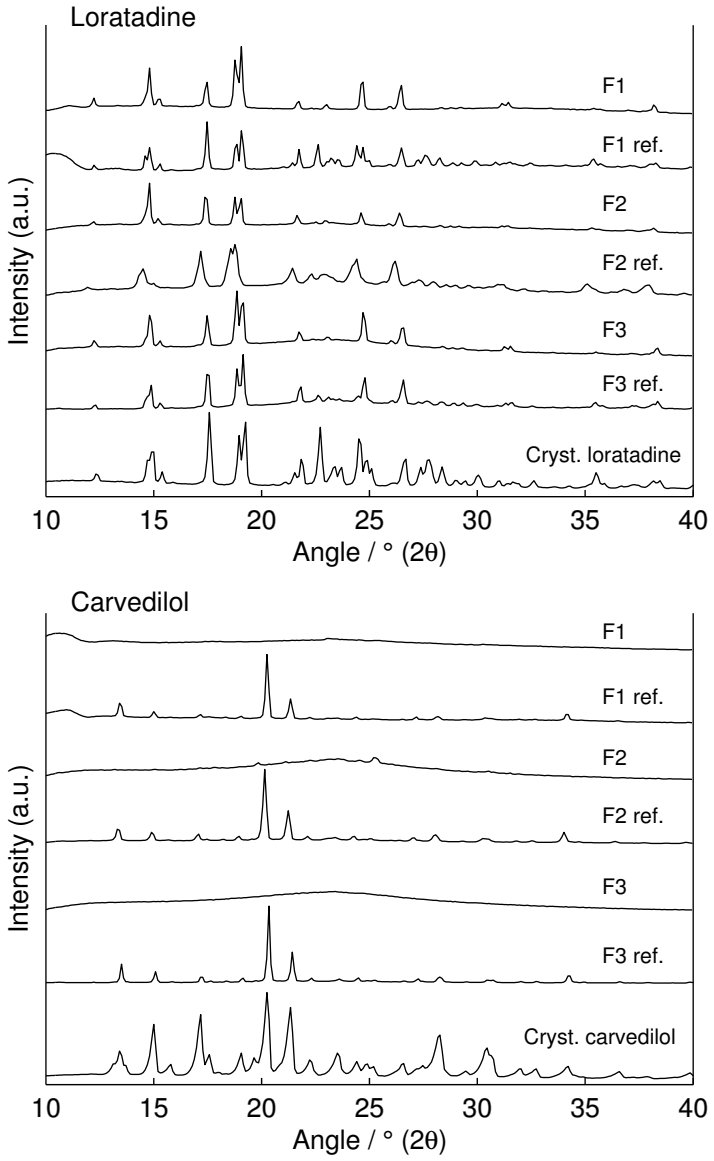

FIGURE 6.6: XRPD pattern of the pellets obtained from the lipolysis of formulation F1, F2, and F3 containing precipitated loratadine (upper plot) and carvedilol (lower plot). As a reference, the XRPD pattern of pure crystalline drug, and of the blank pellets containing the corresponding amount of crystalline drug (F1 ref., F2 ref., F3 ref.) were recorded. The angular range of peaks of precipitated loratadine corresponded to that of the reference patterns, suggesting that loratadine precipitated in crystalline form during digestion. In contrast, the XRPD patterns of precipitated carvedilol revealed no characteristic peak, suggesting that carvedilol precipitated in an amorphous form during digestion.

In contrast, this characteristic peak pattern was almost absent in the pellet with precipitated carvedilol. Only slight peaks were observed in the XRPD pattern of pellets with

precipitated carvedilol, especially with formulation F2. These peaks may indicate a crystallization process, which was very slow compared to the observation period. However, these XRPD patterns suggested that carvedilol mostly precipitated in the amorphous state, while loratadine apparently precipitated in crystalline form during lipolysis.
Comparison of the precipitation behavior of the two drugs in the range of formulations revealed that the extent of precipitation was very similar amongst the three formulations for a given drug. Analogously, no formulation effect was seen for a given drug with respect to the solid-state form of the precipitates.

6.3.5 Re-dissolution

To put the results of solid-state analysis into a biopharmaceutical perspective, we studied the re-dissolution of the precipitates obtained upon lipolysis. The re-dissolution profiles of the pellets containing precipitated drug and of the reference pellets spiked with the corresponding amounts of the crystalline drugs are plotted in Figure 6.7.
The dissolution profiles of precipitated loratadine were very similar to the dissolution profile of the reference pellet, which contained crystalline drug. Hence, almost 100% of the drug re-dissolved within 60 min. In contrast, re-dissolution of precipitated carvedilol was considerably faster in comparison with the reference pellet. The plots of formulations F1 and F2 show that more than 90% of the precipitated carvedilol re-dissolved within 30 min, while the crystalline drug in the reference pellet remained incompletely dissolved after 180 min of re-dissolution. This result supports the finding that precipitated carvedilol differed from the crystalline drug. Interestingly, re-dissolution of loratadine was comparatively fast, although it was in a crystalline state.
Considering loratadine and carvedilol separately, there was no pronounced influence of the (digested) formulation on the drug dissolution profiles. However, an exception occurred for the pellet of formulation F2 containing precipitated carvedilol. Re-dissolution here was notably slower than with the precipitates of F1 and F3. This difference was likely due to the difficulty in disintegrating the pellet phase of system F2, which formed a rather dense aggregate during sample preparation.

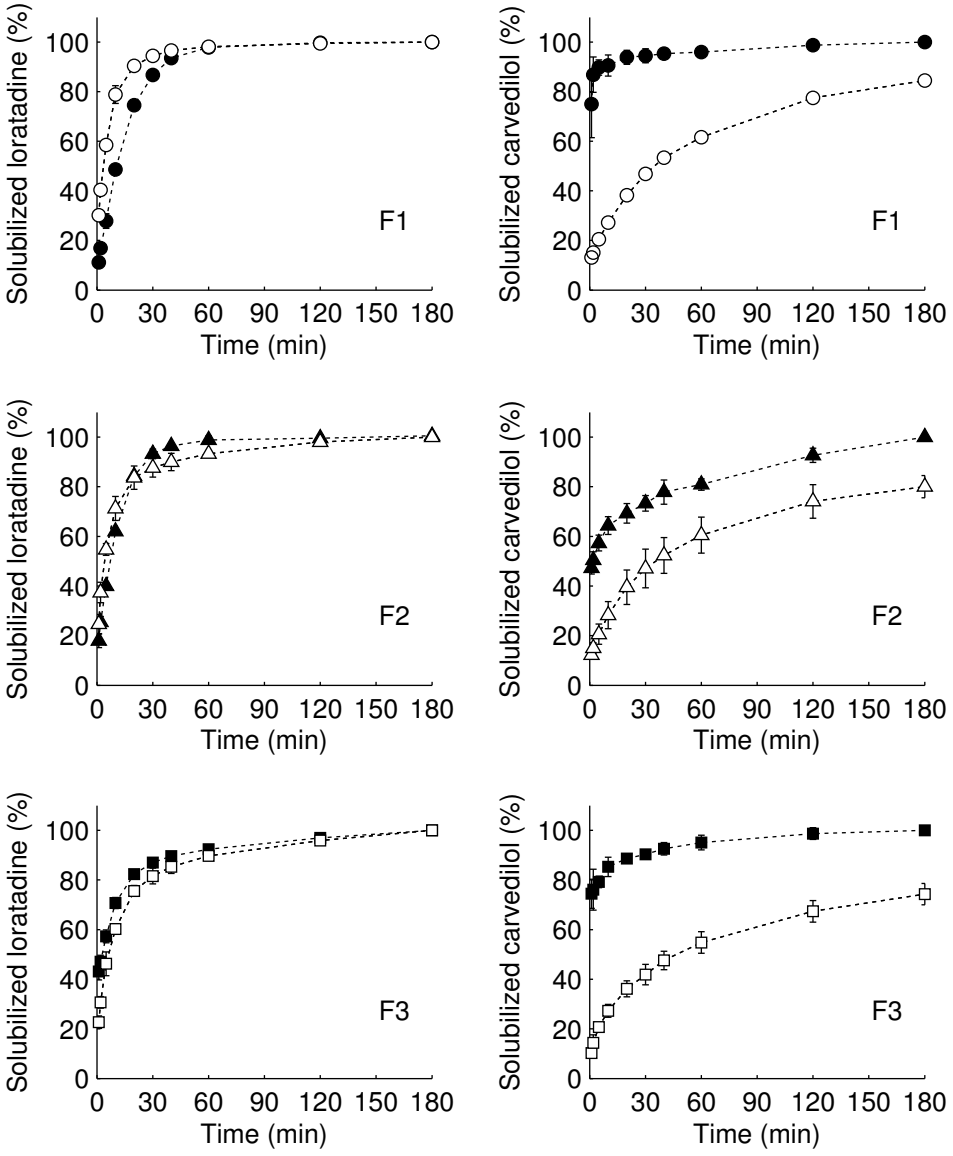

FIGURE 6.7: Re-dissolution profiles of loratadine (left) and carvedilol (right) in pellets obtained from the lipolysis of formulation F1, F2, and F3. Filled symbols represent the dissolution values of pellets containing precipitated drug, open symbols are reference values of blank pellets spiked with crystalline drug (mean ± SD, n=3). The dissolution profiles of precipitated loratadine were very similar to the dissolution profile of the reference pellet that contained crystalline drug. In contrast, the dissolution of precipitated carvedilol occurred considerably faster than that of the reference pellet.

6.4 Discussion

Several *in vitro* assays have been developed to simulate the precipitation of weakly basic drugs during gastrointestinal passage [213, 239, 240, 243, 244]. These are valuable approaches for estimating a drug precipitation profile at intestinal pH in the presence of bile salts and phospholipids. However, when a weak base is administered in an LBF, the drug is not only surrounded by a simple aqueous environment. There are lipidic excipients and hydrolysis products in close proximity to the drug that determine the apparent solubilization capacity of the medium and may influence drug precipitation.
The purpose of this study was to analyze the precipitation behavior of lipophilic weak bases formulated in different LBFs by considering the dispersion and digestion steps separately. Loratadine and carvedilol were selected as model compounds and dissolved in three different LBFs. The pre-concentrates had the same drug saturation ratio of 80% solubility (at 37°C). However, upon formulation dispersion, there was a decrease in solubilization capacity that resulted in a slightly supersaturated state. One formulation (F2) exhibited some precipitation of both loratadine and carvedilol after 60 min of dispersion. The hydrolytic breakdown of formulation lipids notably increased the degree of supersaturation, especially with formulations F1 and F3, which resulted in substantial drug precipitation.
Interestingly, we observed partially different solid-state properties of the precipitates depending on the experimental conditions. During dispersion without lipolytic enzymes, both loratadine and carvedilol precipitated as crystalline materials. Formulation lipolysis also led to the precipitation of crystalline loratadine, but in contrast, carvedilol precipitated as an amorphous drug. It is interesting to compare these results with the findings of Hsieh *et al.* [243], who described the supersaturation and precipitation behaviors of loratadine and carvedilol during potentiometric titration. The drugs were initially dissolved in a simple aqueous medium (without excipients, phospholipids, and bile salts) and pH-induced precipitation resulted in amorphous material for both loratadine and carvedilol [243].
Compared with our study, these findings suggest that precipitation triggered by a pH-change alone should be clearly differentiated from cases in which formulation lipids, medium bile salts, and phospholipids influence the precipitation process. It is well known from chemical engineering that the solid-state of a precipitated substance largely depends on the given precipitation process and on solvent conditions [78]. For example, a compound that precipitates because of a solvent change may have different solid-state properties than the same drug precipitated by a pH-shift. During potentiometric titration in a simple aqueous medium, as it was in the studies of Hsieh *et al.* [243], the pH gradient was the major trigger generating supersaturation and amorphous drug precipitation. However, as seen from our results, during biorelevant formulation processing

there appears to be a complex interplay of factors that should be discussed in more detail.

When a LBF reaches the gastrointestinal fluids, it first disperses to build fine oil droplets or micellar structures. During this process, there is a partitioning of drug between oil droplets, micellar species, and water, which is determined by the relative affinity of the compound to these different phases. Drug partitioning into the aqueous phase determines the free fraction of drug that deprotonates in the basic environment (depending on pK_a). Therefore, the kinetics of drug partitioning is linked to the kinetics of deprotonation to free base, and thus it determines the rate of drug supersaturation. Compared with precipitation in a simple aqueous medium, the use of biorelevant media also implies the presence of several negatively charged counterions such as bile salts, maleate, and chloride ions. These negatively charged species can interact with the base, determine its solubility in the medium and, thus, the extent of drug supersaturation and kinetics of precipitation. A further influence can occur with respect to the stability of supersaturation. When a system reaches a supersaturated state, it is naturally prone to drug precipitation. However, the nucleation induction time is largely determined by the stability of this metastable state, and in a complex medium, it can be notably influenced by the presence of endogenous and exogenous surfactants [55, 56, 70, 245].

When the formulation reaches the intestinal lumen, LBFs are generally digested by lipolytic enzymes [31, 56]. The digestion of formulation lipids results in a substantial transformation of the vehicle toward higher polarity. If the original lipid was a good solvent for the drug, then this process can be viewed as a kind of solvent depletion and is probably a major trigger for drug precipitation. In the case of a weak base there may be an additional effect caused by charge interactions with negatively charged FA, which are produced during hydrolysis of glycerides at the surface of oil droplets. Charged lipolysis products are likely to be in close proximity to ionized weak bases, thereby favoring molecular interactions. It must be kept in mind that this type of interaction is particularly relevant during lipolysis and is not present during formulation dispersion without digestion.

It is worth noting that the formulation performance *in vivo* is expected to be even more complex. First, the unstirred water layer at the intestinal surface is characterized by an acidic microclimate (pH 5.3-6.2) [246–248]. This lower pH favors protonation, and hence, it can improve the solubilization of a weakly basic drug. Secondly, the absorption of drug through the intestinal membrane reduces the total drug concentration in the intestinal lumen. This *in vivo* sink is particularly relevant for highly permeable drugs, for which absorption leads to a fast decrease in drug supersaturation. Care is therefore needed when predicting the extent of precipitation using one-compartmental assays, such as the *in vitro* lipolysis test. For qualitative analyses of the precipitate, this lack of absorptive sink is probably less critical. Moreover, the precipitation behavior of

a weak base may also depend on the nutritional state. In the present study, we used a state-of-the-art method for lipolysis testing, which simulated formulation performance in the fasted state. The gastric passage was neglected, because formulation transfer into the intestine is expected to be rapid. However, drug molecules may still migrate out of oil droplets into the acidic bulk phase, even though the gastric residence time is comparatively short. Partitioning of weak bases in the gastric environment has recently been shown for cinnarizine in equilibrium [80], but the kinetics of such partitioning is currently unknown. However, intestinal drug supersaturation and precipitation may be influenced by such drug partitioning in the gastric environment.

Based on these considerations and on our experimental results it seems that, although a particular chemical compound exhibits some intrinsic propensity to precipitate in either crystalline or amorphous states [249], the solid-state of a drug precipitating in the intestinal environment is hardly predictable *a priori*. The appropriate selection of experimental methods simulating the intestinal lumen is therefore of great importance, as evidenced in recent the works of Psachoulias *et al.* The precipitation of ketoconazole (without excipients) was analyzed *in vivo* [61], and a three compartment *in vitro* model was developed to simulate the gastrointestinal transit of an aqueous ketoconazole solution [240]. In the *in vitro* model, the gastric and intestinal compartments contained an HCl solution (pH 2.5) and fasted state simulating intestinal fluid (FaSSIF-V2plus [61], without digestive enzymes), respectively. The transfer of ketoconazole from the gastric into the luminal compartment resulted in supersaturation and precipitation of crystalline drug *in vitro*. In contrast, amorphous ketoconazole was isolated in luminal aspirates after administration to humans. Therefore, the presence of lipids, digestive enzymes and/or drug absorption clearly influenced the precipitation behavior of ketoconazole *in vivo*.

Such *ex vivo* studies of precipitating material are of high interest. More research is needed to clarify effects of sampling *in vivo* as well as *in vitro*. Sampling effects may affect the determined precipitation kinetics and especially the lag time between sample removal and solid-state analysis could be critical regarding a phase transition of the solid-state. Similarly, the *in vitro* addition of enzyme inhibitor (4-BPBA) could influence the precipitation behavior of the drug so that more studies are needed to this end.

In this study the impact of formulation composition on drug precipitation was also analyzed. The data revealed no specific influence of the formulation on the solid-state properties of precipitated drug. Re-dissolution data indicated that carvedilol dissolved considerably faster than the drug in the control experiment. In contrast, re-dissolution of precipitated loratadine was slower and followed almost the same kinetics as the reference data. This result confirms the solubility advantage of the amorphous precipitate compared with the crystalline material [60, 79]. A superior re-dissolution performance of amorphous drug was also reported in recent studies [33, 80]. Larsen *et al.* analyzed the

in vivo performance of LBFs with cinnarizine in dogs [80]. Although one formulation exhibited amorphous precipitation *in vitro*, the corresponding oral bioavailability was not lower than with the other formulations, which were able to prevent drug precipitation *in vitro*. Therefore, these *in vivo* data may support the view of facilitated re-dissolution from amorphous precipitates during intestinal transit. Other effects mentioned above, such as the *in vivo* sink and stabilization of supersaturated drug, might also have contributed.

Interestingly, re-dissolution of loratadine was rather fast compared with the re-dissolution of crystalline carvedilol. It was therefore assumed that loratadine, although it is in a crystalline state, would re-dissolve during intestinal transit. This is an important aspect: even a crystalline precipitate would not directly indicate poor re-dissolution and erratic drug absorption. The administered drug dose, drug permeability, and the kinetics of drug precipitation and re-dissolution ultimately define the fraction of drug absorbed. Based on these considerations, an improved biopharmaceutical understanding of drug precipitation from LBFs may begin with characterizing its solid-state properties as well as its re-dissolution kinetics.

6.5 Conclusions

The findings of the present study are of high practical importance for the development of oral LBFs with weakly basic drug candidates. Apparently, weak bases do not generally precipitate in a specific form, but the resulting solid-state is largely depending on compound properties as well as on *in vitro* testing conditions. The results also suggested that a classification of weak bases according to their precipitation behavior in a simple pH shift experiment can be only tentatively related to the precipitation of weak bases from LBFs under dispersion/digestion conditions. The extent of drug precipitation and consideration of solid-state properties is of critical importance in LBF development. Therefore, solid-state characterization of precipitated drugs under different experimental conditions should be routinely performed in formulation screening to better understand the biopharmaceutical behavior of LBFs.

This study provided new insights into the likely fate of LBFs in the GI tract and such improved understanding is highly needed to better predict LBF behavior *in vivo*. The finding that the surrounding dispersive or digestive environment affects the solid-state of a precipitate emphasizes the need for an improved mechanistic understanding of the precipitation behavior from LBFs. More research should especially be directed to the activation energy of solid-state phase transitions, as it may significantly determine the resulting precipitate. It also appears very promising to include solid-state properties as well as the re-dissolution behavior into physiologically-based pharmacokinetic models to

improve the simulation of formulation performance *in vivo*. In addition to such physicochemical excipient effects, an LBF can also influence biological processes such as drug permeability, gastrointestinal transit time, and/or pre-systemic clearance. These aspects should be considered when a new formulation is developed. A better understanding of the complex interplay of basic drugs with lipid-based excipients and intestinal media is certainly a key requirement to better design LBFs in the future.

Chapter 7

Comparison of high-resolution ultrasonic resonator technology and Raman spectroscopy as novel PAT tools for drug quantification in SEDDS

Summary

This study evaluates Raman spectroscopy and high-resolution ultrasonic resonator technology (URT) as analytical tools for drug quantification in self-emulsifying drug delivery systems (SEDDS). The model drugs fenofibrate, indomethacin, and probucol were quantitatively assayed in different self-emulsifying formulations. We measured ultrasound velocity and attenuation in the bulk formulationcontaining drug at different concentrations. The formulations were also studied by Raman spectroscopy. We used both, an in-line immersion probe for the bulk formulation and a multi-fiber sensor for measuring through hard-gelatin capsules that were filled with SEDDS. Each method was assessed by calculating the relative standard error of prediction (RSEP) as well as the limit of quantification (LOQ) and the mean recovery.

Raman spectroscopy led to excellent calibration models for the bulk formulation as well as the capsules. The RSEP depended on the SEDDS type with values of 1.5–3.8%,

Stillhart C. *et al.* Comparison of high-resolution ultrasonic resonator technology and Raman spectroscopy as novel PAT tools for drug quantification in SEDDS. *Journal of Pharmaceutical and Biomedical Analysis*, **2012**, 59, 29–37.

while LOQ was between 0.04 and 0.35% (w/w) for drug quantification in the bulk. Similarly, the analysis of the capsules led to RSEP of 1.9–6.5% and LOQ of 0.01–0.41% (w/w). On the other hand, ultrasound attenuation resulted in RSEP of 2.3–4.4% and LOQ of 0.10.6% (w/w). Moreover, ultrasound velocity provided an interesting analytical response in cases where the drug strongly affected the density or compressibility of the SEDDS. We conclude that ultrasonic resonator technology and Raman spectroscopy constitute suitable methods for drug quantification in SEDDS, which is promising for their use as process analytical technologies.

7.1 Introduction

The American Food and Drug Administration (FDA) initiative on process analytical technologies (PATs) has notably increased the interest in novel analytical methods for pharmaceutical product analysis (US FDA PAT Guidance, 2004). A variety of methods for drug quantification in pharmaceutical formulations, such as infrared (IR) spectroscopy or high-performance liquid chromatography (HPLC), require extensive manual sample preparation, are time-consuming, and usually destructive. This is in contrast to the main PAT requirements asking for rapid and non-destructive analytical methods. Today we know about a couple of analytical techniques that are used for process monitoring [250]. However, some processes and drug delivery systems are particularly challenging, so that applied research is needed for the implementation of existing techniques and the evaluation of novel methods.

A highly promising technique is based on ultrasound analytics, since sound waves can propagate through turbid media of liquid and semi-solid pharmaceutical formulations. Ultrasound technology has evolved over time and two main applications have been established: acoustic resonance spectroscopy and high-resolution ultrasonic resonator technology (URT). In spectroscopic analysis, ultrasound velocity and attenuation are measured over a large frequency range. In contrast, URT utilizes a specific ultrasound frequency to determine high-resolution ultrasound velocity and attenuation. Recently, Medendorp *et al.* pioneered the use of acoustic resonance spectroscopy as a PAT tool for drug quantification in semi-solids [251]. Similarly, Chen *et al.* measured the concentration of a model drug and an excipient in acetone solution with this technique [252]. URT was also applied in process analytics [195, 253], but to the best of our knowledge real-time monitoring of drug concentration in pharmaceutical formulations has never been assessed. However, this technology bears great potential as a PAT tool for drug quantification due to the rapid data collection without additional sample preparation,

the relative low-cost instrumentation, the fast computing time, and the possibility of flow-through measurement.

In contrast to the ultrasound-based method, Raman spectroscopy has already gained some importance in several process analytical applications [254]. The high chemical specificity of Raman spectroscopy is one of the key advantages over other tools such as IR spectroscopy. An increasing number of Raman applications have been reported in recent years. Many quantitative Raman methods focused on solid dosage forms such as tablets, capsules, and powders [255–260]. In addition, Gotter *et al.* [261] described the use of Raman spectroscopy for the quantification of a drug suspended in a simple semi-solid formulation consisting of paraffin. More complex solid pharmaceutical formulations were analyzed by Hargreaves *et al.* [255], who established Raman spectroscopy for quantitative analysis of multi-component pharmaceutical capsules. This study demonstrated the suitability for quantifying three low-level excipients in the formulation as well as an active pharmaceutical ingredient (API). To the best of our knowledge, more complex semi-solid formulations such as SEDDS have not been investigated yet.

SEDDS are typically mixtures of up to five excipients (triglyceride oils, mixed glycerides, lipophilic surfactants, hydrophilic surfactants, and water-soluble cosolvents) [9] that undergo self-emulsification if they are exposed to water. Their ability to enhance oral absorption of poorly water-soluble drugs led to a growing interest in formulation research [9]. Some formulations, *e.g.*, ritonavir (Norvir®), saquinavir (Invirase®), and cyclosporine (Sandimmun Neoral®), have already reached the market.
Since SEDDS provide particularly complex matrices, we aimed to use such formulations to evaluate URT as well as Raman spectroscopy for API quantification. Particular emphasis was placed on comparing the two methods with respect to their analytical performance in the different systems. Moreover, we considered two optical Raman configurations: one was intended for in-line measurement in the bulk solution and the other, a multi-fiber sensor, was foreseen for drug quantification through hard-gelatin capsules filled with SEDDS.

7.2 Materials and Methods

7.2.1 Materials

Polysorbate 80 and Miglyol 812 were purchased from Hänseler AG (Herisau, Switzerland), Imwitor® 742 and Imwitor® 988 were supplied by Sasol Germany GmbH (Witten,

Germany), and Cremophor® RH 40 by BASF SE (Ludwigshafen, Germany). Fenofibrate, indomethacin, and probucol were all obtained from Sigma-Aldrich Chemie GmbH (Buchs, Switzerland). Uncolored hard-gelatin capsules Licaps® (size 1) were received from Capsugel (Bornem, Belgium).
For the preparation of the simulated gastric media, we obtained sodium chloride from Carl Roth GmbH (Karlsruhe, Germany), pepsin from Hänseler AG (Herisau, Switzerland), sodium taurocholate from Prodotti chimici ed alimentari S.p.A. (Basaluzzo, Italy), phosphatidylcholine from Lipoid GmbH (Ludwigshafen, Germany), and hydrochloric acid (1 N) from Sigma-Aldrich Chemie GmbH (Buchs, Switzerland).

7.2.2 Samples and analytics

Two different SEDDS consisting of polysorbate 80, Imwitor 988, Miglyol 812 (50/15/35; PO), and Cremophor RH 40, Imwitor 742, Miglyol 812 (40/30/30; CO) were selected as model formulations [48, 91]. For both formulations, we prepared a concentration series with each of the three APIs fenofibrate (Fen), indomethacin (Ind), and probucol (Pro), separately. Therefore, a total of six concentration series, each including 33 samples, were studied.
The oils (Miglyol 812, Imwitor 742, Imwitor 988) and the surfactant (Cremophor RH 40 and polysorbate 80, respectively) were mixed on a magnetic stirrer at 40°C until a clear solution was obtained. Samples of different API concentrations were then prepared by dissolving the drugs in the vehicle at room temperature using a magnetic stirrer.
In the analytical part of the experiment, the drug content was first determined in each bulk formulation by Raman spectroscopy and URT. The formulations were then manually filled into hard-gelatin capsules (∼70% volumetric filling degree). A multi-fiber Raman probe was subsequently used for API quantification through the capsule to compare in-line bulk analytics with a drug assay through the capsule material. Finally, HPLC was used as the reference method for API quantification. A detailed description of each analytical method is given in the following sections.

7.2.2.1 Solubility study

The solubility of the three APIs in PO and CO was determined in triplicate at room temperature. An excess amount of API was added to the formulations and then the suspensions were continuously mixed on a magnetic stirrer. To ensure that the equilibrium was reached, the solubility was determined after 24 h, 48 h, and 72 h. Then, samples were centrifuged at 2000 rpm for 30 min using an Eppendorf centrifuge (model 5415 C)

to separate non-dissolved API from the vehicle. Finally, the drug concentration in the supernatant was assessed by HPLC.

7.2.2.2 Characterization of diluted SEDDS

The model systems were characterized with respect to their self-emulsification behavior upon dilution under physiological conditions. Therefore, formulations with and without API were diluted at 37°C (1:200 w/w) in a medium simulating the stomach in the fasted state (FaSSGF). This medium had a pH of 1.6 and contained minor concentrations of phosphatidylcholine (20 μM) and bile salts (80 μM) according to Vertzoni *et al.* [262]. The diluted samples were gently shaken for a few seconds to mimic the limited mixing stress that occurs physiologically. We measured the particle size on a Zeta Sizer Nano ZS (Malvern Instruments, Malvern, UK), equipped with a 4 mW He-Ne Laser operating at a wavelength of 633 nm. The scattering signal was detected at an angle of 173°, and each sample was measured for 10 min. The result was expressed as intensity averaged particle diameter (nm) and as polydispersity index (PDI).

7.2.3 Instrumental and analytical conditions

7.2.3.1 Raman spectroscopy

Raman spectra were recorded in the backscattering modus using a Raman RXN1 analyzer (Kaiser Optical Systems, Inc., Ann Arbor, MI) equipped with a charge-coupled device (CCD) camera and a diode laser operating at a wavelength of 785 nm. Measurements were carried out with a laser power of 400 mW, and background Rayleigh scattering was removed by a holographic filter during spectra acquisition.
We recorded the Raman spectra of the bulk formulations with a single-fiber optic probe (spot size 0.007 mm^2) by direct immersion of the probe head into the formulation. The vials were wrapped in aluminum foils to avoid the influence of external light on the detection of Raman scattering. To collect Raman spectra through the capsules, a multi-fiber P^hAT probe was used. This sensor had a non-contact sampling optic device with a laser spot diameter of 6 mm. Scattered radiation was then collected by an array of 50 optical fibers and delivered to the CCD detector. Capsules were positioned on an iris holder to locate each capsule at the same position and to avoid displacement during the measurement. A sample holder consisting of a black metal block shielded the samples from external light.
The reference spectra of the pure drugs in powder form and of the empty hard-gelatin capsule were recorded with a non-contact probe. This optics utilizes a single fiber for

excitation and another for collection, and provides a sampling area of 0.007 mm^2 such as the immersion probe.
Spectra were acquired at a resolution of 4 cm^{-1} and processed for subsequent data analysis using the iC Raman Instrument software (Version 3.0, Mettler-Toledo AutoChem Inc., Columbia MD).

7.2.3.2 Ultrasonic resonator technology

High-resolution URT is based on the calculation of the attenuation, A (s^2/m) and velocity, U (m/s) of a sound wave propagating through a sample [263]. In a homogenous liquid the velocity of a sound wave is determined by the density, ρ and the adiabatic compressibility, κ of the fluid. The mathematical relationship is described by the Newton-Laplace equation:

$$U = \frac{1}{\sqrt{\kappa \cdot \rho}} \tag{7.1}$$

Urick [107] generalized this relation to mixtures of different components. Therefore, sound velocity in the mixture U_{12} can be described as (using the subscripts *1* and *2* for the pure components):

$$\frac{1}{U_{12}^2 \cdot \rho_{12}} = \frac{\phi_1}{U_1^2 \cdot \rho_1} + \frac{\phi_2}{U_2^2 \cdot \rho_2} \tag{7.2}$$

where ϕ is the volume fraction and ρ is the density of the two components with the labeled subscripts.
In the ultrasonic experiments, we measured sound velocity U as well as acoustic attenuation A. The latter parameter summarized several contributions to energy loss during sound propagation. It is inversely proportional to the square of sound frequency f, as described by the following equation:

$$A = \frac{\alpha}{f^2} \tag{7.3}$$

The term α refers to the acoustical attenuation factor that describes the absorption of a sound wave with amplitude a traveling a distance x through a medium (a_0 = initial amplitude):

$$\alpha = -\frac{1}{x} \cdot \ln\left(\frac{a}{a_0}\right) \tag{7.4}$$

Ultrasonic velocity and attenuation were measured using the ResoScan® System (TF Instruments Inc., Monmouth Junction, NJ). The ResoScan was equipped with two identical parallel resonator cells having a path length of 7.0 mm (ground wave $\lambda_0 = 14$ mm) with a fundamental frequency of approximately 10 MHz. Since ultrasonic velocity is strongly temperature-dependent, a Peltier-element-controlled thermostat ensured a highly stable temperature in the resonator cavities (resolution 1 mK, stability $\leq \pm 5$ mK). Ultrasound velocity was measured in a range of 1100–1900 m/s and ultrasonic attenuation was measured between 10^{-14} and 10^{-13} s^2/m.
To remove air bubbles, we centrifuged all samples prior to the ultrasonic analysis. Thus, an Eppendorf centrifuge (model 5415 C) was employed for 2 min at 2000 rpm. A sample of about 200 μl was then carefully transferred to the resonator cavities. Since we measured the difference in ultrasound velocity (ΔU) and attenuation (ΔA) between active formulations and placebo formulations, the API-containing formulation was injected into one of the cells, while the placebo formulation was filled in the other. Once thermal equilibrium was reached in both cells, we started the measurement. The analysis was done in triplicate at room temperature.

7.2.3.3 Reference measurements

The drug content of each sample was determined by HPLC. HPLC (Agilent Technologies 1200 Series) analysis was performed with an isocratic pump (G1310A), an autosampler (G1329A), and a variable wavelength detector (G1314B). All measurements were performed on a LiChrospher® 60, RP select B 125-4 (5 μm) column (Merck, Darmstadt, Germany) at a flow rate of 1 ml/min. Before measuring, the samples were diluted with water at a ratio of 1:200, except CO/Pro samples, which were diluted with acetonitrile:water (96:4). The HPLC conditions are detailed in Table 7.1.

Table 7.1: Overview of HPLC methods used for API quantification.

API	Mobile phase	Injection volume	UV detection
Fen	Acetonitrile - ammoniumacetate buffer (pH 3.5; 25 mM) (65:35, v/v)	20 μl	287 nm
Ind	Phosphoric acid (50 mM) - acetonitrile (40:60, v/v)	5 μl	260 nm
Pro	Acetonitrile-water (96:4, v/v)	10 μl	241 nm

7.2.3.4 Density measurements using Coriolis mass flow technology

Density of the six formulations (Fen/CO, Ind/CO, Pro/CO, Fen/PO, Ind/PO, and Pro/PO) at five different drug concentrations (0.5, 1, 2, 3, and 4 % w/w) was measured. We used the Mass Sense Density Meter (Integrated Sensing Systems Inc., Ypsilanti MI, USA) which was equipped with a microelectromechanical system (MEMS) density sensor. This technology used a micromachined tube which was driven into resonance electrostatically while its motion was sensed capacitively by two metal electrodes. The density ρ of the liquid was deduced from the Coriolis force as described by the following equation:

$$\rho = \frac{1}{V} \cdot \left[\left(\frac{K_s}{4 \cdot \pi^2 \cdot f^2} \right) - m_t \right] \tag{7.5}$$

where V is the internal volume of the resonant tube, m_t is the tube mass, K_s is the spring constant of the tube, and f is the resonance frequency of the tube [264]. The density was measured in the range from 0.6 to 1.3 g/ml with an accuracy of ± 0.001 g/ml and values were determined in triplicate at room temperature.

7.2.4 Data analysis

Raman spectra were analyzed by partial least square (PLS) regression. This method establishes a relationship between a set of dependent variables Y and a set of independent variables X (in our case the reference concentration obtained by HPLC and the Raman spectra, respectively). The method performs a principal component analysis based on the independent variable matrix and maximizes the correlation with the dependent variable matrix at the same time. This multivariate analysis was performed using the software iC Quant (Version 1.0, Mettler-Toledo AutoChem Inc., Columbia MD). All spectral data were mean-centered. Further pre-processing steps comprised baseline correction and normalization to unit length.

URT data were analyzed by univariate regression plotting of ΔU and ΔA, separately, versus the reference concentrations obtained by HPLC.

The limit of quantification, LOQ (% w/w), was calculated according to the International Conference of Harmonization (ICH) guidelines [265]. Thus, a calibration curve was modeled using a set of 6–10 samples containing API within an order of magnitude of the estimated quantification limit. Based on the standard deviation σ and the slope S of the calibration curve, the LOQ was expressed as:

$$\mathrm{LOQ} = \frac{10 \cdot \sigma}{S} \tag{7.6}$$

Samples with an API concentration above the calculated LOQ were used for model calibration and validation. Simple and time-saving quantification methods are preferred for process analytical applications. Therefore, we aimed to assess the predictive power of the calibration models that were constructed with a small number of calibration points. We used calibration sets comprising 5–7 samples, while the remaining samples were used to validate the models. This division between calibration and validation samples was maintained for all models.

Relative standard error of prediction, RSEP (%) was calculated according to the equation:

$$\text{RSEP} = \sqrt{\frac{\sum_{i=1}^{n} (c_i^p - c_i^a)^2}{\sum_{i=1}^{n} (c_i^a)^2}} \cdot 100 \tag{7.7}$$

where n is the number of samples, c^a the actual concentration (detected by HPLC), and c^p the predicted concentration (by the model).

Mean recovery (%) was established for each model according to the equation:

$$\text{Mean recovery} = \frac{1}{n} \cdot \sum_{i=1}^{n} \frac{c^p}{c^p} \cdot 100 \tag{7.8}$$

7.3 Results and discussion

7.3.1 SEDDS characterization

We studied two model SEDDS with different drugs for the evaluation of URT and Raman spectroscopy. The model systems were named according to the surfactant so that for the formulation with polysorbate 80, PO was assigned and for the formulations with Cremophor RH 40, the label CO was given. In both systems, a concentration series of the drugs fenofibrate, indomethacin, and probucol was prepared. Table 7.2 shows the main characteristics of the test systems.

The model compounds demonstrated different solubilities in the formulations, but in all cases a wide range of concentrations was enabled, which was beneficial considering the aim of the study. Furthermore, the presence of drug did not strongly alter the dilution characteristics of the SEDDS. This anticipated self-emulsification of the lipid-based formulations (PO and CO), both with and without API, was verified. We analyzed

samples diluted in gastric medium simulating fasted state *in vivo* by dynamic laser light scattering. The mean particle diameter of all formulations was in the range of typical SEDDS [9], as seen in Table 7.2. The CO formulations even formed rather small particles, so that these systems were basically self-microemulsifying drug delivery systems (SMEDDS). Larger swollen micelles were obtained from the dilution of the polysorbate formulations. Furthermore, PO systems were generally more polydisperse upon dilution as opposed to the CO formulations. However, such differences were not considered to be of relevance for the scope of the current analytical research.

Table 7.2: Characterization of lipid formulations used in the study

Formulation	Concentration range [%, w/w] (number of samples)	Solubility[a] ± SD [%,w/w]	Particle diameter[b] (PDI) [nm]
PO	-	-	123.1 (0.269)
PO/Fen	0.01–8.00 (33)	8.58 ± 0.02	138.6 (0.219)
PO/Ind	0.01–4.00 (33)	5.63 ± 0.02	93.3 (0.252)
PO/Pro	0.01–8.00 (33)	11.34 ± 0.01	135.0 (0.192)
CO	-	-	31.2 (0.078)
CO/Fen	0.01–8.00 (33)	14.14 ± 0.11	35.9 (0.069)
CO/Ind	0.01–4.00 (33)	4.61 ± 0.02	34.9 (0.063)
CO/Pro	0.01–8.00 (33)	11.90 ± 0.14	34.8 (0.054)

[a] API concentration measured after 72 h (25°C).
[b] Dilution ratio: 1:200 (w/w) in FaSSGF; temperature: 37°C; API concentration: 8% (w/w) for formulations with Fen and Pro, 4% (w/w) for formulations with Ind.

7.3.2 Raman spectroscopy

Fig. 7.1 shows the Raman spectra of pure APIs (Fen, Ind, and Pro) and excipients (Polysorbate 80, Cremophor RH 40, Imwitor 988, Imwitor 742, Miglyol 812, and the empty capsule). We analyzed these APIs in powder form as well as the empty gelatin capsule with a single-fiber non-contact optic probe. The spectra of the different excipients were instead collected using the immersion probe. All API spectra had some distinct Raman bands in the ranges of 1000–1500 cm^{-1} and 2700–3200 cm^{-1}. In some of these ranges, the different excipients exhibited a comparatively lower Raman activity. To evaluate Raman spectroscopy as a method for drug quantification, we first recorded the spectra of the six concentration series, each with 33 samples, directly from the bulk formulation. Subsequently, following a manual filling of the formulation into hard-gelatin capsules, additional spectra were determined through the capsules using the P^hAT probe. Despite the partially overlapping spectral ranges of pure APIs and excipients, each formulation revealed at least one region where the signal intensity was highly specific for

the API. In these regions, increasing drug concentrations showed peaks with increasing heights as well as areas. This was observed for both measurements in the bulk and through the capsules, as seen in Fig. 7.2 and Fig. 7.3. Based on these preliminary observations, backscatter Raman spectroscopy appeared to be promising for quantitative determination of the model drugs in SEDDS.

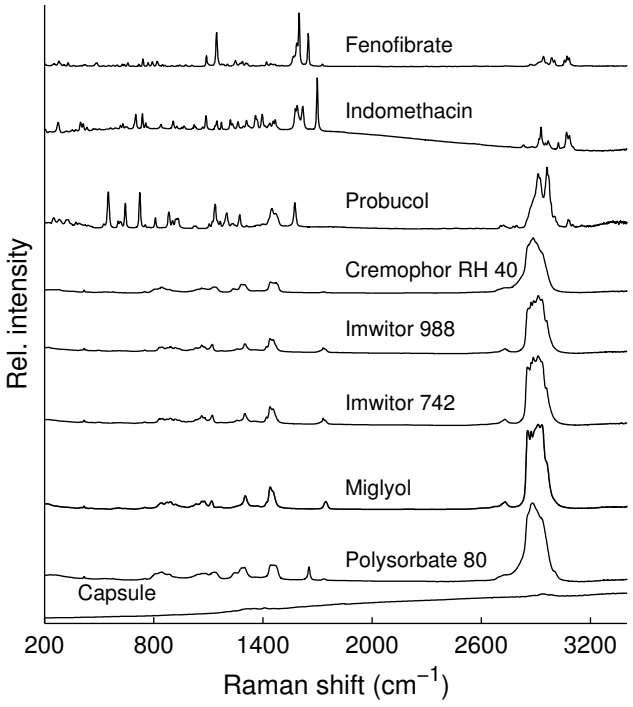

FIGURE 7.1: Raman spectra of pure APIs and excipients.

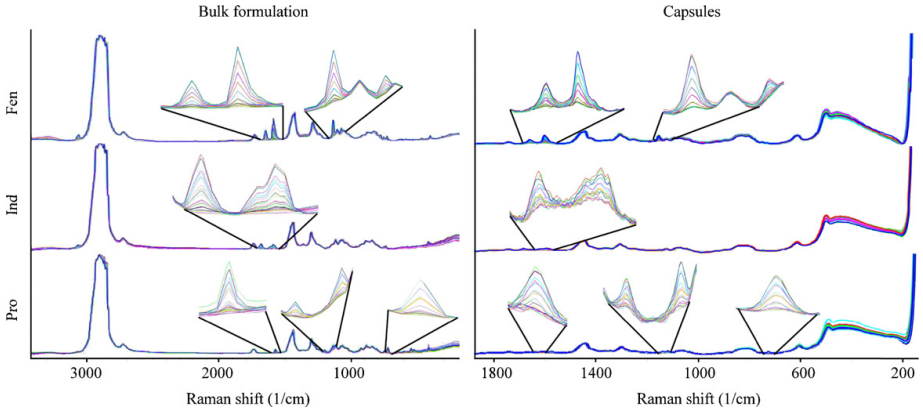

FIGURE 7.2: Raman spectra of CO formulations collected in the bulk (left) and through the capsules (right). The 33 spectra of each concentration series are combined in each illustration, Raman signals generated from APIs are highlighted.

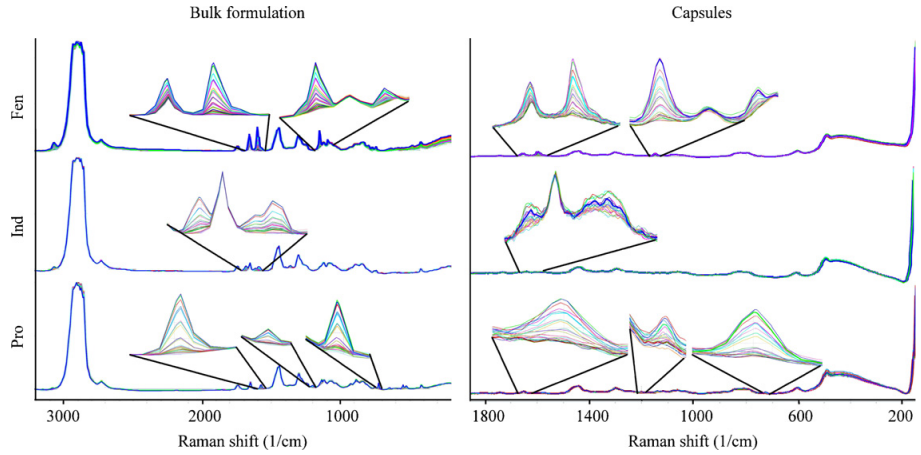

FIGURE 7.3: Raman spectra of PO formulations collected in the bulk (left) and through the capsules (right). The 33 spectra of each concentration series are combined in each illustration, Raman signals generated from APIs are highlighted.

PLS analysis was then performed on the complete data set, while the number of PLS components was determined by cross-validation. Several calibration models constructed on API-specific spectral ranges did not greatly affect the obtained models. Therefore, we always considered the entire spectral ranges of 500–3300 cm^{-1} (bulk formulation) and 500–1800 cm^{-1} (capsules) for multivariate analysis. Table 7.3 lists the values of LOQ, RSEP, and mean recovery of drug quantification in the different formulations. Interestingly, the LOQ values obtained from drug quantification in the capsules were in the range of values obtained from the measurements in the bulk solution. This similar sensitivity was mainly due to the optical devices specifically used for these two analytical tasks. Drug quantification in the capsules required the use of the P^hAT probe. This system, having 50 collected optical fibers, provided a sampling area (28.3 mm^2) that was

TABLE 7.3: Prediction of API concentration in the bulk formulation and in capsules using Raman spectroscopy.

Formulation	Bulk formulation			Capsules		
	LOQ	RSEP	Recovery ± 95% CI	LOQ	RSEP	Recovery ± 95% CI
PO/Fen	0.20	2.32	99.1±1.3	0.05	3.55	99.8±3.3
PO/Ind	0.04	3.83	101.6±2.9	0.41	6.54	99.6±4.8
PO/Pro	0.35	3.18	102.0±3.6	0.06	4.52	102.7±2.8
CO/Fen	0.10	1.99	99.5±2.7	0.34	1.87	100.5±2.1
CO/Ind	0.09	2.96	100.2±1.7	0.01	2.05	100.0±1.1
CO/Pro	0.25	1.48	100.9±1.6	0.02	2.40	99.2±2.8

about 40–900 times larger than that present in conventional dispersive and FT-Raman, so that it had higher sensitivity to scattered radiation than the single-fiber probe. On the other hand, the prediction errors of the calibration models were equal or even smaller for the drug assays in the bulk formulation compared to the capsules. This result can also be inferred from the plots of actual *versus* predicted concentrations (Fig. 7.4 and 7.5). There was a tendency of slightly higher R^2 for drug quantification in the bulk as compared to the capsule (0.9973–0.9995 *versus* 0.9732–0.9991). Such a subtle effect was likely to contribute to some increase in prediction error of drug quantification in the capsules, which was mostly attributable to the experimental setup. Since the laser beam diameter of the P^{h}AT probe slightly exceeded the capsule width, there was some signal noise resulting in an undulating baseline as seen in the spectra (Fig. 7.2 and Fig. 7.3, spectra on the right side). This effect was further enhanced by the transparency of the samples coupled with the short distance covered by the laser beam, leading to a signal noise coming from the background of the sample.

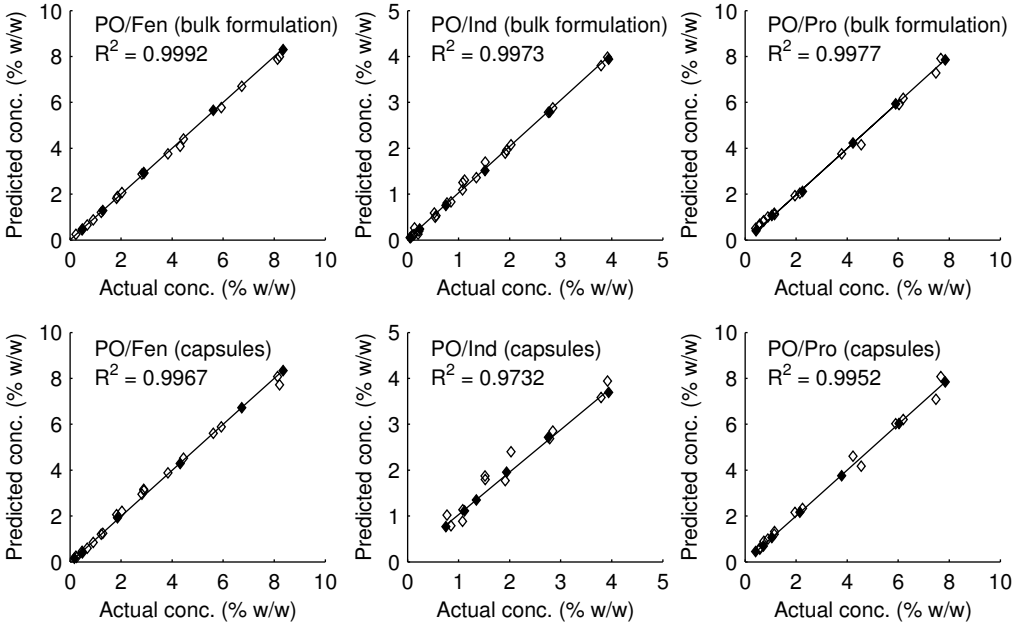

FIGURE 7.4: Drug quantification in PO formulations by Raman spectroscopy in the bulk formulation (top) and through the capsules (bottom).
♦ = calibration data set, ◊ = validation data set.

Regarding the different SEDDS types, drug quantification in PO formulations led to clearly higher prediction errors than those based on CO. This tendency was particularly pronounced for the quantification in capsules, where the predictive ability in PO systems was up to three times lower compared to CO-based formulations (RSEP 3.5–6.5% *versus* 1.9–2.4%). Even though the type of SEDDS affected RSEP, all values were sufficiently

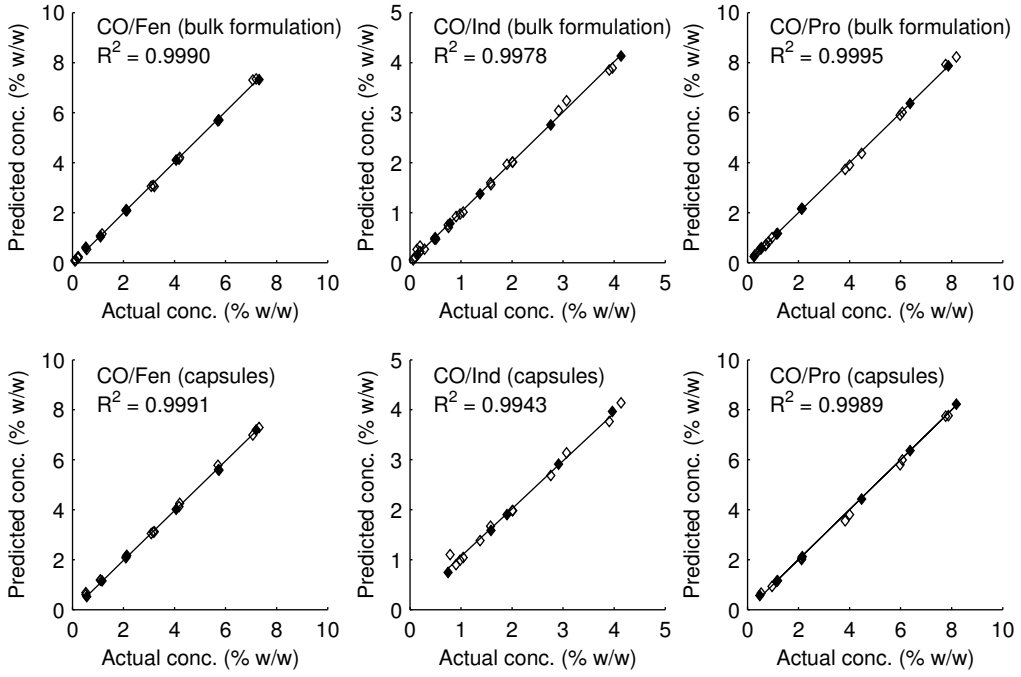

FIGURE 7.5: Drug quantification in CO formulations by Raman spectroscopy in the bulk formulation (top) and through the capsules (bottom).
♦ = calibration data set, ◊ = validation data set.

.

low to fulfill the general acceptance criteria of performance parameters in analytical validation [266]. The obtained results encouraged the use of Raman spectroscopy as an accurate method for API quantification in complex semi-solid formulations. Together with the intrinsic Raman activity of the analyzed substance, it was the type of lipid mixture that apparently influenced the predictive ability of the method.

With respect to the PAT feasibility, the immersion probe can be directly employed as in-line setup for real-time monitoring of the intermediate product (*i.e.*, the capsule fill mass). Raman spectroscopy was very promising for drug quantification through the capsules as well. However, optimization of the instrument setup might even improve its usefulness as a PAT method. Despite the advantages of the large sampling area, the laser beam area should not exceed the capsule size to reduce background noise. Moreover, the analytical procedure was not as fast as the manufacturing of the capsules. Since only a defined portion of the capsules can be transferred to the sample holder, the analysis of the final product was performed at-line.

A similar approach was adopted by Johansson *et al.* [257], where the transmission and the backscatter mode of Raman spectroscopy were compared for the quantitative analysis of tablets and capsules. Spectra were recorded with the P^{h}AT probe. This study demonstrates that transmission Raman leads to even more robust calibration models for solid pharmaceutical formulations as compared to backscatter Raman. In

fact, the transmission setup allows the entire tablet thickness to be analyzed, which is an improvement when compared to the backscatter mode, where only about 10% of a typical tablet is sampled (sampling depth of approximately 5 mm) [257]. The homogenous drug mixtures and transparent capsules used in our study provided an advantageous situation for the backscattering setup so that only limited improvement could be expected from a Raman transmission mode. This expectation was supported by the relatively low RSEP obtained from our experiments. Backscatter Raman demonstrated robust models for this type of drug delivery systems.

7.3.3 URT

In addition to using Raman spectroscopy, we analyzed the six concentration series by ultrasound velocimetry. However, since the ResoScan system was only suitable for analyzing liquid samples, API quantification in capsules was not performed. We determined ultrasound velocity and attenuation as relative values. Thus, two sample cells were always filled, whereby the placebo formulation was filled in the first cell (cell 1) and the drug-containing formulation in the second cell (cell 2). The differences in ultrasound velocity ΔU and attenuation ΔA between the two samples were obtained by subtracting the values measured in cell 1 from the values measured in cell 2, and used for univariate analysis.

Generally, there was a linear relationship for both acoustic responses as a function of API concentration (Fig. 7.6). We noticed the tendency of ΔA to be more sensitive to drug concentration compared to ΔU. The drugs fenofibrate and probucol exhibited smaller quantification limits and prediction errors with ΔA as response, when compared to calibration models built on ΔU (Table 7.4). Indomethacin was different, and the special character of this drug was further underlined by the results of ΔU calibration. The largest ΔA variation was induced by indomethacin and probucol, and this was likely to result in lower LOQs, as observed with these formulations when compared with systems with fenofibrate (Table 7.4). Nevertheless, the analytical performance of ΔA was in a similar range as that of Raman spectroscopy. This was a remarkable result in the context of ultrasound attenuation as a monitoring parameter in complex lipid-based formulations.

Fig. 7.6 shows the double plots of ΔU and ΔA as a function of drug concentration. The values of ΔA generally higher with increasing drug concentrations. The extent of increase and thus the slope of the linear models were mainly affected by the drug type, while there was barely any difference between the formulation types.

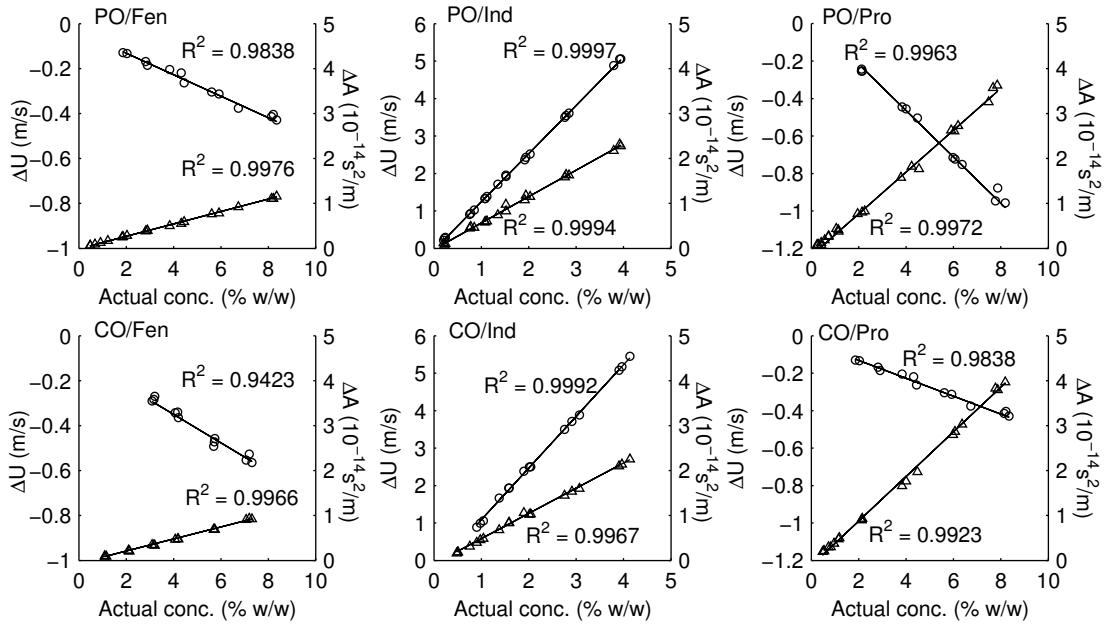

FIGURE 7.6: Variation of ΔU (◯) and ΔA (△) with drug concentration.

With both fenofibrate and probucol, ΔU decreased with increasing drug concentrations. Furthermore, ΔU calibration models of these two drugs led to particularly high values of LOQ and RSEP. Interestingly, analytical performance was different in the case of indomethacin where ultrasound velocity even increased with drug load. For better understanding of this finding, consider Eqs. 7.1 and 7.2. Thus, any change in ultrasound speed is attributed to differences in apparent density or compressibility of the mixture. It was therefore of interest to study how the density of the formulations was affected by different drug amounts.

Five drug concentrations (range 0.5–4 % w/w) were compared with respect to density

TABLE 7.4: Prediction of API concentration in the bulk formulation using URT: evaluation based on ΔU and ΔA

Formulation	ΔU			ΔA		
	LOQ	RSEP	Recovery ± 95% CI	LOQ	RSEP	Recovery ± 95% CI
PO/Fen	1.48	5.43	98.5±6.4	0.40	2.33	101.4±1.9
PO/Ind	0.14	1.08	100.6±1.6	0.20	3.26	101.8±3.5
PO/Pro	2.05	5.43	98.5±3.6	0.13	4.42	103.9±4.2
CO/Fen	2.29	5.34	98.0±4.3	0.64	3.51	97.0±2.9
CO/Ind	0.80	1.35	99.4±1.6	0.48	2.36	97.9±1.8
CO/Pro	1.24	3.44	100.6±2.9	0.39	3.00	101.9±3.7

changes (Fig. 7.7). The results indicated that density in the mixture increased with drug load in all cases. As inferred from the slopes m, the density increase was particularly pronounced for SEDDS containing indomethacin (0.027 [m_{Ind}] *versus* 0.005–0.015 [m_{Pro}, m_{Fen}]). Increasing density would theoretically lead to decreasing values of ΔU, provided that the drug concentration does not change the apparent bulk compressibility in the mixture. The unusual finding for indomethacin could therefore only be explained with a dominating drug effect on the apparent bulk compressibility which appears to have. outweighed the increasing density induced by indomathacin. This drug strongly affected the structure of the lipid mixture, and reduced compressibility originated from a perturbation of the liquid-crystalline structure by the drug. Drugs with a strong effect on the structuring of SEDDS are suitable candidates for analytics based on ultrasound velocity.

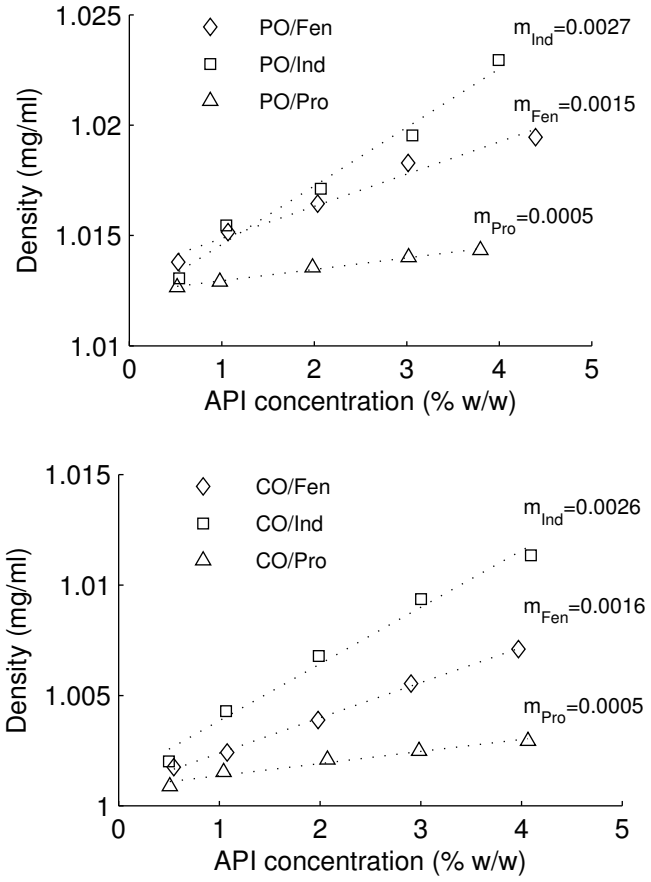

FIGURE 7.7: Variation of density with drug concentration.

7.4 Conclusions

Raman spectroscopy and URT were well suited for rapid and non-destructive drug quantification in complex lipid-based formulations. Therefore, both methods have a high potential for implementation as PAT tools in real-time monitoring the production of SEDDS or other lipid mixtures. These methods are not only useful in process analysis but may also be used when simple and rapid calibration is required, *e.g.*, during formulation development where the composition of the formulations may be varied. Since the development of a formulation-specific method is time-consuming, rapid calibration is clearly advantageous.

Raman spectroscopy has an advantage over URT because it even detects impurities and degradation products. However, the modern ultrasound method has proven to be simple and fast, while showing excellent calibration performance with API quantification in SEDDS. Specifically, the response of ultrasound attenuation resulted in high sensitivity and good predictability. Therefore, ΔA bears the advantage of broad application as a parameter for drug quantification, while ΔU is particularly suitable for predicting drug concentrations if a pronounced influence of the drug is exerted on the apparent compressibility or density of the mixture.

Chapter 8

Final remarks and outlook

The prediction of formulation performance *in vivo* is a key requirement for the rational and effective development of novel formulations. The present thesis aimed at improving the biopharmaceutical understanding of LBF performance in the GI tract using *in vitro* assays, advanced analytical tools, and mathematical modeling.

The quality of biopharmaceutical studies depends on the availability of adequate analytical techniques. There has been an increasing realization that LBF processing in the GI tract is highly dynamic and that conventional analytical tools often fail in detecting these changes accurately. This is particularly true for drug precipitation during LBF dispersion and digestion. Real-time analytics has therefore become a desirable goal, but its application to biopharmaceutical tests was shown to be challenging. This is due, on the on hand, to the complexity and the intrinsic turbidity of testing media. On the other hand, the low absolute concentration of analyte is often below the detection limit of conventional instrumentation.

We identified Raman spectroscopy as an excellent technique for biopharmaceutical testing of LBFs. The chemical specificity and the ability to differentiate between physical states were two main advantages. Additionally, it provided highly time-resolved data, which was appropriate for studying the kinetics of drug precipitation in more detail. In this context, we also found evidence of the experimental drawbacks of off-line techniques for precipitation detection. Ultracentrifugation was the state-of-the-art method for detecting drug precipitation during *in vitro* lipolysis so far. However, we observed that the lag time between sample removal and analysis can lead to further drug precipitation. Care is therefore needed when applying such off-line procedures for the analysis of fast dynamic processes.

Raman spectroscopy bears great potential for further application in biopharmaceutical LBF testing. It is primarily a research tool and may provide major opportunities for

studying drug solubilization during LBF processing on a mechanistic basis. However, the technique could also be implemented in industrial formulation development. A potential direction is the use of Raman spectroscopy in high-throughput formulation screening, and for this purpose, miniaturization of *in vitro* assays and of Raman tools should be considered.

Certain biopharmaceutical processes involving LBFs remain hardly accessible using *in vitro* methods. For example, it is technically difficult to simulate an absorptive sink during formulation lipolysis. We proposed an alternative approach, which was based on the combination of *in vitro* lipolysis with mathematical modeling. This was the very first approach that enabled to study formulation digestion in an absorptive environment. It provided clear evidence that the extent of supersaturation in the intestinal lumen is considerably lower than during *in vitro* lipolysis. Hence, standard *in vitro* lipolysis may overpredict the extent of drug precipitation, whereas formulation digestion *in vivo* is probably less critical than assumed so far. This improved biopharmaceutical understanding provided leads to rationally select appropriate *in vitro* models for LBF testing. Mathematical modeling proved also helpful for improving the mechanistic understanding of drug solubilization during LBF dispersion and digestion. For example, the *non-interacting model* of drug solubilization showed that a loss in excipient interactions can lead to extensive drug precipitation upon dispersion of a formulation. Such an approach may be helpful to identify critical drug loadings in LBFs. Similarly, we introduced an heuristic approach to model drug solubilization during LBF digestion. This model allowed the determination of the kinetics of lipolysis-triggered drug precipitation and drug solubilization in the GI tract.
These advancements may substantially improve the mechanistic understanding of formulation performance *in vivo*. Moreover, excellent opportunities are provided regarding the optimization of physiologically-based models involving LBFs. A drug precipitation step could be included and, to this end, the complex interplay between formulation lipolysis, drug absorption, and the kinetics of precipitation should be further investigated. Additionally, it would be desirable to consider biological effects of drug and excipients (*e.g.*, the influence on efflux mechanisms and on the lymphatic drug transport) in physiologically-based models. Such holistic approaches are a key requirement for better predicting the oral bioavailability of LBFs.

Hence, the present thesis allowed an important step forward toward an accurate prediction of LBF performance *in vivo*. Analytical advancements and mathematical models provided new insights into the formulation processing in the GI environment. The findings were highly encouraging and evidenced that LBFs still bear a great potential for the oral delivery of poorly water-soluble compounds.

Bibliography

[1] G. L. Amidon, H. Lennernas, V. P. Shah, and J. R. Crison. A theoretical basis for a biopharmaceutic drug classification - the correlation of in-vitro drug product dissolution and in-vivo bioavailability. *Pharmaceutical Research*, 12(3):413–420, 1995.

[2] R. J. Ptachcinski, R. Venkataramanan, J. T. Rosenthal, G. J. Burckart, R. J. Taylor, and T. R. Hakala. The effect of food on cyclosporine absorption. *Transplantation*, 40(2):174–176, 1985.

[3] M. U. Mehta, R. Venkataramanan, G. J. Burckart, R. J. Ptachcinski, B. Delamos, S. Stachak, D. H. Vanthiel, S. Iwatsuki, and T. E. Starzl. Effect of bile on cyclosporin absorption in liver-transplant patients. *British Journal of Clinical Pharmacology*, 25(5):579–584, 1988.

[4] L. Di, E. H. Kerns, and G. T. Carter. Drug-like property concepts in pharmaceutical design. *Current Pharmaceutical Design*, 15(19):2184–2194, 2009.

[5] S. Stegemann, F. Leveiller, D. Franchi, H. de Jong, and H. Linden. When poor solubility becomes an issue: From early stage to proof of concept. *European Journal of Pharmaceutical Sciences*, 31(5):249–261, 2007.

[6] H. D. Williams, N. L. Trevaskis, S. A. Charman, R. M. Shanker, W. N. Charman, C. W. Pouton, and C. J. H. Porter. Strategies to address low drug solubility in discovery and development. *Pharmacological Reviews*, 65(1):315–499, 2013.

[7] D. Attwood, L. R. J. Currie, and P. H. Elworthy. Studies of solubilized micellar solutions. I. phase studies and particle size analysis of solutions formed with nonionic surfactants. *Journal of Colloid and Interface Science*, 46(2):249–254, 1974.

[8] R. G. Strickley. *Currently marketed oral lipid-based dosage forms: drug products and excipients.* Informa Healthcare USA, Inc., New York, 2007.

[9] C. W. Pouton. Lipid formulations for oral administration of drugs: non-emulsifying, self-emulsifying and 'self-microemulsifying' drug delivery systems. *European Journal of Pharmaceutical Sciences*, 11:93–98, 2000.

[10] C. W. Pouton. Formulation of poorly water-soluble drugs for oral administration: Physicochemical and physiological issues and the lipid formulation classification system. *European Journal of Pharmaceutical Sciences*, 29(3-4):278–287, 2006.

[11] C. J. H. Porter, C. W. Pouton, J. F. Cuine, and W. N. Charman. Enhancing intestinal drug solubilisation using lipid-based delivery systems. *Advanced Drug Delivery Reviews*, 60(6):673–691, 2008.

[12] F. Seeballuck, E. Lawless, M. B. Ashford, and C. M. O'Driscoll. Stimulation of triglyceride-rich lipoprotein secretion by polysorbate 80: in vitro and in vivo correlation using Caco-2 cells and a cannulated rat intestinal lymphatic model. *Pharmaceutical Research*, 21(12):2320–2326, 2004.

[13] K. Katneni, S. A. Charman, and C. J. H. Porter. Impact of Cremophor-EL and polysorbate-80 on digoxin permeability across rat jejunum: Delineation of thermodynamic and transporter related events using the reciprocal permeability approach. *Journal of Pharmaceutical Sciences*, 96(2):280–293, 2007.

[14] C. J. H. Porter, N. L. Trevaskis, and W. N. Charman. Lipids and lipid-based formulations: optimizing the oral delivery of lipophilic drugs. *Nature Reviews Drug Discovery*, 6(3):231–248, 2007.

[15] D. M. Shackleford, W. A. Faassen, N. Houwing, H. Lass, G. A. Edwards, C. J. H. Porter, and W. N. Charman. Contribution of lymphatically transported testosterone undecanoate to the systemic exposure of testosterone after oral administration of two andriol formulations in conscious lymph duct-cannulated dogs. *Journal of Pharmacology and Experimental Therapeutics*, 306(3):925–933, 2003.

[16] S. M. Khoo, G. A. Edwards, C. J. H. Porter, and W. N. Charman. A conscious dog model for assessing the absorption, enterocyte-based metabolism, and intestinal lymphatic transport of halofantrine. *Journal of Pharmaceutical Sciences*, 90(10): 1599–1607, 2001.

[17] S. M. Khoo, D. M. Shackleford, C. J. H. Porter, G. A. Edwards, and W. N. Charman. Intestinal lymphatic transport of halofantrine occurs after oral administration of a unit-dose lipid-based formulation to fasted dogs. *Pharmaceutical Research*, 20(9):1460–1465, 2003.

[18] D. J. Hauss. Oral lipid-based formulations. *Advanced Drug Delivery Reviews*, 59 (7):667–676, 2007.

[19] A. Dahan and A. Hoffman. The effect of different lipid based formulations on the oral absorption of lipophilic drugs: The ability of in vitro lipolysis and consecutive ex vivo intestinal permeability data to predict in vivo bioavailability in rats. *European Journal of Pharmaceutics and Biopharmaceutics*, 67(1):96–105, 2007.

[20] C. J. H. Porter, A. M. Kaukonen, A. Taillardat-Bertschinger, B. J. Boyd, J. M. O'Connor, G. A. Edwards, and W. N. Charman. Use of in vitro lipid digestion data to explain the in vivo performance of triglyceride-based oral lipid formulations of poorly water-soluble drugs: Studies with halofantrine. *Journal of Pharmaceutical Sciences*, 93(5):1110–1121, 2004.

[21] C. J. H. Porter, A. M. Kaukonen, B. J. Boyd, G. A. Edwards, and W. N. Charman. Susceptibility to lipase-mediated digestion reduces the oral bioavailability of danazol after administration as a medium-chain lipid-based microemulsion formulation. *Pharmaceutical Research*, 21(8):1405–1412, 2004.

[22] A. Larsen, R. Holm, M. L. Pedersen, and A. Müllertz. Lipid-based formulations for danazol containing a digestible surfactant, Labrafil M2125CS: In vivo bioavailability and dynamic in vitro lipolysis. *Pharmaceutical Research*, 25(12):2769–2777, 2008.

[23] N. Thomas, R. Holm, M. Garmer, J. J. Karlsson, A. Mullertz, and T. Rades. Supersaturated self-nanoemulsifying drug delivery systems (super-SNEDDS) enhance the bioavailability of the poorly water-soluble drug simvastatin in dogs. *AAPS Journal*, 15(1):219–227, 2013.

[24] J. P. Reymond, H. Sucker, and J. Vonderscher. In vivo model for ciclosporin intestinal-absorption in lipid vehicles. *Pharmaceutical Research*, 5(10):677–679, 1988.

[25] A. Dahan and A. Hoffman. Use of a dynamic in vitro lipolysis model to rationalize oral formulation development for poor water soluble drugs: Correlation with in vivo data and the relationship to intra-enterocyte processes in rats. *Pharmaceutical Research*, 23(9):2165–2174, 2006.

[26] H. D. Williams, P. Sassene, K. Kleberg, J. C. Bakala-N'Goma, M. Calderone, V. Jannin, A. Igonin, A. Partheil, D. Marchaud, E. Jule, J. Vertommen, M. Maio, R. Blundell, H. Benameur, F. Carriere, A. Müllertz, C. J. H. Porter, and C. W. Pouton. Toward the establishment of standardized in vitro tests for lipid-based formulations, Part 1: Method parameterization and comparison of in vitro digestion profiles across a range of representative formulations. *Journal of Pharmaceutical Sciences*, 101(9):3360–3380, 2012.

[27] H. D. Williams, M. U. Anby, P. Sassene, K. Kleberg, J.-C. Bakala-N'Goma, M. Calderone, V. Jannin, I. Annabel, A. Partheil, D. Marchaud, E. Jule, J. Vertommen, M. Maio, R. Blundell, H. Benameur, F. Carriere, A. Müllertz, C. W. Pouton, and C. J. H. Porter. Toward the establishment of standardized in vitro tests for lipid-based formulations. 2. The effects of bile salt concentration and drug loading on the performance of type I, II, IIIA, IIIB, and IV formulations during in vitro digestion. *Molecular Pharmaceutics*, 9(11):3286–3300, 2012.

[28] H. D. Williams, P. Sassene, K. Kleberg, M. Calderone, A. Igonin, E. Jule, J. Vertommen, R. Blundell, H. Benameur, A. Mullertz, C. W. Pouton, and C. J. H. Porter. Toward the establishment of standardized in vitro tests for lipid-based formulations, Part 3: Understanding supersaturation versus precipitation potential during the in vitro digestion of type I, II, IIIA, IIIB, and IV lipid-based formulations. *Pharmaceutical Research*, in press, 2013.

[29] B. T. Griffin, M. Kuentz, M. Vertzoni, E. S. Kostewicz, Y. Fei, W. Faisal, C. Stillhart, C. O'Driscoll, C. Reppas, and J. B. Dressman. Comparison of in vitro tests at various levels of complexity for the prediction of in vivo performance of lipid-based formulations. submitted, 2013.

[30] A. T. Larsen, P. Sassene, and A. Müllertz. In vitro lipolysis models as a tool for the characterization of oral lipid and surfactant based drug delivery systems. *International Journal of Pharmaceutics*, 417(1-2):245–255, 2011.

[31] C. Stillhart, G. Imanidis, and M. Kuentz. Insights into drug precipitation kinetics during in vitro digestion of a lipid-based drug delivery system using in-line Raman spectroscopy and mathematical modeling. *Pharmaceutical Research*, in press, 2013.

[32] D. B. Warren, M. U. Anby, A. Hawley, and B. J. Boyd. Real time evolution of liquid crystalline nanostructure during the digestion of formulation lipids using synchrotron small-angle X-ray scattering. *Langmuir*, 27(15):9528–9534, 2011.

[33] P. J. Sassene, M. M. Knopp, J. Z. Hesselkilde, V. Koradia, A. Larsen, T. Rades, and A. Mullertz. Precipitation of a poorly soluble model drug during in vitro lipolysis: Characterization and dissolution of the precipitate. *Journal of Pharmaceutical Sciences*, 99(12):4982–4991, 2010.

[34] N. Thomas, R. Holm, A. Mullertz, and T. Rades. In vitro and in vivo performance of novel supersaturated self-nanoemulsifying drug delivery systems (super-SNEDDS). *Journal of Controlled Release*, 160(1):25–32, 2012.

[35] A. T. Larsen, P. Akesson, A. Jureus, L. Saaby, R. Abu-Rmaileh, B. Abrahamsson, J. Ostergaard, and A. Muellertz. Bioavailability of cinnarizine in dogs: effect of SNEDDS loading level and correlation with cinnarizine solubilization during in vitro lipolysis. *Pharmaceutical Research*, in press, 2013.

[36] J. Bevernage, J. Brouwers, P. Annaert, and P. Augustijns. Drug precipitation-permeation interplay: Supersaturation in an absorptive environment. *European Journal of Pharmaceutics and Biopharmaceutics*, 8(2):564–570, 2012.

[37] Y. Fei, E. S. Kostewicz, M.-T. Sheu, and J. B. Dressman. Analysis of the enhanced oral bioavailability of fenofibrate lipid formulations in fasted humans using an in vitro–in silico–in vivo approach. *European Journal of Pharmaceutics and Biopharmaceutics*, in press, 2013.

[38] J. Brouwers, M. E. Brewster, and P. Augustijns. Supersaturating drug delivery systems: The answer to solubility-limited oral bioavailability? *Journal of Pharmaceutical Sciences*, 98(8):2549–2572, 2009.

[39] R. G. Strickley. Solubilizing excipients in oral and injectable formulations. *Pharmaceutical Research*, 21(2):201–230, 2004.

[40] V. Jannin, J. Musakhanian, and D. Marchaud. Approaches for the development of solid and semi-solid lipid-based formulations. *Advanced Drug Delivery Reviews*, 60(6):734–746, 2008.

[41] M. Kuentz. Lipid-based formulations for oral delivery of lipophilic drugs. *Drug Discovery Today: Technologies*, 9(2):e97–e104, 2012.

[42] H. N. Prajapati, D. M. Dalrymple, and A. T. M. Serajuddin. A comparative evaluation of mono-, di- and triglyceride of medium chain fatty acids by lipid/surfactant/water phase diagram, solubility determination and dispersion testing for application in pharmaceutical dosage form development. *Pharmaceutical Research*, 29(1):285–305, 2012.

[43] W. G. Dai, L. C. Dong, X. F. Shi, J. Nguyen, J. Evans, Y. D. Xu, and A. A. Creasey. Evaluation of drug precipitation of solubility-enhancing liquid formulations using milligram quantities of a new molecular entity (NME). *Journal of Pharmaceutical Sciences*, 96(11):2957–2969, 2007.

[44] L. C. Persson, C. J. H. Porter, W. N. Charman, and Christel A. S. Bergström. Computational prediction of drug solubility in lipid based formulation excipients. *Pharmaceutical Research*, in press, 2013.

[45] S. S. Rane and B. D. Anderson. What determines drug solubility in lipid vehicles: Is it predictable? *Advanced Drug Delivery Reviews*, 60(6):638–656, 2008.

[46] M. Sacchetti and E. Nejati. Prediction of drug solubility in lipid mixtures from the individual ingredients. *AAPS PharmSciTech*, 13(4):1103–1109, 2012.

[47] Y. C. Cao, M. Marra, and B. D. Anderson. Predictive relationships for the effects of triglyceride ester concentration and water uptake on solubility and partitioning of small molecules into lipid vehicles. *Journal of Pharmaceutical Sciences*, 93(11): 2768–2779, 2004.

[48] K. Mohsin, M. A. Long, and C. W. Pouton. Design of lipid-based formulations for oral administration of poorly water-soluble drugs: Precipitation of drug after dispersion of formulations in aqueous solution. *Journal of Pharmaceutical Sciences*, 98(10):3582–3595, 2009.

[49] E. T. Cole, D. Cad, and H. Benameur. Challenges and opportunities in the encapsulation of liquid and semi-solid formulations into capsules for oral administration. *Advanced Drug Delivery Reviews*, 60(6):747–756, 2008.

[50] Y. Shi, P. Gao, Y. C. Gong, and H. L. Ping. Application of a biphasic test for characterization of in vitro drug release of immediate release formulations of celecoxib and its relevance to in vivo absorption. *Molecular Pharmaceutics*, 7(5): 1458–1465, 2010.

[51] M. Kataoka, K. Sugano, C. D. Mathews, J. W. Wong, K. L. Jones, Y. Masaoka, S. Sakuma, and S. Yamashita. Application of dissolution/permeation system for evaluation of formulation effect on oral absorption of poorly water-soluble drugs in drug development. *Pharmaceutical Research*, 29(6):1485–1494, 2012.

[52] T. T. Do, M. Van Speybroeck, R. Mols, P. Annaert, J. Martens, J. Van Humbeeck, J. Vermant, P. Augustijns, and G. Van den Mooter. The conflict between in vitro release studies in human biorelevant media and the in vivo exposure in rats of the lipophilic compound fenofibrate. *International Journal of Pharmaceutics*, 414 (1-2):118–124, 2011.

[53] E. Jantratid, N. Janssen, H. Chokshi, K. Tang, and J. B. Dressman. Designing biorelevant dissolution tests for lipid formulations: Case example - Lipid suspension of RZ-50. *European Journal of Pharmaceutics and Biopharmaceutics*, 69(2): 776–785, 2008.

[54] C. M. O'Driscoll and B. T. Griffin. Biopharmaceutical challenges associated with drugs with low aqueous solubility - the potential impact of lipid-based formulations. *Advanced Drug Delivery Reviews*, 60(6):617–624, 2008.

[55] Y. Y. Yeap, N. L. Trevaskis, T. Quach, P. Tso, W. N. Charman, and C. J. H. Porter. Intestinal bile secretion promotes drug absorption from lipid colloidal phases via induction of supersaturation. *Molecular Pharmaceutics*, 10(5):1874–89, 2013.

[56] M. U. Anby, H. D. Williams, M. McIntosh, H. Benameur, G. A. Edwards, C. W. Pouton, and C. J. H. Porter. Lipid digestion as a trigger for supersaturation: Evaluation of the impact of supersaturation stabilization on the in vitro and in vivo performance of self-emulsifying drug delivery systems. *Molecular Pharmaceutics*, 9(7):2063–2079, 2012.

[57] J. Bevernage, J. Brouwers, P. Annaert, and P. Augustijns. Drug precipitation-permeation interplay: Supersaturation in an absorptive environment. *European Journal of Pharmaceutics and Biopharmaceutics*, 8(2):564–570, 2012.

[58] R. Takano, N. Takata, R. Saito, K. Furumoto, S. Higo, Y. Hayashi, M. Machida, Y. Aso, and S. Yamashita. Quantitative analysis of the effect of supersaturation on in vivo drug absorption. *Molecular Pharmaceutics*, 7(5):1431–1440, 2010.

[59] H. D. Williams, N. L. Trevaskis, Y. Y. Yeap, M. U. Anby, C. W. Pouton, and C. J. H. Porter. Lipid-based formulations and drug supersaturation: Harnessing the unique benefits of the lipid digestion/absorption pathway. *Pharmaceutical Research*, in press, 2013.

[60] M. Kuentz and G. Imanidis. In silico prediction of the solubility advantage for amorphous drugs - are there property-based rules for drug discovery and early pharmaceutical development? *European Journal of Pharmaceutical Sciences*, 48 (3):554–562, 2013.

[61] D. Psachoulias, M. Vertzoni, K. Goumas, V. Kalioras, S. Beato, J. Butler, and C. Reppas. Precipitation in and supersaturation of contents of the upper small intestine after administration of two weak bases to fasted adults. *Pharmaceutical Research*, 28(12):3145–3158, 2011.

[62] A. Dahan, A. Beig, V. Ioffe-Dahan, R. Agbaria, and J. M. Miller. The twofold advantage of the amorphous form as an oral drug delivery practice for lipophilic compounds: increased apparent solubility and drug flux through the intestinal membrane. *AAPS Journal*, 15(2):347–353, 2013.

[63] J. W. Mullin. Crystallization, 2001.

[64] D. Kashchiev. *Nucleation: Basic theory and applications*. Butterworth-Heinemann, Oxford, 2000.

[65] Y. Y. Yeap, N. L. Trevaskis, and C. J. H. Porter. The potential for drug supersaturation during intestinal processing of lipid-based formulations may be enhanced for basic drugs. *Molecular Pharmaceutics*, 10(7):2601–2615, 2013.

[66] Y. Y. Yeap, N. L. Trevaskis, and C. J. H. Porter. Lipid absorption triggers drug supersaturation at the intestinal unstirred water layer and promotes drug absorption from mixed micelles. *Pharmaceutical Research*, in press, 2013.

[67] S. Ozaki, T. Minamisono, T. Yamashita, T. Kato, and I. Kushida. Supersaturation-nucleation behavior of poorly soluble drugs and its impact on the oral absorption of drugs in thermodynamically high-energy forms. *Journal of Pharmaceutical Sciences*, 101(1):214–222, 2012.

[68] J. M. Miller, A. Beig, B. J. Krieg, R. A. Carr, T. B. Borchardt, G. E. Amidon, G. L. Amidon, and A. Dahan. The solubility-permeability interplay: mechanistic modeling and predictive application of the impact of micellar solubilization on intestinal permeation. *Molecular Pharmaceutics*, 8(5):1848–1856, 2011.

[69] P. Gao and W. Morozowich. Development of supersaturatable selfemulsifying drug delivery system formulations for improving the oral absorption of poorly soluble drugs. *Expert Opinion Drug Delivery*, 3(1):97–110, 2006.

[70] J. Bevernage, T. Forier, J. Brouwers, J. Tack, P. Annaert, and P. Augustijns. Excipient-mediated supersaturation stabilization in human intestinal fluids. *Molecular Pharmaceutics*, 82(2):424–428, 2012.

[71] D. B. Warren, H. Benameur, C. J. H. Porter, and C. W. Pouton. Using polymeric precipitation inhibitors to improve the absorption of poorly water-soluble drugs: A mechanistic basis for utility. *Journal of Drug Targeting*, 18(10):704–731, 2010.

[72] D. B. Warren, C. A. S. Bergström, H. Benameur, C. J. H. Porter, and C. W. Pouton. Evaluation of the structural determinants of polymeric precipitation inhibitors using solvent shift methods and principle component analysis. *Molecular Pharmaceutics*, 10(8):2823–2848, 2013.

[73] P. Gao, B. D. Rush, W. P. Pfund, T. H. Huang, J. M. Bauer, W. Morozowich, M. S. Kuo, and M. J. Hageman. Development of a supersaturable SEDDS (S-SEDDS) formulation of paclitaxel with improved oral bioavailability. *Journal of Pharmaceutical Sciences*, 92(12):2386–2398, 2003.

[74] P. Gao, M. E. Guyton, T. H. Huang, J. M. Bauer, K. J. Stefanski, and Q. Lu. Enhanced oral bioavailability of a poorly water soluble drug PNU-91325 by supersaturatable formulations. *Drug Development and Industrial Pharmacy*, 30(2): 221–229, 2004.

[75] P. Gao, A. Akrami, F. Alvarez, J. Hu, L. Li, C. Ma, and S. Surapaneni. Characterization and optimization of AMG 517 supersaturatable self-emulsifying drug delivery system (S-SEDDS) for improved oral absorption. *Journal of Pharmaceutical Sciences*, 98(2):516–528, 2009.

[76] J. Bevernage, B. Hens, J. Brouwers, J. Tack, P. Annaert, and P. Augustijns. Supersaturation in human gastric fluids. *European Journal of Pharmaceutics and Biopharmaceutics*, 81(1):184–189, 2012.

[77] C. Stillhart, M. Cavegn, and M. Kuentz. Study of drug supersaturation for rational early formulation screening of surfactant/co-solvent drug delivery systems. *Journal of Pharmacy and Pharmacology*, 65(2):181–192, 2013.

[78] H. Tung, E. L. Paul, M. Midler, and J. A. McCauley. *Properties*. John Wiley and Sons, Hoboken NJ, 2009.

[79] B. C. Hancock and M. Parks. What is the true solubility advantage for amorphous pharmaceuticals? *Pharmaceutical Research*, 17(4):397–404, 2000.

[80] A. T. Larsen, A. G. Ohlsson, B. Polentarutti, R. A. Barker, A. R. Phillips, R. Abu-Rmaileh, P. A. Dickinson, B. Abrahamsson, J. Ostergaard, and A. Mullertz. Oral bioavailability of cinnarizine in dogs: Relation to SNEDDS droplet size, drug solubility and in vitro precipitation. *European Journal of Pharmaceutical Sciences*, 48(1-2):339–350, 2013.

[81] R. Devraj, H. D. Williams, D. B. Warren, K. Mohsin, C. J. H. Porter, and C. W. Pouton. In vitro assessment of drug-free and fenofibrate-containing lipid formulations using dispersion and digestion testing gives detailed insights into the likely fate of formulations in the intestine. *European Journal of Pharmaceutical Sciences*, 49(4):748–760, 2013.

[82] T. R. Kommuru, B. Gurley, M. A. Khan, and I. K. Reddy. Self-emulsifying drug delivery systems (SEDDS) of coenzyme Q(10): formulation development and bioavailability assessment. *International Journal of Pharmaceutics*, 212(2): 233–246, 2001.

[83] S. Nazzal, II Smalyukh, O. D. Lavrentovich, and M. A. Khan. Preparation and in vitro characterization of a eutectic based semisolid self-nanoemulsified drug delivery system (SNEDDS) of ubiquinone: mechanism and progress of emulsion formation. *International Journal of Pharmaceutics*, 235(1-2):247–265, 2002.

[84] E. I. Taha, S. Al-Saidan, A. M. Samy, and M. A. Khan. Preparation and in vitro characterization of self-nanoemulsified drug delivery system (SNEDDS) of

all-trans-retinol acetate. *International Journal of Pharmaceutics*, 285(1-2):109–119, 2004.

[85] L. L. Wei, P. N. Sun, S. F. Nie, and W. S. Pan. Preparation and evaluation of SEDDS and SMEDDS containing carvedilol. *Drug Development and Industrial Pharmacy*, 31(8):785–794, 2005.

[86] F. Buyukozturk, J. C. Benneyan, and R. L. Carrier. Impact of emulsion-based drug delivery systems on intestinal permeability and drug release kinetics. *Journal of Controlled Release*, 142(1):22–30, 2010.

[87] M. Kuentz and M. Cavegn. Critical concentrations in the dilution of oral self-microemulsifying drug delivery systems. *Drug Development and Industrial Pharmacy*, 36(5):531–538, 2010.

[88] C. Goddeeris, F. Cuppo, H. Reynaers, W. G. Bouwman, and G. Van den Mooter. Light scattering measurements on microemulsions: Estimation of droplet sizes. *International Journal of Pharmaceutics*, 312(1-2):187–195, 2006.

[89] R. Pecora. *Dynamic light scattering: applications of photon correlation spectroscopy*. Plenum Press, New York USA, 1985.

[90] S. P. Moulik and B. K. Paul. Structure, dynamics and transport properties of microemulsions. *Advances in Colloid and Interface Science*, 78(2):99–195, 1998.

[91] C. Ditner, R. Bravo, G. Imanidis, and M. Kuentz. A systematic dilution study of self-microemulsifying drug delivery systems in artificial intestinal fluid using dynamic laser light backscattering. *Drug Development and Industrial Pharmacy*, 35(2):199–208, 2009.

[92] K. Sakai, H. Maeda, T. Yoshimori, K. Obata, and Y. Ogawa. High-throughput formulation screening system for self-microemulsifying drug delivery. *Drug Development and Industrial Pharmacy*, 35(6):746–755, 2009.

[93] L. Djordjevic, M. Primorac, and M. Stupar. In vitro release of diclofenac diethylamine from caprylocaproyl macrogolglycerides based microemulsions. *International Journal of Pharmaceutics*, 296(1-2):73–79, 2005.

[94] M. Fanun. Properties of microemulsions based on mixed nonionic surfactants and mixed oils. *Journal of Molecular Liquids*, 150(1-3):25–32, 2009.

[95] M. Fanun. Properties of microemulsions with sugar surfactants and peppermint oil. *Colloid and Polymer Science*, 287(8):899–910, 2009.

[96] N. Thomas, A. Mullertz, A. Graf, and T. Rades. Influence of lipid composition and drug load on the in vitro performance of self-nanoemulsifying drug delivery systems. *Journal of Pharmaceutical Sciences*, 101(5):1721–1731, 2012.

[97] C. J. Newcomb, T. J. Moyer, S. S. Lee, and S. I. Stupp. Advances in cryogenic transmission electron microscopy for the characterization of dynamic self-assembling nanostructures. *Current Opinion in Colloid and Interface Science*, 17 (6):350–359, 2012.

[98] V. Klang, C. Valenta, and N. B. Matsko. Electron microscopy of pharmaceutical systems. *Micron*, 44:45–74, 2013.

[99] P. K. Vinson, Y. Talmon, and A. Walter. Vesicle-micelle transition of phosphatidylcholine and octyl glucoside elucidated by cryo-transmission electron-microscopy. *Biophysical Journal*, 56(4):669–681, 1989.

[100] K. Edwards, J. Gustafsson, M. Almgren, and G. Karlsson. Solubilization of lecithin vesicles by a cationic surfactant - intermediate structures in the vesicle micelle transition observed by cryo-transmission electron-microscopy. *Journal of Colloid and Interface Science*, 161(2):299–309, 1993.

[101] D. G. Fatouros, I. Walrand, B. Bergenstahl, and A. Müllertz. Colloidal structures in media simulating intestinal fed state conditions with and without lipolysis products. *Pharmaceutical Research*, 26(2):361–374, 2009.

[102] K. Kleberg, F. Jacobsen, D. G. Fatouros, and A. Müllertz. Biorelevant media simulating fed state intestinal fluids: Colloid phase characterization and impact on solubilization capacity. *Journal of Pharmaceutical Sciences*, 99(8):3522–3532, 2010.

[103] J. Kuntsche, J. C. Horst, and H. Bunjes. Cryogenic transmission electron microscopy (cryo-tem) for studying the morphology of colloidal drug delivery systems. *International Journal of Pharmaceutics*, 417(1-2):120–137, 2011.

[104] A. Mercuri, A. Passalacqua, M. S. J. Wickham, R. M. Faulks, D. Q. M. Craig, and S. A. Barker. The effect of composition and gastric conditions on the self-emulsification process of ibuprofen-loaded self-emulsifying drug delivery systems: A microscopic and dynamic gastric model study. *Pharmaceutical Research*, 28(7): 1540–1551, 2011.

[105] S. Ajith and A. K. Rakshit. Effect of NaCl on a nonionic surfactant microemulsion system. *Langmuir*, 11(4):1122–1126, 1995.

[106] S. Ajith and A. K. Rakshit. Studies of mixed surfactant microemulsion systems - Brij-35 with Tween-20 and sodium dodecyl-sulfate. *Journal of Physical Chemistry*, 99(40):14778–14783, 1995.

[107] R. J. Urick. A sound velocity method for determining the compressibility of finely divided substances. *Journal of Applied Physics*, 18(11):983–987, 1947.

[108] L. de Campo, A. Yaghmur, N. Garti, M. E. Leser, B. Folmer, and O. Glatter. Five-component food-grade microemulsions: structural characterization by SANS. *Journal of Colloid and Interface Science*, 274(1):251–267, 2004.

[109] C. Goddeeris, B. Goderis, and G. Van den Mooter. Lyotropic, liquid crystalline nanostructures of aqueous dilutions of SMEDDS revealed by small-angle X-ray scattering: Impact on solubility and drug release. *European Journal of Pharmaceutical Sciences*, 40(2):110–117, 2010.

[110] R. P. Hjelm, C. D. Schteingart, A. F. Hofmann, and P. Thiyagarajan. Structure of conjugated bile salt-fatty acid-monoglyceride mixed colloids: Studies by small-angle neutron scattering. *Journal of Physical Chemistry B*, 104(2):197–211, 2000.

[111] A. Spernath, A. Yaghmur, A. Aserin, R. E. Hoffman, and N. Garti. Self-diffusion nuclear magnetic resonance, microstructure transitions, and solubilization capacity of phytosterols and cholesterol in Winsor IV food-grade microemulsions. *Journal of Agricultural and Food Chemistry*, 51(8):2359–2364, 2003.

[112] A. Yaghmur, M. Rappolt, J. Ostergaard, C. Larsen, and S. W. Larsen. Characterization of bupivacaine-loaded formulations based on liquid crystalline phases and microemulsions: The effect of lipid composition. *Langmuir*, 28(5):2881–2889, 2012.

[113] Z. Misic, R. Urbani, T. Pfohl, K. Muffler, G. Sydow, and M. Kuentz. Understanding biorelevant drug release from a novel thermoplastic capsule by considering microstructural formulation changes during hydration. *Pharmaceutical Research*, in press, 2013.

[114] S. Phan, W. K. Fong, N. Kirby, T. Hanley, and B. J. Boyd. Evaluating the link between self-assembled mesophase structure and drug release. *International Journal of Pharmaceutics*, 421(1):176–182, 2011.

[115] A. Yaghmur and M. Rappolt. Structural characterization of lipidic systems under nonequilibrium conditions. *European Biophysics Journal with Biophysics Letters*, 41(10):831–840, 2012.

[116] J. S. Guo, M. S. Elaasser, E. D. Sudol, H. J. Yue, and J. W. Vanderhoff. Phase compositions of styrene oil-in-water microemulsions. *Journal of Colloid and Interface Science*, 140(1):175–184, 1990.

[117] A. Abdalla and K. Mader. Esr studies on the influence of physiological dissolution and digestion media on the lipid phase characteristics of SEDDS and SEDDS pellets. *International Journal of Pharmaceutics*, 367(1-2):29–36, 2009.

[118] A. Ruebe, S. Klein, and K. Mader. Monitoring of in vitro fat digestion by electron paramagnetic resonance spectroscopy. *Pharmaceutical Research*, 23(9):2024–2029, 2006.

[119] D. J. Lurie and K. Mader. Monitoring drug delivery processes by EPR and related techniques - principles and applications. *Advanced Drug Delivery Reviews*, 57(8): 1171–1190, 2005.

[120] M. Vertzoni, C. Markopoulos, M. Symillides, C. Goumas, G. Imanidis, and C. Reppas. Luminal lipid phases after administration of a triglyceride solution of danazol in the fed state and their contribution to the flux of danazol across Caco-2 cell monolayers. *Molecular Pharmaceutics*, 9(5):1189–1198, 2012.

[121] B. K. Kang, J. S. Lee, S. K. Chon, S. Y. Jeong, S. H. Yuk, G. Khang, H. B. Lee, and S. H. Cho. Development of self-microemulsifying drug delivery systems (SMEDDS) for oral bioavailability enhancement of simvastatin in beagle dogs. *International Journal of Pharmaceutics*, 274(1-2):65–73, 2004.

[122] J. Y. Kim and Y. S. Ku. Enhanced absorption of indomethacin after oral or rectal administration of a self-emulsifying system containing indomethacin to rats. *International Journal of Pharmaceutics*, 194(1):81–89, 2000.

[123] A. M. S. Villar, B. C. Naveros, A. C. C. Campmany, M. A. Trenchs, C. B. Rocabert, and L. H. Bellowa. Design and optimization of self-nanoemulsifying drug delivery systems (SNEDDS) for enhanced dissolution of gemfibrozil. *International Journal of Pharmaceutics*, 431(1-2):161–175, 2012.

[124] W. Wu, Y. Wang, and L. Que. Enhanced bioavailability of silymarin by self-microemulsifying drug delivery system. *European Journal of Pharmaceutics and Biopharmaceutics*, 63(3):288–294, 2006.

[125] J. Y. Hong, J. K. Kim, Y. K. Song, J. S. Park, and C. K. Kim. A new self-emulsifying formulation of itraconazole with improved dissolution and oral absorption. *Journal of Controlled Release*, 110(2):332–338, 2006.

[126] R. C. Rossi, C. L. Dias, E. M. Donato, L. A. Martins, A. M. Bergold, and P. E. Froeehlich. Development and validation of dissolution test for ritonavir soft gelatin capsules based on in vivo data. *International Journal of Pharmaceutics*, 338(1-2): 119–124, 2007.

[127] E. Jantratid, N. Janssen, C. Reppas, and J. B. Dressman. Dissolution media simulating conditions in the proximal human gastrointestinal tract: An update. *Pharmaceutical Research*, 25(7):1663–1676, 2008.

[128] Y. Arnold, R. B. Gonzalez, H. Versace, and M. Kuentz. Comparison of different in vitro tests to assess oral lipid-based formulations using a poorly soluble acidic drug. *Journal of Drug Delivery Science and Technology*, 20(2):143–148, 2010.

[129] S. Di Maio and R. L. Carrier. Gastrointestinal contents in fasted state and post-lipid ingestion: In vivo measurements and in vitro models for studying oral drug delivery. *Journal of Controlled Release*, 151(2):110–122, 2011.

[130] R. Holm, A. Mullertz, and H. L. Mu. Bile salts and their importance for drug absorption. *International Journal of Pharmaceutics*, 453(1):44–55, 2013.

[131] E. D. Gamsiz, M. Ashtikar, J. Crison, W. Woltosz, M. B. Bolger, and R. L. Carrier. Predicting the effect of fed-state intestinal contents on drug dissolution. *Pharmaceutical Research*, 27(12):2646–2656, 2010.

[132] E. M. Persson, A. S. Gustafsson, A. S. Carlsson, R. G. Nilsson, L. Knutson, P. Forsell, G. Hanisch, H. Lennernas, and B. Abrahamsson. The effects of food on the dissolution of poorly soluble drugs in human and in model small intestinal fluids. *Pharmaceutical Research*, 22(12):2141–2151, 2005.

[133] The United States Pharmacopeial Convention. *In vitro and in vivo evaluation of dosage forms*, volume 1. The United States Pharmacopeial Convention, Rockville MD, 2009.

[134] J. Dressman, K. Schamp, K. Beltz, and J. Alsenz. *Oral lipid-based formulations: enhancing the bioavailability of poorly water-soluble drugs*, chapter Characterizing release from lipid-based formulations. Informa Healthcare, New York, 2007.

[135] K. J. Frank, U. Westedt, K. M. Rosenblatt, P. Holig, J. Rosenberg, M. Magerlein, M. Brandl, and G. Fricker. Impact of FaSSIF on the solubility and dissolution-/permeation rate of a poorly water-soluble compound. *European Journal of Pharmaceutical Sciences*, 47(1):16–20, 2012.

[136] V. Bakatselou, R. C. Oppenheim, and J. B. Dressman. Solubilization and wetting effects of bile-salts on the dissolution of steroids. *Pharmaceutical Research*, 8(12): 1461–1469, 1991.

[137] D. Juenemann, E. Jantratid, C. Wagner, C. Reppas, M. Vertzoni, and J. B. Dressman. Biorelevant in vitro dissolution testing of products containing micronized or nanosized fenofibrate with a view to predicting plasma profiles. *European Journal of Pharmaceutics and Biopharmaceutics*, 77(2):257–264, 2011.

[138] A. Ruf, J. Worlitschek, and M. Mazzotti. Modeling and experimental analysis of PSD measurements through FBRM. *Particle and Particle Systems Characterization*, 17(4):167–179, 2000.

[139] P. Barrett and B. Glennon. In-line FBRM monitoring of particle size in dilute agitated suspensions. *Particle and Particle Systems Characterization*, 16(5):207–211, 1999.

[140] J. Scholl, L. Vicum, M. Muller, and M. Mazzotti. Precipitation of L-glutamic acid: Determination of nucleation kinetics. *Chemical Engineering Technology*, 29 (2):257–264, 2006.

[141] J. Schoell, C. Lindenberg, L. Vicum, J. Brozio, and M. Mazzotti. Precipitation of alpha L-glutamic acid: determination of growth kinetics. *Faraday Discussions*, 136:247–264, 2007.

[142] Y. Arnold. *Evaluation of lipid-based formulations of poorly water-soluble drugs in the gastro-intestinal tract using in vitro tests*. PhD thesis, University of Basel, 2011.

[143] J.-C. Bakala N'Goma, S. Amara, K. Dridi, V. Jannin, and F. Carriere. Understanding the lipid-digestion process in the GI tract before designing lipid-based drug-delivery systems. *Therapeutic Delivery*, 3(1):105–124, 2012.

[144] J. P. Reymond and H. Sucker. In vitro model for ciclosporin intestinal-absorption in lipid vehicles. *Pharmaceutical Research*, 5(10):673–676, 1988.

[145] J. S. Patton and M. C. Carey. Watching fat digestion. *Science*, 204(4389):145–148, 1979.

[146] L. Sek, C. J. H. Porter, and W. N. Charman. Characterisation and quantification of medium chain and long chain triglycerides and their in vitro digestion products, by HPTLC coupled with in situ densitometric analysis. *Journal of Pharmaceutical and Biomedical Analysis*, 25(3-4):651–661, 2001.

[147] N. H. Zangenberg, A. Mullertz, H. G. Kristensen, and L. Hovgaard. A dynamic in vitro lipolysis model I. controlling the rate of lipolysis by continuous addition of calcium. *European Journal of Pharmaceutical Sciences*, 14(2):115–122, 2001.

[148] N. H. Zangenberg, A. Mullertz, H. G. Kristensen, and L. Hovgaard. A dynamic in vitro lipolysis model II: Evaluation of the model. *European Journal of Pharmaceutical Sciences*, 14(3):237–244, 2001.

[149] Y. Li, M. Hu, and D. J. McClements. Factors affecting lipase digestibility of emulsified lipids using an in vitro digestion model: Proposal for a standardised pH-stat method. *Food Chemistry*, 126(2):498–505, 2011.

[150] H. Ali, A. Siddiqui, and S. Nazzal. The effect of media composition, pH, and formulation excipients on the in vitro lipolysis of self-emulsifying drug delivery systems (SEDDS). *Journal of Dispersion Science and Technology*, 31(2):226–232, 2010.

[151] Z. Vinarov, Y. Petkova, S. Tcholakova, N. Denkov, S. Stoyanov, E. Pelan, and A. Lips. Effects of emulsifier charge and concentration on pancreatic lipolysis. 1. In the absence of bile salts. *Langmuir*, 28(21):8127–8139, 2012.

[152] S. Ren, H. L. Mu, F. Alchaer, A. Chtatou, and A. Mullertz. Optimization of self nanoemulsifying drug delivery system for poorly water-soluble drug using response surface methodology. *Drug Development and Industrial Pharmacy*, 39(5):799–806, 2013.

[153] A. Q. Ye, J. Cui, X. Q. Zhu, and H. Singh. Effect of calcium on the kinetics of free fatty acid release during in vitro lipid digestion in model emulsions. *Food Chemistry*, 139(1-4):681–688, 2013.

[154] M. Hu, Y. Li, E. A. Decker, and D. J. McClements. Role of calcium and calcium-binding agents on the lipase digestibility of emulsified lipids using an in vitro digestion model. *Food Hydrocolloids*, 24(8):719–725, 2010.

[155] LFCS Consortium. http://www.lfcsconsortium.org, 2010-2013.

[156] D. G. Fatouros, G. R. Deen, L. Arleth, B. Bergenstahl, F. S. Nielsen, J. S. Pedersen, and A. Mullertz. Structural development of self nano emulsifying drug delivery systems (SNEDDS) during in vitro lipid digestion monitored by small-angle X-ray scattering. *Pharmaceutical Research*, 24(10):1844–1853, 2007.

[157] S. Fernandez, V. Jannin, J. D. Rodier, N. Ritter, B. Mahler, and F. Carriere. Comparative study on digestive lipase activities on the self emulsifying excipient Labrasol, medium chain glycerides and PEG esters. *Biochimica Et Biophysica Acta-Molecular and Cell Biology of Lipids*, 1771(5):633–640, 2007.

[158] S. Fernandez, J. D. Rodier, N. Ritter, B. Mahler, F. Demarne, F. Carriere, and V. Jannin. Lipolysis of the semi-solid self-emulsifying excipient Gelucire 44/14 by

digestive lipases. *Biochimica Et Biophysica Acta-Molecular and Cell Biology of Lipids*, 1781(8):367–375, 2008.

[159] L. Sek, C. J. H. Porter, A. M. Kaukonen, and W. N. Charman. Evaluation of the in-vitro digestion profiles of long and medium chain glycerides and the phase behaviour of their lipolytic products. *Journal of Pharmacy and Pharmacology*, 54 (1):29–41, 2002.

[160] Z. Vinarov, S. Tcholakova, B. Damyanova, Y. Atanasov, N. D. Denkov, S. D. Stoyanov, E. Pelan, and A. Lips. Effects of emulsifier charge and concentration on pancreatic lipolysis: 2. Interplay of emulsifiers and biles. *Langmuir*, 28(33): 12140–12150, 2012.

[161] K. W. Y. Lee, C. J. H. Porter, and B. J. Boyd. A simple quantitative approach for the determination of long and medium chain lipids in bio-relevant matrices by high performance liquid chromatography with refractive index detection. *AAPS PharmSciTech*, 14(3):927–934, 2013.

[162] J. O. Christensen, K. Schultz, B. Mollgaard, H. G. Kristensen, and A. Mullertz. Solubilisation of poorly water-soluble drugs during in vitro lipolysis of medium- and long-chain triacylglycerols. *European Journal of Pharmaceutical Sciences*, 23 (3):287–296, 2004.

[163] A. Helbig, E. Silletti, E. Timmerman, R. J. Hamer, and H. Gruppen. In vitro study of intestinal lipolysis using pH-stat and gas chromatography. *Food Hydrocolloids*, 28(1):10–19, 2012.

[164] M. W. Rigler, R. E. Honkanen, and J. S. Patton. Visualization by freeze-fracture, invitro and invivo, of the products of fat digestion. *Journal of Lipid Research*, 27 (8):836–857, 1986.

[165] D. G. Fatouros, B. Bergenstahl, and A. Mullertz. Morphological observations on a lipid-based drug delivery system during in vitro digestion. *European Journal of Pharmaceutical Sciences*, 31(2):85–94, 2007.

[166] A. Muellertz, D. G. Fatouros, J. R. Smith, M. Vertzoni, and C. Reppas. Insights into intermediate phases of human intestinal fluids visualized by atomic force microscopy and cryo-transmission electron microscopy ex vivo. *Molecular Pharmaceutics*, 9(2):237–247, 2012.

[167] S. Salentinig, L. Sagalowicz, M. E. Leser, C. Tedeschi, and O. Glatter. Transitions in the internal structure of lipid droplets during fat digestion. *Soft Matter*, 7(2): 650–661, 2011.

[168] S. Phan, A. Hawley, X. Mulet, L. Waddington, C. A. Prestidge, and B. J. Boyd. Structural aspects of digestion of medium chain triglycerides studied in real time using sSAXS and Cryo-TEM. *Pharmaceutical Research*, in press, 2013.

[169] J. P. R. Day, G. Rago, K. F. Domke, K. P. Velikov, and M. Bonn. Label-free imaging of lipophilic bioactive molecules during lipid digestion by multiplex coherent anti-stokes Raman scattering microspectroscopy. *Journal of the American Chemical Society*, 132(24):8433–8439, 2010.

[170] Y.-D. Dong and B. J. Boyd. Applications of X-ray scattering in pharmaceutical science. *International Journal of Pharmaceutics*, 417(1-2):101–111, 2011.

[171] A. Niederquell and M. Kuentz. Introduction of a theoretical splashing degree to assess the performance of low-viscosity oils in filling of capsules. *AAPS PharmSciTech*, 12(1):323–330, 2011.

[172] S. Marze, M. Choimet, and L. Foucat. In vitro digestion of emulsions: diffusion and particle size distribution using diffusing wave spectroscopy and diffusion using nuclear magnetic resonance. *Soft Matter*, 8(42):10994–11004, 2012.

[173] F. Caboi, J. Borne, T. Nylander, A. Khan, A. Svendsen, and S. Patkar. Lipase action on a monoolein/sodium oleate aqueous cubic liquid crystalline phase - a NMR and X-ray diffraction study. *Colloids and Surfaces B-Biointerfaces*, 26(1-2): 159–171, 2002.

[174] C. Wagner, E. Jantratid, F. Kesisoglou, M. Vertzoni, C. Reppas, and J. B. Dressman. Predicting the oral absorption of a poorly soluble, poorly permeable weak base using biorelevant dissolution and transfer model tests coupled with a physiologically based pharmacokinetic model. *European Journal of Pharmaceutics and Biopharmaceutics*, 82(1):127–138, 2012.

[175] D. G. Fatouros, F. S. Nielsen, D. Douroumis, L. J. Hadjileontiadis, and A. Mullertz. In vitro-in vivo correlations of self-emulsifying drug delivery systems combining the dynamic lipolysis model and neuro-fuzzy networks. *European Journal of Pharmaceutics and Biopharmaceutics*, 69(3):887–898, 2008.

[176] S. F. Han, T. T. Yao, X. X. Zhang, L. Gan, C. L. Zhu, H. Z. Yua, and Y. Gan. Lipid-based formulations to enhance oral bioavailability of the poorly water-soluble drug anethol trithione: Effects of lipid composition and formulation. *International Journal of Pharmaceutics*, 379(1):18–24, 2009.

[177] C. A. Barta, K. Sachs-Barrable, F. Feng, and K. M. Wasan. Effects of monoglycerides on P-glycoprotein: Modulation of the activity and expression in Caco-2 cell monolayers. *Molecular Pharmaceutics*, 5(5):863–875, 2008.

[178] E. V. Batrakova, H. Y. Han, V. Y. Alakhov, D. W. Miller, and A. V. Kabanov. Effects of pluronic block copolymers on drug absorption in Caco-2 cell monolayers. *Pharmaceutical Research*, 15(6):850–855, 1998.

[179] M. M. Nerurkar, P. S. Burton, and R. T. Borchardt. The use of surfactants to enhance the permeability of peptides through Caco-2 cells by inhibition of an apically polarized efflux system. *Pharmaceutical Research*, 13(4):528–534, 1996.

[180] D. M. Woodcock, M. E. Linsenmeyer, G. Chojnowski, A. B. Kriegler, V. Nink, L. K. Webster, and W. H. Sawyer. Reversal of multidrug resistance by surfactants. *British Journal of Cancer*, 66(1):62–68, 1992.

[181] T. Gershanik, E. Haltner, C. M. Lehr, and S. Benita. Charge-dependent interaction of self-emulsifying oil formulations with Caco-2 cells monolayers: binding, effects on barrier function and cytotoxicity. *International Journal of Pharmaceutics*, 211 (1-2):29–36, 2000.

[182] S. Fernandez, V. Jannin, S. Chevrier, Y. Chavant, F. Demarne, and F. Carriere. In vitro digestion of the self-emulsifying lipid excipient labrasol by gastrointestinal lipases and influence of its colloidal structure on lipolysis rate. *Pharmaceutical Research*, in press, 2013.

[183] S. Fernandez, S. Chevrier, N. Ritter, B. Mahler, F. Demarne, F. Carriere, and V. Jannin. In vitro gastrointestinal lipolysis of four formulations of piroxicam and cinnarizine with the self emulsifying excipients Labrasol and Gelucire 44/14. *Pharmaceutical Research*, 26(8):1901–1910, 2009.

[184] R. Devraj, H. D. Williams, D. B. Warren, A. Mullertz, C. J. H. Porter, and C. W. Pouton. In vitro digestion testing of lipid-based delivery systems: Calcium ions combine with fatty acids liberated from triglyceride rich lipid solutions to form soaps and reduce the solubilization capacity of colloidal digestion products. *International Journal of Pharmaceutics*, 441(1-2):323–333, 2013.

[185] S. M. Caliph, W. N. Charman, and C. J. H. Porter. Effect of short-, medium-, and long-chain fatty acid-based vehicles on the absolute oral bioavailability and intestinal lymphatic transport of halofantrine and assessment of mass balance in lymph-cannulated and non-cannulated rats. *Journal of Pharmaceutical Sciences*, 89(8):1073–1084, 2000.

[186] T. T. Kararli. Comparison of the gastrointestinal anatomy, physiology, and biochemistry of humans and commonly used laboratory-animals. *Biopharmaceutics and Drug Disposition*, 16(5):351–380, 1995.

[187] H. A. Merchant, E. L. McConnell, F. Liu, C. Ramaswamy, R. P. Kulkarni, A. W. Basit, and S. Murdan. Assessment of gastrointestinal ph, fluid and lymphoid tissue in the guinea pig, rabbit and pig, and implications for their use in drug development. *European Journal of Pharmaceutical Sciences*, 42(1-2):3–10, 2011.

[188] R. Verger. *Pancreatic lipases*. Elsevier Inc., London, GB, 1984.

[189] J. M. DeSesso and C. F. Jacobson. Anatomical and physiological parameters affecting gastrointestinal absorption in humans and rats. *Food and Chemical Toxicology*, 39(3):209–228, 2001.

[190] R. N. Gursoy and S. Benita. Self-emulsifying drug delivery systems (SEDDS) for improved oral delivery of lipophilic drugs. *Biomedicine Pharmacotherapy*, 58(3): 173–182, 2004.

[191] A. Dahan and A. Hoffman. Evaluation of a chylomicron flow blocking approach to investigate the intestinal lymphatic transport of lipophilic drugs. *European Journal of Pharmaceutical Sciences*, 24(4):381–388, 2005.

[192] C. M. O'Driscoll. Lipid-based formulations for intestinal lymphatic delivery. *European Journal of Pharmaceutical Sciences*, 15(5):405–415, 2002.

[193] R. G. Alany, I. G. Tucker, N. M. Davies, and T. Rades. Characterizing colloidal structures of pseudoternary phase diagrams formed by oil/water/amphiphile systems. *Drug Development and Industrial Pharmacy*, 27(1):31–38, 2001.

[194] S. Hickey, S. A. Hagan, E. Kudryashov, and V. Buckin. Analysis of phase diagram and microstructural transitions in an ethyl oleate/water/Tween 80/Span 20 microemulsion system using high-resolution ultrasonic spectroscopy. *International Journal of Pharmaceutics*, 388(1-2):213–222, 2010.

[195] R. B. Shah, A. S. Zidan, T. Funck, M. A. Tawakkul, A. Nguyenpho, and M. A. Khan. Quality by design: Characterization of self-nano-emulsified drug delivery systems (SNEDDS) using ultrasonic resonator technology. *International Journal of Pharmaceutics*, 341(1-2):189–194, 2007.

[196] A. Munoz, J. P. Guichard, and P. Reginault. Micronized fenofibrate. *Atherosclerosis*, 110:45–48, 1994.

[197] D. Kashchiev and G. M. van Rosmalen. Review: Nucleation in solutions revisited. *Crystal Research and Technology*, 38(7-8):555–574, 2003.

[198] S. H. Yalkowsky. *Solubilization by cosolvents*, chapter 6, pages 180–235. Oxford University Press, Washington NY, 1999.

[199] S. H. Yalkowsky. *Solubilization by surfactants*, pages 236–320. Oxford University press, Washington NY, 1999.

[200] Y. Ran, L. Zhao, Q. Xu, and S. H Yalkowsky. Solubilization of Cyclosporin A. *AAPS PharmSciTech*, 2(1), 2001.

[201] A. P. Sarvazyan. Ultrasonic velocimetry of biological compounds. *Annual Review of Biophysics and Biophysical Chemistry*, 20:321–342, 1991.

[202] A. B. Wood. *A textbook of sound*. G. Bell, London, second edition, 1941.

[203] J. F. Cuine, C. L. McEvoy, W. N. Charman, C. W. Pouton, G. A. Edwards, H. Benameur, and C. J. H. Porter. Evaluation of the impact of surfactant digestion on the bioavailability of danazol after oral administration of lipidic self-emulsifying formulations to dogs. *Journal of Pharmaceutical Sciences*, 97(2):995–1012, 2008.

[204] Y. E. Arnold, G. Imanidis, and M. Kuentz. Study of drug concentration effects on in vitro lipolysis kinetics in medium-chain triglycerides by considering oil viscosity and surface tension. *European Journal of Pharmaceutical Sciences*, 44(3):351–358, 2011.

[205] G. A. Kossena, W. N. Charman, B. J. Boyd, and C. I. H. Porter. Influence of the intermediate digestion phases of common formulation lipids on the absorption of a poorly water-soluble drug. *Journal of Pharmaceutical Sciences*, 94(3):481–492, 2005.

[206] G. A. Kossena, B. J. Boyd, C. J. H. Porter, and W. N. Charman. Separation and characterization of the colloidal phases produced on digestion of common formulation lipids and assessment of their impact on the apparent solubility of selected poorly water-soluble drugs. *Journal of Pharmaceutical Sciences*, 92(3): 634–648, 2003.

[207] J. Cornel, C. Lindenberg, and M. Mazzotti. Quantitative application of in situ ATR-FTIR and Raman spectroscopy in crystallization processes. *Industrial Engineering Chemistry Research*, 47(14):4870–4882, 2008.

[208] Y. R. Hu, J. K. Liang, A. S. Myerson, and L. S. Taylor. Crystallization monitoring by Raman spectroscopy: Simultaneous measurement of desupersaturation profile and polymorphic form in flufenamic acid systems. *Industrial Engineering Chemistry Research*, 44(5):1233–1240, 2005.

[209] A. Caillet, F. Puel, and G. Fevotte. In-line monitoring of partial and overall solid concentration during solvent-mediated phase transition using Raman spectroscopy. *International Journal of Pharmaceutics*, 307(2):201–208, 2006.

[210] T. Ono, J. H. ter Horst, and P. J. Jansens. Quantitative measurement of the polymorphic transformation of L-glutamic acid using in-situ Raman spectroscopy. *Crystal Growth Design*, 4(3):465–469, 2004.

[211] J. Scholl, D. Bonalumi, L. Vicum, M. Mazzotti, and M. Muller. In situ monitoring and modeling of the solvent-mediated polymorphic transformation of L-glutamic acid. *Crystal Growth Design*, 6(4):881–891, 2006.

[212] N. Pienack and W. Bensch. In-situ monitoring of the formation of crystalline solids. *Angewandte Chemie-International Edition*, 50(9):2014–2034, 2011.

[213] Y. E. Arnold, G. Imanidis, and M. T. Kuentz. Advancing in-vitro drug precipitation testing: new process monitoring tools and a kinetic nucleation and growth model. *Journal of Pharmacy and Pharmacology*, 63(3):333–341, 2011.

[214] M. M. Reis, P. H. H. Araujo, C. Sayer, and R. Giudici. Spectroscopic on-line monitoring of reactions in dispersed medium: Chemometric challenges. *Analytica Chimica Acta*, 595(1-2):257–265, 2007.

[215] C. W. Garner. Boronic acid inhibitors of porcine pancreatic lipase. *Journal of Biological Chemistry*, 255(11):5064–5068, 1980.

[216] P. Geladi, D. Macdougall, and H. Martens. Linearization and scatter-correction for near-infrared reflectance spectra of meat. *Applied Spectroscopy*, 39(3):491–500, 1985.

[217] R. J. Barnes, M. S. Dhanoa, and S. J. Lister. Standard normal variate transformation and de-trending of near-infrared diffuse reflectance spectra. *Applied Spectroscopy*, 43(5):772–777, 1989.

[218] A. Rinnan, F. van den Berg, and S. B. Engelsen. Review of the most common preprocessing techniques for near-infrared spectra. *Trac-Trends in Analytical Chemistry*, 28(10):1201–1222, 2009.

[219] P. Geladi and B. R. Kowalski. Partial least-squares regression - a tutorial. *Analytica Chimica Acta*, 185:1–17, 1986.

[220] C. Stillhart and M. Kuentz. Comparison of high-resolution ultrasonic resonator technology and Raman spectroscopy as novel process analytical tools for drug quantification in self-emulsifying drug delivery systems. *Journal of Pharmaceutical and Biomedical Analysis*, 59:29–37, 2012.

[221] Y. R. Hu, H. Wikstrom, S. R. Byrn, and L. S. Taylor. Analysis of the effect of particle size on polymorphic quantitation by Raman spectroscopy. *Applied Spectroscopy*, 60(9):977–984, 2006.

[222] J. Boetker, T. Rades, J. Rantanen, A. Hawley, and B. J. Boyd. Structural elucidation of rapid solution-mediated phase transitions in pharmaceutical solids using in situ synchrotron SAXS/WAXS. *Molecular Pharmaceutics*, 9(9):2787–2791, 2012.

[223] J. F. Cuine, W. N. Charman, C. W. Pouton, G. A. Edwards, and C. J. H. Porter. Increasing the proportional content of surfactant (Cremophor EL) relative to lipid in self-emulsifying lipid-based formulations of danazol reduces oral bioavailability in beagle dogs. *Pharmaceutical Research*, 24(4):748–757, 2007.

[224] K. Kleberg, J. Jacobsen, and A. Müllertz. Characterising the behaviour of poorly water soluble drugs in the intestine: application of biorelevant media for solubility, dissolution and transport studies. *Journal of Pharmacy and Pharmacology*, 62(11): 1656–1668, 2010.

[225] B. D. Anderson and M. T. Marra. Chemical and related factors controlling lipid solubility. *Bulletin Technique Gattefosse*, pages 11–19, 1999.

[226] B. Borgstrom and H. L. Brockman. Lipases, 1983.

[227] R. Birner-Grunberger, H. Scholze, K. Faber, and A. Hermetter. Identification of various lipolytic enzymes in crude porcine pancreatic lipase preparations using covalent fluorescent inhibitors. *Biotechnology and Bioengineering*, 85(2):147–154, 2004.

[228] C. S. Wang, A. Kuksis, and F. Manganaro. Studies on the substrate-specificity of purified human-milk lipoprotein-lipase. *Lipids*, 17(4):278–284, 1982.

[229] F. H. Mattson and R. A. Volpenhein. Digestion and absorption of triglycerides. *Journal of Biological Chemistry*, 239(9):2772–, 1964.

[230] D. G. Fatouros and A. Mullertz. In vitro lipid digestion models in design of drug delivery systems for enhancing oral bioavailability. *Expert Opinion on Drug Metabolism and Toxicology*, 4(1):65–76, 2008.

[231] J. Najib. Fenofibrate in the treatment of dyslipidemia: A review of the data as they relate to the new suprabioavailable tablet formulation. *Clinical Therapeutics*, 24(12):2022–2050, 2002.

[232] A. Avdeef and K. Y. Tam. How well can the Caco-2/madin-darby canine kidney models predict effective human jejunal permeability? *Journal of Medicinal Chemistry*, 53(9):3566–3584, 2010.

[233] V. P. Shah, Y. Tsong, P. Sathe, and J. P. Liu. In vitro dissolution profile comparison - statistics and analysis of the similarity factor, f(2). *Pharmaceutical Research*, 15(6):889–896, 1998.

[234] M. Grove, G. P. Pedersen, J. L. Nielsen, and A. Mullertz. Bioavailability of seocalcitol I: Relating solubility in biorelevant media with oral bioavailability in rats - effect of medium and long chain triglycerides. *Journal of Pharmaceutical Sciences*, 94(8):1830–1838, 2005.

[235] K. Sugano. *Biopharmaceutics modeling and simulations*. Wiley, Hoboken NJ, USA, 2012.

[236] S. S. Davis, J. G. Hardy, and J. W. Fara. Transit of pharmaceutical dosage forms through the small-intestine. *Gut*, 27(8):886–892, 1986.

[237] R. Sanghvi, E. Mogalian, S. G. Machatha, R. Narazaki, K. L. Karlage, P. Jain, S. E. Tabibi, E. Glaze, P. B. Myrdal, and S. H. Yalkowsky. Preformulation and pharmacokinetic studies on antalarmin: A novel stress inhibitor. *Journal of Pharmaceutical Sciences*, 98(1):205–214, 2009.

[238] S. Carlert, P. Akesson, G. Jerndal, L. Lindfors, H. Lennernas, and B. Abrahamsson. In vivo dog intestinal precipitation of mebendazole: A basic BCS class II drug. *Molecular Pharmaceutics*, 9(10):2903–2911, 2012.

[239] E. S. Kostewicz, M. Wunderlich, U. Brauns, R. Becker, T. Bock, and J. B. Dressman. Predicting the precipitation of poorly soluble weak bases upon entry in the small intestine. *Journal of Pharmacy and Pharmacology*, 56(1):43–51, 2004.

[240] D. Psachoulias, M. Vertzoni, J. Butler, D. Busby, M. Symillides, J. Dressman, and C. Reppas. An in vitro methodology for forecasting luminal concentrations and precipitation of highly permeable lipophilic weak bases in the fasted upper small intestine. *Pharmaceutical Research*, 29(12):3486–3498, 2012.

[241] S. Carlert, A. Palsson, G. Hanisch, C. von Corswant, C. Nilsson, L. Lindfors, H. Lennernas, and B. Abrahamsson. Predicting intestinal precipitation - A case example for a basic BCS class II drug. *Pharmaceutical Research*, 27(10):2119–2130, 2010.

[242] S. Klein, N. L. Buchanan, and C. M. Buchanan. Miniaturized transfer models to predict the precipitation of poorly soluble weak bases upon entry into the small intestine. *AAPS PharmSciTech*, 13(4):1230–1235, 2012.

[243] Y. L. Hsieh, G. A. Ilevbare, B. Van Eerdenbrugh, K. J. Box, M. V. Sanchez-Felix, and L. S. Taylor. pH-induced precipitation behavior of weakly basic compounds: determination of extent and duration of supersaturation using potentiometric titration and correlation to solid state properties. *Pharmaceutical Research*, 29(10): 2738–2753, 2012.

[244] E. S. Kostewicz, U. Brauns, R. Becker, and J. B. Dressman. Forecasting the oral absorption behavior of poorly soluble weak bases using solubility and dissolution studies in biorelevant media. *Pharmaceutical Research*, 19(3):345–349, 2002.

[245] Y. Li and D. J. McClements. New mathematical model for interpreting pH-stat digestion profiles: Impact of lipid droplet characteristics on in vitro digestibility. *Journal of Agricultural and Food Chemistry*, 58(13):8085–8092, 2010.

[246] Y. F. Shiau, P. Fernandez, M. J. Jackson, and S. McMonagle. Mechanisms maintaining a low-pH microclimate in the intestine. *American Journal of Physiology*, 248(6 Pt 1):G608–17, 1985.

[247] M. L. Lucas, W. Schneider, F. J. Haberich, and J. A. Blair. Direct measurement by pH-microelectrode of the pH microclimate in rat proximal jejunum. *Proceedings of the Royal Society B: Biological Sciences*, 192(1106):39–48, 1975.

[248] M. Ikuma, H. Hanai, E. Kaneko, H. Hayashi, and T. Hoshi. Effects of aging on the microclimate ph of the rat jejunum. *Biochimica et Biophysica Acta (BBA) - Biomembranes*, 1280(1):19–26, 1996.

[249] D. Mahlin, S. Ponnambalam, M. H. Hockerfelt, and C. A. S. Bergstrom. Toward in silico prediction of glass-forming ability from molecular structure alone: A screening tool in early drug development. *Molecular Pharmaceutics*, 8(2):498–506, 2011.

[250] K. Bakeev. *Process analytical technology*. Wiley, Chichester, West Sussex, 2nd edition, 2010.

[251] J. Medendorp, R. G. Buice, and R. A. Lodder. Acoustic-resonance spectrometry as a process analytical technology for the quantification of active pharmaceutical ingredient in semi-solids. *AAPS PharmSciTech*, 7(3):8, 2006.

[252] R. R. Chen, T. Zelesky, N. Ilasi, and S. S. Sekulic. Simultaneously measuring concentrations of a model drug and a model excipient in solution using ultrasonic spectrometry. *Journal of Pharmaceutical and Biomedical Analysis*, 37(2):239–247, 2005.

[253] M. Cavegn, R. Douglas, G. Akkermans, and M. Kuentz. Study of an ultrasound-based process analytical tool for homogenization of nanoparticulate pharmaceutical vehicles. *Journal of Pharmaceutical Sciences*, 100(8):3374–3385, 2011.

[254] J. Rantanen. Process analytical applications of Raman spectroscopy. *Journal of Pharmacy and Pharmacology*, 59(2):171–177, 2007.

[255] M. D. Hargreaves, N. A. Macleod, M. R. Smith, D. Andrews, S. V. Hammond, and P. Matousek. Characterisation of transmission Raman spectroscopy for rapid quantitative analysis of intact multi-component pharmaceutical capsules. *Journal of Pharmaceutical and Biomedical Analysis*, 54(3):463–468, 2011.

[256] S. Mazurek and R. Szostak. Quantitative determination of diclofenac sodium in solid dosage forms by FT-Raman spectroscopy. *Journal of Pharmaceutical and Biomedical Analysis*, 48(3):814–821, 2008.

[257] J. Johansson, A. Sparen, O. Svensson, S. Folestad, and M. Claybourn. Quantitative transmission Raman spectroscopy of pharmaceutical tablets and capsules. *Applied Spectroscopy*, 61(11):1211–1218, 2007.

[258] T. M. Niemczyk, M. Delgado-Lopez, F. S. Allen, J. T. Clay, and D. L. Arneberg. Quantitative assay of bucindolol in gel capsules using infrared and Raman spectroscopy. *Applied Spectroscopy*, 52(4):513–518, 1998.

[259] C. Eliasson, N. A. Macleod, L. C. Jayes, F. C. Clarke, S. V. Hammond, M. R. Smith, and P. Matousek. Non-invasive quantitative assessment of the content of pharmaceutical capsules using transmission Raman spectroscopy. *Journal of Pharmaceutical and Biomedical Analysis*, 47(2):221–229, 2008.

[260] A. Szep, G. Marosi, B. Marosfoi, P. Anna, I. Mohammed-Ziegler, and M. Viragh. Quantitative analysis of mixtures of drug delivery system components by Raman microscopy. *Polymers for Advanced Technologies*, 14(11-12):784–789, 2003.

[261] B. Gotter, W. Faubel, S. Heiler, J. Hein, and R.H.H. Neubert. Determination of drug content in semisolid formulations by non-invasive spectroscopic methods: FTIR - ATR, - PAS, - Raman and PDS. *Journal of Physics: Conference Series*, 214(1):1–5, 2010.

[262] M. Vertzoni, J. Dressman, J. Butler, J. Hempenstall, and C. Reppas. Simulation of fasting gastric conditions and its importance for the in vivo dissolution of lipophilic compounds. *European Journal of Pharmaceutics and Biopharmaceutics*, 60(3): 413–417, 2005.

[263] F. Eggers. Ultrasonic velocity and attenuation measurements in liquids with resonators, extending the mhz frequency-range. *Acustica*, 76(5):231–240, 1992.

[264] R. Smith, D. R. Sparks, D. Riley, and N. Najafi. A MEMS-based coriolis mass flow sensor for industrial applications. *Ieee Transactions on Industrial Electronics*, 56(4):1066–1071, 2009.

[265] ICH Topic Q2B. Validation of analytical procedures: Methodology., 1996.

[266] J. Ermer and J. H. Miller. *Method Validation in Pharmaceutical Analysis: A Guide to Best Practice*. Wiley-VCH Verlag GmbH, Weinheim (D), 2005.

List of Abbreviations

4-BPBA	4-bromophenylboronic acid
BCS	Biopharmaceutical classification system
API	Active pharmaceutical ingredient
CARS	Coherent anti-Stokes Raman scattering
CCD	Charge-coupled device
CI	Confidence interval
CMC	Critical micelle concentration
CO	Cremophor system
DG	Diglycerides
DLS	Dynamic light scattering
EPR	Electron paramagnetic resonance
F1	Formulation 1
F2	Formulation 2
F3	Formulation 3
FA	Fatty acids
FaSSGF	Fasted state simulated gastric fluid
FaSSIF	Fasted state simulated intestinal fluid
FBRM	Focused beam reflectance measurement
FDA	Food and Drug Administration
Fen	Fenofibrate
FeSSIF	Fed state simulated intestinal fluid
GI	Gastro-intestinal
HPLC	High-performance liquid chromatography
Ind	Indomethacin
ICH	International conference of harmonization

IR	Infrared
i.v.	intravenous
LBDDS	Lipid-based drug delivery systems
LBF	Lipid-based formulation
LFCS	Lipid formulation classification system
LOQ	Limit of quantification
LP	Lipolysis products
LP1	Lipolysis products generated from triglycerides
LP2	Lipolysis products generated from surfactants
MEMS	Microelectromechanical system
MG	Monoglycerides
MSC	Multiple scattering correction
NaCl	Sodium chloride
NaOH	Sodium hydroxide
NaTDC	Sodium taurodeoxycholate
NMR	Nuclear magnetic resonance
PAT	Process analytical technology
PBPK	Physiologically-based pharmacokinetic
PC	Phosphatidylcholine
PDI	Polydispersity index
PLS	Partial least square
PK	Pharmacokinetic
p.o.	peroral
PO	Polysorbate system
Pro	Probucol
PTFE	Polytetrafluoroetylene
PVDF	Polyvinyldifluoride
RMSEC	Root-mean-square error of calibration
RMSECV	Root-mean-square error of cross-validation
RSEP	Relative standard error of prediction
SANS	Small-angle neutron scattering
SAXS	Small-angle X-ray scattering
SD	Standard deviation

SEDDS	Self-emulsifying drug delivery system
SF	Surfactant
SG	Savitzky–Golay
SGF	Simulated gastric fluid
SMEDDS	Self-microemulsifying drug delivery system
SNEDDS	Supersaturated self-nanoemulsifying drug delivery system
SNV	Standard normal variate
SR	Saturation ratio
TG	Triglycerides
TRFQ	Time-resolved fluorescence quenching
URT	Ultrasonic resonator technology
USP	United States Pharmacopeia
UV	Ultraviolet
XRPD	X-ray powder diffraction

List of Symbols

a	Amplitude
a_0	Initial amplitude
c^a	Actual drug concentration
c^p	Predicted drug concentration
f	Surface expansion factor (in Chapter 5)
f	Sound frequency (in Chapter 7)
f_2	Similarity factor
g	Order of particle growth
k	Boltzmann constant
$k_{dig,SF}$	Kinetic constant of SF digestion
$k_{dig,TG}$	Kinetic constant of TG digestion
k_{el}	Kinetic constant of drug elimination
k_g	Particle growth coefficient
k_{gd}	Kinetic constant of formulation dispersion in gastric fluid
k_{ge}	Kinetic constant of gastric emptying
k_{id}	Kinetic constant of formulation dispersion in intestinal fluid
k_{pt}	Kinetic constant of drug distribution from plasma to peripheral tissue
k_{tp}	Kinetic constant of drug distribution from peripheral tissue to plasma
m	Slope
m_t	Mass of the tube
n	Number of samples
n_{SF}	Order of kinetics for SF digestion
n_{TG}	Order of kinetics for TG digestion
r	Intestinal radius
t	Time

t_g	Time point of beginning of particle growth
t_{ind}	Induction time
t_n	Time point of beginning of nucleation
t_x	Time point of transition between 1^{st} and 2^{nd} stage of lipolysis
x	Distance
A	Kinetic parameter of the nucleation rate equation (Chapter 4)
A	Ultrasound attenuation (Chapter 7)
A'	Kinetic parameter of the nucleation rate equation
B	Thermodynamic parameter of the nucleation rate equation
C^*	Solubility
C_{co}	Concentration of co-solvent
$C_{eq,co}$	Drug solubility in diluted co-solvent
$C_{eq,meas}$	Measured equilibrium solubility
$C_{eq,model}$	Theoretical drug solubility in diluted formulation
$C_{eq,surf}$	Drug solubility in diluted surfactant
$C_{eq,w}$	Drug solubility in water
C_{form}	Drug concentration in the formulation
C_{id}	Concentration of solubilized drug in dispersed LBF in the intestine
C^*_{LP1}	Drug solubilization caused by LP1
$\hat{C}^*_{LP1}$	Relative drug solubility in LP1
C^*_{LP2}	Drug solubilization caused by LP2
$\hat{C}^*_{LP2}$	Relative drug solubility in LP2
$C^*_{m,t}$	Drug solubility in the lipolysis medium at time t
C_p	Drug concentration in plasma
C_{pr}	Concentration of precipitated drug
C^*_{SF}	Drug solubilization caused by surfactants
$\hat{C}^*_{SF}$	Relative drug solubility in surfactants
C_{sol}	Concentration of solubilized drug
$C_{sol,max}$	Maximum concentration of solubilized drug
C_{surf}	Concentration of surfactant
C_{theor}	Theoretical concentration of solubilized drug
C^*_{TG}	Drug solubilization caused by triglycerides

$\hat{C}^*_{TG}$	Relative drug solubility in triglycerides
D_{gd}	Drug mass in dispersed formulation in the stomach
D_{gu}	Drug mass in undispersed formulation in the stomach
D_{id}	Drug mass in dispersed formulation in the intestine
D_{iu}	Drug mass in undispersed formulation in the intestine
D_p	Drug mass in plasma
D_t	Drug mass in peripheral tissue
F_a	Fraction absorbed
FA_{titr}	Amount of titrated FAs
FA^{tot}_{titr}	Total amount of ionized and unionized FAs
G	Growth rate
J	Nucleation rate
K_s	Spring constant
$LP2_{tot}$	Total amount of LP2
M_1	Moles of TG and DG digested into MG
M_2	Moles of digested MG
M_i	Ratio between C and C_{max} in modeled profile
N_{SF}	Molar amount of SF in undigested formulation
N_{TG}	Molar amount of TG in undigested formulation
P_{eff}	Effective permeability coefficient
$P_{eff,FF}$	Effective permeability coefficient for fenofibrate
$P_{eff,LP}$	Effective permeability coefficient for lipolysis products
Q^2	Coefficient of cross-validation
R^2	Coefficient of correlation
S	Supersaturation ratio (Chapter 3)
S	Slope of the calibration curve (Chapter 5)
S_{theor}	Theoretical supersaturation ratio
SF	Molar amount of undigested surfactant (Chapter 5)
SF_0	Total amount of surfactants at t=0
$SF_{id,mic}$	Amount of surfactant in micellar structures in the intestine
$SF_{id,oil}$	Amount of surfactant in oil droplets in the intestine
SF_{mic}	Amount of surfactant in micellar structures
SF_{oil}	Amount of surfactant in oil droplets

SF_{tot}	Total amount of surfactant
SR	Supersaturation ratio
SR^M	Maximum supersaturation ratio
T	Temperature
T_i	Ratio between C and C_{max} in experimental profile
TG	Molar amount of undigested triglycerides (Chapter 5)
TG_{id}	Amount of triglycerides in dispersed LBF in the intestine
TG_{iu}	Amount of triglycerides in undispersed LBF in the intestine
TG_{tot}	Total amount of triglycerides
U	Ultrasound velocity
V	Volume
V_d	Volume of distribution
V_i	Volume of intestinal fluid
X_{gd}	Amount of SF or TG in dispersed LBF in the stomach
X_{gu}	Amount of SF or TG in undispersed LBF in the stomach
X_{iu}	Amount of SF or TG in undispersed LBF in the intestine

α	Acoustical attenuation factor
ϕ	Volume fraction
γ	Interfacial energy
κ	Adiabatic compressibility
κ'	Surfactant solubilization power
λ	Wave length
λ_0	Ground wave
μ	Chemical potential
μ_{eq}	Chemical potential at equilibrium
ν_0	Molecular volume
ρ	Density
σ	Standard deviation
σ'	Co-solvent solubilization power
τ_{ind}	Induction time

List of Figures

List of Tables

Acknowledgments

The present thesis would not have been possible without the great support of many people – I owe an enormous *Thank You* to all of them.

I wish to express my deep gratitude to *Prof. Dr. Georgios Imanidis* for giving me the opportunity to carry out this PhD thesis at the University of Basel and the University of Applied Sciences and Arts Northwestern Switzerland. Thank you for many fruitful scientific discussions and for giving me the freedom to pursue my own ideas.

My sincere thanks also go to *Prof. Dr. Martin Kuentz* for valuable input, interesting discussions, and for his great enthusiasm toward the topic of the thesis.

I am also very grateful to *Prof. Dr. Jörg Huwyler* for being co-referee of the thesis and to *Prof. Dr. Matthias Hamburger* for kindly accepting to chair the defense.

Many thanks to the members of the LFCS consortium Dispersion Working Group for giving me the opportunity to participate in this interesting project. I also owe many thanks to *Dr. Brendan Griffin* for his valuable input and collaboration in the biopharmaceutical modeling study.

To my colleagues at the Institute of Pharma Technology – the time with you was amazing! Thank you for sharing lunches and coffee breaks, cakes and tiramisus, sportive and cultural events, many, many interesting discussions, and – above all – thank you for sharing your laughter and friendship, which made the time at the IPT really irreplaceable. *Andreas, Berndt, Carla, David, Fabienne, Georg, Jan, Jiri, Jonas, Katerina, Lukas, Marc, Martin C., Martin K., Mathias, Michael, Miriam, Myriam, Nicolas, Sheela, Stüdi, Urs, Ursula, Verena, Veronika, Yvonne, Zdravka* – Thank you all!!

Special thanks go to *Yvonne Arnold* for introducing me to several analytical techniques at the very beginning of my PhD thesis, to *Martin Cavegn, Michael Lanz, Fabienne Thönen*, and *Stefan Winzap* for immediate help with any technical issue in the lab.

I owe many thanks to *Thomas Denz, Michaela Werfeli*, and *Desirée Dürr*, for their valuable contribution to my projects during their Bachelor's and Master's theses.

Karen, Jimmy, Sara, Pelle, Sara bio – anche per me il capitolo unibas sta volgendo al termine, ed è quindi un'ottima occasione per ringraziarvi di cinque anni indimenticabili trascorsi in vostra compagnia!

Mein allerherzlichstes Dankeschön gilt *meiner Familie*. Ihr habt mir diesen Weg ermöglicht und mich stets ermutigt und unterstützt, dafür bin ich Euch unendlich dankbar. Danke für alles!

E per finire un sincero *grazie di cuore* a te, *Patrick*. Non immagini quanto sia stato prezioso per me il tuo sostegno! *Grazie. Grazie infinite.*

'How did science surprise you?', a voice asks. Here, too, I don't have to search for the answer very long: 'I expected solitary research and had no inkling of how much the community of other scientists would shape and enrich my life.' Great scientific discoveries are the children of solitude, yet they are never born in isolation. We scientists are working on a cathedral whose completion none of us will ever see. The community of our work gives us the strength to keep on going.

Gottfried Schatz

in *A matter of wonder –*

What biology reveals us about us, our world, and our dreams